The Roles of CD38 and NAADP in Cardiac Tissue



Wee Khang Lin

Green Templeton College

University of Oxford

A thesis submitted for the degree of

Doctor of Philosophy

Trinity 2017

Dedication

In memory of my dearest pet dog, Lucky

For the joy and warmth you brought

For the irreplaceable void you left

You shall not be forgotten

Acknowledgements

I must firstly thank my supervisor Derek Terrar for all his guidance and encouragement, without which this work could not have been done. I also owe a debt of gratitude to my second supervisor, Antony Galione, who provided many valuable insights and generously allowed me to use his lab equipment and reagents.

I have also benefited greatly from help given by academic staff and non academic staff including, but not limited to, Ming, Fran, Paula, Hilary and Clive. I am also very grateful to my lab mates and many members from other labs who have provided many useful discussions.

I would also like to express my greatest gratitude to all those including Emma Bolton, Dhivina Gagoomal, Danni Zhu and James Lua who have provided companionship throughout my time in Oxford. Special thanks should go to Peter Watson and T.O.M. Samuels who have spent significant amount of time with me on a daily basis, and who have also been there during my ups and downs.

Last but not least, I must thank my parents for their endless love and for supporting their son in the pursuit of his dream.

Publications

Lin, W. K., Bolton, E. L., Cortopassi, W. A., Wang, Y., O'Brien, F., Maciejewska, M., Jacobson, M. P., Garnham, C., Ruas, M., Parrington, J. and Lei, M., Sitsapesan, R., Galione, A., and Terrar D. A. (2017). Synthesis of the Ca^{2+}-mobilising messengers, NAADP and cADPR, by intracellular CD38 enzyme in mouse heart: role in β-adrenoceptor signaling. *Journal of Biological Chemistry* 10.1074/jbc.M117.789347. **[includes material presented in Chapter 4, 5, and 6 of this thesis]**

※Capel, R. A., ※Bolton, E. L., ※**Lin, W. K.**, Aston, D., Wang, Y., Liu, W., Wang, X., Burton, R. A. B., Bloor-Young, D., Shade, K. T., Ruas, M., Parrington, J., Churchill G. C., Lei, M., Galione, A., and Terrar D. A. (2015). Two-pore channels (TPC2s) and nicotinic acid adenine dinucleotide phosphate (NAADP) at lysosomal-sarcoplasmic reticular junctions contribute to acute and chronic β-adrenoceptor signaling in the heart. *Journal of Biological Chemistry* **290**, 30087-30098. **[includes material presented in Chapter 3 of this thesis]**

※Wang, Y.,※**Lin, W. K.**, Crawford, W., Ni, H., Bolton, E. L., Khan, H., Shanks, J., Bub, G., Wang, X., Paterson, D. J., Zhang, H., Galione, A., Ebert, S., Terrar, D. A., and Lei, M. (2017). Optogenetic control of heart rhythm by selective stimulation of cardiomyocytes derived from $Pnmt^{+}$ cells in murine heart. *Scientific Reports* 10.1038/srep40687.

※Wang, R., ※Wang, Y., **Lin, W. K.**, Zhang, Y., Liu, W., Huang, K., Terrar, D. A., Solaro, R. J., Wang, X., Ke, Y., and Lei, M. (2014). Inhibition of angiotensin II-induced cardiac hypertrophy and associated ventricular arrhythmias by a p21 activated kinase 1 bioactive peptide. *PloS ONE*, 10.1371/journal.pone.0101974.

※ **These authors contributed equally.**

Abbreviations

ADP	adenosine diphosphate
ADPR	adenosine diphosphate-ribose
ADPRP	adenosine diphosphate-ribose-2'-phosphate
Akt	RAC-α serine/threonine-protein kinase, protein kinase B
Ang-II	angiotensin II
ANOVA	analysis of variance
ARC	adenosine diphosphate-ribosyl cyclase
Asp	aspartic acid
ATP	adenosine triphosphate
bpm	beats per minute
BST-1	bone marrow stromal cell antigen-1
Ca^{2+}	calcium (ions)
cADPR	cyclic adenosine diphosphate-ribose
CAM	coronary artery myocyte
CaMKII	calcium/calmodulin-dependent protein kinase II
cAMP	cyclic adenosine monophosphate
CD	cluster of differentiation
cDNA	complementary deoxyribonucleic acid
CD38$^{-/-}$	model with homozygous knock-out of the CD38 gene
cGPDR	cyclic guanine diphosphate-ribose
cIDPR	cyclic inosine diphosphate-ribose
CPA	cyclopiazonic acid
DHAB	4,4'-dihydroxy azobenzene
DMEM	Dulbecco's Modified Eagle Medium
DMSO	dimethyl sulphoxide
DSEVC	discontinuous single electrode voltage clamp
DTT	dithiothreitol
EC coupling	excitation-contraction coupling
ECG	electrocardiogram
EGTA	ethylene glycol-bis(β-aminoethyl ether)-N,N,N',N'-tetraacetic acid
EM-CCD	electron multiplying charge coupled device
ER	endoplasmic reticulum
Erk	extracellular signal-regulated kinase
ES	embryonic stem
FGF4	fibroblast growth factor 4
FRET	Förster resonance energy transfer
GDP	guanine diphosphate
Glu	glutamic acid
GPI	glycosylphosphatidyl-inositol

GPN	Gly-Phe β-naphthylamide
GTP	guanosine-5'-triphosphate
H.M.S.O.	Her Majesty's Stationery Office
HA	human influenza hemagglutinin
HEPES	4-(2-Hydroxyethyl) piperazine-1-ethanesulfonic acid, N-(2-Hydroxyethyl) piperazine-N'-(2-ethanesulfonic acid
HSR	heavy sarcoplasmic reticulum (fraction)
IC_{50}	concentration of an inhibitor where the response (or binding) is reduced by half
IR	ischemia/reperfusion
ISO	isoprenaline
K_d	dissociation constant
kDa	kilodalton
KO	knock-out
LAMP-2	lysosome-membrane associated protein 2
LSR	light sarcoplasmic reticulum (fraction)
MALDI-TOF	matrix-assisted laser desorption/ionisation time-of-flight
MAP	monophasic action potential
MEF	mouse embryonic fibroblast
MEF2C	myocyte enhancer factor 2C
MM/GBSA	Molecular Mechanics/Generalised Born Surface Area
MnTBAP	Mn(III) tetrakis(4-benzoic acid)porphyrin chloride
MTRP1	mucolipin transient receptor potential channel 1
Na^+	sodium
NA	nicotinic acid
NAADP	nicotinic acid adenine dinucleotide phosphate
NAADP-AM	acetoxymethyl ester derivative of NAADP
NAD	nicotinamide adenine dinucleotide
NADP	nicotinamide adenine dinucleotide phosphate
NHD	nicotinamide hypoxanthine dinucleotide
NMN	nicotinamide mononucleotide
NO	nitric oxide
PBS	phosphate-buffered saline
PDB	Protein Data Bank
PI(3,5)P2	phosphatidylinositol 3,5-bisphosphate
PI3 kinase	phosphatidylinositol-4,5-bisphosphate 3-kinase
PKA	protein kinase A
PKC	protein kinase C
PLC	phospholipase C
PMSF	phenylmethyl-sulphonic fluoride
PPADS	pyridoxal phosphate-6-azo(benzene-2,4-disulphonic acid) tetrasodium salt

PSS	physiological salt solution
PVB	premature ventricular beats
r.f.u.	relative fluorescence unit
ROS	reactive oxygen species
RT-PCR	real-time reverse transcription polymerase chain reaction
RyR	ryanodine receptor
RyR2	ryanodine receptor 2
SERCA	sarco-endoplasmic reticulum adenosine triphosphatases
siRNA	small interfering ribonucleic acid
SR	sarcoplasmic reticulum
SRMP	sarcoplasmic reticulum-enriched membrane preparation
TEMPO	2,2,6,6-tetramethyl-1-piperidinyloxy
TGF	transforming growth factor
Thr	threonine
TPC	two-pore channel
***Tpcn2*$^{-/-}$**	model with homozygous knock-out of the TPCN2 gene
Trp	tryptophan
TRP	transient receptor potential
2KC1	two-kidney one clip
VT	ventricular tachycardia
WT	wild type
Zn^{2+}	zinc ions

Abstract

Nicotinic acid adenine dinucleotide phosphate (NAADP) is an endogenous molecule that releases calcium ions (Ca^{2+}) from acidic endolysosomal stores. This Ca^{2+}-mobilising molecule is known to play a role in modulating cardiac excitation-contraction coupling and pathophysiology.

The first part of the thesis focuses on understanding the mechanistic details of NAADP actions, particularly during the flight and fight response of the heart. Paced ventricular myocytes, which had genetically- (*Tpcn2*$^{-/-}$) or pharmacologically-impaired (bafilomycin-A1 treatment) NAADP signalling pathways, had blunted responses to isoprenaline. Further investigations revealed that NAADP actions are dependent of functional CaMKII proteins but independent of L-type Ca^{2+} channels.

The main part of the thesis focuses on understanding the enzymatic production of NAADP in the heart. Although CD38, which belongs to the ADP-ribosyl cyclase (ARC) family, has been shown to catalyse the synthesis of NAADP in other mammalian tissue, whether CD38 is responsible for the production of NAADP in the heart remains debatable. Membrane fractions from *CD38*$^{-/-}$ mouse hearts were not able to generate NAADP through catalysing the base-exchange reaction. Experiments involving the permeabilisation of cardiac myocytes also revealed the intracellular expression of CD38 on the sarcoplasmic reticulum (SR). The SR-enriched membrane preparation (SRMP) from sheep heart is also capable of catalysing NAADP production and showed properties associated with those of CD38. Upon isoprenaline addition, paced *CD38*$^{-/-}$ myocytes had smaller Ca^{2+} transients and contraction amplitudes, compared to those of wild type animals. In addition, impairing NAADP signalling using bafilomycin-A1 did not affect the effect of isoprenaline on *CD38*$^{-/-}$ myocytes. highlighting the role of CD38 in coupling NAADP action to β-adrenoceptor signalling.

Lastly, a novel ARC inhibitor, SAN4825, was also shown to inhibit NAADP synthesis in both mouse and sheep cardiac preparations, through targeting CD38. *CD38*$^{-/-}$ hearts or SAN 4825-treated hearts were resistant to isoprenaline-induced arrhythmias. These observations support the hypothesis that NAADP is generated by intracellular CD38 in the heart, which contributes to the positive inotropic and pro-arrhythmic effects of the β-adrenoceptor activation.

Contents

1 Introduction **1**

1.1 General introduction 1

1.2 CD38/ADP-ribosyl cyclase as an enzyme 3

1.2.1 The discovery of CD38 3

1.2.2 Distributions of CD38/ADP-ribosyl cyclase 4

1.2.3 CD38 and its homologues 5

1.2.4 Biological reactions catalysed by CD38 6

1.2.5 Acid dependency of CD38-associated enzymatic activities 8

1.2.6 Physiological concentration of substrates of CD38 10

1.2.7 Enzymatic structure of CD38 11

1.2.7.1 Essential catalytic residues in the enzymatic pocket of CD38 11

1.2.7.2 Cysteine residues of CD38 12

1.2.7.3 Dimerisations/tetramerisations of CD38 14

1.2.7.4 Glycosylations of CD38 14

1.2.8 Topological paradox of CD38 15

1.2.9 Observations of non-CD38 ARCs in mammalian tissue 17

1.2.10 Relationships between CD38 and endogenous concentrations of NAADP and cADPR 21

1.2.11 Enzymatic role of CD38/ADP-ribosyl cyclase in physiology and pathophysiology of the heart 23

1.2.11.1 Physiological roles of enzymatic products of CD38 in the heart 23

1.2.11.2 Gender and temperature dependent effect of CD38 KO on cardiac tissue 25

1.2.11.3 Hormonal regulation of CD38/ADP-ribosyl cyclase 27

1.2.11.4 Cardiac development and CD38 29

1.2.11.5 CD38, ROS and ischemic/reperfusion injury 30

1.2.11.6 Hypertrophy and CD38 . . . 32
1.2.11.7 Arrhythmias and CD38 . . . 33
1.3 NAADP as an endogenous Ca^{2+}-mobilising agent . . . 35
1.3.1 Ca^{2+} release properties of NAADP in sea urchin egg homogenates . . . 35
1.3.2 Endolysosomes as an acidic store of Ca^{2+} . . . 37
1.3.3 Molecular targets of NAADP . . . 39
1.3.4 TPCs are essential for the NAADP-regulated Ca^{2+} release . . . 41
1.3.5 Roles of NAADP in the cardiac physiology . . . 46
1.3.6 NAADP and cardiac diseases . . . 50
1.4 General remarks . . . 52

2 Methods and Materials **55**
2.1 Animals . . . 55
2.2 Mouse ventricular cardiomyocyte isolation . . . 56
2.3 Rabbit ventricular and atrial cardiomyocyte isolation . . . 57
2.4 Cell superfusion . . . 58
2.4.1 Bulk superfusion system . . . 58
2.4.2 Rapid switch system . . . 59
2.5 Ca^{2+} fluorescence imaging . . . 60
2.5.1 Line scanning confocal microscopy . . . 60
2.5.2 Spinning disk confocal microscopy . . . 61
2.6 Electrical field stimulation . . . 62
2.7 Contraction studies . . . 62
2.8 L-type Ca^{2+} current measurement . . . 63
2.9 Sheep sarcoplasmic reticulum-enriched membrane preparation . . . 66
2.10 Mouse mixed membrane preparation . . . 67
2.11 The measurement of NAADP using sea urchin egg homogenate assay . . . 68
2.12 The measurement of ADP-ribosyl cyclase activity . . . 69
2.12.1 Detection of cGDPR formation using an NGD assay . . . 69
2.12.2 Detection of cADPR using sea urchin egg homogenate assay . . . 70
2.13 Permeabilisation . . . 71
2.14 Protein quantification . . . 71
2.15 Immunocytochemistry . . . 72
2.16 Monophasic action potential recording . . . 73

2.17 Drug docking studies . . . 75
2.17.1 Blind docking with SwissDock server . . . 75
2.17.2 Docking simulation with Glide . . . 76
2.18 Recipes for solutions . . . 77
2.19 Suppliers of drugs and chemical compounds . . . 77
2.20 Statistical analysis . . . 79

3 NAADP action in mouse myocytes 81
3.1 Background . . . 82
3.2 Methods . . . 84
3.3 Results . . . 85
3.3.1 The application of NAADP-AM increased Ca^{2+} transient amplitudes in mouse ventricular cardiomyocytes . . . 85
3.3.2 NAADP-mediated positive inotropy was abolished in ventricular myocytes from *Tpcn2*$^{-/-}$ mice . . . 87
3.3.3 *Tpcn2*$^{-/-}$ mice showed a blunted increase in Ca^{2+} transient amplitudes during β-adrenoceptor activation . . . 89
3.3.4 Bafilomycin-A1 reduced the increase in Ca^{2+} transients amplitude of mouse single ventricular cardiomyocytes during β-adrenoceptor activation . . . 91
3.3.5 Activation of the NAADP/TPC pathway did not alter the amplitude of L-type Ca^{2+} currents of mouse ventricular myocytes . . . 93
3.3.6 KN-93, an inhibitor of CaMKII, abolished the NAADP-AM-induced increase in Ca^{2+} transient amplitudes . . . 94
3.3.7 An active NAADP signalling pathway was not detected in mouse ventricular cardiomyocytes under conditions where β-adrenoceptors were not stimulated . . . 96
3.4 Discussion . . . 99
3.4.1 Does the increased level of NAADP during β-adrenoceptor stimulation contribute to the cardiac fight or flight response? . . . 99
3.4.2 How does NAADP-regulated Ca^{2+} release give rise to a positive inotropic effect in ventricular cardiomyocyte? . . . 104
3.4.3 Is the NAADP signalling pathway constitutively active under the condition when β-adrenoceptors are not stimulated? . . . 111
3.5 Conclusion . . . 113

4 NAADP synthesis in sheep SRMP 115
4.1 Background . . . 115

4.2 Method . . . 118
4.3 Results . . . 119
4.3.1 NAADP, cADPR and cGDPR synthesis was detected in SRMP from sheep hearts . . . 119
4.3.2 cGDPR synthesis was inhibited by NAD or NADP and NAADP synthesis was inhibited by NAD at pH 7.2 . . . 122
4.3.3 NAADP synthesis at pH 4.5 was enhanced and unaffected by the presence of NAD . . . 125
4.3.4 Effects of Zn^{2+} on NAADP and cGDPR synthesis . . . 127
4.3.5 Effects of catalytic subunit of PKA on NAADP and cGDPR synthesis 130
4.4 Discussion . . . 133
4.4.1 Is there evidence for the existence of a non-CD38 in the SRMP from sheep hearts? . . . 133
4.4.2 Is the assessment of ARC activity in this chapter reliable? . . . 137
4.4.3 Do observations in this thesis support the existence of an ARC in the cardiac SR? . . . 139
4.4.4 Would SR be a suitable place for an ARC enzyme? . . . 141
4.5 Conclusion . . . 143

5 Effects of CD38 KO on hearts 145

5.1 Background . . . 145
5.2 Methods . . . 147
5.3 Results . . . 148
5.3.1 Lack of cardiac cGDPR and NAADP synthesis in membrane preparation from *CD38*$^{-/-}$ mice at pH 7.2 . . . 148
5.3.2 Lack of cardiac NAADP synthesis in the membrane preparation from *CD38*$^{-/-}$ mice at pH 4.5 . . . 151
5.3.3 Lack of NAADP synthesis in intact cardiac myocytes from *CD38*$^{-/-}$ . . . 153
5.3.4 Permeabilisation with Triton X-100 or saponin increased NAADP synthesis rate in single ventricular cardiomyocytes from mice . . . 154
5.3.5 Permeabilisation with Triton X-100 revealed CD38 labelling in ventricular cardiomyocytes isolated from WT but not *CD38*$^{-/-}$ mice . . . 159
5.3.6 Immunolabelling of CD38 and RyR2 on ventricular and atrial cardiomyocytes from rabbits . . . 164
5.3.7 Single ventricular cardiomyocytes from *CD38*$^{-/-}$ mice showed blunted Ca^{2+} transient amplitudes and sarcomere shortening magnitudes during β-adrenoceptor stimulation . . . 173

5.3.8 Bafilomycin-A1 blunted Ca^{2+} transient amplitudes in single ventricular cardiomyocytes from WT but not *CD38*$^{-/-}$ mice during β-adrenoceptor stimulation . . . 175

5.3.9 Langendorff-perfused hearts from *CD38*$^{-/-}$ mice were more resistant to isoprenaline-induced arrhythmogenocity . . . 178

5.3.10 Langendorff-perfused hearts from *CD38*$^{-/-}$ mice showed reduced isoprenaline-induced positive chronotropic effect . . . 183

5.4 Discussion . . . 185

5.4.1 Is CD38 the main enzyme responsible for NAADP and cADPR synthesis in the heart? . . . 185

5.4.2 Is CD38 expressed as an ectoenzyme in the hearts? . . . 188

5.5 Conclusion . . . 190

6 Effects of SAN4825 on hearts 193

6.1 Background . . . 193

6.2 Methods . . . 195

6.3 Results . . . 196

6.3.1 SAN4825 inhibited cGDPR and cADPR synthesis in sheep cardiac SRMP at pH 7.2 . . . 196

6.3.2 SAN4825 inhibited NAADP synthesis in sheep cardiac SRMP at pH 7.2199

6.3.3 Lack of SAN4825 inhibition of NAADP synthesis in sheep cardiac SRMP at pH 4.5 . . . 200

6.3.4 *In vitro* and *in silico* evidence supports CD38 as the target of SAN4825 in mouse cardiac tissue . . . 202

6.3.5 *In silico* observation predicts human CD38 as the target of SAN4825 . 207

6.3.6 Effects of SAN4825 on magnitudes of Ca^{2+} transients and sarcomere shortenings in mouse ventricular myocytes under basal conditions and during the activation of β-adrenoceptors . . . 209

6.3.7 Effects of SAN4825 on isoprenaline-induced arrhythmogenocity in Langendorff-perfused mouse hearts . . . 213

6.3.8 Langendorff-perfused mouse hearts treated with SAN4825 showed blunted isoprenaline-induced positive chronotropic effects . . . 217

6.4 Discussion . . . 219

6.4.1 Does SAN4825 target CD38? . . . 219

6.5 Conclusion . . . 222

7 General discussion and future work 225

7.1 General discussion and conclusion . . . 225

7.2 Future work 233
7.2.1 Type-III CD38 in the heart 233
7.2.2 Contribution of CD38 in atrial tissue 234
7.2.3 Relationship of CaMKII and NAADP/CD38 235
7.2.4 Possible complementary actions of NAADP and cADPR 236
References . . . . .

List of Figures

1 Schematic diagram of enzymatic activities catalysed by CD38, CD157 and *Aplysia* cyclase 7

2 Schematic diagram of stimulation protocols in arrhythmias studies 75

3 Effect of NAADP-AM on Ca^{2+} transient amplitudes of paced ventricular myocytes from mice 87

4 Lack of NAADP-AM effect on Ca^{2+} transient amplitudes of paced ventricular myocytes from mice without functional TPC2 protein (*Tpcn2*$^{-/-}$) 88

5 The effect of β-adrenoceptor stimulation on Ca^{2+} transients evoked by electrical stimulation were smaller in ventricular myocytes from *Tpcn2*$^{-/-}$ hearts as compared to those from WT hearts 90

6 Pretreatment with bafilomycin-A1 blunted the Ca^{2+} transient amplitudes of single ventricular cardiomyocytes from mice during β-adrenoceptor activation 92

7 The post-isoprenaline amplitude of L-type Ca^{2+} currents was comparable in ventricular cardiomyocytes from *Tpcn2*$^{-/-}$ and WT mice 94

8 NAADP-mediated increase in Ca^{2+} transient amplitude of paced ventricular cardiomyocytes is dependent on functional CaMKII 95

9 Ca^{2+} transients of WT ventricular cardiomyocytes were comparable to those of myocytes lacking TPC2 and to those of myocytes pretreated with KN93 . . 98

10 NADP and NAADP displacement of photoaffinity radioactive 5-azido-NAADP labelling in SKBR3 whole cell lysates 101

11 The proposed mechanism for the contribution of the NAADP signalling pathway in the β-adrenoceptor-mediated positive inotropy 110

12 Synthesis of NAADP, cADPR and cGDPR by SRMP from sheep hearts . . . 122

13 Substrate competition studies of ARC from SRMP at pH 7.2 124

14 Influence of pH on NAADP synthesis and on inhibition of NAADP synthesis by NAD 126

15 Influence of Zn^{2+} on NAADP and cGDRP synthesis 130

16 Influence of PKA and DTT on cGDPR and NAADP synthesis 133

17 *In vitro* NAADP and cGDPR synthesis was not detectable in cardiac membrane preparation from *CD38*$^{-/-}$ mice at pH 7.2 150

18 *In vitro* NAADP synthesis remained undetectable at pH 4.5 in cardiac membrane preparation from $CD38^{-/-}$ mice 152

19 NAADP synthesis was undetectable in single ventricular cardiac myocytes isolated from *CD38$^{-/-}$ mice* 154

20 Permeabilisation of ventricular cardiomyocytes with saponin (0.01% w/v) and Triton X-100 (0.1% v/v) led to an increased rate of NAADP synthesis 158

21 Effects of H_20, Triton X-100, saponin and DMSO on the sea urchin egg homogenate bioassay 159

22 Permeabilisation with Triton X-100 revealed immunolabelling of CD38 in ventricular cardiomyocytes isolated from WT but not *CD38$^{-/-}$* mice 163

23 Rabbit anti-human CD38 polyclonal antibodies were able to stain both permeabilised and intact spleen tissue 163

24 Immunolabelling of CD38 on rabbit ventricular myocytes showed a similar pattern to that observed in mouse ventricular myocytes 168

25 Immunolabelling of CD38 on rabbit atrial myocytes showed a striated pattern instead of a membrane-like staining pattern 169

26 Z series scan of rabbit atrial myocytes labelled by the rabbit polyclonal anti-CD38 antibody 171

27 Dual immunolabelling of rabbit atrial myocytes by anti-CD38 and anti-RyR2 antibodies 173

28 Single ventricular cardiomyocytes from *CD38$^{-/-}$* mice showed blunted Ca^{2+} transients amplitudes and sarcomere shortenings during β-adrenoceptor stimulation 175

29 Pretreatment with bafilomycin-A1 did not alter the Ca^{2+} transient amplitudes of single ventricular cardiomyocytes from *CD38$^{-/-}$* mice during activation of β-adrenoceptors 177

30 Langendorff-perfused from *CD38$^{-/-}$* mice showed resistance to isoprenaline-induced arrhythmogenocity 182

31 The basal heart rate, heart rate in the presence of isoprenaline and post-isoprenaline refractory periods of Langendorff-perfused hearts from WT and *CD38$^{-/-}$* mice 185

32 cGDPR and cADPR synthesis carried out by sheep cardiac SRMP were inhibited by SAN4825 at pH 7.2 198

33 NAADP synthesis carried out by sheep cardiac SRMP was inhibited by SAN4825 at pH 7.2 200

34 SAN4825 failed to inhibit sheep cardiac NAADP synthesis at pH 4.5 while its inhibition of cADPR synthesis remain intact 202

35 *In vitro* evidence of SAN4825 inhibiting the synthesis of NAADP and cADPR through targeting CD38 205

36 *In silico* evidence of SAN4825 inhibiting the synthesis of NAADP and cADPR through targeting CD38 207

37 *In silico* observations support the hypothesis that SAN4825 can inhibits the enzymatic of human CD38 by occupying its active site 209

38 Lack of SAN4825 effect on the amplitudes of Ca^{2+} transients and cell shortenings in mouse ventricular cardiac myocytes under basal conditions and during β-adrenoceptor stimulation 212

39 Whole hearts treated with SAN4825 showed resistance to isoprenaline-induced arrhythmogenocity 216

40 The basal heart rate, heart rate in the presence of isoprenaline, and post-isoprenaline refractory periods of mouse hearts preincubated with either DMSO or SAN4825 219

List of Tables

2.1 Perfusion Solutions 77
2.2 Myocyte Isolation Solution 77
2.3 Additional buffers 78
4.1 Summary of properties of the CD38, non-CD38 cardiac specific ARC and ARC from sheep cardiac SRMP 138
6.1 Mean, SEM and n number of Ca^{2+} transient and sarcomere shortening measurements of ventricular myocytes with and without the preincubation of SAN4825 from Figure 6.3.6 213

Chapter 1

Introduction

1.1 General introduction

The heart is an organ that pumps blood around the body in order to maintain sufficient oxygen and nutrients for all organs and tissues. It consists of contractile muscle cells (myocytes) that contract and relax in response to action potentials. These myocytes are connected through gap junctions and this allows the heart to function as an electrical syncytium.

Ca^{2+} ions (Ca^{2+}) play a paramount role in the excitation-contraction coupling (EC coupling) in the cardiac muscle (see review by Bers 2002). During each membrane depolarisation, L-type Ca^{2+} channels open, allowing the influx of Ca^{2+} ions. This Ca^{2+} influx causes a subsequent release of Ca^{2+} ions from the sarcoplasmic reticulum (SR) through ryanodine receptors (RyRs), resulting in a global rise of the cytosolic concentration of Ca^{2+}. The cardiac muscle contraction occurs when Ca^{2+} ions bind

to troponin C proteins and facilitate the formation of the actin-myosin cross-bridges. In order for the heart muscle to relax, the cytosolic level of Ca^{2+} is restored to the basal level through at least four mechanisms: i) The reuptake by sarco-endoplasmic reticulum ATPases (SERCA), ii) The extrusion by Na^{+}/Ca^{2+}-exchanger protein, iii) The extrusion by sarcolemmal Ca^{2+}-ATPases, iv) The uptake by mitochondrial Ca^{2+} uniporters (see review by Bers 2002).

In the past, the roles of several second messengers in this EC coupling have been investigated. Among them, cyclic adenosine monophosphate (cAMP) that is produced upon activation of β-adrenoceptors has received the most attention, particularly in regards to its stimulation of protein kinase A (PKA), which in turn phosphorylates several key proteins such as RyRs, SERCAs and L-type Ca^{2+} channel (see review by Bers 2002). This increases the level of systolic intracellular Ca^{2+} as well as Ca^{2+} load in the SR, resulting in stronger contractions, namely the positive inotropic effect. Similarly, Ca^{2+}/calmodulin dependent kinase II (CaMKII) that can be activated by Ca^{2+} is known to phosphorylate these key proteins too (see review by Maier and Bers 2007). IP_3 that is able to mobilise Ca^{2+} from IP_3-sensitive stores, also modulates EC coupling, especially in atrial myocytes (see review by Hohendanner et al. 2014). More recently, cyclic adenosine diphosphate-ribose (cADPR) and nicotinic acid adenine dinucleotide phosphate (NAADP) were shown to contribute to the cardiac EC coupling through regulating Ca^{2+} from acidic lysosomes and SR respectively (see reviews by Rakovic and Terrar 2002 and Terrar 2015). The formation of these two endogenous Ca^{2+}-mobilising molecules was hypothesised to be catalysed by CD38/ADP-ribosyl cyclase (ARC) (see review by Lee 2001).

The aim of this thesis is to investigate the enzymatic production of NAADP

in the heart by CD38/ARC and further evaluate the roles of the NAADP/CD38 pathway in cardiac physiology and pathophysiology, particularly in the context of the flight or fight response (activation of β-adrenoceptors). Although this thesis mainly focuses on the contribution of the Ca^{2+} signalling pathway in EC coupling, it is important to highlight that Ca^{2+} is also involved in other cardiac signalling pathways that regulate myocyte growth, mitochondrial energetics, and transcriptional gene expression (Kang and Lebeche, 2013). In addition, anomalies in Ca^{2+} handling are factors and consequences of cardiac diseases such as hypertrophy, cardiac arrhythmias, ischemic heart diseases and heart failure (Talukder et al., 2009; Cartwright et al., 2011; Kang and Lebeche, 2013). Therefore, the understanding of the CD38/NAADP pathway will undoubtedly advance the cardiac Ca^{2+} signalling field beyond the context of EC coupling.

1.2 CD38/ADP-ribosyl cyclase as an enzyme

1.2.1 The discovery of CD38

The CD (cluster of differentiation, cluster of designation or classification determinant) nomenclature was established in the first International Workshop and Conference on Human Leukocyte Differentiation Antigens (HLDA), which was held in Paris in 1982. When two or more murine monoclonal antibodies are shown to bind to a surface molecule, the surface molecule is assigned a CD number. In 1980, CD38 (also known as T10) was identified by E.L. Reinherz and co-workers in thymocytes and lymphocytes (Reinherz et al., 1980). The gene encoding human CD38 is located at chromosome 4 (Katz et al., 1983). This gene was isolated and

cloned by Jackson and Bell in 1990 (Jackson and Bell, 1990). The human CD38 cDNA (complementary deoxyribonucleic acid) sequence predicts a polypeptide consisting of a short N-terminal cytoplasmic tail (21 residues), a single transmembrane segment and a carboxyl-terminal extracellular domain carrying the four potential N-linked glycosylation sites around 32 kDa.

1.2.2 Distributions of CD38/ADP-ribosyl cyclase

As mentioned above, CD38 expression was first observed in thymocytes and T lymphocytes (Reinherz et al., 1980). Consistently, its expressions in lymphocytes demonstrated stage-related variations and agonistic antibodies against CD38 were shown to trigger a wide range of responses in various types of blood cells (see reviews by Malavasi et al. 1992, 1994). However, it was later revealed that CD38 is not lymphocyte/thymocyte-specific, but is ubiquitously expressed in many other tissues including the brain, eye, gut, pancreas, kidney, bone, and heart (Fernandez et al., 1998; Malavasi et al., 2008). Contrary to the idea that it is a surface antigen, it has been shown that its expression is not limited on cell surfaces but also in various intracellular organelles, such as the endoplasmic reticulum (ER), ribosome, small vesicle, mitochondria as well as the nucleus (Yamada et al., 1997; Adebanjo et al., 1999; Keng et al., 2000; Sun et al., 2002; Ceni et al., 2003b; Yalcintepe et al., 2005; Cosker et al., 2010).

In heart tissue, Mészáros et al. (1997) reported that cardiac sarcolemmal fractions contained CD38-like ARCs, while non-CD38 ARCs were found in the SR-enriched non-sarcolemmal fractions. This was the first discovery of ARC-associated activity on the cardiac SR membrane. Similar the SR-enriched membrane preparation (SRMP)

has since been used by several group to study the ARCs of the heart (Xie et al., 2005; Kannt et al., 2012). Apart from the SR, cardiac ARC activity was also observed in mitochondria-enriched preparation (Xie et al., 2003).

1.2.3 CD38 and its homologues

CD38 belongs to the ARC family that catalyses the conversion of nicotinamide adenine dinucleotide (NAD) to cADPR. Together with CD38, there are four members identified in this family and they have about 20% to 30% similarity among their protein sequences (see review by Lee 2006). *Aplysia* cyclase was first member to be discovered in this family (Hellmich and Strumwasser, 1991; Lee and Aarhus, 1991). Unlike CD38 that is a glycosylated transmembrane protein, *Aplysia* cyclase a soluble protein of 256 residues that is abundant in *Aplysia* ovotestis (Hellmich and Strumwasser, 1991; Lee and Aarhus, 1991). On the other hand, CD157 (or bone marrow stromal cell antigen-1, BST-1) is a 42 – 45 kDa glycosylphosphatidylinositol(GPI)-anchored antigen and the only mammalian homologue of CD38 identified to date (Itoh et al., 1994). A fourth member of the cyclase family, which is another GPI-anchored protein, was discovered in *Schistosoma mansoni*, a human parasite (Goodrich et al., 2005). The highly conserved active site region (referred to as the TLED signature domain) is highly conserved among the CD38, CD157, and *Aplysia* cyclase while the protein sequence of *S. mansoni* cyclase also possesses a high degree of similarity (47%) within this domain when compared to other homologues (Goodrich et al. 2005 and see review by Lee 2006). Another conservative feature among these 4 homologues is the ten critical cysteine residues which are necessary for the 5 conserved intra-disulphide bonds, and which can be aligned among their protein sequences (Prasad et al., 1996;

Goodrich et al., 2005). All of them (in their relative capabilities *Aplysia* cyclase > CD38 > CD157 > *S. mansoni* cyclase) are able to produce cADPR from NAD (Goodrich et al. 2005 and see the review by Malavasi et al. 2008). In addition, apart from CD157, all homologues catalyse the base-exchange reaction that forms NAADP from nicotinamide adenine dinucleotide phosphate (NADP) and nicotinic acid (NA) (Goodrich et al. 2005 and see reviews by Lee 2006; Malavasi et al. 2008). An enzyme, which synthesises NAADP but not cADPR, was also discovered in sea urchin sperm (Vasudevan et al., 2008); however, as whether it is a homolog of CD38 remains to be investigated.

1.2.4 Biological reactions catalysed by CD38

A sequence comparison shows that approximately 30% of the amino acid residues from ARC isolated from *Aplysia* cyclase are identical to CD38 (States et al., 1992). This was the first piece of evidence that shows the structural homogeneity of CD38 and the *Aplysia* cyclase, suggesting a possible role of CD38 as the mammalian ARC. Like the *Aplysia* cyclase, CD38 was shown to catalyse the cyclisation of NAD to cADPR (Lee and Aarhus, 1991; Howard et al., 1993; Kim et al., 1993; Takasawa et al., 1993). However, unlike *Aplysia* cyclase, CD38 also hydrolyses the substrate (NAD) as well as the product (cADPR) to ADP-ribose (ADPR). Apart from the formation and degradation of cADPR, CD38 also plays a role in synthesising and hydrolysing NAADP (Aarhus et al., 1995; Graeff et al., 2006). In the presence of NA, CD38 catalyses a base-exchange reaction involving the exchange of nicotinamide group of NADP with NA. At neutral pH or in the absence of NA, CD38 preferentially hydrolyses NADP into ADP-ribose 2'-phosphate (ADPRP) (Aarhus et al., 1995). It can also utilise NAADP as a substrate and hydrolyse it to ADP-ribose 2'-phosphate

(ADPRP) at an acidic pH. Due to the capability of catalysing multiple biological reactions, CD38 is regarded as a multifunctional enzyme. A comparison of enzymatic reactions catalysed by *Aplysia* cyclase, CD157 and CD38 is shown in **Figure 1**.

Figure 1

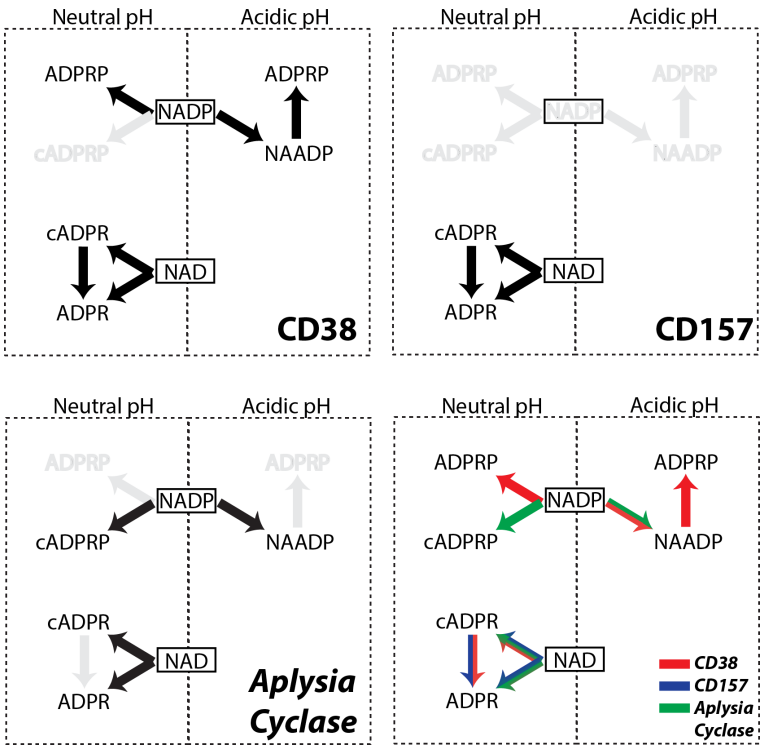


Figure 1: Schematic diagram of enzymatic activities catalysed by CD38, CD157 and *Aplysia* cyclase

Solid black fonts and arrows represents reactions that are catalysed, while greyed out fonts and arrows represent reactions that are not catalysed, by CD38 (top left), CD157 (top right) and *Aplysia* cyclase (bottom left). A summary (bottom right) showing comparison of catalytic activities of these enzymes with color coded arrows representing CD38 (red), CD157 (blue) and *Aplysia* cyclase (green). The schematic reactions are categorised according to their favourable pH. (Howard et al., 1993; Aarhus et al., 1995; Torti et al., 1999; Malavasi et al., 2008)

1.2.5 Acid dependency of CD38-associated enzymatic activities

It has been shown that the formation and hydrolysis of NAADP, as well as the formation of cADPR, by CD38 are pH-dependent (Aarhus et al. 1995; Graeff et al. 2006, see also **Figure 1** for scheme).

By supplementing 1 mM NADP and 30 mM NA, Aarhus et al. (1995) showed that the rate of formation of NAADP by both CD38 and *Aplysia* cyclase was at its maximum between pH 4 and 5, and decreased as the pH increased from 5 to 10. They reported a drastic change of the rate of NAADP formation by CD38 from 22 μmol mg^{-1} min^{-1} to less than 1 μmol mg^{-1} min^{-1} when the pH was increased from 4 to 7. This demonstrated that formation of NAADP through the base-exchange reaction was greatly enhanced at the acidic pH.

Interestingly, Aarhus et al. (1995) showed that when CD38 was incubated with NADP and NA, the rate of formation of ADPRP was roughly 10 μmol mg^{-1} min^{-1} at pH 7, roughly 2 times quicker than its formation at pH 4. On the other hand, Graeff et al. (2006) has shown that the rate of hydrolysis NAADP to ADPRP is at its maximum (resolution of 1 pH) when CD38 was incubated with NAADP at pH 5 . At pH 4 and pH 7, the rate of hydrolysis of NAADP by CD38 was reported by Graeff et al. (2006) to be approximately 80 % and 15 % of its maximum rate, respectively.

These observations do not necessarily contradict each other. In Aarhus's experiment, the reactions were dynamic as NADP and NA were both incubated with CD38; formation of ADPRP can be achieved either from the hydrolysis of NADP itself or the product of the base-exchange reaction, NAADP. The formation

of ADPRP could also be hindered by the formation of NAADP as different substrates could compete for the same active site of CD38. Since Graeff et al. (2006) has shown the enhanced hydrolysis of NAADP at an acidic pH with a more simple and elegant experiment, the hypothesis that NAADP hydrolysis occurs at a greater rate in an acidic environment is favoured.

Some have challenged the physiological relevance of the synthesis of NAADP by CD38 since NAADP formation occurs preferentially at an acidic pH (Aarhus et al., 1995) and CD38 hydrolyses NAADP (Schmid et al., 2011). On the other hand, some have proposed that NAADP synthesis occurs in a compartmentalised, acidic environment such as the acidic endolysosome (Davis et al., 2008; Cosker et al., 2010). It should be pointed out that the half-maximal effective concentration of NAADP in mobilising Ca^{2+} is about 30 nM in sea-urchin egg homogenates (Lee and Aarhus, 1995). Nanomolar concentration of NAADP was also shown to have an effect on cardiomyocytes (Macgregor et al., 2007a; Nebel et al., 2013). Perhaps, CD38 does not have to operate anywhere near its maximal potential to synthesise physiologically relevant amounts of NAADP, and a low production of NAADP at neutral pH can still be sufficient to trigger relevant signalling pathways. The view of the author of this thesis is that the term "rate of synthesis of NAADP" (in many reports including Aarhus's experiment) does not simply mean the actual amount of NAADP being produced by these enzymes in a given length of time, but the amount of measurable NAADP after a given length of time. As CD38 is capable of degrading NAADP, the measurable "rate of synthesis" of NAADP by CD38 could be lower than the real rate of NAADP production. The dynamic interactions between the formation and degradation of NAADP by CD38 and the activation of NAADP receptors in a real biological system remains to be addressed.

To a lesser extent, the formation of cADPR from NAD by CD38 was also affected by the pH. Increasing the pH from 4 to 7 resulted in an increase of cADPR formation rate from approximately 400 μmol mg^{-1} min^{-1} to 700 μmol mg^{-1} min^{-1} (Aarhus et al., 1995). A summary of pH dependency of CD38 is depicted in **Figure 1**.

1.2.6 Physiological concentration of substrates of CD38

The half-maximal concentrations of NADP and NA needed are about 0.2 mM and 10 mM for the base exchange reaction, while the half-maximal concentration of NAD needed for cyclisation is around 50 μM (Graeff et al., 1998, 2001). The total concentration of reduced form of NAD and NADP (NADH and NADPH) was estimated to be around 100 μM (Yu and Heikal, 2009). While the reported ratios of total intracellular NAD : NADH are around 3 – 10 in mammals, the reported ratios of NADP : NADPH are much lower (between 0.001 and 0.015, Veech et al. 1969). In addition, intracellular concentrations of NADP and NADPH are expected to be lower than their non-phosphorylated forms (see reviews byLin and Guarente 2003; Pollak et al. 2007). Cytosolic concentration of NA is also expected to be much lower than 10 mM as the quantified blood concentrations of NA are relatively low (approximately 100 nM, see review by Cantó et al. 2015). These estimations of cytosolic concentrations of NADP and NA suggest that CD38 is not working near its half-maximal rate for its base-exchange reaction. As whether there are other accessory proteins (see (Liu et al., 2017)) or physiological ions which might alter the enzymatic properties of CD38 remains to be investigated.

1.2.7 Enzymatic structure of CD38

1.2.7.1 Essential catalytic residues in the enzymatic pocket of CD38

A mutagenesis study carried out in Lee's group has revealed at least five important amino acid residues for the catalytic activities of human CD38. These are Asp155, Trp125, Trp189 and Glu146 and Glu226 (Munshi et al., 2000). The most important residue seems to be Glu226, as changing it to other residues like Asp, Asn, Gln, Leu or Gly completely eliminated most of the enzymatic activities of CD38. While the alteration of Glu146 caused a reduction in enzymatic rate of formation and hydrolysis of cADPR, the alteration of Asp155 resulted in an increase in the GDP (guanosine diphosphate)-ribosyl cyclase activity specifically. Their results also showed that mutations of the two tryptophans (Trp125 and Trp189) reduced the rate of enzymatic activities of CD38. Using nicotinamide mononucleotide (NMN) as a substrate analogue of NAADP, crystallography studies have supported this mutagenesis study by showing CD38-bound NMN was indeed very close to all five mentioned residues (see the review by Lee 2006). In addition, the ring of Trp189 in CD38 was shown to be parallel to and stacked with the nicotinamide ring of NMN, supporting that this residue is crucial in coordinating the binding of substrates.

Two out of these five residues (Glu146 and Asp155) were suggested to confer the pH dependency of CD38 activities (Graeff et al., 2006). Changing Glu146 or Asp155 to uncharged residues by the site-directed mutagenesis eliminated the strong pH dependence of both CD38-catalysed NAADP hydrolysis and synthesis. Changing Asp155 to a charged residue such as Glu, in contrast, preserved the dependence. As Glu146 and Asp155 are negatively charged at neutral pH, it was proposed that

the electrostatic repulsion between the negatively charged residues and the charged NA group of NAADP would prevent the substrate binding to the active site and, therefore, hindering its hydrolysis. Similarly, during formation of NAADP by the base-exchange reaction, it was suggested that these acidic residues might play a role in positioning the NA and therefore the repulsion between NA and the residues will be a hindrance for the NAADP synthesis at neutral pH. At an acidic pH such as 4.5, the protonation of NA is encouraged and the repulsion among these amino acid residues and substrates will be lessened, favouring both the hydrolysis and synthesis of NAADP.

1.2.7.2 Cysteine residues of CD38

10 cysteine residues are perfectly aligned and conserved between the Aplysia enzymes and human CD38 (Tohgo et al., 1994). In a site-directed mutagenesis study, two additional cysteines (residues 119 and 201) of CD38 were found to be essential for the hydrolysis of cADPR by CD38. Mutating these cysteines residues resulted in the loss of cADPR hydrolase activities in CD38. While the *Aplysia* cyclase does not hydrolyse cADPR in its wild-type form, changing its residues that correspond to residues 119 and 201 of human CD38 to cysteines make it capable of hydrolysing cADPR (Tohgo et al., 1994).

On the other hand, De Flora and co-workers showed that the cysteine residues in ARC did not take part directly in the enzymatic activities of CD38 and *Aplysia* cyclase (Guida et al., 1995). They showed the lack of effect of a thiol-modifying agent on CD38 and *Aplysia* cyclase, in terms of their cADPR forming and hydrolysing activities. However, β-mercaptoethanol, which is capable of reducing disulphide bonds, inactivated the CD38 but not *Aplysia* cyclase. The authors

proposed that β-mercaptoethanol inactivated CD38 by inducing its extensive oligomerisation. They subsequently showed that mildly fixing the CD38 with glutaraldehyde prevented the inactivation of enzymatic activities by β-mercaptoethanol, since β-mercaptoethanol could not induce oligomerisation on fixed CD38. They concluded that these β-mercaptoethanol-sensitive disulphide bonds do not have a direct catalytic role, but they might be important in maintaining the monomeric, catalytically-active structure of CD38 (Guida et al., 1995; Zocchi et al., 1995). (Note: CD38 can also form dimers and/or tetramers with comparable catalytic properties on the cell surface (Bruzzone et al., 1998; Moreno-García et al., 2004)).

The NADase activity of CD38 from *Escherichia* coli cells expressing human CD38 and the membrane of retinoic acid-treated HL-60 cells was shown to be inhibited by dithiothreitol (DTT), a reducing agent (Kontani et al., 1993). In addition, Berthelier et al. (2000) also showed that the NADase activity of immunopurified CD38 from HL-60 cells were reduced to 10% by 10 mM DTT. They reported that DTT incubation led to the loss of the binding of specific monoclonal antibodies to CD38. This provides evidence that is consistent with the notion that disulphide bridges in CD38 are important in maintaining the catalytically active form of CD38. Interestingly, using a specific antibody which recognises a particular disulphide bridge (C254-C275) of human CD38, Zhao et al. (2011) demonstrated that this disulphide bridge of cytosolic and soluble CD38 (engineered) remained intact even in the reducing environment such as the cytosol.

1.2.7.3 Dimerisations/tetramerisations of CD38

As mentioned above, De Flora's group has suggested β-mercaptoethanol inactivated CD38 through oligomerisation of CD38. However, it was reported by Chidambaram et al. (1998) that CD38 from pig hearts showed a series of bands (45 – 285 kDa) under a non-reducing condition, while only the 45 kDa monomer was detected under a reducing condition in a protein immunoblot analysis, using an antiserum to recombinant rat CD38. They have also observed that oligomers of CD38 displayed a higher ARC activity than that of the monomer. While crystallised bovine CD38 appeared to be homodimers (Egea et al., 2012), both human CD38 on the surface of transfected HeLa cells and mouse CD38 on lymphocytes was reported to be expressed as both dimers and tetramers (Bruzzone et al., 1998; Moreno-García et al., 2004; Hara-Yokoyama et al., 2012). Furthermore, mouse CD38 was reported to form tetramers by the dimerisation of CD38 dimers (Hara-Yokoyama et al., 2012). This tetramerisation was reported to be essential for the catalytic activity and localisation of CD38. Perhaps, a specific-pattern oligomerisation is important to maintain the catalytic activity of CD38 and De Flora's observation of the inactivation of CD38 by the β-mercaptoethanol is through a non-specific oligomerisation.

1.2.7.4 Glycosylations of CD38

It was predicted that CD38 has four potential glycosylation sites (Jackson and Bell, 1990). It was later shown that treating the CD38 protein with a deglycosylating agent, endoglycosidase-H, reduced the molecular weight of CD38 from 45 kDa to 36 KDa, suggesting that high mannose N-linked carbohydrates contribute at least

20 % of the molecular weight of the CD38 (Alessio et al., 1990). These N-linked glycosylations of CD38 were reported to have a role in maintaining the structure stability by preventing the formation of inter-molecular cross-links in human CD38 (Gao and Mehta, 2007) and a role in maintaining the enzymatic activities of rat and bovine CD38 (Chidambaram and Chang, 1998; Muller-Steffner et al., 2010). An unglycosylated type-III human CD38, which is 35 kDa and which has a cytosol-facing active site has also been reported (Zhao et al., 2011, 2012, 2015). In contrast to the view that glycosylations of rat and bovine CD38 are pivotal to its enzymatic activities (Chidambaram and Chang, 1998; Muller-Steffner et al., 2010), this unglycosylated type-III human CD38 was shown to retain its enzymatic activity (Zhao et al., 2011).

1.2.8 Topological paradox of CD38

Since CD38 was discovered, it has long been predicted and assumed to be a type-II transmembrane protein, which has an extracellular, catalytic C-domain (Jackson and Bell, 1990). While this orientation suits the receptorial role of CD38 in signalling pathways in the immune system (see review by Malavasi et al. 2008), it is not well-understood how this accommodates its enzymatic role to catalyse reactions of intracellular substrates such as NAD and NADP. Moreover, the products of CD38, such as cADPR and NAADP have intracellular targets, therefore they would have to be transported across the plasma membrane after being produced extracellularly. This topological inconsistency has provoked further investigations and resulted in two major non-exclusive hypotheses.

Firstly, a vesicular/transporter mechanism has been proposed, suggesting that CD38 can be internalised into endo-lysosomes, along with proteins which facilitate

transfers of substrates and products, such as connexin 43 and nucleoside transporters (Bruzzone et al., 2001; Guida et al., 2002; Davis et al., 2008). This hypothesis was reviewed by De Flora et al. 2004, Bruzzone et al. 2012, and Lee and Zhao 2014.

More recently, an alternative transmembrane orientation of CD38 has been proposed. In contrast to the conventional type-II CD38, this CD38 is expressed as a type-III transmembrane protein with a cytosol facing, catalytic C-domain. Considering the fact that the N-terminal of CD38 has a net positive charge of three, while the C-terminal side has a charge of two instead, the expression of a type-III CD38, at the first thought, might violate the "positive inside rule" — the more positively charged side of a single-pass transmembrane segment of a protein should be facing the cytosol (von Heijne, 1989). However, it is worth pointing out that the charge difference between the two sides of CD38 is very small and that some proteins with a small charge difference between their two sides do exhibit more than one orientation (von Heijne, 2006). Observations of the type-III CD38 in native cells has also been reported by several groups (Adebanjo et al., 1999; Zhao et al., 2012, 2015). As mentioned before (see section 1.2.7 on page 11), the disulphide bridges in CD38 are essential for its enzymatic activity and this has raised concerns regarding whether these disulphide bridges will be stable under the reducing condition of the cytosol. However, Lee's group has demonstrated that the type-III CD38 is enzymatically functional inside the cytosol (Zhao et al., 2011). They also showed that altering the serine residues of CD38 to aspartate, which is functionally equivalent to phosphorylation of CD38, resulted in expression of the type-III CD38 instead of the type-II CD38 (Zhao et al., 2012, 2015). This highlights the possibility of a mechanism of regulating the CD38 orientation through the endogenous phosphorylation of the serine residues of the nascent N-terminal tails of CD38.

Perhaps, the orientations of CD38 are not necessarily mutually exclusive and different orientations might serve different purposes. It was suggested that a type-II CD38 is more suitable for long term responses to agonists, due to the slower kinetics involving activations of receptors, internalisations, and transportations of substrates and products. On the other hand, a type-III CD38 could maintain the basal levels of products and mediate fast responses upon various stimulations (Zhao et al., 2015).

Besides the two hypotheses mentioned above, in order to resolve the topological paradox of CD38, several groups have sought to explore other candidates that catalyse the formation of cADPR and/or NAADP. They have reported the existence of an intracellular non-CD38 ARC that could have a cytosolic catalytic site. This will be discussed in the next section.

1.2.9 Observations of non-CD38 ARCs in mammalian tissue

They have been reports regarding other non-CD38 ARCs in mammalian tissues over the years:

i) Kidney

In rat kidneys, a discovery of a non-CD38 ARC was reported by Kim's group (Nam et al., 2006). Unlike human CD38, the enzymatic cyclisation reaction of the ARC from rat kidneys was not inhibited by DTT (up to 30 mM). While the enzymatic activity (NGD cyclisation) of human CD38 was potentiated by zinc ions (Zn^{2+}), this enzyme from rat kidneys was inhibited by Zn^{2+}. They further supported their discovery by showing a drug, 4,4'-dihydroxy azobenzene (DHAB), at 200 μM, specifically blocked the enzymatic activity of ARCs from kidneys but had no effect on those from hearts (see Gul et al. 2008 for contradictory observations of the effect

of DHAB on cardiac ARC activity), brains, and spleens, as well as purified human CD38. DHAB also blocked the cADPR-mediated increase in cytosolic Ca^{2+} concentration in rat mesangial cells but not Jurkat T cells that were thought to express CD38 exclusively.

ii) Skeletal tissue

Similar Zn^{2+} and DTT-related biochemical differences were observed in heavy SR fractions (HSR) isolated from rabbit skeletal muscle by Bacher and co-workers' study (Bacher et al., 2004). In their study, they showed that Zn^{2+} and Cu^{2+} ions inhibited ARC activity from HSR, in contrast to the observations that the ARC activity of CD38 and CD157/BST-1 was activated by Zn^{2+} ions (Hirata et al., 1994; Kukimoto et al., 1996). On the other hand, DTT failed to affect the enzymatic cyclisation observed in the skeletal HSR. While CD38 from Jurkat T-lymphocytes was labelled by anti-CD38 antibodies in their experiments, no labelling was detected at the molecular mass of interest (35 – 45 kDa) in the HSR from skeletal muscle.

iii) Brain

In the brain, Ceni et al. (2003a, 2006) reported a detectable ARC activity (that can be inhibited by Zn^{2+}) from adult *CD38*$^{-/-}$ brains. The NADase activity from adult *CD38*$^{-/-}$ brains examined *in vitro* using protein extracts and cells was 3 orders of magnitude lower compared with the CD38-dependent NADase activities found in the same preparations isolated from wild-type mouse brains (Ceni et al., 2003a). In the brain synaptosomes, Ceni et al. (2006) also showed that despite the observation that these CD38-independent ARCs were incapable of cyclising NGD to cGDPR, NGD was able to inhibit these cADPR-forming enzymes.

iv) Heart tissue

There are at least three reports which mentioned the existence of non-CD38 ARCs

in the heart. Using differential centrifugation to separate dog and rat cardiac muscles into different fractions, Mészáros et al. (1997) reported that the plasma membrane (sarcolemmal)-bound ARC was sensitive to DTT and could be labelled by anti-CD38 antibodies, therefore showing high resemblance to a CD38 enzyme. On the other hand, the SR-associated ARC activity was not inhibited by DTT and was not recognised by these CD38 antibodies. In addition, this SR-associated enzyme was inhibited by endogenous protein kinase C (PKC)-dependent phosphorylation. From a rat SR-membrane enriched preparation, Xie et al. (2005) partially purified the cardiac ARC, which has a molecular mass of approximately 42 kDa. They showed that this rat cardiac ARC had no cross-reactivity with CD38 antibodies and was inhibited by Cu^{2+} but not DTT. They have also reported that this enzyme showed no sign of similarity with the sequence of CD38 using matrix-assisted laser desorption/ionisation time-of-flight (MALDI-TOF) analyses. Kannt et al. (2012) later discovered two small-molecule inhibitors, SAN4825 and SAN2589 that completely abolished the enzymatic activity of the cardiac ARCs from rat and pig SR membrane preparation. In contrast to the complete inhibition of cardiac ARC activities, both SAN4825 and SAN2589, even though at higher concentration, only partially inhibited the ARC activities of purified human CD38 or *Aplysia* cyclase from transfected Spodoptera frugiperda cell line SF9. In consistent with Xie's study, Kannt's partially purified cardiac ARC showed a molecular mass of approximately 35 kDa and was inhibited by Zn^{2+} (Xie et al., 2005; Kannt et al., 2012).

V) Other tissue

The discovery of non-CD38 ARCs was also reported in the membrane fractions of both rat vascular smooth muscles and bovine retinal rod outer segments, based on the difference in effect of Zn^{2+} and Cu^{2+} on these enzymes and CD38 (De Toledo

et al., 2000; Fabiano et al., 2011). In addition, anti-CD38 antibodies were shown to potentiate the cyclisation rate of CD38-expressed HL-60 cells, but did not affect those from the membrane fraction of vascular smooth muscle. 10 μmol L^{-1} of gangliosides GT1b was also able to inhibit the ARC activity in rat vascular smooth muscles, in contrast to those from the CD38-expressing HL-60 cells for gangliosides inhibition of CD38 (De Toledo et al. 2000, see also Hara-Yokoyama et al. 1996, 2001 for the inhibition of CD38 by gangliosides). However, in de Toledo's experiments, despite the difference in pharmacological and Zn^{2+} and Cu^{2+}-related biochemical properties of their enzyme of interest and CD38, they showed that their enzymes were labelled by an antibody targeting rat CD38 (De Toledo et al., 2000). Furthermore, in contrast to CD38 as a membrane protein, a soluble ARC has also been reported in T-lymphocytes (Guse et al., 1999).

One of the limitations of most of these studies was the lack of evidence from a CD38 knock-out (KO) model. In order to demonstrate the existence of non-CD38 ARCs, it is important to show a detectable ARC activity in the tissue of interest from a CD38 KO model. A difference in biochemical properties, in the author's opinion, is not sufficient to validate the existence of a non-CD38 ARC. In addition, it is unknown whether divalent ions such as Zn^{2+} and Cu^{2+} have a direct effect on either CD38, CD157 or the non-CD38 ARCs. Given that researchers often compared their newly discovered ARCs from an animal model to human CD38 from a cell line from a different source, it is possible that the difference in Zn^{2+} and Cu^{2+} arises from the difference in environments or species. Perhaps, experiments involving both CD38 and the non-CD38 ARC are purified from the same source can provide more convincing evidence. One puzzling thought is that despite these studies being consistent regarding the Zn^{2+} inhibition of their non-CD38 ARCs, there is no evidence that they were indeed studying a similar group of enzymes. Some of the pharmacological properties of these enzymes were

distinctive among themselves in addition to CD38. For example, the kidney specific ARC could be inhibited by DHAB, but DHAB could not inhibit the brain or heart-specific ARCs (Nam et al., 2006). In addition, contradictory observations have also been reported showing inhibition of ARC activity by DHAB in cardiac SR-enriched preparation and cardiac myocytes (Kannt et al., 2012; Gul et al., 2008).

1.2.10 Relationships between CD38 and endogenous concentrations of NAADP and cADPR

Studies using KO models have established that CD38 is responsible for the synthesis of cADPR *in vivo* and *in vitro*, because most tissue (apart from the brain, see Ceni et al. 2003b, 2006) in the CD38 KO mice had a significant and substantial decrease in the endogenous level of cADPR. (Partida-Sánchez et al., 2001). It was also shown that CD38 contributed to the increased level of cADPR resulted from activation of receptors by glucose, acetylcholine and isoprenaline. (Kato et al., 1999; Fukushi et al., 2001; Gul et al., 2016).

The role of CD38 in catalysing NAADP through the base-exchange reaction has been observed *in vitro* experiments. To date, the base-exchange reaction is the only viable method to generate NAADP *in vitro* and it has been shown in many tissues that this *in vitro* reaction requires functional CD38 to be present. However, the questions of whether CD38 is responsible for the endogenous production of NAADP remains controversial (Chini and Dousa, 1995; Partida-Sánchez et al., 2001; Soares et al., 2007). It has been shown in some tissues including the heart that the levels of NAADP were comparable between wild type (WT) and *CD38*$^{-/-}$ animals at basal levels and upon stimulations of histamine and β-adrenergic receptors (Soares et al., 2007; Gul

et al., 2016). In contrast, in pancreatic acinar cells, the cholecystokinin-induced increase in the level of NAADP was abolished in the *CD38*$^{-/-}$ animals, showing that CD38 is required for endogenous NAADP generation (Cosker et al., 2010). Similar observations were made in hepatic stellate cells and lymphokine-activated killer cells from *CD38*$^{-/-}$ mice that were incapable of elevating the levels of NAADP in response to angiotensin and interleukin-8 (Kim et al., 2010; Rah et al., 2010). Perhaps, the discrepancy is due to the difficulty in measuring the minute amount of endogenous NAADP using current methodologies (Graeff and Lee, 2002; Lewis et al., 2007). When present in high concentration, the existence of endogenous molecules (such as NADP) that share structural resemblance with NAADP could also potentially interfere with the measurement of NAADP (Lewis et al., 2007).

Even though it remains to be explored whether CD38 plays a role in the degradation of cADPR and NAADP in the physiological environment, the CD38 capability of hydrolysing both cADPR and NAADP has been demonstrated *in vitro* and should not be overlooked (Takasawa et al., 1993; Aarhus et al., 1995; Graeff et al., 2006; Schmid et al., 2011). It was suggested that a single enzyme that catalysed both the synthesis and degradation of these Ca^{2+} messengers would be advantageous, because this would facilitate subsequent removal of the Ca^{2+} messengers once their signalling purposes were accomplished, preventing the excessive accumulation of these Ca^{2+}-mobilising molecules. However, how such an enzyme regulates its multiple complex functions in terms of the qualitative, quantitative and temporal aspects remains to be addressed.

1.2.11 Enzymatic role of CD38/ADP-ribosyl cyclase in physiology and pathophysiology of the heart

1.2.11.1 Physiological roles of enzymatic products of CD38 in the heart

cADPR and NAADP are the most potent endogenous Ca^{2+}-mobilising agents that are catalysed by CD38 (see review by Lee 2001). Both cADPR and NAADP were first discovered as Ca^{2+}-mobilising molecules in sea urchin egg homogenates (Clapper et al., 1987). The Ca^{2+}-mobilising mechanism of cADPR in the sea urchin egg homogenates showed a property of homologous desensitisation and is inhibited by ryanodine, ruthenium red and caffeine, but is not affected by prior additions of IP_3 or NAADP (Galione et al., 1991; Lee and Aarhus, 1995). Conversely, cADPR desensitises the homogenates to caffeine and ryanodine (Galione et al., 1991).

In cardiac tissue, it was suggested that the cADPR mechanism is mainly associated with the SR Ca^{2+} release. Addition of cADPR to SR vesicles was shown to elicit Ca^{2+} efflux (Meszaros et al., 1993; Lahouratate et al., 1997; Kumasaka et al., 1999; Bak et al., 2001). As to whether this cADPR-mediated SR Ca^{2+} release is associated with RyRs remains controversial. Evidence from single channel studies (where RyRs were incorporated into artificial lipid bilayers) shows that the addition of cADPR to a chamber corresponding to the cytosolic compartment of the cell increased the open probability of RYRs. However, subsequent studies reported contradictory observations demonstrating the lack of an effect of cADPR on similar single channel experiments (Fruen et al., 1994; Copello et al., 2001). On the other hand, Sitsapesan et al. (1994) demonstrated that cADPR enhanced the probability of RyR opening in the absence of ATP, but decreased the probability of RyR opening in the presence of ATP. In studies involving islet microsomes, cADPR was

also shown to bind to FK12.6 binding proteins that normally bind to RyRs (Noguchi et al., 1997), however, the role of these FK506 binding proteins in modulating RyRs remains controversial (see the review by Venturi et al. 2012).

The first evidence that cADPR modulates EC coupling in intact cardiomyocytes was provided by the observations made in the Terrar's laboratory. It was found that the intracellular application of 8-amino-cADPR, a cADPR inhibitor, reduced the amplitudes of Ca^{2+} transients and contractions, in electrically paced guinea-pig ventricular myocytes (Rakovic et al., 1996; Iino et al., 1997). The intracellular application of cADPR through photorelease of caged-cADPR also increased the magnitudes of Ca^{2+} transients and the frequency of Ca^{2+} sparks in these cells (Cui et al., 1999; Macgregor et al., 2007b). While the intracellular application of cADPR for 10 min enhanced the SR Ca^{2+} load, the effects of the acute application of 8-amino-cADPR and the acute intracellular application of cADPR (less than 3 minutes) occurred without changes in L-type Ca^{2+} currents and SR Ca^{2+} loads. These effects were also prevented by the prior application of ryanodine and thapsigargin. Similar findings were reported by other researchers, showing the positive inotropic effects of the intracellular application of cADPR (increasing Ca^{2+} transients and the frequency of Ca^{2+} sparks) were inhibited by ryanodine, thapsigargin or 8-amino-cADPR (Lukyanenko and Gyorke, 1999; Prakash et al., 2000; Lukyanenko et al., 2001; Zhang et al., 2009b). The application of isoprenaline was also found to increase the level of cADPR in guinea pig and mouse hearts (Lewis et al., 2012; Gul et al., 2016). This elevated level of cADPR could play a role in the β-adrenoceptor-mediated arrhythmogenesis, as shown in single cell experiments (Rakovic et al., 1999). Rakovic et al. (1999) have demonstrated that cytosolic injections of inhibitors of cADPR (8-amino-cADPR or 8-bromo-cADPR) could inhibit β-adrenoceptor-mediated arrhythmogenic events such as spontaneous

oscillations, intracellular Ca^{2+} waves, spontaneous action potentials and after-depolarisations. Similar anti-arrhythmogenic effects of cADPR inhibitors were also demonstrated in Rakovic's experiments where ouabain was used to trigger arrhythmias instead of isoprenaline (Rakovic et al., 1999). All together, the observations from these experiments highlight the role of cADPR in mediating the EC coupling of the heart and in contributing to the development of arrhythmias (probably when it is present in excess).

The Ca^{2+}-mobilising properties and physiological relevance of NAADP will be discussed in detail in section 1.3 on page 35.

1.2.11.2 Gender and temperature dependent effect of CD38 KO on cardiac tissue

Takahashi et al. (2003) reported a gender-dependent effect of CD38 KO on mice hearts. While hearts from both male and female mice had an 85% reduction in their endogenous levels of cADPR, they claimed that male but not female *CD38*$^{-/-}$ mice (of unknown age) developed cardiac hypertrophy. This cardiac hypertrophy developed in the absence of any pharmacological or physiological stressor and was independent of alterations in systolic blood pressure and heart rate. In addition, the expression level of ventricular SERCA2 protein and the ratio of expression level of ventricular SERCA2 to PLB proteins were significantly increased in *CD38*$^{-/-}$ mice of both genders, while the protein level of ventricular RyR2 was only significantly higher in female *CD38*$^{-/-}$ mice.

Besides, they revealed a temperature-dependent observation of cardiac parameters between papillary muscles from *CD38*$^{-/-}$ and WT mice. They also

showed that none of the parameters for Ca^{2+} transients and contraction forces of isolated papillary muscles were significantly different between *CD38*$^{-/-}$ and WT mice at 37 °C. In contrast to the observations at 37 °C, papillary muscles isolated from *CD38*$^{-/-}$ mice had significantly higher peak Ca^{2+} transients and significant accelerations in the Ca^{2+} decay and muscle relaxation at 27 °C,. Given that cADPR has been shown to be a potent positive inotropic agent at 37 °C (Iino et al., 1997), they suggested that *CD38*$^{-/-}$ hearts might have a compensatory mechanism for Ca^{2+} handling and force development despite having an impaired cADPR signalling system. The existence of these compensatory mechanisms in *CD38*$^{-/-}$ hearts might provide an explanation for the temperature-dependent difference between WT and *CD38*$^{-/-}$ mice — at the lower temperature, cADPR was unable to enhance Ca^{2+} release from the SR of WT while the presumably temperature-independent compensatory mechanism of *CD38*$^{-/-}$ gave rise to the apparently greater amplitude of Ca^{2+} transient and faster muscle relaxation.

Gan et al. (2011) also detected a significant enhancement in the myocardial contractility, contraction, and relaxation velocities in male but not female *CD38*$^{-/-}$ mice. Although this observation is consistent with the hypothesis of a gender-dependent effect of CD38 KO, the authors detected this difference in cardiac parameters at 37 °C. Like Takahashi's study (Takahashi et al., 2003), they also provided evidence of an increase in levels of mRNAs that are responsible for the expressions of RyR2, SERCA2 and Na^{+}/Ca^{2+}-exchanger protein 1 (NCX1), and α-myosin heavy chain. Supported by the observations that i) *CD38*$^{-/-}$ male mice had a marked decrease in the level of mRNA for androgen receptor expression, ii) *CD38*$^{-/-}$ male mice had an increase in the level of testosterone, iii) and that the differences in cardiac parameters and mRNA levels in *CD38*$^{-/-}$ mice could be reversed by flutamide, an antagonist for androgen receptors, the researchers

hypothesised that this gender-dependent effect of CD38 KO is mediated by the enhanced level of testosterone.

1.2.11.3 Hormonal regulation of CD38/ADP-ribosyl cyclase

i) Angiotensin receptor

Higashida et al. (2000) provided evidence that the activation of angiotensin receptors could be the upstream mechanism of cADPR formation in neonatal rat myocytes. The administration of angiotensin II (Ang-II) administration enhanced the cardiac ARC activity in membrane preparations from rat neonatal myocytes and this enhancement could be abolished by incubation of Cholera toxin A and B subunits. Treatment with guanosine-5'-triphosphate (GTP) was also shown to affect the ARC activity of the cardiac membrane preparations in a bell shaped dose-response manner, which peaked around 10 nM (Higashida et al., 2000). Gul et al. (2008) further showed that the stimulation of ARC upon activation of Ang-II receptors requires a functional IP_3 signalling pathway involving tyrosine-protein kinase Src, phosphatidylinositol-4,5-bisphosphate 3-kinase (PI3 kinase) and phospholipase C (PLC). Based on their observations using pharmacological agents, the authors suggested that Ang-II activates Ang-II type 1 receptors that subsequently activate Src and PI 3-kinase, resulting in the phosphorylation of Akt (in the Akt and PLC-γ1 complex) and an enhanced production of IP_3. It remains unknown how the IP_3-regulated Ca^{2+} release leads to an enhanced enzymatic activity of ARC since the physiological range of Ca^{2+} has no effect on CD38 and a higher concentration of Ca^{2+} has an inhibitory rather than stimulatory effect on CD38 (Liu et al., 2008).

ii) P2Y11 purinergic receptor

In rat ventricular cardiomyocytes, Djerada and Millart (2013) and Djerada et al. (2013) demonstrated that the activation of P2Y11 purinergic receptors by extracellular NAADP or NF 564 (specific P2Y11 agonist) leads to an increase in the cytosolic levels of cADPR and NAADP, while this accumulation of intracellular cADPR and NAADP was reduced by more than 50 % in the condition where P2Y11 antagonist NF157 was present. Although whether NAADP is a real agonist for P2Y11 purinergic receptors remains debatable, this evidence suggests that the activation of P2Y11 purinergic receptors can lead to an enhanced enzymatic activity of CD38/ARCs.

iii) β-adrenoceptor

Using membrane preparations from ventricular myocytes of rats aged from 0 to 4 weeks, Higashida et al. (1999) also showed that the application of isoprenaline increased the rate of ARC activity in these membrane preparations, suggesting a role of the β-adrenoceptor in enhancing ARC activity in the heart. This effect was abolished in the presence of propranolol.

Rakovic and Terrar (2002) have reported that the catalytic subunit of PKA was able to increase the ARC activity observed in SR-enriched membrane preparations from guinea pig hearts. Consistent with this finding, Xie et al. (2005) showed that the incubation of ventricular homogenates from rat hearts with isoprenaline (2 μM), forskolin or cAMP resulted in an enhanced cyclisation reaction of the cardiac ARC. This enhancement was abolished by the pretreatment with H89, a PKA inhibitor. Xie et al. (2005) further showed that intracellular application of the purified cardiac ARC into resting rat cardiomyocytes resulted an increased intracellular Ca^{2+}, in a dose-dependent manner. This effect was blocked by 8-Br-cADPR, a cADPR antagonist. In addition, they showed that the cAMP-induced increase in the intracellular Ca^{2+}

concentration of resting cardiomyocytes was also inhibited by 8-Br-cADPR and H89. These findings suggest that the enhancement of cardiac ARC activity could be a downstream effect of β-adrenoceptor activation via cAMP/PKA signalling, leading to an increase in the level of cADPR and subsequently an increase in the level of intracellular Ca^{2+}.

In Langendorff whole heart experiments, it was shown that the levels of NAADP and cADPR were elevated upon the application of isoprenaline (Macgregor et al., 2007b; Lewis et al., 2012). Lewis et al. (2012) pointed out that the increase in the level of NAADP peaked transiently at the first minute followed by a slower rise while the the level of cADPR increase gradually over 5 min. More recently, Gul et al. (2016) have reported corroborating observations, showing isoprenaline increased the levels of cADPR and NAADP in cardiac ventricular myocytes from mouse hearts . This increase was prevented by the preincubation of PKA and cAMP antagonist. They also showed that the level of cADPR (but not NAADP) in cardiac myocytes from *CD38*$^{-/-}$ was not elevated upon β-adrenoceptor activation, providing evidence that CD38 is indeed a direct or indirect downstream target of the β-adrenoceptor pathway (Gul et al., 2016).

1.2.11.4 Cardiac development and CD38

The role of CD38 in the cardiomyogenesis of mouse embryonic stem (ES) cells has been recently investigated (Wei et al., 2012). It was reported that the overexpression of CD38 in mouse ES cells significantly inhibited the differentiation of cardiomyocytes. This claim was supported by observations showing beating cells appeared earlier and were more abundant in CD38 knockdown colony. This finding was further supported by real-time reverse transcription polymerase chain reaction

(RT-PCR) and Western blot analyses, revealing that the upregulation of the expression of several cardiac markers, including transcription factor GATA-4, myocyte enhancer factor 2C (MEF2C), cardiac homeobox protein NKX2.5, and α-myosin light chain in CD38 knockdown group. There were also more cardiac troponin T-positive cardiomyocytes in CD38 knockdown or 8-Br-cADPR-treated groups. Wei et al. (2012) also showed that the CD38/cADPR signalling pathway negatively modulated the fibroblast growth factor 4 (FGF4)/extracellular signal-regulated kinase (Erk)1/2 cascade, which is important for the cardiomyocyte differentiation of ES cells. Since the link between reactive oxygen species (ROS) and CD38/cADPR/Ca^{2+} signalling has been established (see section 1.2.11.5), the researchers hypothesised that CD38 could alter the redox state of the cell which could in turn affect the binding ability of certain proteins on the FGF4 gene. This could lead to the inhibition of FGF4 transcription and subsequently preventing Erks 1/2 activation during the differentiation stage of mouse ES cells.

1.2.11.5 CD38, ROS and ischemic/reperfusion injury

Xie et al. (2003) showed that homogenates from hearts that were subjected to ischemia/reperfusion (IR) injury had a 2-fold increase in their ARC activity and a 4-fold increase in their cADPR contents, compared with the control group. Further investigation revealed that ARC activities from the sarcolemmal and mitochondrial fractions but not the cytosolic fraction of hearts with IR injury were significantly increased. They also showed that the exposure to t-butyl hydroperoxide, an oxidant, to rat cardiomyocytes could mimic the effect of IR injury on ARC activity and cADPR content, consistent with the well established observation that the elevated level of ROS contributed significantly to IR injury (see the review by Kalogeris et al. 2014).

They also demonstrated that the increased cADPR level and increased ARC activity of homogenates from hearts with IR injury could be abolished by administrations of ROS scavengers, 2,2,6,6-tetramethyl-1-piperidinyloxy (TEMPO) and mannitol. This study proposed that ARCs could play a role during cardiac IR injury and contribute to the elevated intracellular Ca^{2+} through the overproduction of cADPR (Xie et al., 2003).

Reyes et al. (2015) also reported the increased in ARC activity during IR injury of the mouse hearts by showing a decrease in the level of NADP(H) (a substrate of CD38) and increase in the level of ADPRP (a product of CD38). This NADPH depletion could be prevented by the pharmacological inhibition of CD38, genetic knockdown of CD38, or by the pretreatment of a superoxide dismutase mimetic, Mn(III) tetrakis(4-benzoic acid)porphyrin chloride (MnTBAP), providing evidence for the activation of CD38 by ROS during IR injury. In addition, they revealed that the pharmacological inhibition of CD38 with α-NAD or NADPH supplementation enhanced the recovery of contractile functions and decreased the infarction in post-ischemic hearts, suggesting a role of CD38 and its marked activation of the NAD(P)ase activity during IR injury. Although the main focus of the paper emphasised the importance of NADP(H) as the source of reducing equivalents in the endothelial nitric oxide (NO) signalling pathway, the cardiac NO signalling pathway has important roles in cardiac tissue too (see the review by Massion et al. 2003). This indicates there could an unaddressed role for CD38 in the cardiac NO signalling pathway.

The CD38/cADPR pathway was also shown to be involved in Ang-II-induced cardiac hypertrophy (Gul et al., 2008). In rat cardiomyocytes, Ang-II activated the NAD(P)H oxidase through the IP3/PKC pathway to initiate the generation of ROS. The ROS subsequently stimulated cardiac ARC to synthesise cADPR (Gul et al.,

2008). The cADPR/CD38 pathway could sustain ROS production through the further activation of the NAD(P)H oxidase complex via Rac1, ultimately leading to cardiac hypertrophy (Gul et al., 2012). This could imply the existence of a positive feedback mechanism between CD38 and ROS. In addition, since CD38 can deplete NAD, which is the product of NAD(P)H oxidase, activation of CD38 could also lead to the formation of ROS by shifting the equilibrium of the NAD(P)H oxidase reaction (Xu et al., 2013).

As to how ROS activates CD38, some have proposed that the mechanism involves oxidative modifications of CD38, particularly its disulphide bridge which has been shown to be pivotal for its catalytic activity (see section 1.2.7.2 on page 12). Besides that, in mouse coronary arterial myocytes, it was reported that a redox activation of CD38 could result in the internalisation of membrane-associated CD38, providing the greater access to its intracellular substrates (NADP and NAD) and generating a greater yield of products (Xu et al., 2013).

1.2.11.6 Hypertrophy and CD38

Using a rat angiotensin-dependent model of hypertension, 2K1C (two-kidney one-clip), a positive correlation of Ang-II activation and ARC activity in cardiac myocytes has been reported (Higashida et al., 2000; Gul et al., 2008). It was further shown that this 2K1C model developed cardiac hypertrophy which could be prevented by the administration of a small molecule inhibitor, DHAB, that inhibits ARC activity. In contrast to Takeshi's and Gan's studies that showed CD38 KO has a positive or no effect on cardiac hypertrophy development respectively (Takahashi et al., 2003; Gan et al., 2011), Gul's study suggested that the inhibition of ARC activity can be protective against angiotensin-II induced hypertrophy. They have also provided

evidence from experiments involving histology and molecular biology, showing the upregulation of pro-hypertrophic molecules in their models.

In 2016, Gul et al. (2016) further investigated the role of CD38 in cardiac myocytes. Beside mediating the Ang-II-induced hypertrophy, they showed that CD38 also has a role in the β-adrenoceptor-induced hypertrophy. The chronic treatment of isoprenaline in whole animals has lead to an increase in cell sizes, heart weight/body weight ratios and cardiac fibrosis in WT but not *CD38*$^{-/-}$ mice. The elevated levels of hypertrophic and fibrosis markers (fibronectin and transforming growth factor (TGF)-β1) were also observed in the WT but not *CD38*$^{-/-}$ mice. They proposed that *CD38*$^{-/-}$ mice were more resistant to the β-adrenoceptor-induced hypertrophy and that these mice retained a better cardiac function compared to WT hearts when exposed to chronic isoprenaline infusion. Capel et al. (2015) also reported that *TPC2*$^{-/-}$ mice, which are insensitive to NAADP (one of the products catalysed by CD38), were resistant to β-adrenoceptor-induced hypertrophy.

1.2.11.7 Arrhythmias and CD38

Kannt et al. (2012) have shown that the papillary muscle isolated from guinea pigs were less prone to arrhythmias when they were treated with cardiac specific ARC inhibitors SAN4825 or SAN2589, as shown in their significantly reduced number of spontaneous action potentials following high frequency electrical pacing. Similarly, an intravenous administration of 3 mg kg^{-1} of SAN4825 was capable of delaying the occurrence of Ca^{2+} overload-induced ventricular fibrillation and cardiac arrest in whole guinea pigs infused with ouabain. Consistent with Kannt's study, Warszta et al. (2014) reported that SAN4825 at micromolar level was capable of preventing

the β-adrenoceptor-induced spontaneous Ca^{2+} transients in electrically paced murine cardiac myocytes. All together, these observations highlight a role of CD38/ARC in the arrhythmogenicity of hearts.

As discussed above, the cardiac β-adrenoceptor stimulation was also shown to be accompanied by an increased production of cGDPR, cADPR and NAADP in cardiac tissue (see section 1.2.11.3 on page 27). With evidence from experiments involving KO animals and pharmacological inhibition of relevant pathways, the Ca^{2+}-mobilising molecules, NAADP and cADPR, were also reported to be pro-arrhythmogenic (Rakovic et al., 1999; Nebel et al., 2013; Capel et al., 2015). Rakovic et al. (1999) showed that the intracellular application cADPR inhibitors, 8-Br-cADPR or 8-amino-cADPR, reduced the propensity of guinea pig ventricular cardiac myocyte towards arrhythmias, which were induced by the activation of β-adrenoceptors or by ouabain-mediated Ca^{2+} overload. Capel et al. (2015) also reported that $TPC2^{-/-}$ mice, which are insensitive to NAADP, were resistant to both acute and chronic β-adrenoceptor-induced arrhythmias. Consistent with Capel's study, Nebel et al. (2013) also provided pharmacological evidence, showing that the administration of BZ194, an inhibitor of NAADP effect on RyRs Dammermann et al. (2009), was capable of reducing the occurrence of isoprenaline induced-spontaneous diastolic Ca^{2+} transients and arrhythmias in single mouse cardiac myocytes and awake mice respectively.

Therefore, it is likely that the CD38/ARC pathways contribute to the development of cardiac arrhythmias, partially if not entirely through producing an excess amount of Ca^{2+}-mobilising agents, causing Ca^{2+} mishandling in the short term. In the long run, other complications due to the sustained or heightened CD38/ARC activity such as hypertrophy, might also contribute to the development of arrhythmias.

1.3 NAADP as an endogenous Ca^{2+}-mobilising agent

1.3.1 Ca^{2+} release properties of NAADP in sea urchin egg homogenates

In sea urchin egg homogenates, the application NAADP caused Ca^{2+} release (half-maximal effect at 30 nM), but this Ca^{2+} release was insensitive to pretreatment of antagonists of IP_3 and cADPR such as heparin and 8-amino-cADPR respectively, as well as inhibitors of SERCA such as thapsigargin or cyclopiazonic acid (CPA) (Lee and Aarhus, 1995; Genazzani et al., 1996). Given SERCA inhibitors are capable of inhibiting IP_3 and cADPR-mediated Ca^{2+} release in sea urchin egg homogenates, the NAADP-mediated Ca^{2+} release is therefore distinct from those of IP_3 and cADPR, and is released from a different source other than ER Ca^{2+} stores. Furthermore, in sea urchin egg homogenates, NAADP-induced Ca^{2+} release is less pH-sensitive compared with Ca^{2+} release mediated by IP_3 or cADPR. Changing the pH of the experimental media, from 7.2 to 6.7, NAADP mediated Ca^{2+} release was only slightly affected, whilst IP_3- and cADPR-mediated Ca^{2+} release were almost abolished in the acidic environment (Genazzani et al., 1997).

It is worth mentioning that though in the broken cell preparation, NAADP-mediated Ca^{2+} release is independent of other Ca^{2+}-mobilising pathways, in intact cells, the interactions between Ca^{2+}-mobilising messengers are more dynamic. In the presence of functionally active IP_3Rs, RyRs and ER stores, NAADP was shown to trigger a series of Ca^{2+} oscillations across the cell (Aarhus et al., 1996; Churchill and Galione, 2001). In the case where IP_3R, RyR, or SERCA antagonists were present, the observed NAADP-triggered Ca^{2+} release was non-regenerative but

rather a propagation across the cell from the region where NAADP was applied. Pharmacological agents including L-type voltage-gated Ca^{2+} and K^{+} channel antagonists (Genazzani et al., 1997), the nonselective P2 purinergic antagonist pyridoxal phosphate-6-azo(benzene-2,4-disulphonic acid) tetrasodium salt (PPADS, Billington and Genazzani 2007), and the novel NAADP antagonists, BZ194 (inhibiting NAADP action on RyRs) (Dammermann et al., 2009) and Ned-19 (Naylor et al., 2009), were shown to inhibit NAADP-mediated Ca^{2+} release.

In sea urchin egg and its homogenates, subthreshold amounts (100 pM to 2 nM) of NAADP that could not elicit a detectable Ca^{2+} release, could fully and irreversibly inactivate the NAADP-sensitive Ca^{2+} release mechanism in a concentration and time-dependent manner (Genazzani et al., 1996; Aarhus et al., 1996). Without depleting the NAADP-sensitive Ca^{2+} stores, this preceding subthreshold amount of NAADP was able to abolish the Ca^{2+} release ability of subsequent additions of NAADP (Genazzani et al., 1996; Aarhus et al., 1996). This inactivation mechanism was independent of the concentration of subsequent NAADP addition and independent of small pH changes. While Genazzani et al. (1996) suggested that this inactivation mechanism was independent of enzymatic activity as this mechanism remained intact in the presence of general kinase inhibitor staurosporine (10 μM) or at 4 °C, the molecular basis of this intriguing desensitisation property of NAADP-regulated Ca^{2+} release remains unknown. Since it was shown that Ned-19.4 which is an analogue of NAADP, could selectively block NAADP-induced desensitisation without affecting NAADP-evoked Ca^{2+} release (Rosen et al., 2009), the hypothesis that the inactivation mechanism involved a different NAADP binding site on NAADP-targeted proteins was put forward.

1.3.2 Endolysosomes as an acidic store of Ca^{2+}

As mentioned in the previous section, NAADP releases Ca^{2+} from a store, which was not affected by SERCA, IP_3, and cADPR inhibitors. Evidence from sea urchin egg stratification studies also supports that NAADP mobilises Ca^{2+} from ER-distinct organelles. These experiments showed that upon the egg centrifugation, various organelles became localised in opposite poles of the sea urchin egg and that while IP_3 and cADPR mobilised Ca^{2+} from one pole that contained ER, NAADP-regulated Ca^{2+} release originated from the opposite pole of the cell (Lee and Aarhus, 2000). Further pharmacological and biochemical studies revealed that these NAADP-targeted organelles in sea urchin eggs were reserve granules, which are functionally equivalent to lysosomes (Churchill et al., 2002). In mammalian pancreatic acinar and β cells, NAADP-regulated Ca^{2+} release was also demonstrated to be originated from lysosome-related organelles (Yamasaki et al., 2004).

Lysosomes were discovered by Christian de Duve in the 1950s (Bainton, 1981). They are membrane-enclosed organelles that contain acid hydrolases. Lysosomes were also shown to have proton-pumping vacuolar ATPases, which maintain the luminal environment at a pH of 4.6 – 5.0 (Mellman et al., 1986). Lysosomes play a role in receiving and degrading macromolecules from the secretory, endocytic, autophagic and phagocytic membrane-trafficking pathways (Luzio et al., 2007). The luminal Ca^{2+} concentration of lysosomes was estimated to be 0.4 – 0.6 μM and was proposed to be regulated by its luminal pH (Christensen et al., 2002; Lloyd-Evans et al., 2008).

In sea urchin eggs, NAADP-regulated Ca^{2+} release was shown to be dependent on a proton gradient maintained by an ATP-dependent vacuolar-type proton pump (Churchill et al., 2002). It was proposed that the Ca^{2+} uptake mechanism of a

lysosome or reserve granule is driven by this proton gradient through Ca^{2+}/H^{+} exchangers. This is further supported by the observations that lysosomal Ca^{2+} uptake in sea urchin eggs is abolished in the presence of a protonophore, nigericin, and a vacuolar-type H^{+}-ATPase inhibitor, bafilomycin-A1. Consistent with the above findings, the alkalinisation of lysosomes upon NAADP application was also observed in both sea urchin eggs and mammalian cells (Morgan and Galione, 2007; Collins et al., 2011).

This model of Ca^{2+} reuptake model was recently challenged by Garrity et al. (2016). By measuring the lysosomal Ca^{2+} content through the Ca^{2+} release evoked by a cell permeant mucolipin transient receptor potential channel 1 (MTRP1) agonist, they showed that although the pH of lysosomes was elevated, the lysosomal Ca^{2+} content was not affected by treatment of bafilomycin-A1 (5 μM). Instead, they proposed that the lysosomal Ca^{2+} content and the Ca^{2+} refilling process relied on a functional ER Ca^{2+} store. However, the authors did not address whether there was a change in the rate of lysosomal Ca^{2+} refilling process in the presence of bafilomycin-A1. The effect of bafilomycin-A1 on MTRP1-regulated Ca^{2+} release could be masked by an alternative Ca^{2+} refilling mechanism, which compensate for the loss of pH-gradient driven Ca^{2+} reuptake. The store might be refilled to a similar level, but the refilling process might require a longer time in the absence of functional proton pumps. Another major concern is that responses from a MTRP1 agonist in the presence of bafilomycin-A1 have a larger standard error of mean compared to the control, despite having a bigger sample size (figure 1H of Garrity et al. 2016). This could be an indicator of a pooled data from responsive and non-responsive cells. Perhaps, a greater n number is needed to justify these data. In addition, the second and third Ca^{2+} responses from MTRP1 agonist applications were often higher than the first response, according to the authors. However, these apparently larger second and third Ca^{2+} responses from

MTRP1 agonist applications were not observed in the presence of bafilomycin-A1, which could be interpreted as bafilomycin-A1 having an inhibitory effect on lysosomal Ca^{2+} content (figure 1H, Garrity et al. 2016). The authors also stated several p values which are lower than 0.05 in the figure legend (figure 1H, Garrity et al. 2016), and yet considered the difference of data to be insignificant without further justifications. As a matter of opinion, the author of this thesis believes that more observations are needed before the inhibitory effect of bafilomycin-A1 on lysosomal Ca^{2+} refilling process is invalidated.

1.3.3 Molecular targets of NAADP

As described in section 1.3.1 on page 35, the NAADP sensitive receptor is pharmacologically and physically distinct from RyRs and those of cADPR and IP_3. Several receptors including the transient receptor potential channels (TRP channels), the purinergic receptors and the two-pore channels (TPCs), were the main candidates being proposed as the NAADP receptors.

Zhang and Li (2007) have reported obeservations of NAADP-sensitive currents from single channel recording experiments involving the reconstitution of lysosomal membrane proteins from rat liver microsomes into lipid bilayers. With Cs^+ on both the cis and trans chambers as the charge carriers, the addition of NAADP increased the open probability of the lysosomal channels, in a bell shaped dose-dependent manner, from concentrations ranging from 1 nM to 100 μM. While the NAADP-sensitive current was not affected by high concentrations of ryanodine or an IP_3 inhibitor (2-APB) , it could be inhibited by L-type Ca^{2+} channel inhibitors (diltiazem, verapamil and nifedipine), consistent with previous observations by Genazzani et al. (1997).

Interestingly, an anti-TRP-mucolipin 1 antibody was shown to inhibit this NAADP-sensitive current too, suggesting TRP-ML1 as the NAADP-targeted receptor. This hypothesis was further supported by the study of Zhang et al. (2009a) using TRP-ML1 small interfering RNA (siRNA) to knockdown the expression of TRP-ML1 in bovine coronary artery myocytes (CAMs). They showed the application endothelin-1, which induced a local Ca^{2+} burst from lysosomes followed by a global Ca^{2+} release in CAMs was significantly attenuated in TRP-ML1 siRNA-pretreated CAMs. The opening probability of lysosomal NAADP-sensitive channels from these pretreated CAMs was also reduced by 71.5 $\pm$ 18.5%, measured in single channel recording experiments. Consistent with the hypothesis that TRP-ML1 is the NAADP targeted channel, these lysosomal NAADP-sensitive currents observed in bovine CAMs were also abolished by immunoprecipitation or blockade of anti-TRP-ML1 antibodies.

There were also studies reporting NAADP as the agonist of extracellular receptors such as the purinergic receptors (Heidemann et al., 2005; Singaravelu and Deitmer, 2006; Moreschi et al., 2008; Djerada and Millart, 2013; Djerada et al., 2013). Extracellular NAADP (100 μM) triggered a concentration-dependent increase in intracellular Ca^{2+} in 1321N1 cells transfected with human P2Y11, but not in wild-type cells (Moreschi et al., 2008). In rat astrocytes, extracellular application of 10 μM NAADP also evoked Ca^{2+} spikes and this effect was abolished by P2Y11 antagonist but surprisingly not by bafilomycin-A1 and GPN (Gly-Phe β-naphthylamide) that disrupt lysosomes (Singaravelu and Deitmer, 2006). However, in Heidemann's experiments, they showed incubation of GPN reduced the number of astrocytes which responded to the extracellular NAADP (5 μM) addition. They also further demonstrated that the effect of extracellular NAADP addition was reduced in the presence of antagonists of both non-adenosine purinergic (suramin and PPADS), and adenosine receptors (CGS-15943) (Heidemann et al.,

2005). The extracellular application of metabolites such as NADP, NAAD and NAD was also shown to trigger responses similar to those of NAADP (Heidemann et al., 2005; Moreschi et al., 2006; Mutafova-Yambolieva et al., 2007). This raises a question of whether the response mediated by high concentrations of extracellular NAADP was a direct effect on extracellular receptors or an indirect effect through its metabolic products. Nevertheless, a direct effect of NAADP at micromolar range is unlikely to be physiological due to its endogenous availability.

The role of TPCs as NAADP receptors will be discussed in detail in the next section.

1.3.4 TPCs are essential for the NAADP-regulated Ca^{2+} release

TPC1 was first cloned from rat kidneys (Ishibashi et al., 2000). The protein encodes 819 amino acids and comprises two domains, each with six transmembrane segments (S1-S6) with two conserved positively charged voltage sensor segments (S4), similar to those found in voltage-gated Ca^{2+} and Na^{+} channels. TPC1 mRNA expression was found in several other tissues including rat liver, lung and spleen (Ishibashi et al., 2000). Recently, the crystal structure of plant TPC1 from *Arabidopsis thaliana* has also been discovered. TPCs have three isoforms (TPC1, TPC2 and TPC3) and they are all present in sea urchins and most of the vertebrate species (Calcraft et al., 2009; Zhu et al., 2010). However, TPC3 is absent in mice, rats, and primates (including humans), while being present in most other mammals (such as guinea pigs).

Several studies in 2009 have established the pivotal link between TPCs and NAADP-mediated Ca^{2+} release (Brailoiu et al., 2009; Calcraft et al., 2009). Northern blot analysis was carried out and demonstrated that mRNA responsible for TPC1 and TPC2 expressions could be detected in various human tissues including liver, kidney, brain, pancreas and heart (Zong et al., 2009; Calcraft et al., 2009). The expression of TPC2 proteins on acidic lysosomes has been identified using immunocytochemistry studies. Immunofluorescence labelling using an anti-hTPC2 antibody revealed staining with a punctate pattern that colocalised with the staining of lysosome-membrane associated protein 2 (LAMP-2) in the cytoplasm in HEK293 cells (Calcraft et al., 2009). In hemagglutinin (HA)-tagged hTPC2 expressed cell lines (hTPC2 cells), the HA-tagged protein overlapped with LAMP-2 and LAMP-1 but not with markers for early and late endosomes or those for ER, Golgi, or mitochondria (Zong et al., 2009; Calcraft et al., 2009). On the other hand, TPC1 and TPC3 proteins were found to be expressed in late endosomes and other unidentified cellular compartments, showing little overlapping with TPC2 proteins.

In hTPC2 cells, the photorelease of caged NAADP elicited a biphasic Ca^{2+} response, beginning with a slow rise (10 – 180 s) of Ca^{2+} concentration followed by a larger Ca^{2+} transient, while in WT cells with no TPC2 expressions, only small and short-lived Ca^{2+} release events were observed, lacking both the ramp-like phase and secondary transient. Both phases were suppressed by bafilomycin-A1, while the second Ca^{2+} transient phase was sensitive to heparin and thapsigargin, suggesting that the initial ramp phase occurred as a result of NAADP-mediated Ca^{2+} release from lysosomes and the second Ca^{2+} transient was dependent on IP3 receptors and ER Ca^{2+} stores, which were presumably activated by the lysosomal NAADP-mediated Ca^{2+} release. These observations are consistent with the two-pool

hypothesis proposed by Churchill and Galione (Churchill and Galione, 2001).

Calcraft et al. (2009) also generated a Tpcn2 KO (*Tpcn2*$^{-/-}$) mouse model using a gene trap strategy. They showed that the NAADP-mediated Ca^{2+} release from a lysosomal compartment in pancreatic β-cells and the subsequent activation of a plasma membrane Ca^{2+} sensitive inward current was successfully demonstrated in WT mice but not in *Tpcn2*$^{-/-}$ mice.

Similarly, in mouse embryonic fibroblasts (MEFs), the administration of NAADP-AM (acetoxymethyl ester derivative of NAADP), a cell-permeant analogue of NAADP, triggered robust Ca^{2+} signals which were abolished by preincubation with bafilomycin-A1, GPN, nigericin and Ned-19 (Ruas et al., 2015). Consistent with the two-pool hypothesis (Churchill and Galione, 2001), CPA, ryanodine and 2-aminoethoxydiphenyl borate (2-APB) abolished the NAADP-AM-stimulated Ca^{2+} signals. In single-KO MEFs lacking either TPC1 or TPC2, the NAADP responses were still present but significantly reduced whereas in double-KO MEFs lacking both TPC1 and TPC2, the NAADP responses were completely abolished. To confirm that the loss of NAADP responsiveness in double-KO MEFs was specifically due to the absence of TPCs, the authors showed that the re-expression of TPCs (but not TRPML-1 or mutant TPC2 channels with a reduced or negligible Ca^{2+} permeability) rescued NAADP-triggered Ca^{2+} responses.

Although the evidence is clear that NAADP-mediated Ca^{2+} release requires the expression of TPCs, there has been discussion of whether TPCs are indeed the NAADP-targeted lysosomal Ca^{2+} channels. Wang et al. (2012) performed electophysiogical experiments on vacuolin-enlarged endolysosomes and claimed that TPCs were instead Na^{+}-selective channels activated by phosphatidylinositol 3,5-bisphosphate (PI(3,5)P2), and were not activated by NAADP. The hypothesis

that TPCs are Na^{+} channels was also supported by other studies (Cang et al., 2013, 2014). Wang et al. (2012) also showed that the Ned-19 sensitive glucose-induced Ca^{2+} responses in pancreatic islets were not significantly reduced in KO models lacking both TPC1 and TPC2.

Surprisingly, despite the fact that NAADP-induced lysosomal Ca^{2+} release was observed in their pancreatic β-cell lines, the authors failed to detect any measurable NAADP-activated whole-endolysosomal current (Wang et al., 2012). Since TPC variants with more than 91 % of the native full-length sequence could still be produced in the KO model used by Wang et al. (2012), the validity of their KO models was also challenged by Galione's group (Ruas et al., 2015). The authors demonstrated that by mimicking Wang's N-terminally truncated proteins ($\geq$ 91 % of the full-length sequence), they showed that ΔN69-TPC1 or ΔN49-TPC2 proteins (with 69 or 49 deleted amino acid residues) were not only NAADP-sensitive, they were localised to endolysosomes and were capable of restoring the NAADP-sensitivity in Ruas's version of TPCs double KO model. Jha et al. (2014) used a similar approach as Wang et al. (2012). They conducted electrophysiological measurements on vacuolin-enlarged lysosomes and reported that TPC2 current was indeed regulated by NAADP, in a Mg^{2+}-sensitive manner (Jha et al., 2014). In addition, different groups have reported observations of TPCs being permeant to Ca^{2+}, or to Ca^{2+} surrogates using various experimental models, such as protein incorporation into lipid bilayers (TPC2, (Pitt et al., 2010); TPC1, (Pitt et al., 2014; Rybalchenko et al., 2012), single-organelle planar patch-clamp (Schieder et al., 2010), or TPCs targeted to the plasma membrane (Brailoiu et al., 2009; Yamaguchi et al., 2011; Jha et al., 2014).

The findings that TPCs are required for NAADP-mediated Ca^{2+} release

eventually raise the question of whether NAADP directly binds to TPCs to activate them. Even though the immunoprecipitation of sea urchin TPCs resulted in immunocomplexes with high affinity [^{32}P]-NAADP binding (Ruas et al., 2010), the overexpression of TPC2 in HEK cells only caused a 3-fold increase in the binding of NAADP, as measured using radioactive-ligand binding protocol (Calcraft et al., 2009). Moreover, using a photoaffinity labelling approach involving 5-azido-[^{32}P]-NAADP, low molecular weight proteins of 30, 40 and 45 kDa were labelled in sea urchin egg membranes, whereas cytosolic proteins of around 22 – 23 kDa were labelled in mammalian pancreas (Lin-Moshier et al., 2012; Walseth et al., 2012). These proteins were all considerably lower than the molecular weight of TPC1 and TPC2 (expected to be 94 and 85 kDa, respectively). Recent evidence also reveals that high-affinity [^{32}P]-NAADP binding still occurs in double KO tissue lacking of both TPC1 and TPC2 proteins from mouse livers (Ruas et al., 2015). All together, these data suggest that NAADP might bind to small accessory proteins rather than binding to TPCs directly. As to whether these accessory proteins have a role in regulating the NAADP-mediated Ca^{2+} release through their interactions with TPCs is yet to be addressed.

The controversies regarding the role of TPCs in NAADP signalling were summarised in a recent review by Morgan and Galione (2014). The authors outlined concerns regarding the limitations in studies with contradictory observations and the variability of the experimental setups and conditions. They concluded that there is still a considerable body of evidence supporting the link between TPCs and NAADP-mediated Ca^{2+} release and it is therefore, currently premature to discard TPCs as the NAADP-regulated Ca^{2+} channel without further investigation.

1.3.5 Roles of NAADP in the cardiac physiology

In early studies that examined enzymatic production of NAADP in cardiac tissue, Rusinko and Lee demonstrated the presence of an NAADP-synthesising enzyme in extracts from rabbit hearts (Rusinko & Lee, 1989). Chini and Dousa subsequently showed that rat cardiac tissue was capable of synthesising NAADP (Chini and Dousa, 1995). Synthesis rate of NAADP have been estimated to be 0.4 nmol min^{-1} mg^{-1} protein in mouse hearts (Chini et al., 2002) while the endogenous level of NAADP was estimated to be 0.22 nmol (Macgregor et al., 2007a) and 0.4 pmol (Lewis et al., 2012) mg^{-1} protein in guinea pig hearts.

Using a radioactive analogue of NAADP, [^{32}P]-NAADP, two binding sites of NAADP (dissociate constants (K_d) of 130 pM and 4 nM) were identified in rabbit heart microsomes by Bak et al. (2001). Despite the high NAADP binding affinities of this preparation, the EC_{50} of NAADP-triggered Ca^{2+} release in this preparation was 323 $\pm$ 14 nM. The authors suggested that similar difference has been observed in NAADP-mediated Ca^{2+} release in sea urchin egg and the difference might arise from the different kinetics of release versus binding. With a Hill slope coefficient of approximately 2 in both NAADP binding and Ca^{2+} release curve, the authors proposed a positive co-operativity binding mode for NAADP binding in the heart. Since the NAADP-mediated Ca^{2+} release from cardiac microsomes (observed upon application of 1 μM NAADP) was not affected by heparin, 8-amino-cADPR or ruthenium red, the NAADP-mediated Ca^{2+} release was suggested to be independent from cADPR-, RyR- and IP3-mediated Ca^{2+} release mechanisms.

Copello and colleagues have reported the lack of effect of NAADP on SR microsomes from canine hearts (Copello et al., 2001). Furthermore, in their single

channel recording experiments where RyRs incorporated in an artificial lipid bilayer, NAADP (from 0.1 to 10 μM) did not affect the opening probability of cardiac as well as skeletal RyRs. However, it is also important to note that Copello and co-workers also failed to demonstrate the effect of cADPR addition on Ca^{2+} release from SR microsomes (see the review by Venturi et al. 2012). Recently, evidence was provided by Pitt et al. (2010) from similar single channel recordings, showing that NAADP concentrations up to 1 μM had no significant effects on the opening probability of rabbit skeletal and cardiac RyRs.

Contrary to all the studies mentioned above, Mojzisová et al. (2001) have reported observations showing that NAADP-(from 3 to 10 μM) induced Ca^{2+} release from rat cardiac microsomes. In their experiments, NAADP, over a concentration range of 1 – 10 μM, was shown to increase the opening probability of cardiac RyR2s isolated from dog hearts and incorporated into lipid bilayers.

The first evidence for a functional role of NAADP in single cardiac myocytes was performed and carried out in Terrar's laboratory. Under the condition without any activation of receptors by drugs or external supply of NAADP, Macgregor et al. (2007a) demonstrated that antagonists of NAADP such as bafilomycin-A1 (a vacuolar proton pump inhibitor) and high, desensitising concentrations of NAADP (0.1 to 1 mM) reduced cell contractions and Ca^{2+} transient amplitudes in paced guinea pig ventricular myocytes. This suggests that the level of NAADP in myocytes is above a functional threshold and there is a role for this endogenous NAADP in the basal EC coupling. In paced ventricular cardiomyocytes and atrial cardiomyocytes isolated from guinea pig hearts, the intracellular application of NAADP by photoreleasing caged NAADP (which was introduced into the cells by patch electrodes) or by cell-permeant NAADP-AM led to an increase in Ca^{2+}

transient amplitude (Macgregor et al., 2007a; Collins et al., 2011). These effects could be abolished by the disrupting the lysosomal function using bafilomycin-A1 or GPN, by desensitising NAADP mechanisms using high concentrations of NAADP, or by the suppressing the SR function with ryanodine or thapsigargin.

They further showed that the intracellular application of NAADP increased the caffeine-triggered the Ca^{2+} release of the SR both in atrial and ventricular myocytes. This suggests NAADP application could lead to an increase in SR Ca^{2+} load and SR Ca^{2+} release. They also showed that the amplitude of Ca^{2+} influx through L-type Ca^{2+} channels remain unchanged upon administration of NAADP (Macgregor et al., 2007a; Collins et al., 2011). Taken together, these observations are consistent with the hypothesis that NAADP has a role in EC coupling of cardiac muscle, through mediating the Ca^{2+} release from bafilomycin-A1-sensitive lysosomal acidic stores; this Ca^{2+} release enhances SR Ca^{2+} release, Ca^{2+} transient amplitudes and magnitudes of cell-shortening, partly if not completely through a directly or indirectly stimulatory effect on SR Ca^{2+} load.

While the above experiments were performed on paced (not resting) guinea pig cardiomyocytes involving photoreleasing of caged NAADP or superfusing NAADP-AM as the means to introduce NAADP intracellularly, Nebel et al. (2013) has demonstrated the effect of direct application of NAADP through patch pipettes on resting mouse cardiomyocytes. They have shown that the application of NAADP led to a global Ca^{2+} transient in 60 s which could be inhibited by bafilomycin-A1, ruthenium red and BZ194, which is a small molecule inhibitor of NAADP. The dose response curve of NAADP exhibited a bell-curve shape, peaking at around 30 nM. However, this was not observed in the previous attempts to introduce NAADP directly through patch pipette onto guinea pig cardiomyocytes in Terrar's lab

(Macgregor, 2014). This discrepancy could be due to the capability of mouse cardiomyocytes to retain a high level of Ca^{2+} in SR stores in their resting states (when they are not paced) while guinea pig cardiomyocytes tend to lose Ca^{2+} from the SR quickly when they are not paced (personal communication, Derek A. Terrar). Consistent with the observation that the NAADP effect was independent of changes in L-type Ca^{2+} current, BZ194 did not alter the Ca^{2+} influx through L-type Ca^{2+} channels (Nebel et al., 2013).

The involvement of NAADP in the β-adrenoceptor pathway has also been reported. First of all, in the presence of an activator of β-adrenoceptors, isoprenaline, photorelease of caged NAADP resulted in a smaller increase in Ca^{2+} transient amplitudes in paced guinea pig ventricular cardiomyocytes, suggesting the possible overlapping roles of NAADP and β-adrenoceptors (Macgregor et al., 2007a). In addition, in the presence of isoprenaline, the inhibition of the NAADP pathway (by high, desensitising concentrations of NAADP) resulted in a greater reduction in the magnitude of cell-shortening in paced guinea pig ventricular myocytes (Macgregor et al., 2007a). Capel et al. (2015) have also shown that a blunted response to β-adrenoceptor-mediated increase in Ca^{2+} transient amplitudes was observed when isoprenaline was applied to cardiomyocytes in the presence of bafilomycin-A1 or Ned-19 (a small molecule inhibitor of NAADP). Consistent with the findings mentioned above, Ned-19 did not seem to affect the β-adrenoceptor-mediated increase in L-type Ca^{2+} current (Capel et al., 2015). In the case of atrial myocytes, application of isoprenaline with the presence of GPN or bafilomycin-A1 has led to a blunted response to β-adrenoceptor-mediated increase in Ca^{2+} transient amplitude (Collins et al., 2011). These observations are consistent with the hypothesis that the activation of β-adrenoceptor enhanced the level of NAADP and this elevated level of NAADP contributed to the positive inotropic

effect mediated by β-adrenoceptor. This hypothesis is also consistent with the observations that CD38 was regulated by β-adrenoceptors (see section 1.2.11.3 on page 27).

1.3.6 NAADP and cardiac diseases

Consistent with the observations that CD38 may play a role in the development of cardiac arrhythmias and hypertrophy, the contribution of the NAADP pathway has been demonstrated in these cardiac diseases (Nebel et al., 2013; Capel et al., 2015; Gul et al., 2016). While a high concentration of isoprenaline (200 nM) caused an increase in the frequency of spontaneous Ca^{2+} transients (one of the indicators of cardiac arrhythmias), Nebel et al. (2013) have shown that the preincubation of bafilomycin-A1 or BZ194 in ventricular cardiomyocytes prevented the arrhythmogenic effect of β-adrenoceptor activation. They also demonstrated the effect of this NAADP antagonist, BZ194, in preventing the development of arrhythmias *in vivo*. Mice, which received two intraperitoneal injections of isoprenaline (2 mg kg^{-1} body weight), developed a variety of cardiac arrhythmias such as premature ventricular beats (PVB), salves of PVBs, bigeminy, and ventricular tachycardia (VT). On the other hand, mice, which received the BZ194 treatment (180 mg kg^{-1} body weight) 4 hours prior to the isoprenaline administration, had approximately 91% reduction in frequencies of PVB and bigeminy and 88% reduction in frequencies of salves of PVBs and VTs. Capel et al. (2015) also demonstrated the contribution of the NAADP pathway to arrhythmias using *Tpcn2*$^{-/-}$ mice (Note: the cardiomyocytes from these mice did not response to NAADP-AM application. (see section 3.3.2 on page 87). From the whole heart monophasic action potential recordings, they showed that hearts from these

NAADP-insensitive mice had increased thresholds (in terms of currents or pacing frequency) for arrhythmias following the acute activation of β-adrenoceptors (by perfusing hearts with 50 nM isoprenaline) or following the chronic activation of β-adrenoceptors (by administrating 10 mg kg^{-1} day^{-1} of isoprenaline via osmotic mini pumps for 14 days) (Capel et al., 2015).

Capel et al. (2015) also showed that *Tpcn2*$^{-/-}$ mice were more resistant to β-adrenoceptor-induced cardiac hypertrophy (measured by ratio of heart weight/tibia length, end diastolic left ventricular posterior wall thickness and mass of left ventricles) and retained better cardiac function (measured by reduction of fractional shortening). Similarly, Gul et al. (2016) reported that *CD38*$^{-/-}$ mice were more resistant to cardiac hypertrophy. Taken together, these findings highlight the possible contribution of NAADP towards the development of cardiac arrhythmias and hypertrophy.

NAADP-mediated Ca^{2+} signalling has also been studied in IR injury in the heart. Davidson et al. (2015) also showed NAADP levels in hearts were highly regulated during IR. They further showed that a novel antagonist of NAADP, Ned-K, reduced Ca^{2+} oscillations and improved the survival of cardiomyocytes after ischaemia and reoxygenation. In their experiments, *Tpcn1*$^{-/-}$ mice and mice administered with Ned-K had reduced post-reperfusion myocardial infarct sizes. Both Ned-K and bafilomycin-A1 significantly delayed the opening of the mitochondrial permeability transition pores, which is a link to cell death and IR injury. The authors hypothesised that during cardiac reperfusion, NAADP could play a role in contributing to Ca^{2+} oscillations via TPC1 which subsequently lead to the opening of the mitochondrial permeability transition pores and cell death. On the other hand, extracellular NAADP (1 μM) was found to be cardioprotective

during IR injury in terms of functional recovery, necrosis and arrhythmogenesis via the activation of purinergic P2Y11 (Djerada and Millart, 2013; Djerada et al., 2013). However, as whether Djerada's experiments was relevant to NAADP-mediated lysosomal Ca^{2+} remains unexplored.

1.4 General remarks

In addition to being an enzyme which catalyses the production of Ca^{2+}-mobilising molecules, CD38 also plays a role as a receptor for ligands such as CD4 and CD31 (see the review by Malavasi et al. 2008). Although this is not discussed extensively in this thesis, expression of CD38 as a surface antigen and receptor is particularly important in immune cells such as lymphocytes and monocytes. For example, the high expression of CD38 in some malignant cells (multiple myeloma and chronic lymphoid leukaemia) has prompted effort into investigating whether CD38 can be a good drug target for cancer treatment (see review by Sanchez et al. 2016). Indeed, daratumumab (Darzalex^{TM}) has recently been approved by the US Food and Drug Administration. Furthermore, CD38 is also recognised as a biomarker for AIDS (Benito et al., 2004). The experimental model, *CD38*$^{-/-}$ mice also showed other defects apart from cardiac defects, including impaired insulin secretion (Kato et al., 1999), disordered osteoclast formation and function (Sun et al., 2002), altered airway responsiveness (Guedes et al., 2015), impairment of dendritic cell trafficking and reduced humoral immune response (Partida-Sánchez et al., 2001), impairment of α-adrenoceptor-stimulated contraction in the aorta (Mitsui-Saito et al., 2003), and depression of oxytocin release and abnormal social behaviour (Jin et al., 2007).

On the other hand, NAADP plays important roles in various signalling pathways

in plants and animals including humans, which include hormonal secretions, smooth muscle contractions, immune responses, fertilisation and neuromodulation (see reviews by Lee 2001; Galione 2014). Importantly, the NAADP signalling pathway has been shown to modulate VEGF-regulated angiogenesis (Favia et al., 2014), making it a potential target for restricting angiogenesis in cancer progression. A study in 2015 also showed that Ebola virus entry into host cells is dependent on the NAADP-regulated TPC proteins (Sakurai et al., 2015).

Taken together, this highlights the ubiquitousness of CD38 and NAADP, as well as the wide range of physiological functions that they mediate. As the heart is one of the most vital organs, a better understanding of these CD38 and NAADP-related pathways in the heart will not only assist in the search for treatments for cardiac diseases but also will provide valuable insights for potential cardiac side effects when these pathways are used as targets in designing novel therapies to combat other diseases.

Chapter 2

Methods and Materials

2.1 Animals

The C57BL6 mice and New Zealand white rabbits were obtained from Envigo (UK) or Charles River Laboratories (USA).

The *CD38*$^{-/-}$ mouse line was developed by Cockayne et al. (1998) and obtained from Jackson laboratory (*CD38*^{tm1Lnd}/J). This CD38 KO model was achieved by replacing Exon 2 and 3 of the *CD38* gene of a C57BL6 mouse that are responsible for encoding the catalytic site for CD38, with the neomycin resistance gene (Cockayne et al., 1998), resulting in the loss of CD38 protein expression. This (*CD38*$^{-/-}$) model was further verified by the lack of CD38-specific mRNA transcripts and immunolabelling by the rat anti CD38 antibody, and by the dramatically reduced NAD glycohydrolase activity (Cockayne et al., 1998).

The *Tpcn2*$^{-/-}$ mouse line was developed by Dr Margarida da Silva from Professor

Antony Galione's lab. This *Tpcn2* KO model was achieved by using a gene trap mutation in the *Tpcn2* gene of a YHD437 mouse (Calcraft et al., 2009; Ruas et al., 2015).

2.2 Mouse ventricular cardiomyocyte isolation

This single mouse cell isolation was adapted from that previously described by Powell et al. (1980). Male adult mice (10 – 24 weeks) were stunned and killed by cervical dislocation in accordance with the Home Office Guidance on the Operation of the Animals (Scientific Procedures) Act 1986 (H.M.S.O.). The heart was excised within minimal amount of time and put in a dissection chamber filled with Mouse Myocytes Isolation Solution (see **Table 2.2** in section 2.18). The thymi were separated to reveal the aorta (identified by its characteristic arch with three branches). The heart was then cannulated with a blunted syringe needle through the aorta. For some experiments, the heart was perfused with physiological salt solution (PSS, see **Table 2.1** in section 2.18), supplemented with heparin (10 units ml^{-1}) to minimise clotting of blood in the coronary vessels, and with streptokinase (100 units ml^{-1}) to digest any clotted blood. The heart, together with the cannula, was then mounted onto a Langendorff perfusion system, where it was perfused with Mouse Myocytes Isolation Solution (36 ^{o}C). Whenever blood clots were observed (identified by the presence of black dots upon shining light through the heart), gentle pressure was applied using the finger tips to the ventricle wall to facilitate the removal of blood. Within 3 minutes, the perfusion solution was replaced with Mouse Myocytes Isolation Solution containing 0.5 – 0.8 mg ml^{-1} of collagenase (type-II, Worthington Biochemical Corp., Lakewood, NJ, USA). The enzymatic digestion would then typically be carried out for 5 – 8 min before removing the heart from the

cannula upon softening of the ventricle wall. By this stage, the heart should have a similar touch sensation of water-filled latex balloon. The ventricles were cut into pieces and titurated with a pipette to dissociate individual cells. The solution containing the cells was filtered through a 250 μm gauze. The filtered solution containing single isolated cells was then collected and stored either in a high potassium solution or a Tyrode solution (see **Table 2.1** and **2.3** in section 2.18).

The procedures were optimised through trial and improvement until they produced good yields of healthy ventricular myocytes, judged according to their morphology (rod-like shape and visible cross striations) and their resting state (quiescent and no spontaneous contractions). All single cell experiments reported in this thesis were carried out on viable, healthy myocytes. Variations of the procedures were kept to a minimum in each set of experiments.

2.3 Rabbit ventricular and atrial cardiomyocyte isolation

The isolation of myocytes from the rabbit heart was carried out by Dr. Daniel Aston using the protocol described in Aston et al. (2017). Male New Zealand White rabbits (approximately 1 kg) were sacrificed by intravenous overdose of sodium pentobarbitone. The heart was rapidly excised, washed in heparin-containing solution (5 units ml^{-1}), and mounted on a Langendorff apparatus for perfusion with Rabbit Myocytes Isolation Solution (see **Table 2.2** in section 2.18). Within 2 minutes, the digestion was initiated using a similar solution, spiked with 0.5 mg ml^{-1} of collagenase (type-II, Worthington Biochemical Corp., Lakewood, NJ, USA),

and 100 μM $CaCl_2$ (to replace ethylene glycol-bis(β-aminoethyl ether)-N,N,N',N'-tetraacetic acid, EGTA) and allowed to proceed for a further 30 – 35 minutes. Ventricular tissue or atrial tissue was then isolated, cut into pieces and titurated. The isolated, individual myocytes were centrifuged and stored in Dulbecco's Modified Eagle Medium (DMEM).

2.4 Cell superfusion

Most of the experiments involving Ca^{2+} imaging, contraction and electrophysiology studies on live cells were carried out using a superfusion system (unless stated otherwise) described as below:

2.4.1 Bulk superfusion system

Single myocytes were transferred onto a glass coverslip, which was attached to the bottom of a rectangular Perspex chamber glued on by silicon grease (RS Components Ltd., UK). This bath was placed onto the stage of an inverted microscope, and a perfusion system was used to provide a continuous flow of PSS across the bath. The perfusion system was either driven gravitationally or by a peristaltic pump at a flow rate of approximately 3.5 ml min^{-1}. Cells were left to settle and attach to the cover slip for at least 5 minutes before being superfused. These cells were superfused continuously with bicarbonate-buffered PSS (gassed with 95% O_2 and 5% CO_2) or HEPES- (4-(2-Hydroxyethyl)piperazine -1-ethanesulfonic acid, N-(2-Hydroxyethyl)piperazine-N'-(2-ethanesulfonic acid) buffered Tyrode solution. The temperature of the inflow solution was regulated by a

heating block, to ensure that the average temperature at the centre of the bath chamber was 36 ^{o}C. An outflow tube was placed on the other end (opposite the inflow tube) of the bath chamber to maintain the depth of the solution, through applying vacuum suction generated by a dish tank pump or a peristaltic pump. The exchange of the superfusate was achieved either by the use of a set of voltage-activated, 3-way solenoid valves (Lee Products Ltd., UK), which allowed the switching of the solution, or by direct modification of the superfusion solution by adding drugs into the reservoir. The former method has the advantage of smaller dead space, but may generate a greater mechanical disturbance due to potentially trapped bubbles being released.

2.4.2 Rapid switch system

In some experiments, in order to preserve the use of drugs, a local superfusion system was set up. This system is named as a rapid switch system. A triple-barrelled square glass capillary tube (Harvard Apparatus Ltd, UK) was held by a holder. The control solution and a solution containing the drug were passed through the first and the third glass tube respectively. The first glass tube was placed near to the target cell to provide superfusion. Two different solutions flowed out from both tube 1 and 3 continuously. Switching of the local inflow solution can be achieved through the rapid lateral movement of the capillary tubes, driven by a stepper motor. This allowed an exchange of the superfusate in minimum time and ensured a minimal amount of drugs were consumed. However, bulk superfusion (see section 2.4.1 on the facing page) was still required to maintain the temperature of the bath.

2.5 Ca^{2+} fluorescence imaging

For the single cell experiments in this thesis, Fluo-5F was used as the fluorescent Ca^{2+} indicator to measure intracellular Ca^{2+}. Fluo-5F has very similar properties to conventional Fluo-3 or Fluo-4; the main difference is that Fluo-5F has a lower affinity towards Ca^{2+} (K_d of Fluo-5F is 2.3 μM, while K_d of Fluo-4 is around 500 nM). Due to its higher K_d, Fluo-5F also provides better signal resolution when measuring Ca^{2+} signals from action potential-triggered Ca^{2+} transient of myocytes, which are in the range of 10^{-6} M. In addition, there should be less buffering of Ca^{2+} signals Fluo-5F compared with other high affinity Ca^{2+} dyes. However, Fluo-based dyes do not have a significant spectral shift (in either their emission or excitation wavelength) when they are bound Ca^{2+} ions, so they are non-ratiometric. The Ca^{2+}-bound Fluo-5F can be excited with light at 488 nm and emitted fluorescence upon excitement can be expected at $\geq$ 510 nm.

2.5.1 Line scanning confocal microscopy

A Leica TCS NT confocal scanning head was used in conjunction with a Leica DMIRB inverted light microscope with a $100x$ oil immersion objective lens (1.4 numerical aperture, Leica Microsystems, UK). Excitation light was provided by an air-cooled 488 nm Argon ion laser system (Uniphase Ltd, USA) while emitted light was passed through a 515 nm long pass filter before detection by photomultiplier tubes. Assuming the average peak amplitude of the Ca^{2+} transient at any given area of the cell was comparable during an episode of global transient event, the whole cell Ca^{2+} transients were recorded in the line-scan mode at a scanning speed of 450 lines per second. A line of one pixel thickness was placed across the shorter axis in

the middle of a cell (to minimise movement artefacts caused by contractions of the cardiomyocytes), and this area was repetitively scanned upon excitation with lasers. 10 to 20 Ca^{2+} transients were evoked by a series of electrical field stimulations (1 Hz) and recorded continuously before the addition of drugs. At least 20 continuous Ca^{2+} transients were recorded every min for 5 min after the application of drug. The Ca^{2+} transient amplitudes were analysed using imageJ (NIH, USA) and Python (Python Software Foundation, https://www.python.org/). For analysis, background fluorescence was subtracted and multiple transients were averaged in order to collect data at a given time point. Data are presented as F/F_0 such that fluorescence signal is presented relative to the diastolic fluorescence. The average of Ca^{2+} transient amplitudes was either plotted with time points or the highest average Ca^{2+} transient amplitude (averaged min by min) was presented as the peak Ca^{2+} transient.

2.5.2 Spinning disk confocal microscopy

Excitation light of 488 nm was provided by an argon laser (Coherent, USA). The light passed through a Zeiss disc confocal scanning unit (CSU-10) before entering the side port of a Nikon Axiovert 200 microscope and delivered through a $40x$ oil immersion objective to the cells. The fluorescence signal was collected through the objective and filter, and directed through the CSU-10 before being detected by an Andor iXON897 electron multiplying charge coupled device (EM-CCD) camera. Images were taken at a rate of 50 frames per sec. At least 10 Ca^{2+} transients were evoked by a series of electrical field stimulation (1 Hz) and recorded continuously before the addition of drugs. A minimum of 10 continuous Ca^{2+} transients were recorded at every min for 5 min after the application of drug. The Ca^{2+} transient amplitudes were analysed using both Andor IQ software (Andor Technology, UK)

and Clampfit software (Axon Instruments, USA). For analysis, background fluorescence was subtracted and multiple transients were averaged in order to collect data at a given time point. Data are presented as F/F_0 such that fluorescence signal is reported relative to the diastolic fluorescence. The average of Ca^{2+} transient amplitudes was either plotted with time points or the highest average Ca^{2+} transient amplitude (averaged min by min) was presented as the peak Ca^{2+} transient.

2.6 Electrical field stimulation

In some experiments, Ca^{2+} transients or contraction of cardiac myocytes were triggered by electrical pulses. These cells were placed in a bath chamber equipped with two carbon fibre electrodes on the longitudinal sides of the chamber. These electrodes were connected to a stimulator, which can generate a potential difference across the electrodes (across the bath), thus forming an electrical field. In all the electrical field stimulation experiments, the cells were stimulated by delivering electrical pulses with an amplitude of 20 – 30 V and a pulse duration of 2 – 3 ms at a frequency of 1 Hz.

2.7 Contraction studies

Contraction measurements in this thesis were carried out by Dr. Emma Bolton. The contraction strengths of the ventricular cardiomyocytes were quantified by measuring the amplitude of their sarcomere shortenings during each contraction. This was achieved using an IonOptix MyoCam system (IonOptix Corp., Milton, MA, USA) with an inverted microscope (Olympus, IX-70, Leeds Precision Ltd,

Minneapolis, MN, USA). Cells were superfused with PSS or HEPES-buffered Tyrode solution and electrically paced (see section 2.6 on the preceding page). The sarcomeres of the cells were visualised through a $40x$ oil objective lens using IonOptix MyoCam (IonOpix Corp.). Images were sampled at a rate of 240 frames per sec.

The alternating light and dark bands of the contractile machinery gives rise to a optical density profile with a sinusoidal pattern, whose period can be computed into the sarcomere length through a fast Fourier transformation. A minimum of 7 sarcomeres (from a single myocyte) were selected during each recording. The measurement system was calibrated using a stage micrometre with 2 μm graduations. The peak amplitude of sarcomere shortening was defined as the difference between the minimum systolic sarcomere length and maximum diastolic sarcomere length. The peak amplitude of sarcomere shortening was expressed in μm. Analysis was performed using IonWizard 5 software (IonOptix Corp.). All values represented an average of at least 10 contractions.

2.8 L-type Ca^{2+} current measurement

Ventricular myocytes were superfused with PSS and viewed on a $10x$ objective lens of an inverted microscope. A patch electrode was placed into a Perspex holder, which was itself mounted into a headstage (HS-2A, Axon instruments, USA). An electrical connection was established between the headstage and the electrode using an Ag/AgCl-coated wire from the headstage. This wire was put through the glass electrode and was in contact with the whole patch solution (pipetted into the glass electrode, see **Table 2.3** in section 2.18) throughout the experiments.

Electrophysiological measurements were recorded with reference to a electrode making contact with the bath (extracellular) solution.

Action potential and voltage clamp recordings were made using an Axoclamp 2 (or 2A) amplifier (Axon Instruments, USA). Electrophysiological recording equipment and other nearby instruments including the microscope were grounded or shielded with aluminium foil to minimise electrical noise. The tip potential was zeroed when the microelectrode was placed into the bath solution. Electrophysiological recording of the cardiomyocytes was firstly carried out in the current clamp-bridge mode of the amplifier where the tip potential of the microelectrode voltage was measured continuously. A small negative current of 1.1 nA with a pulse width of 200 ms was passed through the microelectrode at a frequency of 0.2 Hz. This current caused a change in potential difference due to the resistance of the microelectrode, which was compensated using the bridge balance adjustment on the amplifier. This bridge balance adjustment corresponded to the resistance of the pipette, which should lie around 3 – 4 MΩ. A lower resistance could indicate a broken glass electrode and a higher resistance could indicate a blocked glass electrode, both cases not being ideal for recording.

Using a micromanipulator, the microelectrode was positioned above the targeted cell and lowered until it caused a dim on the surface of the cell. The contact between the microelectrode and cell could be identified was reflected by a drop in the voltage recording. A gentle suction was applied using a 10 ml syringe attached to the microelectrode with a rubber tubing, in order to form a high resistance seal (approximately 200 MΩ) between the cell surface and the tip of the microelectrode. Whole-cell configuration was achieved by rupturing the cell membrane by the means of suction. A successful patch would give a measurement of resting membrane

potential in the range of -70 to -85 mV and the action potentials could then be evoked by applying brief (2 ms) depolarising current pulses (3 to 5 nA), delivered at 1 Hz.

L-type Ca^{2+} current of mouse ventricular cardiomyocytes was measured in the whole-cell configuration under voltage clamp conditions. This was achieved in the discontinuous single electrode voltage clamp (DSEVC) or “switched" clamp” (switching between current and voltage clamp). Before switching to this DSEVC mode, the capacitance compensations were carried out in discontinuous current clamp mode. Current pulses were injected into the microelectrode, and the voltage response monitored on an oscilloscope. The capacitance neutralisation control was adjusted to maximise the rate of the rise of the voltage response without causing the overshoot of the input signal or inducing circuit oscillations. L-type Ca^{2+} currents were measured by clamping the membrane potential at -35 to -40 mV (in order to inactivate the Na^{+} and T-type Ca^{2+} channels) and subsequently applying a 200 ms step depolarisations to 0 mV at a frequency of 1 Hz. The low frequency allowed L-type Ca^{2+} channels to fully recover from inactivation between step depolarisations. The L-type Ca^{2+} current was defined as the difference between the maximum inward current and the baseline (holding current at 0 mV). Data were acquired and digitised using a Digidata 1322A analogue-to-digital converter and Clampex software (Axon Instruments, USA), and analysed with Clampfit software (Axon Instruments, USA).

2.9 Sheep sarcoplasmic reticulum-enriched membrane preparation

The ingredients for solutions mentioned in this section can be found in **Table 2.3** in section 2.18. Collection of sheep hearts from a local abattoir was carried out by Rebecca Sitsapesan's lab.

The sheep hearts were transported from a local abattoir to the laboratory in an ice-cold cardioplegic solution. The left ventricular tissue, including the septal wall, was isolated and halved, with fat and connective tissue trimmed. The cardiac muscle was then stored in liquid N_2. The frozen tissues were pulverised with a pestle and mortar and homogenised in SRMP solution 1 with a blender (Braun GmbH, Kronberg, Germany) followed by further homogenisation with a Ultra-Turrax homogeniser (IKA Werke GmbH & Co. KG, Staufen, Germany). The homogenised tissue was then centrifuged for 20 min in a GSA Sorvall rotor (Fisher Scientific UK Limited, Loughborough, UK) at 6500 x g. The supernatant was subsequently centrifuged for 1 hr in a Sorvall A-641 rotor at 100,000 x g. The resulting pellet containing mixed membrane vesicles was resuspended in SRMP solution 2 and centrifuged for 2 hr in a Sorvall AH629 swing out rotor at 100,000 x g in SRMP solution 2 with a discontinuous sucrose gradient of 20%, 30% and 40% w/v. The different membrane fractions were separated according to their densities. The 30 – 40% sucrose interface contained a fraction with a high density of RyR channels (HSR), were collected and resuspended in SRMP solution 3. The LSR fraction, containing K^+ and Cl^- channels but very few RyR channels, were collected from the 20 – 30% interface and resuspended in SRMP solution 3. The two membrane fractions were then centrifuged for 1 hr in a Sorvall T865 rotor at 100,000 x g,

resuspended in a minimum volume of SRMP solution 4, frozen with liquid N_2 and stored at -80 °C. This preparation (either HSR or LSR) was termed SRMP.

2.10 Mouse mixed membrane preparation

The ingredients for solutions mentioned in this section can be found in **Table 2.3** in section 2.18.

6 mouse hearts were isolated and excised from mice killed by cervical dislocation in accordance with the Home Office Guidance on the Operation of the Animals (Scientific Procedures) Act 1986 (H.M.S.O.). After the removal of atrial tissue and blood (by gentle squeezing), hearts were kept in an ice-cold cardioplegic solution. The cardiac muscle was then stored in liquid N_2. The frozen tissues were pulverised with a pestle and mortar and homogenised in SRMP solution 1 using a blender (Braun GmbH, Kronberg, Germany), followed by a fine homogenisation with the Ultra-Turrax (IKA Werke GmbH & Co. KG, Staufen, Germany). The homogenised tissue was centrifuged in a GSA Sorvall rotor (Fisher Scientific UK Limited, Loughborough, UK) at 6500 x g. The supernatant was centrifuged for 1 hr in a Sorvall A-641 rotor at 100,000 x g. The final pellets were resuspended in a minimum volume of SRMP solution 4, frozen with liquid N_2 and stored at -80 °C. This preparation was termed the (mixed) membrane preparation.

2.11 The measurement of NAADP using sea urchin egg homogenate assay

Sea urchin egg homogenates were prepared by members of Galione's lab using the method described by Galione (2014). In brief, egg shedding by the female sea urchin (*Lytechinus pictus*) was stimulated by intracoelomical injection of 0.5 M KCl. Eggs were dejellied by passing them through nylon net filters (100 μm), washing with Ca^{2+}-free artificial sea water, and centrifuging at 800 x g, 10 °C for 2 – 5 min. Pellets were collected and washed in GluIM buffer (**Table 2.3** in section 2.18). Homogenisation of the eggs was carried out using Dounce glass tissue homogeniser and a size A pestle (6 strokes) before the homogenised eggs were centrifuged at 13000 x g and at 4 °C for 10 sec and stored at -80 °C.

An aliquot of sea urchin egg homogenate (approximately 50% v/v) was defrosted for 30 min in a cooling tank at 18 ^{o}C. The homogenates were further diluted sequentially with GluIM buffer at 18 ^{o}C over 3 hours to allow effective Ca^{2+} loading into intracellular stores. The final concentration of the sea urchin egg homogenate was 5% v/v or 2.5% v/v. This sea urchin egg homogenate was then stored at -80 ^{o}C.

To be used as a Ca^{2+} release bioassay, the sea urchin egg homogenate (5% v/v or 2.5% v/v) was defrosted in the cooling tank at 18 ^{o}C for at least 30 min. A final concentration of 3 μM Fluo-3 was added into the homogenate as the Ca^{2+} indicator. Free Ca^{2+} was measured using 99 μl of sea urchin egg homogenates in a a Novostar plate reader (BMG Labtech, UK) at excitation and emission wavelengths of 490 nm and 535 nm respectively. Additions were made to the well in 1 μL volumes and the changes in relative fluorescence units (r.f.u.) were measured.

Protein samples were pre-diluted to the desired concentration in solution 5, while cells were incubated in the high potassium solution (**Table 2.3** in section 2.18). To synthesise NAADP, NADP (500 μM, final concentration) and NA (7 mM, final concentration) were preincubated with the protein sample or cells at 37 ^{o}C. Then, the protein-substrate or cell-substrate mixtures were diluted before adding them to the sea urchin egg homogenates. After 5 min, purified NAADP (500 nM, final concentration) was added to the sea-urchin egg homogenates to elicit a Ca^{2+} release response. This Ca^{2+} release induced by saturating 500 nM NAADP concentration was expressed in the percentage of the control (Ca^{2+} release induced by 500 nM NAADP with vehicle preincubation). The Ca^{2+} release response to 500 nM NAADP is specifically dependent on the subthreshold concentration of the NAADP in the preceding addition (Genazzani et al., 1996). Hence, the concentration of NAADP can be quantified through interpolation of a standard dose response curve from known concentrations of purified NAADP.

2.12 The measurement of ADP-ribosyl cyclase activity

2.12.1 Detection of cGDPR formation using an NGD assay

The ARC activity of a given cell or tissue homogenates can be detected by a continuous assay, using nicotinamide guanine dinucleotide (NGD) as the enzyme substrate. NGD is an analogue of NAD where the adenine group has been replaced with guanine. When NGD is converted to cyclic GDP-ribose (cGDPR) through cyclisation by the ARC, its production can be detected using a fluorimetric method

via the fluorescence of cGDPR (Graeff et al., 1994). Protein sample was diluted in solution 5 and a final concentration of 500 μM NGD was added to the protein sample to initiate the enzymatic reaction. The production of the fluorescent product, cyclic GDP-ribose, was measured using a Novostar plate reader (BMG Labtech, UK). The cGDPR formation was monitored through its fluorescence intensity at 410 $\pm$ 5 nm during its excitation with light of wavelength 300 $\pm$ 10 nm. The rate of cyclase activity of each reaction mixture was then defined by the change in fluorescence with time, which is the slope of the curve in the fluorescence versus time plot, obtained by linear regression.

2.12.2 Detection of cADPR using sea urchin egg homogenate assay

The synthesis of cADPR was achieved by incubating protein or cell samples with 2.5 mM NAD in solution 5 and the high potassium solution respectively (**Table 2.3** in section 2.18). The protein-substrate or cell-substrate mixture was then diluted before adding into the 2.5% v/v or 5% v/v sea urchin egg homogenate bioassay that contained 3 μM Fluo-3 as Ca^{2+} indicators. An increase in the fluorescence reading upon the addition of the diluted sample implies a Ca^{2+} release induced by the presence of cADPR (converted from NAD). This Ca^{2+} release was calibrated with known concentrations of cADPR. Since cADPR is more susceptible to hydrolysis compared with cGDPR, the NGD assay (described in section 2.12.1 on the preceding page) is generally a more reliable way to quantify the enzymatic activity of ARC. However, it is important in some experiments to show that the measurement of ARC activity using an analogue is at least quantitatively similar when the physiological substrate, NAD is used. Hence, the sea urchin egg

homogenate assay was used to detect the presence of cADPR, in order to provide a further validation to the results obtained from NGD assay in some experiments.

2.13 Permeabilisation

For experiments investigating the enzymatic activities of permeabilised myocytes, myocytes were preincubated with high potassium solution (see **Table 2.3** in section 2.18 for ingredients) containing either saponin (0.01 % w/v) or Triton X-100 (0.1 % v/v) for 15 min before 500 μM NADP and 7 mM NA was added to the incubation to initiate the base exchange reaction.

2.14 Protein quantification

A standard bicinchoninic acid assay was used for the quantification of protein in samples. Briefly, 10 μL of sample was preincubated with 200 μL of dye reagent (a solution containing bicinchoninic acid solution and 4% (w/v) copper sulphate solution in a 50:1 ratio) in a 96-well plate at room temperature or at 37 °C for 30 min. The absorbance of each well was then measured at 595 nm using TECAN SunRise Remote Control plate reader and calibrated with known concentrations of protein (bovine serum albumin).

2.15 Immunocytochemistry

Cells were left to settle on a Superfrost plus slides (VWR International Ltd, UK) for at least 30 min and fixed with phosphate-buffered saline (PBS) with 4% paraformaldehyde (Sigma-Aldrich Company Ltd, UK) for 15 min before being washed in PBS (3 changes, 5 min each). In some experiments, the permeabilisation of cell membranes was achieved by incubating cells with PBS with 0.1% Triton X-100 (Sigma-Aldrich Company Ltd, UK) for 10 min and washed with PBS (3 changes, 5 min each). Cells were subsequently incubated with 1% bovine serum albumin for 60 min to block non-specific binding sites prior to an overnight incubation with primary antibodies at 4 ^{o}C. The next day, cells were first washed with PBS (3 changes, 5 min each) before being incubated with secondary antibodies for 2 hours (either AlexaFluor 488 conjugated donkey anti-rabbit or Dylight 550 donkey anti-mouse, 1: 1000 dilution) and then being washed with PBS (6 changes, 5 min each). Finally, slides were covered with coverslips using Vectashield (Vector Laboratories Ltd, UK) and sealed with nail polish to preserve the moisture of the sample. Cells were stored in the dark at 4 ^{o}C and visualised within 2 days.

For control experiments, similar procedures were performed with the omission of the primary antibodies, or with cells from KO model when available. Primary antibodies against CD38 (sc-15362, Santa Cruz, USA) and ryanodine (ab2827, Abcam, UK) were used at a 1: 100 and 1 : 200 dilution respectively. Observations were carried out using a Nikon A1 confocal laser scanning microscope equipped with a $60x$ objective. The settings on the laser power, sensitivity of detectors and pinhole size ($\leq$ 1 airy units) were adjusted until no fluorescence was observed in the negative control group and subsequently kept the same for the same set of experiments. Images were analysed and processed using imageJ software (NIH, USA).

2.16 Monophasic action potential recording

Male adult mice (10 – 24 weeks) were stunned and killed by cervical dislocation in accordance with the Home Office Guidance on the Operation of the Animals (Scientific Procedures) Act 1986 (H.M.S.O.). The chest cavity of the mouse was exposed and the heart was isolated and put in a dissection chamber filled with Krebs solution (see **Table 2.1**). The thymi were torn apart to reveal the aorta and the heart was cannulated through the aorta, and perfused with Krebs solution (bubbled with 95% O_2 and 5% CO_2) at a flow rate of 3.5 – 4 ml min^{-1}.

The heart were left to settle for 30 min to achieve a stable, continuous heart beat. In some experiments where preincubation of drug with the heart was required, drugs or vehicles were introduced in the Krebs solution during this 30 min stabilisation stage.

A recording electrode was placed on the left ventricle to measure the monophasic action potential (MAP) while an pacing electrode was placed on the ventricular septum to delivered programmed pulses to stimulate the heart. A schematic diagram is included to show the four protocols used (**Figure 2**).

a) Frequency-varying burst pacing protocol

For frequency-varying burst pacing protocol, a cycle of three trains of stimuli was delivered to the heart. Each train of stimuli consists of 50 stimuli and was separated by a pacing-free interval of 2 s. The interval between each stimulus was progressively reduced from 100 ms (10 Hz) to 20 ms (50 Hz) in 10 ms decrements after each cycle.

b) Amplitude-varying burst pacing protocol

For amplitude-varying burst pacing protocol, a cycle of three trains of stimuli was

delivered to the heart. Each train of stimuli consists of 50 stimuli with interval of 20 ms and was separated by a pacing-free interval of 2 s. After each cycle, the current amplitude was increased progressively by factors of the pacing threshold current or by 1 mA, i.e. the minimum current to evoke an action potential in a 1:1 manner. The protocol was terminated when a ventricular arrhythmias was observed or a current of 32 mA was reached.

c) Dynamic pacing

Cycles of 100-stimulus (S1) drive train were applied at a pacing interval of 135 ms initially. Pacing interval was progressively reduced by 5 ms between successive cycles until a pacing interval of 10 ms was reached.

d) S1S2 pacing

Cycles of 9 stimuli comprising eight S1 stimuli (8 Hz) followed by an extra stimulus (S2). Initially, the interval between S1 and S2 was set to be 125 ms and was progressively reduced by 1 ms between successive cycles until the heart became refractory i.e. when S2 stimulus was no longer able to evoke an action potential.

Ventricular arrhythmia was defined as six or more consecutive regular premature waveforms or irregular fibrillating waveforms. The arrhythmogenicity of the heart was determined by number of protocols that successfully triggered arrhythmias. A scoring system was devised on this basis. For example, the score for arrhythmogenicity is 3 when a heart exhibited signs of arrhythmias under 3 out of 4 protocols. (note: the maximum score was 4 when all four protocols successfully triggered arrhythmias)

The heart rate was derived from the beat-to-beat intervals. A minimum of 10 beat-to-beat intervals were used to calculate the average heart rate.

Figure 2

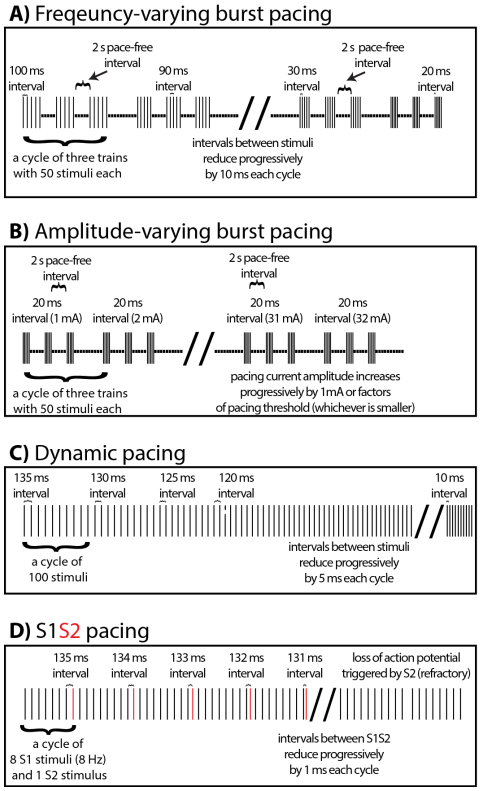


Figure 2: Schematic diagram of stimulation protocols in arrhythmias studies

Protocols for frequency-varying burst pacing, amplitude-varying burst pacing, dynamic pacing and S1S2 pacing are shown in **A**, **B**, **C** and **D** respectively.

2.17 Drug docking studies

2.17.1 Blind docking with SwissDock server

Blind docking using the SwissDock webserver (Grosdidier et al., 2011) was performed to predict the binding sites of SAN4825 in human CD38 and mouse CD38. This docking methodology is based on the EADock DSS engine, an approach that has been able to successfully determine small molecules binding modes to

proteins (Grosdidier et al., 2011). In brief, when a protein and ligand of interest were submitted to SwissDock webserver, the structure of the target protein, as well as that of the ligand are automatically prepared SwissDock. Then, typically 5000 to 15000 binding modes were generated in potential pockets of the entire protein surface (blind docking). The CHARMM energies of the binding modes were estimated (Brooks et al., 2009) and the most favourable energies were listed on the top of the results, with the consideration of solvent effect using the FACTS implicit solvation model (Haberthur and Caflisch, 2008).

2.17.2 Docking simulation with Glide

This method is carried out in collaboration with Dr. Wilian Cortopassi. A conformational search in an implicit solvent (water) with an OPLS_2005 force field (Jorgensen et al., 1996) was performed for SAN4825 using MacroModel Schrödinger Release 2017-1. An adapted blind docking of all possible conformations in the mouse CD38 (PDB ID: 2EG9, chain A) was performed with Glide (Friesner et al., 2004; Halgren et al., 2004) considering all possible pockets, as determined by SiteMap (Halgren, 2009). Preparation of the CD38 protein was achieved using the protein preparation tool available in Maestro. The missing side chains and loop are filled with Prime (Jacobson et al., 2002, 2004). The resulting structure was minimised energetically with OPLS_2005 force field. Binding energies after docking simulations were calculated for ranking the best docking poses using the Molecular Mechanics/Generalised Born Surface Area (MM/GBSA) scoring function. For the scoring, residues close to ligand docking sites (within 5 Å) were considered flexible in order to allow the optimisation of the docking conformations.

2.18 Recipes for solutions

	Kreb's Solution	Physiological Saline Solution (PSS)	Tyrode Solution
NaCl	120	125	134
KCl	4	5.4	4
$MgSO_4$	1.3		
$MgCl_2$		1	1.2
NaH_2PO_4	1.2	1.2	
$NaHCO_3$	25.2	25	
HEPES			10
Glucose	5.8	5.5	11.1

Table 2.1: Perfusion Solutions
Note: Solutions with HEPES were titrated to pH 7.4 with NaOH while solutions with $NaHCO_3$ were bubbled with 5% CO_2.

	Mouse	Rabbit
NaCl	135	136
KCl	5.4	5.4
$MgCl_2$	1	1
NaH_2PO_4	0.33	1.2
$NaHCO_3$	25.2	12
HEPES	10	
Glucose	10	5
Na pyruvate		1
EGTA		0.04

Table 2.2: Myocyte Isolation Solution
Note: Solutions with HEPES were titrated to pH 7.4 with NaOH while solutions with $NaHCO_3$ were bubbled with 5% CO_2.

2.19 Suppliers of drugs and chemical compounds

All the common chemical compounds were purchased either from Sigma (USA) or VWR (USA) unless specified.

The SAN4825 compound was a kind gift from Sanofi (France).

Buffer	Ingredient
High potassium solution	KCl 70, $MgCl_2$ 5, K glutamine 5, taurine 20, EGTA, 0.04, succinic acid 5, KH_2PO_4 20, glucose 10, HEPES 5 (mM); pH 7.2 with KOH
Whole patch solution	K aspartate 110, KCl 10, NaCl 8, $MgCl_2$ 5.2, HEPES 5, K_2ATP 5; pH 7.2 with KOH
cardioplegic solution	NaCl 102, KCl 21.4, $MgCl_2$ 16, Na-lactate 28.7, $CaCl_2$ 2.4, procaine 1; pH 7.4 with NaOH
SRMP solution 1	phenylmethylsulphonic fluoride (PMSF) 1, sucrose 300, piperazine-N,N'-bis(2-ethanesulphonic acid) (PIPES) 20, aprotinin 0.0003, leupeptin 0.001, benzamidine 1, DTT 2.5 (mM); pH 7.4 with KOH
SRMP solution 2	KCl 400, $CaCl_2$ 0.1, EGTA 0.1, PIPES 5, 10% w/v sucrose (mM); pH 7.2 with KOH
SRMP solution 3	KCL 400, PIPES 10 (mM); pH 7.2 with KOH
SRMP solution 4	sucrose 400, HEPES 5 (mM); pH 7.2 with Tris
SRMP solution 5	KCL 150, $MgCl_2$ 0.5, HEPES 10 (mM); pH 7.2 with KOH
GluIM	K gluconate 250, N-methylglucamine 250, HEPES 20, $MgCl_2$ 1, MgATP 0.5, phosphocreatine 10 (mM); creatine phosphokinase 10 (units ml^{-1}); pH 7.2 with glacial acetic acid

Table 2.3: Additional buffers

NAADP-AM was synthesised in Grant Churchill's lab by the author of this thesis and by Ana Tusie.

β-NGD, bafilomycin-A1, creatine phosphokinase (from rabbit muscle), (–)-isoprenaline hydrochloride, PKA catalytic subunit (from bovine heart), saponin (from quillaja bark), streptokinase (from β-haemolytic Streptoccocus) were purchased from Sigma (USA).

Collagenase (type-II) was purchased from Worthington Biochemical (USA).

DMEM was purchase from Life Technologies (USA).

Fluo-4 salt and Fluo-5F AM was purchased from Molecular Probes (USA).

2.20 Statistical analysis

All statistical comparisons involving continuous data were made by two-tailed Student's t-tests. When more than two comparisons were made, an analysis of variance (ANOVA) was used, followed by Bonferroni's or Dunnett's post-hoc tests as appropriate. Mann-Whitney test and Fisher's exact test were used to compare arrhythmogenocity score and categorical data respectively, in the arrhythmias studies. An one sample t-test was used for statistical analysis in **Figure 30F**. All data are expressed as the mean ± SEM.

Chapter 3

The NAADP Signalling Pathway Contributes to β-Adrenoceptor-Mediated Positive Inotropy in Mouse Ventricular Cardiomyocytes

Part of the material presented in this chapter was published in Journal of Biological Chemistry (Capel et al. 2015). © the American Society for Biochemistry and Molecular Biology.

3.1 Background

In both guinea pig ventricular and atrial cardiomyocytes, NAADP has been shown to be a positive inotropic agent by Terrar's group (Macgregor et al., 2007a; Collins et al., 2011). It was shown that the photorelease of NAADP from caged-NAADP increased the amplitudes of the action potential triggered-Ca^{2+} transient of these cardiomyocytes while the superfusion of the cell-permeant NAADP-AM increased the frequency and amplitudes of Ca^{2+} sparks as well as the amplitudes of contraction. In these experiments, the intracellular application of NAADP also increased the level of Ca^{2+} in the SR. The positive inotropic effects mediated by NAADP were inhibited by bafilomycin-A1, ryanodine, and thapsigargin, consistent with a cross-talk between lysosomes and SR.

In addition, roles of NAADP in basal EC coupling have been studied extensively (Macgregor et al., 2007a; Collins et al., 2011). Under basal conditions where no drugs were applied, the patch application of a high, inactivating concentration of NAADP (1 mM) was reported to decrease the amplitudes of Ca^{2+} transients in ventricular cardiomyocytes while superfusion of bafilomycin-A1 (100 nM, to interfere with lysosomal function) decreased the amplitudes of Ca^{2+} transients in atrial cardiomyocytes. These results suggested that the resting concentration of NAADP was at a suprathreshold level.

The observations that application of intracellular NAADP further increased the amplitudes of Ca^{2+} transient suggested that the endogenous NAADP-mediated positive inotropy has not reached its ceiling effect (i.e. the maximal effect of this pathway requires the presence of extra NAADP) (Macgregor et al., 2007a). This suggests that at a given time and upon given a stimulus, the NAADP level can be

tuned to alter the properties of EC coupling. This hypothesis is supported by two substantial pieces of evidence: i) Following the application the β-adrenoceptor agonist, isoprenaline (at 60 nM for 5 min or at 100 nM for 1 min), the level of NAADP in whole heart was reported to be increased by approximately 2-fold (Macgregor et al., 2007a; Lewis et al., 2012), ii) In both guinea pig ventricular and atrial myocytes, the effects of isoprenaline-induced positive inotropy were blunted when the NAADP signalling pathway was suppressed (Capel et al., 2015).

Ned-19, which is structurally similar to NAADP, is an NAADP antagonist (Naylor et al., 2009). Like the bafilomycin-A1 (1 μM) or high concentration of NAADP (1 mM), Ned-19 was shown to have an inhibitory effect on the NAADP signalling pathway of guinea pig ventricular and atrial myocytes (Capel et al., 2015). The application of Ned-19 (1 μM) reduced the effect of isoprenaline-induced increase in the Ca^{2+} transients amplitudes of these myocytes.

While these experiments have shed light on the contribution of NAADP to EC coupling in both the absence and presence of β-adrenoceptor stimulation, little was known about the mechanistic details of these pathways. Endolysosomal TPCs are the most widely discussed candidate for the NAADP receptor. It is hypothesised that TPCs are the channel responsible for the NAADP-regulated Ca^{2+} release. The genetic KO of TPCs has been shown to cause NAADP-insensitivity in various tissues (see section 1.3.4 on page 41). In cardiac tissue, the KO of TPC2 but not TPC1, was shown to abolish the NAADP-mediated positive inotropy (Elson et al., 2010).

Most if not all of the experiments mentioned above were carried out in guinea pig cardiac myocytes. The aim of the experiments presented in this chapter is therefore to use an NAADP-insensitive TPC2 KO mouse model ($Tpcn2^{-/-}$) to investigate whether the NAADP signalling pathway plays a role in

β-adrenoceptor-mediated positive inotropy in mice. Further aims are to determine mechanistically how activation of the NAADP signalling pathway contributes to β-adrenoceptor signalling.

3.2 Methods

The methods used to carry out experiments in this chapter are described in detail in Chapter 2. C57BL6 mice (aged 12-20 weeks) were killed by cervical dislocation and their hearts were rapidly excised. Ventricular cardiomyocytes were isolated from a type-II collagenase-digested Langendorff-perfused heart. Cardiomyocytes were left to settle onto a coverslip attached to a perspex bath, and superfused with PSS (95% O_2/ 5% CO_2, 36^{o}C, pH 7.4) or with Tyrode solution (HEPES buffered, 36^{o}C, pH 7.4). NAADP-AM was applied to ventricular cells via a rapid switch system, while isoprenaline was applied through the bulk superfusion. In the experiments where bafilomycin-A1 and KN93 were used, the cells were preincubated with bafilomycin-A1 (10 μM), KN93 (1 μM) or with PSS containing an equivalent amount of the solvent, DMSO, for 30 minutes before they were left to settle on a coverslip.

For the measurement of Ca^{2+} transients, ventricular cardiomyocytes were incubated with Fluo-5F-AM (10 μM) for 20 – 30 minutes and electrically field stimulated to evoke action potentials at 1 Hz. Global Ca^{2+} transients were recorded with a Leica line scanning microscope (450 lines per second) or a Nipkow spinning disc confocal microscope (50 frames per second).

For the measurement of L-type Ca^{2+} currents, cardiac myocytes were patched in the whole cell configuration using glass microelectrodes. Electrophysiological

experiments were carried out using an Axoclamp 2 amplifier. L-type Ca^{2+} currents were activated by 200 ms step depolarisations from a holding potential of -40 mV to 0 mV. Data analysis was performed using Clampfit 9.2 and Prism 6 software.

3.3 Results

3.3.1 The application of NAADP-AM increased Ca^{2+} transient amplitudes in mouse ventricular cardiomyocytes

NAADP is a polar molecule with negative charges, rendering it cell-impermeant. In order to apply NAADP intracellularly, a cell-permeant analogue of NAADP, NAADP-AM was synthesised (for methods, see Parkesh et al. 2008). Once NAADP-AM crosses the cell membrane, the cytosolic liberation of NAADP can be achieved when the ester bonds are cleaved by intracellular esterases in the cells. Ventricular cardiomyocytes isolated from mouse hearts were incubated with Fluo-5F-AM (20 μM) and electrically paced using field stimulation at 1 Hz. 5 min exposure to NAADP-AM (240 nM) through a rapid switch system resulted in a significant increase in the amplitude of Ca^{2+} transients in these ventricular myocytes, compared with the pre-exposure level, while treatment with DMSO did not. (NAADP-AM: 16.4 $\pm$ 4.9 %, n = 20 myocytes; DMSO: 2.8 $\pm$ 1.2 %, n = 5 myocytes; 5 min after NAADP-AM addition, $p < 0.05$, **Figure 3**). This is consistent with the observations that photorelease of NAADP increased Ca^{2+} transients in guinea pig ventricular cardiomyocytes (Macgregor et al., 2007a).

NAADP-AM is a convenient tool for intracellular application of NAADP as

compared to the photorelease of caged-NAADP, as it does not require one to introduce the analogue of NAADP through a whole-cell patch. However, the photorelease of NAADP from a caged compound provides a better control of the release of NAADP in terms of the temporal aspect and magnitude, while the intracellular application of NAADP through the NAADP-AM depends on the de-esterification NAADP-AM, which in turn relies on the enzymatic activities of esterases inside the cells.

Figure 3

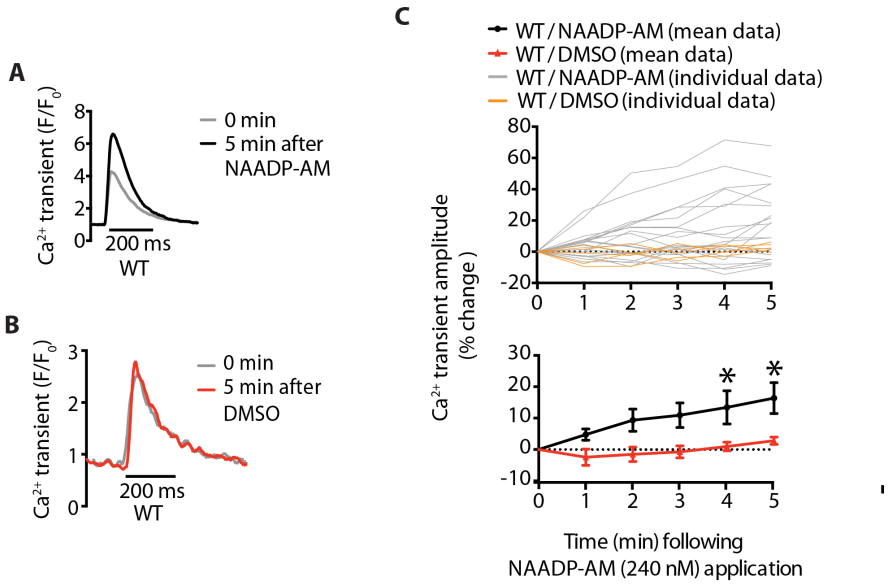


Figure 3: Effect of NAADP-AM on Ca^{2+} transient amplitudes of paced ventricular myocytes from mice

A shows superimposed Ca^{2+} transients before and during NAADP-AM application (240 nM, 5 min) in paced myocytes from WT mice.
B shows superimposed Ca^{2+} transients before and during DMSO application (0.1%, 5 min) in paced myocytes from WT mice.
C shows the individual Ca^{2+} transient amplitudes plots (upper panel) and average percentage increase in Ca^{2+} transient amplitudes (lower panel, relative to measurements at time 0) recorded in paced mouse ventricular myocytes over time after NAADP-AM/DMSO application (NAADP-AM, n = 20 myocytes; DMSO, n = 5 myocytes).

Note: Myocytes were preincubated with Fluo-5F-AM for 20 – 30 min, electrically paced at 1 Hz and imaged with a line scanning confocal microscope (36 °C and pH 7.4). Images were analysed with ImageJ and Python. There was no observed significant increase in the amplitude of Ca^{2+} transients in myocytes treated with DMSO. 50% of cardiac myocytes elicit a positive response upon NAADP-AM application (positive response was assumed when the increase in Ca^{2+} transient amplitudes was $\geq$ 15%) and none of the cardiac myocytes showed such as response upon DMSO application. Numerical data in lower panel of **C** are reported as the mean ± SEM. * denotes $p < 0.05$ relative to measurement at 1 min, determined by Student's t-test.

3.3.2 NAADP-mediated positive inotropy was abolished in ventricular myocytes from *Tpcn2*$^{-/-}$ mice

It has been reported that functional TPCs are essential for the NAADP-regulated Ca^{2+} release from lysosomes in pancreatic β cells (Calcraft et al., 2009). Here, the expression of TPC2 was shown to be pivotal for the observed NAADP-AM-mediated increase in Ca^{2+} transient amplitude (see section 3.3.1) in electrically-paced ventricular cardiomyocytes. Application of NAADP-AM (240 nM) for 5 min resulted in an increase in the Ca^{2+} transient amplitudes in electrically stimulated (1 Hz) ventricular myocytes from WT mice but not *Tpcn2*$^{-/-}$ mice, as shown in **Figure 4** (WT :16 ± 5%; *Tpcn2*$^{-/-}$: -6 ± 4%; 5 min after NAADP-AM

addition; n = 20 myocytes for both groups; $p < 0.05$). This observation is interpreted as the expression of functional *Tpcn2* being essential for the NAADP signalling pathway in ventricular myocytes, and therefore *Tpcn2*$^{-/-}$ mice can be used as NAADP-impaired models to investigate the contribution of the NAADP signalling pathway during activation of the β-adrenoceptor pathway in the heart.

Figure 4

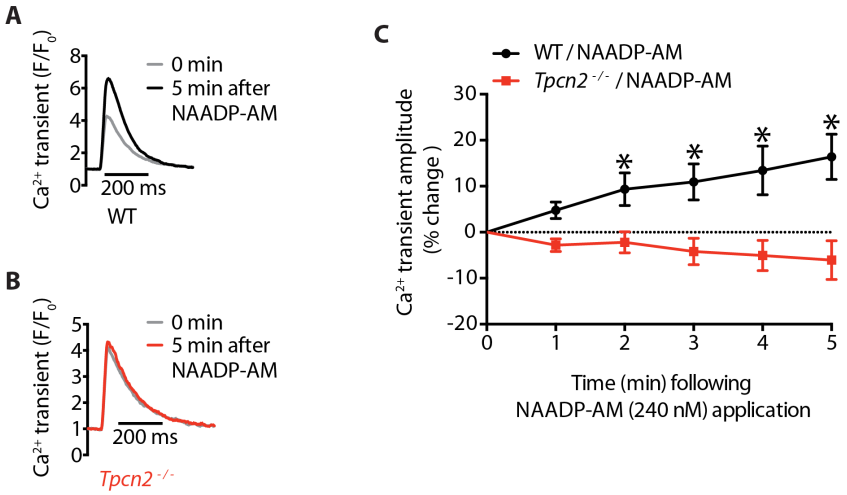


Figure 4: Lack of NAADP-AM effect on Ca^{2+} transient amplitude of paced ventricular myocytes from mice without functional TPC2 protein (*Tpcn2*$^{-/-}$)

A shows superimposed Ca^{2+} transients before and during application of NAADP-AM (240 nM, 5 min) in ventricular myocytes from WT mice.
B shows superimposed Ca^{2+} transients before and during application of NAADP-AM (240 nM, 5 min) in ventricular myocytes from *Tpcn2*$^{-/-}$ mice.
C shows the mean percentage increase (relative to measurements at time 0) in Ca^{2+} transient amplitudes recorded in paced WT and *Tpcn2*$^{-/-}$ ventricular myocytes over time after the application of NAADP-AM (n = 20 myocytes for both groups).

Note: Myocytes were preincubated with Fluo-5F-AM for 20 – 30 min, electrically paced at 1 Hz and imaged with a line scanning confocal microscope (36 °C and pH 7.4). Images were analysed with ImageJ and Python. Numerical data in **C** are reported as the mean ± SEM. * denotes $p < 0.05$ relative to *Tpcn2*$^{-/-}$, determined by multiple t-test with Bonferroni's correction.

3.3.3 *Tpcn2*$^{-/-}$ mice showed a blunted increase in Ca^{2+} transient amplitudes during β-adrenoceptor activation

To evaluate the contribution of the NAADP signalling pathway towards β-adrenoceptor-mediated positive inotropy, the peak percentage increase of the Ca^{2+} transient amplitudes upon addition of isoprenaline (with respect to the Ca^{2+} transient amplitude before the addition of isoprenaline) was compared between WT mice and *Tpcn2*$^{-/-}$ mice. Isoprenaline (3 nM), an agonist of β-adrenoceptors, was applied to electrically paced, Fluo-5F-AM-loaded ventricular cardiomyocytes isolated from both WT and *Tpcn2*$^{-/-}$ hearts. **Figure 5B** shows that paced *Tpcn2*$^{-/-}$ cardiomyocytes had a significantly milder response to addition of isoprenaline (3 nM) in terms of the increase in Ca^{2+} transient amplitudes (*Tpcn2*$^{-/-}$: $57 \pm 17\%$; WT: $123 \pm 24\%$; n = 15 myocytes for both group; $p < 0.05$; 4 min after isoprenaline addition). This observation is consistent with the blunted increase in contraction amplitudes upon the application of isoprenaline in *Tpcn2*$^{-/-}$ in both Langendorff heart and single cell studies (Capel et al., 2015). The blunted response to isoprenaline application was interpreted to be a consequence of the lack of functional TPC2 proteins and therefore the lack of functional NAADP signalling pathways. These observations are consistent with the findings that have been reported in guinea pig cardiomyocytes (Capel et al., 2015) and mouse cardiomyocytes stimulated with isoprenaline in the presence of Ned-19 or bafilomycin-A1 (see section 3.3.4 on page 91), agents that suppress the NAADP pathway . These observations together support the hypothesis regarding a non-redundant role of the NAADP signalling pathway in the β-adrenoceptor-mediated positive inotropy.

Figure 5

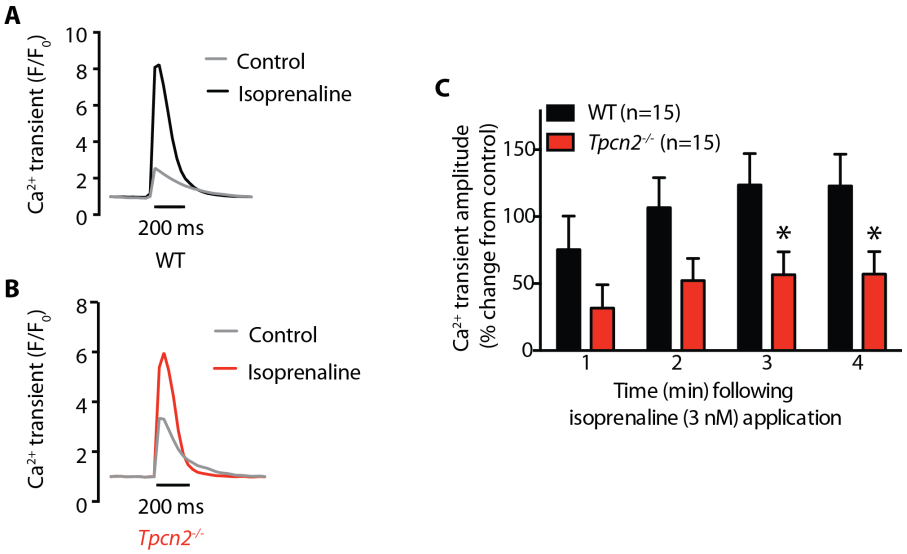


Figure 5: The effect of β-adrenoceptor stimulation on Ca^{2+} transients evoked by electrical stimulation were smaller in ventricular myocytes from *Tpcn2*$^{-/-}$ hearts as compared to those from WT hearts

A shows superimposed Ca^{2+} transients before and during application of isoprenaline (3 nM, 4 min) in myocytes from WT mice.
B shows superimposed Ca^{2+} transients before and during application of isoprenaline (3 nM, 4 min) in myocytes from *Tpcn2*$^{-/-}$ mice.
C shows the mean percentage increase (relative to measurements at time 0) in Ca^{2+} transient amplitudes recorded in paced WT and *Tpcn2*$^{-/-}$ ventricular myocytes over time after the application of isoprenaline (n = 15 myocytes for both data sets).

Myocytes were preincubated with Fluo-5F-AM for 20 – 30 min, electrically paced at 1 Hz and imaged with a spinning disk confocal microscope (36 °C and pH 7.4). Images were analysed with ImageJ and Python. Numerical data in **C** are reported as the mean ± SEM. * denotes $p < 0.05$ relative to the WT control, determined by Student's t-test.

3.3.4 Bafilomycin-A1 reduced the increase in Ca^{2+} transients amplitude of mouse single ventricular cardiomyocytes during β-adrenoceptor activation

Bafilomycin-A1 is a potent vacuolar H^+-ATPase inhibitor that has been shown to antagonise the NAADP signalling pathway (Crider et al., 1994; Churchill et al., 2002; Collins et al., 2011). It was postulated that the Ca^{2+} concentration within the lysosome is maintained via Ca^{2+} proton exchangers. Bafilomycin-A1 disrupts the pH gradient and subsequently causes alkalinisation of acidic lysosomes through its inhibition on the vacuolar proton pumps (Collins et al., 2011). This ultimately affects the Ca^{2+} refilling process and thus abolishes the NAADP-regulated Ca^{2+} release from lysosomes (Calcraft et al., 2009). Indeed, bafilomycin-A1 has been shown to inhibit effects of NAADP in the heart (Macgregor et al., 2007b; Collins et al., 2011). In **Figure 6A** and **B**, preincubation with bafilomycin-A1 (10 μM) resulted in weaker Ca^{2+} transient amplitudes of during β-adrenoceptor activation (without bafilomycin-A1: 5.7 $\pm$ 0.3 (F/F_0), n = 21, 84 $\pm$ 12% increase upon isoprenaline addition , n = 10; with bafilomycin-A1: 4.4 $\pm$ 0.2 (F/F_0), n = 25, 42 $\pm$ 8% increase upon isoprenaline addition , n = 15; n = number of myocytes, $p < 0.05$; **Figure 6A** and **B**). Representative records are shown in **Figure 6C**. This observation further supports a role for the NAADP signalling pathway in mediating β-adrenoceptor-associated positive inotropy in the heart.

Figure 6

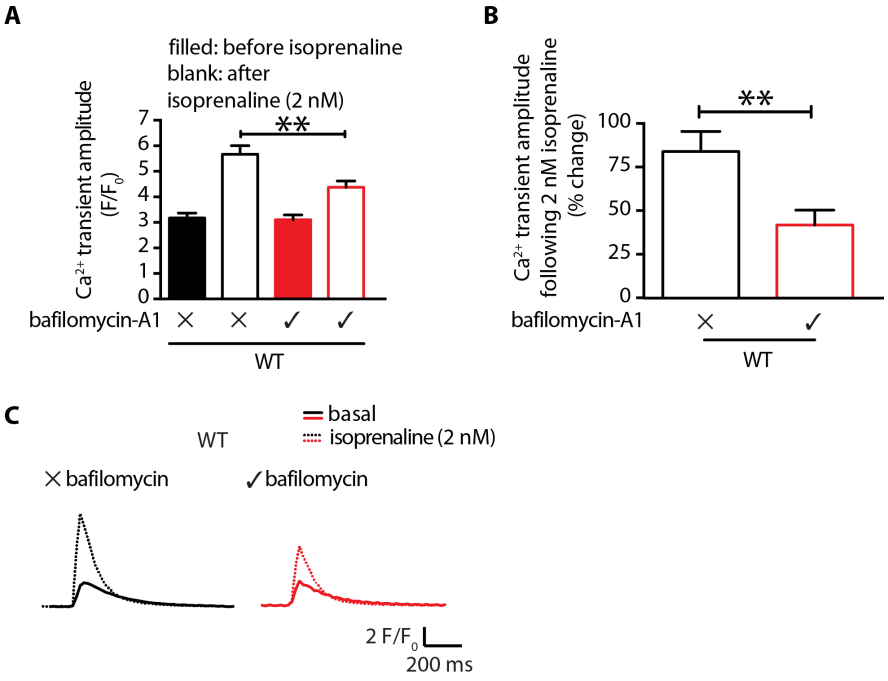


Figure 6: Pretreatment with bafilomycin-A1 blunted the Ca^{2+} transient amplitudes of single ventricular cardiomyocytes from mice during β-adrenoceptor activation

A shows the mean Ca^{2+} transient amplitude before and after the addition of 2 nM isoprenaline of WT single ventricular cardiomyocytes pretreated either with bafilomycin-A1 (10 μM) or DMSO (n = 21 – 25 cardiomyocytes).
B shows the mean percentage increase (relative to measurements at time 0) in Ca^{2+} transient amplitudes recorded in paced WT single ventricular cardiomyocytes pretreated either with bafilomycin-A1 (10 μM) or DMSO (n = 10 – 15 cardiomyocytes).
C shows the representative traces of Ca^{2+} transients before and after the addition of 2 nM isoprenaline of WT single ventricular cardiomyocytes pretreated either with bafilomycin-A1 (10 μM) or DMSO.

Note: Myocytes were electrically paced at 1 Hz, superfused with Tyrode solution and imaged with a spinning disk confocal microscope (after incubation with Fluo-5F-AM and bafilomycin-A1/DMSO for 20 – 30 min) at 36 °C and pH 7.4. Fluorescence data were analysed with Andor software. Numerical data in **A** and **B** are reported as the mean ± SEM. ** denotes $p < 0.01$ relative to the DMSO control, determined by Student's t-test.

3.3.5 Activation of the NAADP/TPC pathway did not alter the amplitude of L-type Ca^{2+} currents of mouse ventricular myocytes

In guinea pig ventricular myocytes, the application of intracellular NAADP failed to increase the L-type Ca^{2+} currents and Ned-19 that antagonises NAADP also failed to decrease the L-type Ca^{2+} currents (Macgregor et al., 2007a; Capel et al., 2015). Consistent with the observations in guinea pig myocytes, the administration of isoprenaline increased the amplitude of L-type Ca^{2+} currents of ventricular cardiomyocytes from *Tpcn2*$^{-/-}$ and WT mice in a comparable manner (*Tpcn2*$^{-/-}$: 81 ± 15%; WT: 78 ± 6%; maximum percentage increase within 5 min exposure to 3 nM isoprenaline; n = 7 myocytes for both sets; p = 0.88; **Figure 7**). These observations suggest that under both conditions with and without β-adrenoceptor activation, the positive inotropic effect mediated by the TPC2-regulated NAADP signalling pathway is unlikely to be through an augmentation of Ca^{2+} influx through L-type Ca^{2+} channels.

Figure 7

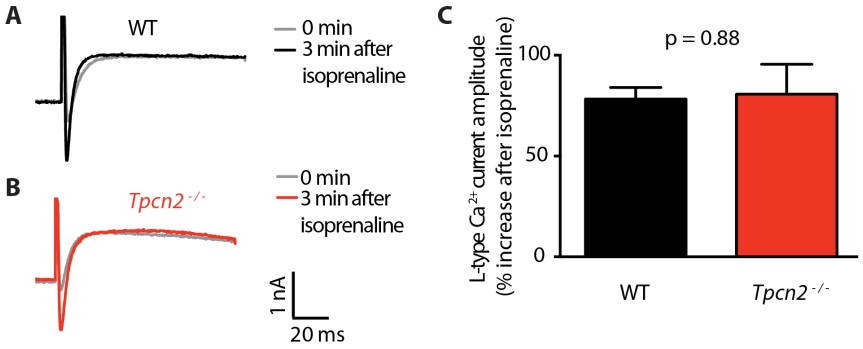


Figure 7: The post-isoprenaline amplitude of L-type Ca^{2+} currents was comparable in ventricular cardiomyocytes from *Tpcn2*$^{-/-}$ and WT mice

A shows superimposed traces of L-type Ca^{2+} current before and during application of isoprenaline (3 nM, 3 min) in myocytes from WT mice.
B shows superimposed traces of L-type Ca^{2+} current before and during application of isoprenaline (3 nM, 3 min) in myocytes from *Tpcn2*$^{-/-}$ mice.
C shows the mean of maximum percentage increase of amplitude of L-type Ca^{2+} currents (relative to measurements at time 0) recorded in WT and *Tpcn2*$^{-/-}$ ventricular myocytes over time after application of isoprenaline (n = 7 myocytes for both groups, $p > 0.05$).

Note: Myocytes were superfused with PSS (36 °C and pH 7.4) and L-type Ca^{2+} currents were activated by 200 ms step depolarisations from a holding potential of -40 mV to 0 mV. Numerical data in **C** are reported as the mean ± SEM. Student's t-test was used to compare the difference of means.

3.3.6 KN-93, an inhibitor of CaMKII, abolished the NAADP-AM-induced increase in Ca^{2+} transient amplitudes

KN-93 (1 μM), an inhibitor of CaMKII, abolished the NAADP-AM (240 nM)-induced increase in Ca^{2+} transient amplitudes in WT mice (NAADP-AM: 13 ± 5%, n = 20 myocytes; NAADP-AM + KN-93: -0.8 ± 2%, n = 9 myocytes; 4 min after NAADP-AM addition; $p < 0.05$; **Figure 8**). Inhibition of CaMKII in guinea pig ventricular and atrial myocytes with KN-93 (but not KN-92) and AIP respectively, also blocked the effect of photorelease of caged-NAADP on Ca^{2+} transient amplitudes (Capel et al., 2015). CaMKII, which is activated by high concentration of localised Ca^{2+} (Maier and Bers, 2007), could be inducing phosphorylation at the Thr 17 site of phospholamban thus removing its inhibition on SERCA pumps, leading to an enhanced SERCA activity and therefore an increase in the SR Ca^{2+} load (as reported by (Macgregor et al., 2007a; Collins et al., 2011). It is possible that CaMKII is one of the downstream targets of the NAADP signalling pathway, which amplifies the Ca^{2+}

intake of SR upon the activation of CaMKII by the NAADP-mediated Ca^{2+} release, ultimately leading to a heightened global Ca^{2+} transient amplitude.

Figure 8

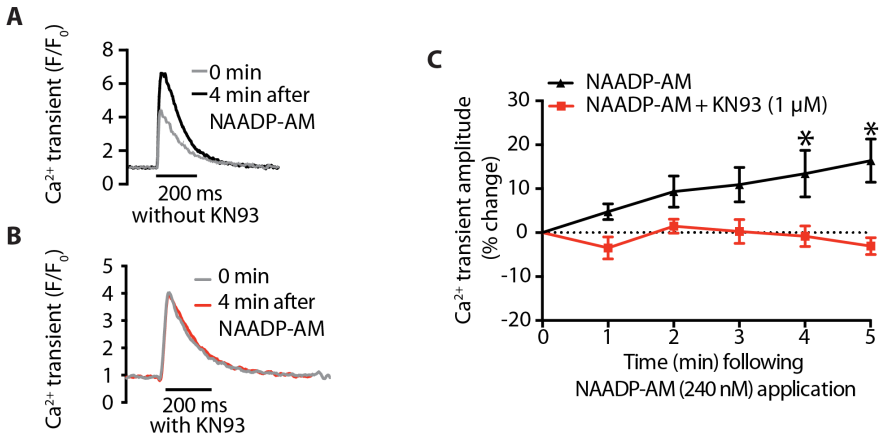


Figure 8: NAADP-mediated increase in Ca^{2+} transient amplitude of paced ventricular cardiomyocytes is dependent on functional CaMKII

A shows superimposed Ca^{2+} transients before and during application of NAADP-AM (240 nM, 4 min) in ventricular myocytes in the absence of KN93.
B shows superimposed Ca^{2+} transients before and during application NAADP-AM (240 nM, 4 min) in ventricular myocytes preincubated with 1 μM KN93.
C shows the mean percentage increase (relative to measurements at time 0) in Ca^{2+} transient amplitudes recorded in paced mouse ventricular myocytes over time after application of NAADP-AM with and without the preincubation of 1 μM KN93 (NAADP-AM, n = 20 myocytes; NAADP-AM + KN93, n = 9 myocytes).

Note: Myocytes were preincubated with Fluo-5F-AM and/or KN93 (1 μM) for 20 – 30 min, electrically paced at 1 Hz and imaged with a line scanning confocal microscope (36 °C and pH 7.4). Images were with ImageJ and Python. Numerical data in **C** are reported as the mean ± SEM. * denotes $p < 0.05$ relative to the control (without KN93), determined by Student's t-test.

3.3.7 An active NAADP signalling pathway was not detected in mouse ventricular cardiomyocytes under conditions where β-adrenoceptors were not stimulated

Under conditions where β-adrenoceptors were not stimulated, exposure of guinea pig ventricular myocytes to either bafilomycin-A1 or self-inactivating concentration of NAADP (0.1 or 1 mM) caused a reduction in Ca^{2+} transient amplitudes (Macgregor et al., 2007a). Similarly in electrically paced guinea pig atrial myocytes, superfusion of bafilomycin-A1 reduced the Ca^{2+} transient amplitudes (Collins et al., 2011). This suggested that there might be a constitutively active NAADP signalling pathway in resting condition where β-adrenoceptors are not stimulated. This "background" NAADP signalling pathway is likely to play a role in the cardiac EC coupling. Unexpectedly, the Ca^{2+} transient amplitude of WT and *Tpcn2*$^{-/-}$ mice were comparable in the absence of any β-adrenoceptor stimulation (*Tpcn2*$^{-/-}$: 4.7 $\pm$ 0.3 (F/F_0), n = 39 myocytes; WT: 4.2 $\pm$ 0.2 (F/F_0), n = 38 myocytes; p = 0.13; **Figure 9**). Consistent with this finding, the Ca^{2+} spark frequency and contraction magnitude were not significantly different between mouse ventricular cardiomyocytes from WT and *Tpcn2*$^{-/-}$ mice when β-adrenoceptors were not stimulated (Elson, 2011). Furthermore, preliminary data also showed that Ned-19, an NAADP antagonist did not reduce the Ca^{2+} transient amplitude of the mouse ventricular cardiomyocytes (Elson, 2011). As KN93 was established to inhibit the NAADP action in mouse myocytes (see section 3.3.6 on page 94), the observation showing comparable Ca^{2+} transient amplitudes with and without the presence of KN93 in the WT animals provides further support of the hypothesis regarding the lack of a constitutively active NAADP signalling pathway in mouse ventricular myocytes (WT: 4.2 $\pm$ 0.2 (F/F_0), n = 38 myocytes; KN93: 3.3 $\pm$ 0.2 (F/F_0), n = 9

myocytes; p = 0.13; **Figure 9**). In section 3.3.4, it was also demonstrated that the resting electrically triggered Ca^{2+} transients were not significantly different in mouse myocytes with or without preincubation of bafilomycin-A1 (without bafilomycin-A1: 3.2 ± 0.2 (F/F_0), n = 21 myocytes; with bafilomycin-A1: 3.1 ± 0.2 (F/F_0), n = 25 myocytes; p = 0.80; **Figure 6A**), in contrast to experiments performed in guinea pig myocytes (Macgregor et al., 2007a; Collins et al., 2011). Possible explanations for these different findings from observations in guinea pig cardiomyocytes and mouse cardiomyocytes are species difference and compensatory mechanisms arising from genetic KO (see discussions in section 3.4.3 on page 111).

Figure 9

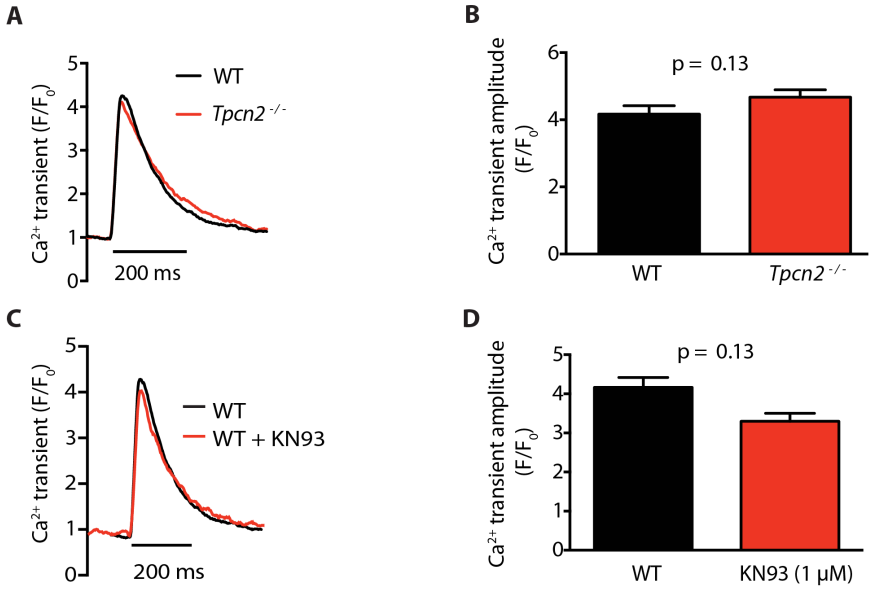


Figure 9: Ca^{2+} transient WT ventricular cardiomyocytes were comparable to those of myocytes lacking TPC2 and to those of myocytes pretreated with KN93

A shows superimposed basal Ca^{2+} transients of ventricular myocytes from WT and *Tpcn2*$^{-/-}$ mice.
B shows the mean of basal Ca^{2+} transient amplitudes of ventricular myocytes from WT (n = 38 myocytes) and *Tpcn2*$^{-/-}$ (n = 39 myocytes) mice.
C shows superimposed Ca^{2+} transients of ventricular myocytes from WT mice in the presence or absence of KN93 (unpaired samples).
D shows the mean of Ca^{2+} transient amplitudes of ventricular myocytes from WT in the presence (n = 9 myocytes) and absence of 1 μM KN93 (n = 38 myocytes).

Note: These Ca^{2+} transient measurements were made in the absence of isoprenaline. Myocytes were preincubated with Fluo-5F-AM and/or KN93 (1 μM) for 20 – 30 min, electrically paced at 1 Hz and imaged with a line scanning or spinning disk confocal microscope (36 °C and pH 7.4). Images were analysed with ImageJ and Python. Numerical data are reported as the mean ± SEM. Student's t-test was used to compare the difference of means.

3.4 Discussion

3.4.1 Does the increased level of NAADP during β-adrenoceptor stimulation contribute to the cardiac fight or flight response?

The conventional view of the fight or flight response of the heart heavily focussed on the roles of the PKA/cAMP pathway. The activation of this pathway, which is initiated by the stimulation of β-adrenoceptors/adenylyl cyclases, leads to enhanced activity of various channels/enzymes including RyRs, SERCA and L-type Ca^{2+} channels. In the past, it has been shown that levels of cADPR and NAADP increased during β-adrenoceptor stimulation (Macgregor et al., 2007a; Lewis et al., 2012; Gul et al., 2016). Both cADPR and NAADP have been shown to be potent endogenous Ca^{2+}-mobilising agents across the taxonomic kingdoms (see review by Lee 2012). Evidence in this chapter supports a role of this increased level of NAADP in the β-adrenoceptor-mediated positive inotropy.

Firstly, in this chapter, the intracellular application of NAADP through a cell-permeant precursor, NAADP-AM, was shown to increase the Ca^{2+} transient amplitudes of mouse ventricular cardiomyocytes. The photorelease of caged-NAADP has also been shown to give rise to a similar effect in ventricular cardiomyocytes from guinea pig hearts (Macgregor et al., 2007a). In addition to showing NAADP is a positive inotropic agent, evidence presented here shows that mouse models with impaired NAADP signalling pathway (cardiomyocytes from *Tpcn2*$^{-/-}$ mice and/or myocytes preincubated with bafilomycin-A1) have significantly blunted responses to the stimulation of the β-adrenoceptor pathway,

both in the aspects of increased Ca^{2+} transient amplitude (from this thesis) and cardiac contraction (Capel et al., 2015). Pharmacological blockade of the NAADP signalling pathway using bafilomycin-A1 and Ned-19 in guinea pig ventricular and atrial cardiomyocytes during β-adrenoceptor stimulation has also resulted in similar blunted responses (Capel et al., 2015).

One could argue that the genetic KO of *Tpcn2*, the inhibitory effect of bafilomycin-A1 as well as the inhibitory effect of Ned-19 are not specific or limited to the NAADP signalling pathway; the apparent blunted response of cardiomyocytes towards a β-adrenoceptor agonist could be due to a disrupted lysosomal signalling pathway that is not necessarily unique to the NAADP-regulated Ca^{2+} release. In 2009, Calcraft has elucidated the quintessential role of *Tpcn2* in mediating NAADP-regulated Ca^{2+} release (see section 1.3.4 on page 41). In experiments where TPC2 channels were incorporated into artificial lipid bilayer, it has been showed that NAADP increases the opening probability of TPC2 and Ned-19 (1 μM) decreases the opening probability of TPCs (Pitt et al., 2010). Despite compiling evidence supporting the hypothesis that *Tpcn2* is a NAADP receptor, this hypothesis was challenged by several reports (see section 1.3.4 on page 41). For example, Wang et al. (2012) performed electrophysiological experiments on vacuolin-enlarged lysosomes, showing current carried by TPCs are not sensitive to the presence of NAADP and is a predominantly Na^{+} rather than Ca^{2+} current. However, these experiments are not without their limitations, and this topic was reviewed by Morgan and Galione (2014).

Although it was shown in Calcraft's paper that an increase in TPC expression led to an increase in NAADP binding (measured by radioligand binding assay), it was later reported that direct binding of NAADP to TPC was not detected with

the photoaffinity labelling technique using 5-azido-NAADP ([^{32}P-5N$_3$]NAADP) (Lin-Moshier et al., 2012; Walseth et al., 2012). The existence of possible NAADP binding proteins was proposed in these two reports. The author of this thesis believes that it is rare in the biological system that a molecule only interacts with one group of specific proteins. A figure (**Figure 10**) extracted from Lin-Moshier's paper showed that displacing radioactive (hot) NAADP with non-radioactive (cold) NAADP resulted in a disappearance of not just a single but several bands (Lin-Moshier et al., 2012). Moreover, a single band is not necessarily restricted to a single protein; in most cases, a single band contains multiple proteins.

Figure 10

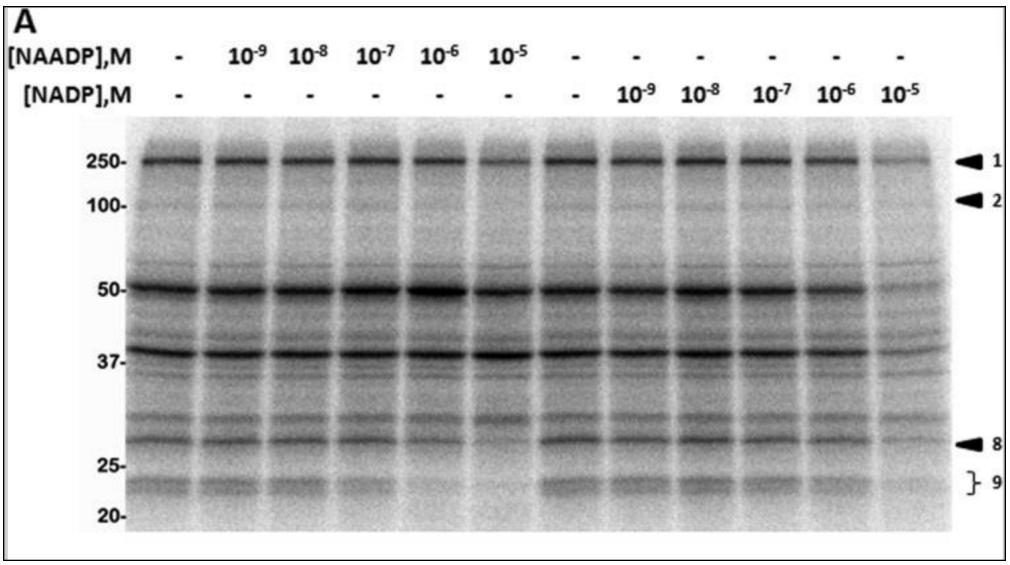


Figure 10: NADP and NAADP displacement of photoaffinity radioactive 5-azido-NAADP labelling in SKBR3 whole cell lysates

A Representative photoaffinity labelling image showing effects of increasing concentrations of NAADP (lanes 2 to 6) and NADP (lanes 8 to 12) on the photoaffinity labelling of radioactive 5-azido-NAADP. Lanes 1, 2, 8 and 9 showed a decrease in the density radioactive label, which was dependent on the concentration of non-radioactive NAADP or NADP.

Note: **Figure 10** was originally published in Journal of Biological Chemistry. (Lin-Moshier et al., 2012) © the American Society for Biochemistry and Molecular Biology.

An example of a substance binding to multiple proteins is noradrenaline, which is known to have a high affinity towards α-adrenoceptors, but does bind to β-adrenoceptors and is sequestered into the synapses through various transporters and degraded by various enzymes. Noradrenaline interacts with many other proteins others than its "true" receptor. NAADP could also have interactions with other proteins such as enzymes responsible for its synthesis and degradation, active transporters and channels. It is important to investigate whether this presence or absence of NAADP-binding protein is pivotal for the observed NAADP-regulated Ca^{2+} release. If NAADP-binding proteins are indeed a determinant for NAADP-regulated Ca^{2+} release, then the interpretation of the experimental results from single channel recordings, lysosomal patching, heterologous expression of TPC on cell-lines (see section 1.3.4 on page 41) will have to be reconsidered based on whether functional NAADP-binding proteins were preserved in these models.

A less likely possibility would be the "true" receptor responsible for NAADP-regulated Ca^{2+} release has a lower binding affinity for NAADP that could be masked in the techniques used. The fact that binding of 5-azido-NAADP ([^{32}P-5N$_3$]NAADP) can be displaced by increasing amount of NAADP (as well as NADP) only showed that these molecules have overlapping binding targets, but it is important to note that whether quantitative and qualitative binding profiles [^{32}P-5N$_3$]NAADP is identical to the native NAADP requires further investigation.

As the lysosomal Ca^{2+} proton exchanger is driven by a proton gradient, bafilomycin-A1 abolishes this Ca^{2+} refilling process by inhibiting the lysosomal proton pumps, and therefore disrupting the pH gradient of the lysosomes (Crider et al., 1994; Churchill et al., 2002; Morgan and Galione, 2007; Collins et al., 2011). It is true that it is not only the Ca^{2+}-proton exchanger is affected by this change in

pH, and many proteins such as receptors and enzymes are pH sensitive. Therefore it is reasonable to propose that the functionality of the NAADP receptor is not the sole protein affected by the alkalinising effect of bafilomycin-A1. Ned-19 is an analogue of NAADP which was shown to inhibit the NAADP-regulated Ca^{2+} release in sea urchin egg homogenates and mammalian cells, at an IC_{50} below 1 μM (Naylor et al., 2009), while up to 100 nM Ned-19 was shown to potentiate opening probability of human TPC2 in single channel experiments (Pitt et al., 2010). Ned-19 was also reported to inhibit the NAADP binding in sea-urchin egg homogenates (Rosen et al., 2009; Naylor et al., 2009). Application of Ned-19 through a patch pipette or directly to a TPC2 channel incorporated on a lipid bilayer has been shown to antagonise the action of NAADP at a concentration of 1 μM (Elson et al., 2016; Capel et al., 2015; Pitt et al., 2010). NAADP actions were also abolished with 10 μM Ned-19 that was applied extracellularly on T-cells (Davis et al., 2012). In several reports, a higher concentration (100 μM) of Ned-19 was applied extracellularly in order to abolish the NAADP signalling pathway (Ruas et al., 2010; Favia et al., 2014; Arredouani et al., 2015; Favia et al., 2016). In cardiomyocytes, 100 μM Ned-19 was shown to decrease SR-content, lower spark frequency, reduce Ca^{2+} transient amplitude and in some cases (30%), it completely eliminated Ca^{2+} transient evoked by electrical stimulation (Davidson et al., 2015). The reduction in spark frequencies, Ca^{2+} transient amplitude, and SR-content support the current proposal regarding the NAADP signalling pathway. However, the observed complete elimination of Ca^{2+} transient could be due to an off-target of this high concentration of Ned-19.

Although the idea of TPC being the NAADP receptor has been challenged and questions have been raised about the specificity of the pharmacological agents, the common consequence that results from the KO of TPCs, application of Ned-19, and

application of bafilomycin-A1 is the disruption of the NAADP signalling pathway. Together with the evidence of NAADP being a positive inotropic agent, the impaired NAADP signalling pathway is likely to account for the blunted β-adrenoceptor response, observed in mouse *Tpcn2*$^{-/-}$ myocytes and cardiomyocytes pretreated with Ned-19 and bafilomycin-A1. Therefore, observations from these experiments are consistent with the hypothesis that endolysosomal NAADP signalling pathway is essential to elicit the maximum positive inotropic effect during activation of β-adrenoceptors.

3.4.2 How does NAADP-regulated Ca^{2+} release give rise to a positive inotropic effect in ventricular cardiomyocyte?

In this chapter, it is shown that the amplitude of the action potential-evoked Ca^{2+} transients of ventricular cardiomyocytes, on average, shows an approximately 15% increase after being superfused with 240 nM NAADP-AM. This increase in the amplitude of Ca^{2+} transients is relatively small compared with the percentage difference of the increase in Ca^{2+} transient amplitudes between the NAADP-insensitive model (*Tpcn2*$^{-/-}$ or bafilomycin-A1 preincubated cardiomyocytes) and the control group (WT mouse cardiomyocytes or DMSO-preincubated cardiomyocytes) during β-adrenoceptor activation (which is approximately 40 – 50%).

The use of an NAADP-AM does not allow a precise control over the final concentration in the cells as the accumulation of intracellular NAADP does not only rely on the permeability of the NAADP-AM, it also depends on the activity of esterases to cleave the NAADP-AM into its active form. The accumulation of the

NAADP could be opposed by the degradation of NAADP by NAADP-degrading enzymes (Schmid et al., 2012). Though the synthesis of NAADP-AM was challenging, the AM-ester form of NAADP provides a convenient way to introduce NAADP into the cytoplasm of cells. This technique has a limited control over the magnitude aspect (the concentration of NAADP introduced), temporal aspect (the time when NAADP is introduced), and the spatial aspect (the locations exposed to NAADP). These aspects are influenced by the amount of NAADP-AM accumulated inside the cell, the enzymatic kinetics of esterases inside the cell, and the distribution of esterases inside the cell. Other methods of applying NAADP intracellularly are the photorelease of caged-NAADP and applying NAADP through patch pipette. These methods have advantages over the superfusion of NAADP-AM in terms of the aspects discussed above. However, these methods tend to be harder in practice as their implementation require some experience with electrophysiology experiments.

While the application of 240 nM NAADP-AM was sufficient to demonstrate the NAADP-mediated increase in Ca^{2+} transient amplitudes and the importance of TPC2 expression for this effect, it was not known whether this concentration of NAADP-AM was sufficient to elicit the maximal effect of NAADP signalling pathway. The photorelease of caged-NAADP (5 μM) in guinea pig myocytes has resulted in a greater increase (40%) in Ca^{2+} transient amplitudes. Although this is a cross-species comparison, it is likely that the maximal effect of NAADP has not been achieved by applying 240 nM NAADP-AM in mouse cardiac myocytes. In addition, since only half of the WT cardiomyocytes had a positive response to application of NAADP-AM, the measurements from non-responding WT cardiomyocytes could lower the mean in the data, resulting in an underestimated effect of NAADP-AM. As whether these cardiomyocytes were not responding due to

the lower dose of NAADP-AM, slower rate of de-esterification and/or other reasons remain to be explored. On the other hand, the 3 nM isoprenaline might have resulted in accumulation of higher concentration of NAADP in the cells, and consequently, the WT and *Tpcn2*$^{-/-}$ show a greater observed difference in Ca^{2+} transient amplitudes. Another consideration is the possibility that there could be complementary effects (positive co-operativity) among NAADP and other molecules and proteins that constitute the β-adrenoceptor pathway, and therefore a simple linear model cannot be assumed. Future work can be carried out to construct the dose response of NAADP-AM and determine maximum of effect of NAADP-AM on the Ca^{2+} transient amplitudes.

Although Nebel et al. (2013) have shown that direct patch application of NAADP to resting mouse ventricular cardiomyocytes triggered Ca^{2+} release, a substantial increase in intracellular Ca^{2+} signal in a non-paced (resting) cardiomyocytes from guinea pig has not been detected (Macgregor, 2014). This could be due to the difference in Ca^{2+} handling of these two species. Guinea pig cardiomyocytes tend to have a smaller Ca^{2+} transient evoked by an action potential after a long resting time (compared to Ca^{2+} transients from steady continuous pacing), while mouse cardiomyocytes tend to have a bigger Ca^{2+} transient evoked by an action potential after a long resting time. This is hypothesised to be the difference in SR Ca^{2+} loading of these two species — ventricular cardiomyocytes from mice, compared to those from guinea pig, are better at retaining Ca^{2+} in SR over time during resting state (personal communication, Derek Terrar).

Macgregor's studies showed that the photorelease of caged-NAADP not only led to an increase in Ca^{2+} transient amplitudes, but also caused an increase in SR Ca^{2+} load of guinea pig cardiomyocytes (Macgregor et al., 2007a). It is possible that this

increase in SR Ca^{2+} load is a prerequisite for the observed increase in Ca^{2+} transient amplitudes. There are several possible routes to achieve an increase in the SR Ca^{2+} load such as i) the increase in Ca^{2+} influx, ii) the decrease in Ca^{2+} efflux, iii) and the increase in Ca^{2+} uptake. It is difficult to address whether the observed increase in Ca^{2+} transient amplitudes and increase in SR Ca^{2+} load are purely due to Ca^{2+} ions from NAADP-sensitive stores being released and transferred to the SR. It is likely that Ca^{2+} ions being released from lysosomes which are found in close proximity to the SR (Aston et al., 2017), like any other homogeneous Ca^{2+} ions will be sequestered by SERCA pumps. However, this process will be competed by various Ca^{2+} uptake mechanisms of nearby mitochondria and lysosomes, leading to a reduced efficiency of Ca^{2+} transfer (to SR). Therefore, it might be insufficient to lead to a substantial increase in Ca^{2+} load in SR.

The data showing the comparable augmentation of L-type Ca^{2+} current by the β-adrenoceptor stimulation in both WT and *Tpcn2*$^{-/-}$ mice indicates that the endolysosomal NAADP signalling pathway does not regulate the properties of the L-type Ca^{2+} current. These experiments also suggested that the integrity of the β-adrenoceptor pathway involving the cAMP/PKA signalling cascade is likely to remain intact in the *Tpcn2*$^{-/-}$ models. Therefore, the apparent difference in Ca^{2+} handling of WT and *Tpcn2*$^{-/-}$ is not likely to arise from the difference in the any alterations of β-adrenoceptors, L-type Ca^{2+} channels or from the difference extent of activation of the cAMP/PKA pathway. This is further confirmed by the observation that the density of β-adrenoceptor was shown to be comparable between these two groups of mice measured from experiments involving Western blots (Aston, 2017).

One interesting hypothesis would be the observed increase in SR Ca^{2+} load (after the intracellular application of NAADP) could be a result of the alteration of SERCA

property, mediated by the NAADP-TPC pathway. Both KN93 and AIP but not KN92 preincubation have been shown to abolish the positive inotropic effect of intracellular application of NAADP in mouse and guinea pig cardiomyocytes (see section 3.3.6 on page 94 and Capel et al., 2015). In other words, the expected NAADP-mediated increase in Ca^{2+} transient amplitude was not observed, in the presence of CaMKII inhibitors. Given that CaMKII is Ca^{2+} sensitive, these observations revealed a possible role of CaMKII as the protein which interacts directly with the NAADP-regulated Ca^{2+} release. Since an increase in SR Ca^{2+} load but not the enhancement of L-type Ca^{2+} current was observed upon intracellular application of NAADP, this NAADP-CaMKII pathway might play a role in amplifying the Ca^{2+} intake into the SR.

Although other possibilities that might result in the increase in SR Ca^{2+} load could not be excluded, the experimental evidence in this chapter is consistent with the following hypothesis: upon activation of β-adrenoceptors, the enzymatic synthesis of NAADP increases and this leads to an increase in the TPC2-sensitive NAADP-regulated Ca^{2+} release from lysosomes; this increase in local Ca^{2+} concentration subsequently activates CaMKII, which in turn carries out phosphorylation on the Thr17 site of phospholamban and removing phospholamban inhibition of SERCA, resulting in an increase in SR Ca^{2+} load. This increase in SR Ca^{2+} load then promotes the increase in Ca^{2+} transient amplitudes, as observed after the addition of intracellular NAADP (for scheme, see Figure **11**). This possible interaction between SR and lysosomal proteins is further corroborated by data from electron microscopy showing lysosomes are found in close proximity (25 nm) to the SR (Capel et al., 2015; Aston et al., 2017).

Although off-target of KN93 has been reported, especially in the context of inhibiting L-type Ca^{2+} channel (Gao et al., 2006) and IP3 receptor (Smyth et al.,

2002), the hypothesis mentioned above is supported by i) the application of AIP that is commonly accepted to be a more specific peptide inhibitor of CaMKII, resulted in the similar observation with the application of KN93 (Capel et al., 2015), ii) and the application of KN92, which is a structural analogue of KN93 that does not inhibit CaMKII, had no effect on the NAADP-mediated increase in Ca^{2+} transient amplitudes (Capel et al., 2015). There is no knowledge to date whether these drugs have an direct inhibitory effect on the NAADP-regulated Ca^{2+} release. Future experiments can be carried out to further evaluate the involvement of CaMKII as a downstream mediator of the NAADP signalling pathway (see section 7.2 on page 233)

Figure 11

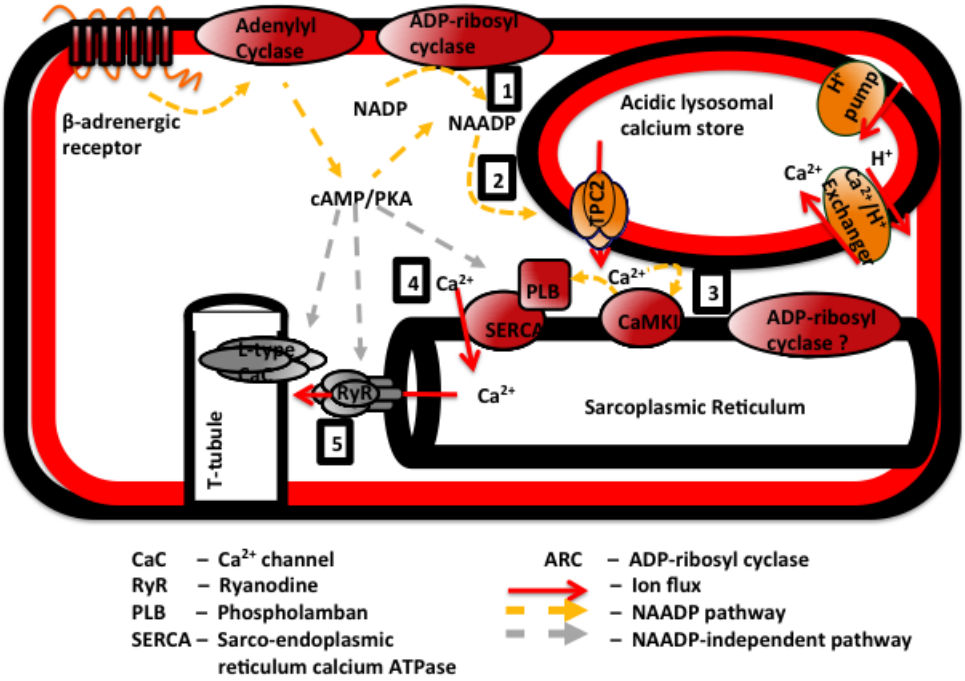


Figure 11: The proposed mechanism for the contribution of the NAADP signalling pathway to the β-adrenoceptor-mediated positive inotropy

1) The activation of the β-adrenoceptor pathway leads to an increase in the level of NAADP in the heart. **2)** NAADP induces Ca^{2+} release from acidic lysosomal stores. (note: this NAADP-mediated release of Ca^{2+} requires functional TPC2 proteins) **3)** CaMKII activated by elevated local Ca^{2+} concentrations phosphorylates phospholamban on the Thr17 site. **4)** Phosphorylated phospholamban removes its inhibition of SERCA, causing an increase in Ca^{2+} uptake into SR, and thus an increase in SR Ca^{2+} load. **5)** This leads to more Ca^{2+} being released during each Ca^{2+}-induced Ca^{2+} release event, thus giving rise to a positive inotropic effect.

3.4.3 Is the NAADP signalling pathway constitutively active under the condition when β-adrenoceptors are not stimulated?

In the guinea pig atrial and ventricular cardiac myocytes, the impairment of the NAADP pathway using bafilomycin-A1, Ned-19 and inactivating concentrations of NAADP has given rise to a negative inotropic effect, such as a decrease in Ca^{2+} transient amplitudes (Macgregor et al., 2007a; Collins et al., 2011). This occurred under the resting condition where no drugs were used to activate the β-adrenoceptors or other receptors. At least in the case of guinea pig cardiac tissue, the evidence is convincing that there is a constitutively active NAADP signalling pathway.

Conversely, the basal (in the absence of drugs) Ca^{2+} transient amplitude of a NAADP-insensitive mouse model, *Tpcn2*$^{-/-}$ was not significantly different from the WT mouse model. Data from another researcher from Terrar's group also provides further support of this observation, showing the comparable contraction magnitude and Ca^{2+} spark frequency between these two mouse models (Elson, 2011). One might postulate that there are possible compensatory mechanisms arisen from the genetic KO of TPC2, masking the importance of a constitutively active NAADP signalling pathway. However, preliminary data showing acute inhibition of the NAADP pathway using Ned-19 on WT mouse cardiomyocytes did not alter their Ca^{2+} transient amplitudes (Elson, 2011). In addition, although preincubation with KN93 or bafilomycin-A1 interfere with the NAADP action in mouse ventricular myocytes, mouse ventricular myocytes preincubated with KN93 or bafilomycin-A1 did not have significantly different Ca^{2+} transient amplitudes compared to their corresponding control groups (see section 3.3.4 on page 91 and section 3.4.3 on page 111). Three independent groups have published similar results showing the lack of

an effect of KN93 in mouse cardiomyocytes in the absence of the β-adrenoceptor stimulation, with some reporting that the KN93-associated negative inotropic effect was only observed in the condition where β-adrenoceptors are stimulated (Yang et al., 2011; Curran et al., 2014; Huang et al., 2015).

If the NAADP signalling pathway is active and is activating the CaMKII pathway under this condition, the KN93 preincubation should in theory produce a negative inotropic effect. This evidence is in line with the idea that the NAADP signalling pathway in mouse cardiac tissue is mostly not activated, especially if the NAADP-CaMKII pathway that was postulated in the previous section is true. While NAADP was detectable in the WT mouse heart as well as myocytes (Gul et al., 2016), it might be below the threshold to activate the NAADP signalling pathway. Hence, the explanation for the dichotomous findings as whether the NAADP signalling pathway is constitutively active might be the species difference. One alternative explanation might be the effect size of the basal NAADP signalling pathway is relatively smaller in mice and render it inseparable from the noise.

So far, in the cardiac tissue, only the β-adrenoceptor activation has been reported to increase the level of NAADP (Macgregor et al., 2007a; Lewis et al., 2012). The observations presented here show that there is no evidence to support a constitutively active NAADP signalling pathway but the contribution of this pathway to the β-adrenoceptor-mediated positive inotropy was significant. Due to the comparable baseline between the WT and NAADP-insensitive model, it can be implied that the blunted response of *Tpcn2*$^{-/-}$ cardiomyocytes or bafilomycin-A1-preincubated cardiomyocytes during β-adrenoceptor activation is mainly due to the lack of the contribution of a receptor-activated NAADP signalling pathway during activation of the β-adrenoceptors but not due to lack of the basal or

constitutively active NAADP signalling pathway . In the guinea pig model, the baseline parameters were different between groups with and without a functional NAADP signalling pathway; therefore, it is not easy to dissect the relative contributions of the constitutively active NAADP signalling pathway and the receptor-activated NAADP signalling pathway towards the apparent blunted response of the β-adrenoceptor activation. This receptor-activated NAADP signalling pathway observed in the mouse cardiac tissue has been proposed and observed in other tissues such as, immune cells, tracheal smooth muscle, pancreatic cells, and vascular smooth muscle cells (Cosker et al., 2010; Rah et al., 2010; Aley et al., 2013; Arredouani et al., 2015; Favia et al., 2014).

3.5 Conclusion

In conclusion, observations presented in this chapter provide strong support for a role for NAADP and TPC2 proteins in contributing to the β-adrenoceptor-mediated positive inotropy in mouse ventricular cardiomyocytes. The TPC-NAADP signalling pathway in these myocytes is activated upon β-adrenoceptor stimulation (as opposite to being active constitutively) and involves a component of CaMKII proteins but not L-type Ca^{2+} channels.

Chapter 4

NAADP synthesis in sarcoplasmic reticulum-enriched membrane preparation from sheep hearts

Part of the material presented in this chapter was published as supplementary data in Journal of Biological Chemistry (Lin et al., 2017). © the American Society for Biochemistry and Molecular Biology.

4.1 Background

The enzyme known to catalyse cADPR and NAADP formation, ARC was first purified from *Aplysia californica* (Lee and Aarhus, 1991). Two mammalian homologues, CD38 and CD157/BST-1 were then identified based on sequence comparison (Itoh et al., 1994; States et al., 1992). Most of the members in the ARC

family are known to catalyse the *in vitro* formation of cADPR when they are incubated with NAD through cyclisation; and the *in vitro* formation of NAADP when they are incubated with NADP and NA (see section 1.2.3 on page 5 and section 1.2.4 on page 6). The formation of NAADP involves the swapping of the nicotinamide moiety of NADP with NA through a base-exchange reaction (Aarhus et al., 1995).

Compelling evidence has been reported regarding CD38 as the main enzyme in catalysing the *in vitro* formation of cADPR from NAD in the heart, spleen, uterus, kidney and liver (Soares et al., 2007). Attempts have been carried out to measure the endogenous concentration of cADPR between *CD38*$^{-/-}$ and WT animals. This has resulted in published results in accordance with the findings from *in vitro* experiments (Fukushi et al., 2001; Lee, 2006; Soares et al., 2007; Gul et al., 2016), whilst other reports disagree (Partida-Sánchez et al., 2001). While CD157 could be participating in catalysing the endogenous formation of cADPR such as in the brain as reported (Higashida et al., 2017), data regarding its distribution in other tissues is still scant (Malavasi et al., 2008). In addition, given that both CD38 and CD157 are regarded as ectoenzymes that have extracellular active sites, their access to the intracellular substrates (NAD and NADP) and the delivery of their products (cADPR and NAADP) to intracellular targets are restricted. This is currently thought as the topological paradox of CD38 (see section 1.2.8 on page 15). While some authors suggested a transport system as a possible mechanism to resolve this paradox, some have suggested the possibility of intracellularly expressed enzymes that are distinct from CD38, which may be present to compensate for the CD38 deficiency (see section 1.2.8 on page 15 and section 1.2.9 on page 17). This view was further supported by results from Lund's group showing that the endogenous concentrations of cADPR in organs such as the kidney, brain and heart remained

detectable in the *CD38*$^{-/-}$ models and the differences of cADPR content between WT and *CD38*$^{-/-}$ models in these tissue were smaller, compared to spleen tissue and thymus tissue (Partida-Sánchez et al., 2001).

Mészáros et al. (1997) showed that there were at least two groups of pharmacologically-distinct and location-specific ARCs expressed in rat and dog hearts. The ARC activity of the sarcolemmal-dominant microsomes was potentiated by an anti-CD38 antibody. Similar to CD38, the ARC enzymes in their sarcolemmal fraction were inhibited by lectin and DTT, while the ARCs in their SR-enriched fraction were unaffected by all these compounds. Consistent with above findings, Xie et al. (2005), as well as Kannt et al. (2012), showed that the enzymatic activity of the purified rat cardiac ARC was inhibited by Zn^{2+} unlike the human CD38, which was potentiated by Zn^{2+}. Xie et al. (2005) also reported that this purified rat cardiac ARC has no cross reactivity with the anti-CD38 antibody and the predicted sequence of the cardiac ARC from MALDI-TOF proteomic analysis did not show any similarity with the sequence of CD38. In addition, Kannt et al. (2012) also developed two potent compounds, SAN4825 ($IC_{50} \approx 10^{-7}$ M) and SAN2589 ($IC_{50} \approx 10^{-7}$ M) which selectively inhibited the ARC activity of the purified cardiac enzyme but only partially inhibited that of human CD38 and the *Aplysia* cyclase at higher concentration ($\gg 10^{-6}$ M) (Kannt et al., 2012). Overall, these studies have provided evidence for the existence of an intracellularly-expressed, non-CD38 ARC that could be a new member of the ARC family. These studies have mainly focussed on the formation of cADPR while the capability of these SR-associated enzymes to catalyse the production of NAADP in the heart has not been studied. Using SRMP from sheep hearts, this study investigates the synthesis of NAADP in this preparation and further evaluates and compares the associated properties of the ARC in sheep cardiac SRMP to those exhibited by human CD38.

4.2 Method

SRMP were prepared and isolated from sheep hearts as described in section 2.9 on page 66.

To initiate the NAADP production, 500 μM NADP and 7 mM NA were preincubated with the protein sample and the formation of NAADP was measured using sea urchin egg homogenate assay (see section 2.11 on page 68).

To initiate the cADPR production, 2.5 mM NAD was preincubated with the protein sample and the formation of cADPR was measured using sea urchin egg homogenate assay (see section 2.12.2 on page 71).

To initiate the cGPDR production, 500 μM β-NGD was added to the protein sample and the formation of cGDPR was measured using fluorimetry (see section 2.12.1 on page 69).

The pH of the incubation was maintained with HEPES or acetate-based buffers at pH 7.2 or 4.5 respectively.

4.3 Results

4.3.1 NAADP, cADPR and cGDPR synthesis was detected in SRMP from sheep hearts

NAADP-mediated Ca^{2+} release in sea urchin egg homogenates was reported to have a dose-dependent homologous inactivation mechanism (Aarhus et al., 1996; Genazzani et al., 1996). It was shown that the maximum amount of Ca^{2+} that can be released by an NAADP addition depends on the concentration of NAADP added previously. This unique property allows us to use this preparation as a bioassay to detect and measure NAADP production specifically at a low concentration, from approximately 10^{-10} to 10^{-8} M. Example traces and a calibration curve are shown in **Figure 12A** and **B**.

SRMP was prepared by following a modified protocol originally published by Sitsapesan and Williams (1990). The SRMP can be further fractioned into i) the LSR that was collected from the less dense band on a sucrose gradient column and was reported to have less RyRs, thus was thought to contain the non-junctional SR, ii) and the HSR that was collected from the denser band on a sucrose gradient column and was reported to have more RyRs, thus was thought to contain the junctional SR (Inui et al., 1988). SRMP was able to synthesise NAADP when they were preincubated with NADP (500 μM) and NA (7 mM). These substrate concentrations were based on Heather's research on NAADP production of sea-urchin egg homogenates and arterial pulmonary tissue, aiming to produce an optimal rate of NAADP production (Wilson, 1998). The enzymatic rate of NAADP synthesis between two different fractions, LSR and HSR, were comparable at pH 7.2

(**Figure 12C** and **D**; LSR: 1.3 ± 0.4 nmol min^{-1} mg^{-1} protein; HSR: 1.2 ± 0.6 nmol min^{-1} mg^{-1} protein, n = 4 sheep hearts for both group; p = 0.93). The absence of either NADP or NA resulted in an undetectable NAADP-mediated Ca^{2+} release response (**Figure 12E** and **F**). This implies that the *in vitro* NAADP production by cardiac ARCs requires the presence of both NADP and NA.

A widely accepted conventional NGD assay was used to gauge the rate of cADPR synthesis (Graeff et al., 1994). This assay allows the nicotinamide-sensitive cyclisation of NGD (an analogue of NAD) into cyclic GDP-ribose (cGDPR, a fluorescent analogue of cADPR) to be detected. Data presented here shows that SRMP is capable of synthesising cGDPR, when being incubated with NGD (500 μM) (**Figure 12G**). Another approach is to take advantage of the ability of sea urchin egg homogenates to show Ca^{2+} release in response to addition of cADPR (Clapper et al., 1987). This property was used to detect cADPR production by SRMP. NAD (2.5 mM) and SRMP were first co-incubated for 15 min, and a sample of the mixture was added to the sea urchin egg homogenates to cause a Ca^{2+} release that was thought to be mediated by cADPR synthesised from the NAD substrate. 500 nM NAADP was added at the end of the experiment to trigger an appreciable Ca^{2+} release, showing that the NAD-SRMP-induced Ca^{2+} release is independent of the NAADP-induced Ca^{2+} release (**Figure 12H**).

Figure 12

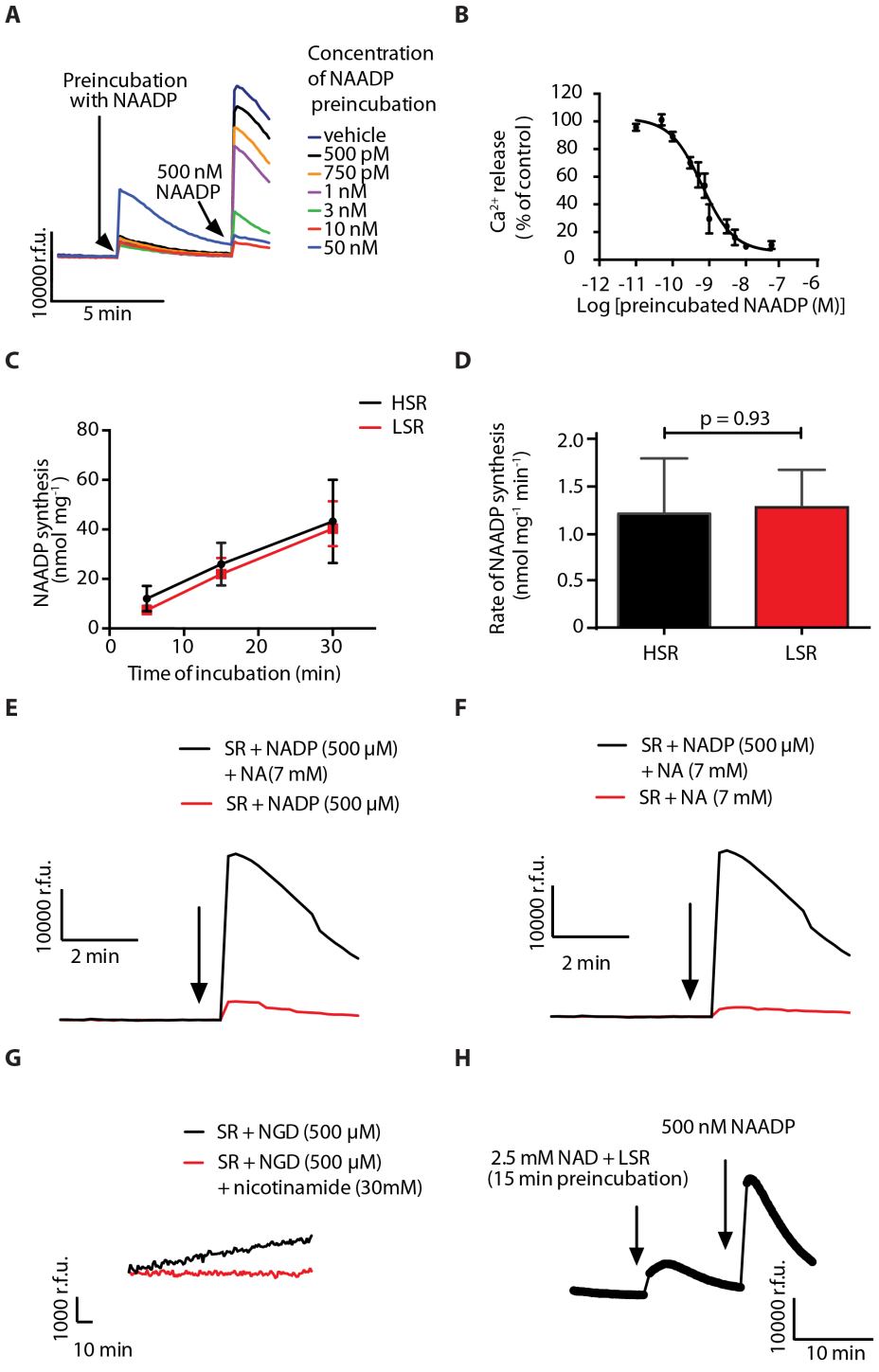

A
Preincubation with NAADP
500 nM NAADP
Concentration of NAADP preincubation
vehicle
500 pM
750 pM
1 nM
3 nM
10 nM
50 nM
10000 r.f.u.
5 min
B
Ca2+ release (% of control)
120
100
80
60
40
20
0
-12 -11 -10 -9 -8 -7 -6
Log [preincubated NAADP (M)]
C
HSR
LSR
NAADP synthesis (nmol mg-1)
80
60
40
20
0
0 10 20 30
Time of incubation (min)
D
p = 0.93
Rate of NAADP synthesis (nmol mg-1 min-1)
2.0
1.5
1.0
0.5
0
HSR
LSR
E
SR + NADP (500 µM) + NA(7 mM)
SR + NADP (500 µM)
10000 r.f.u.
2 min
F
SR + NADP (500 µM) + NA (7 mM)
SR + NA (7 mM)
10000 r.f.u.
2 min
G
SR + NGD (500 µM)
SR + NGD (500 µM) + nicotinamide (30mM)
1000 r.f.u.
10 min
H
500 nM NAADP
2.5 mM NAD + LSR (15 min preincubation)
10000 r.f.u.
10 min

Figure 12: Synthesis of NAADP, cADPR and cGDPR by SRMP from sheep heart

A shows representative traces of dose-dependent homologous inactivation of NAADP-mediated Ca^{2+} release in sea urchin egg homogenates.
B shows an example of a calibration curve of **A** produced with known concentrations of NAADP (n = 3 series of calibrations).
C and **D** show the time course and the average rate of NAADP production, respectively, by HSR and LSR fractioned from SRMP (n = 4 sheep hearts in each group). Both preparations were incubated with 500 μM NADP and 7 mM NA.
E and **F** show representative traces of NAADP-mediated Ca^{2+} release in sea urchin egg homogenates triggered by samples where 7 mM NA (**E**) or 500 μM NADP (**F**) was omitted from the solution where SRMP was incubated. These trends were observed in 3 out of 3 independent experiments and samples were diluted by 20 times before addition (indicated by black arrows).
G shows a representative trace of cGDPR synthesis (indicated by an increase in fluorescence) by SRMP when supplemented with NGD (500 μM). This synthesis was inhibited by 30 mM nicotinamide. This inhibition was observed in 3 out of 3 independent experiments.
H shows a representative trace demonstrating a Ca^{2+} release response in sea urchin egg homogenates triggered by a sample of 1 μl from the incubation of SRMP and NAD (2.5 mM). This Ca^{2+} release is thought to be mediated by the conversion of cADPR from NAD and is therefore independent of the NAADP-mediated Ca^{2+} release. This cADPR-mediated Ca^{2+} release was observed in 3 out of 3 independent experiments.

Note: All experiments were conducted at pH 7.2. NGD assays were conducted at 37 °C. Measurements of NAADP and cADPR using sea urchin egg homogenates were conducted at 17 °C and samples from incubations (37 °C) were diluted accordingly before addition, in order to achieve optimal measurements. Numerical data in **B**, **C** and **D** are reported as the mean ± SEM. Student's t-test was used to compare the difference of means. "mg^{-1}" refers to "per mg protein found in the incubation". "r.f.u." refers to "relative fluorescence unit".

4.3.2 cGDPR synthesis was inhibited by NAD or NADP and NAADP synthesis was inhibited by NAD at pH 7.2

Despite being a multifunctional enzyme that binds to different substrates and catalyses several distinct reactions, such as the hydrolysis, cyclisation and

base-exchange reactions, the CD38 and *Aplysia* cyclase were reported to have a single active-site (Lee, 2006). It was shown that the binding of the substrates and the reactions were dependent on the same amino acid residues (Asp155, Trp125, Trp189 and Glu146 and Glu226 of human CD38) on the active site, regardless of which reaction was taking place. As to whether this property is exhibited by cardiac ARC is evaluated in this section. If the substrates for different reactions occupy the same active site of cardiac ARC, they will compete for the active site of the enzyme and therefore suppress each other's synthesis.

The rate of cGDPR production from NGD by SRMP was inhibited by NAD (1 mM NAD: 35 ± 3% of control; $p < 0.05$; **Figure 13A**) ,and by NADP and NA (1 mM NADP and 1 mM NA: 41 ± 7% of control; $p < 0.05$; **Figure 13B**), in a concentration-dependent manner. Since NA is essential for the NAADP production, it was initially surprising to note that NADP alone was capable of inhibiting the cyclisation of NGD (3 μM NADP 13 ± 6% of control; $n = 4$, $p < 0.01$; **Figure 13B**). However, *Aplysia* cyclase was known to catalyse the production of cADPR-phosphate from NADP, while CD38 was known to hydrolyse NADP to ADPRP, both occurring in their respective active sites, when NA is absent (Lee and Aarhus, 1997). On the other hand, NA alone did not affect cGDPR synthesis (**Figure 13B**). Consistent with the observation in **Figure 13A and 13B**, the NAADP production was found to be hindered by the presence of NAD at pH 7.2 (control: 1.3 ± 0.6 nmol mg^{-1} protein min^{-1}; 2.5 mM NAD: 0.18 ± 0.1 mg^{-1} protein min^{-1} $n = 4$; $p < 0.05$; **Figure 13C and 13D**) , supporting the hypothesis that a single active site enzyme is responsible for the synthesis of both NAADP and cADPR.

Figure 13

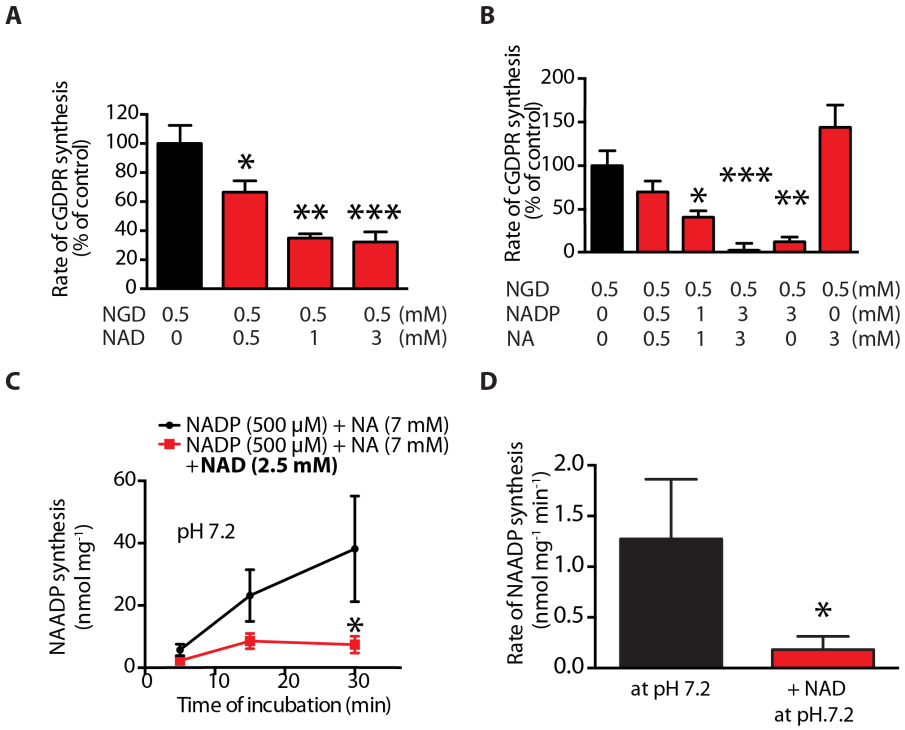


Figure 13: Substrates competition studies of ARC from SRMP at pH 7.2

A shows the bar graph of NAD inhibition on cGDPR synthesis in a dose-dependent manner in sheep SRMP.
B shows the bar graph of NADP and NA inhibition on cGDPR synthesis in a dose-dependent manner in sheep SRMP. NA alone did not inhibit the synthesis of cGPDR.
C and **D** show the time course and the average rate of NAADP production, respectively, by SRMP with and without the presence of NAD (2.5 mM).

Note: All experiments were conducted at pH 7.2. NGD assays were conducted at 37 °C. Measurements of NAADP using sea urchin egg homogenates were conducted at 17 °C and samples from incubations (37 °C) were diluted accordingly before addition, in order to achieve optimal measurements. Numerical data are reported as the mean ± SEM (n = 3 to 7 experiments with SRMP from at least 3 sheep hearts in each group). * denotes $p < 0.05$; ** denotes $p < 0.01$; *** denotes $p < 0.001$ relative to the control (represented by black bars or symbols), determined by Student's t-test or one-way ANOVA with post-hoc Dunnett's test. "mg^{-1}" refers to "per mg protein found in the incubation".

4.3.3 NAADP synthesis at pH 4.5 was enhanced and unaffected by the presence of NAD

NAADP synthesis was observed to be enhanced at lower pH (Aarhus et al., 1995), which leads to the hypothesis that NAADP synthesis is more efficient in acidic environments such as acidic lysosomes. A site-directed mutagenesis study has revealed that Glu146 of CD38 is responsible for controlling the pH dependence of NAADP synthesis (Graeff et al., 2006). While WT human CD38 has maximal enzymatic activity at pH 5, the loss of the pH dependence of NAADP synthesis was observed when the Glu146 of human CD38 was changed to glycine. It was proposed that at neutral pH, both NA and Glu146 was negatively charged and the electrostatic repulsion between them would reduce substrate binding and consequently decrease the reaction rate. On the other hand, an environment with acid pH will encourage the protonation of NA and hence promote the synthesis of NAADP by reducing the electrostatic repulsion between the acidic residue Glu146 and NA.

Consistent with this hypothesis, a higher yield of NAADP was observed at pH 4.5 (5.4 ± 1 nmol mg^{-1} protein min^{-1}), compared to at pH 7.2 (1.3 ± 0.6 nmol mg^{-1} protein min^{-1}, **Figure 14A**). In contrast to the finding that NAD inhibited NAADP synthesis at pH 7.2 (**Figure 13C**), the cADPR substrate, NAD, did not affect the synthesis of NAADP in SRMP at pH 4.5 (**Figure 14B**). This observation implies that NAD fails to compete with NADP for the enzyme active site at pH 4.5, despite the formation of both NAADP and cADPR taking place at the same active site of the ARC. It has also been reported that the rate of cADPR synthesis was roughly 2-fold lower at pH 4.5 than at pH 7.2 (Aarhus et al., 1995). Perhaps factors contributing to a lower rate of cADPR formation and a higher rate of NAADP synthesis give rise

to, especially in the current assay described in this chapter, the comparable rates of NAADP synthesis.

Figure 14

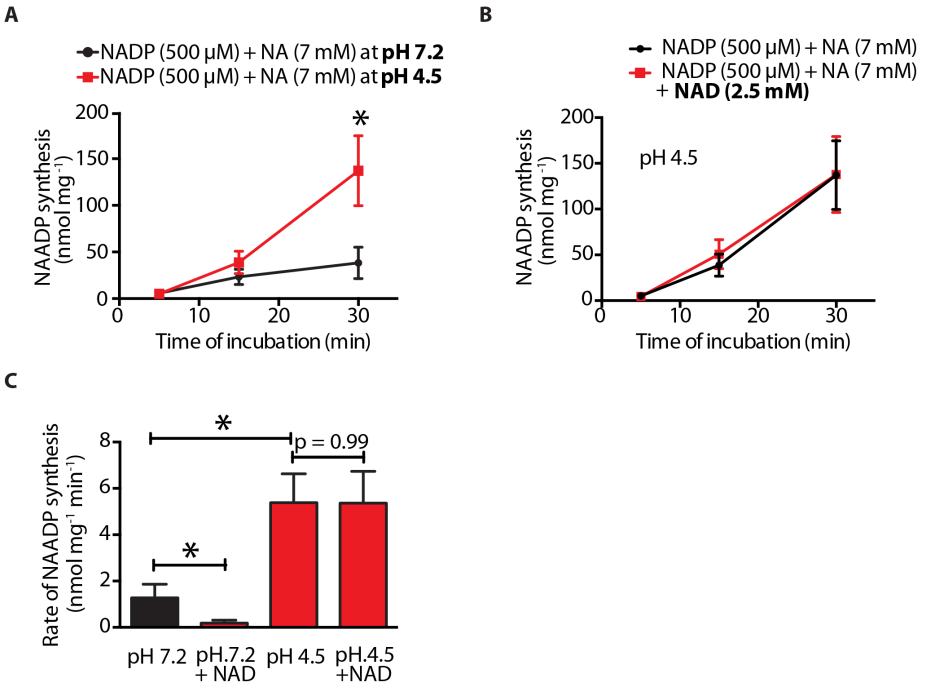


Figure 14: Influence of pH on NAADP synthesis and on inhibition of NAADP synthesis by NAD

A shows the time course of NAADP synthesis by SRMP at pH 7.2 and pH 4.5.
B shows the time course of NAADP synthesis by SRMP with and without the presence of NAD (2.5 mM) at pH 4.5 .
C shows the average rate of NAADP production by SRMP under four different conditions: at pH 7.2 without NAD, at pH 7.2 with NAD, at pH 4.5 without NAD and at pH 4.5 with NAD.

Note: NGD assays were conducted at 37 °C. Measurements of NAADP using sea urchin egg homogenates were conducted at 17 °C and samples from incubations (37 °C) were diluted accordingly before addition, in order to achieve optimal measurements. Numerical data are reported as the mean ± SEM (n = 4 experiments with SRMP from 4 sheep hearts in each group). * denotes $p < 0.05$ relative to the control (represented by black bars or symbols), determined by Student's t-test. "mg^{-1}" refers to "per mg protein found in the incubation".

4.3.4 Effects of Zn^{2+} on NAADP and cGDPR synthesis

As described in section 1.2.9 on page 17, some groups have reported the possibility of a cardiac-specific ARC in a similar SRMP. Since the identities of these cardiac-specific ARCs have not been solved, the enzymes were characterised indirectly by assessing their biochemical properties, which were reported to be different from those of human CD38.

The presence of Zn^{2+} was reported to induce a conformational change in human CD38 and increase the net production of cADPR of CD38 by shifting its preference from predominantly carrying out a glycohydrolase activity to predominantly carrying out a cyclase activity (Kukimoto et al., 1996; Zielinska et al., 2004). Human CD38 Therefore, the influence of Zn^{2+} was investigated, and there appeared to be an enhancement of NAADP synthesis by the presence of Zn^{2+}, which is consistent with the properties of CD38 (5 mM Zn^{2+}: 280 $\pm$ 50% of control; n = 6; p $<$ 0.01; **Figure 15A**).

However, in the fluorimetric experiment to measure cGDPR formation, addition of Zn^{2+} in the SRMP mixture caused an increase in the fluorescence readout in the absence of NGD (**Figure 15B**). The increase in fluorescence after the addition of Zn^{2+} (5 mM) reached plateau after 30 min. Once the plateau was achieved, addition of NGD further increased the fluorescence.

Extra caution needs to be taken when interpreting these measurements. In addition to the artefactual increase in fluorescence reading caused by Zn^{2+} addition, the turbidity of samples also seemed to increase with the increase in concentration of Zn^{2+} (**Figure 15C**). This observation indicates that addition of Zn^{2+} might have led to the formation of insoluble particles or segregation of molecules, contributing

to the light scattering effect that increases fluorescence reading and to the turbidity which gave rise to the cloudiness of the solution. The signal to noise ratio of the NGD assay would be lower with the increase in turbidity of the solution, possibly masking or undermining the potentiation effect of Zn^{2+} ions on the rate of cGDPR formation of SRMP. As a result of other issues mentioned above, it is difficult to justify fluorimetrically whether the rate of cGDPR formation is really potentiated in the presence of Zn^{2+}. Nevertheless, it is clear that the abolition of ARC enzymatic activities (cGDPR and NAADP synthesis) by Zn^{2+} was not observed, in contrast to observations reported by the other groups (Xie et al., 2005; Kannt et al., 2012).

Since the NAADP measurement assay is free of the issue mentioned above (due to the fact that samples were diluted significantly and that fluorescence readout and NAADP measurement are derived from the second addition of NAADP), the favoured hypothesis is that the Zn^{2+} has a potentiation effect on the enzymatic activity of SRMP, which is consistent with the effect of Zn^{2+} on human CD38 (Xie et al., 2005; Kannt et al., 2012).

Figure 15

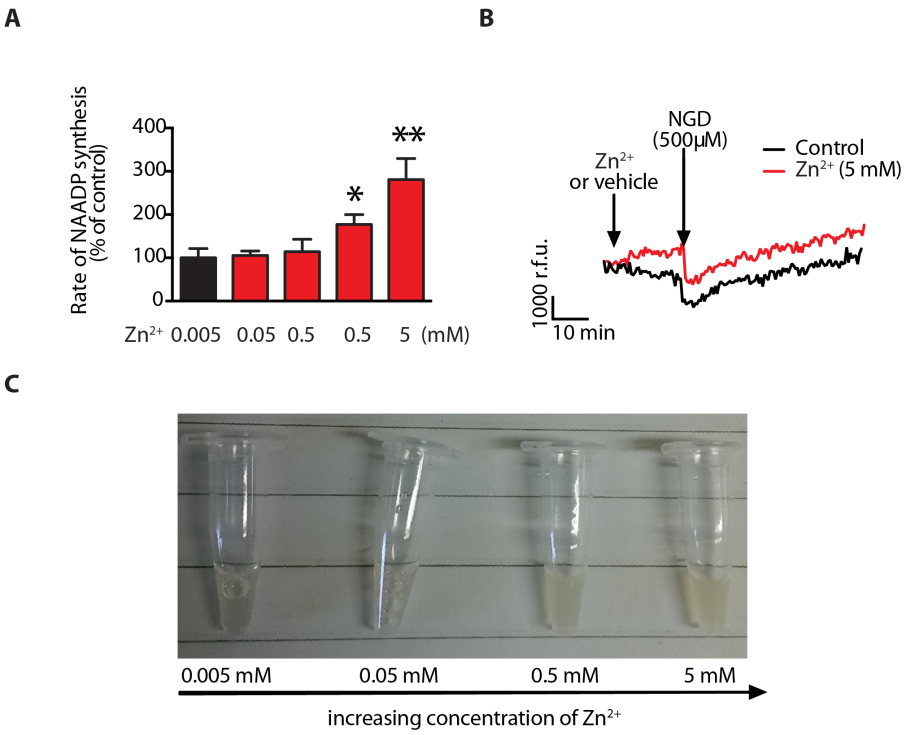

A
B
Rate of NAADP synthesis (% of control)
400
300
200
100
0
*
**
Zn2+ 0.005 0.05 0.5 0.5 5 (mM)
NGD (500μM)
Zn2+ or vehicle
Control
Zn2+ (5 mM)
1000 r.f.u.
10 min
C
0.005 mM
0.05 mM
0.5 mM
5 mM
increasing concentration of Zn2+

Figure 15: Influence of Zn^{2+} on NAADP and cGDRP synthesis

A shows the average rate of NAADP production by sheep SRMP in increasing concentration of Zn^{2+}. Numerical data are reported as the mean ± SEM (n = 4 to 6 experiments using SRMP from 3 hearts in each group).
B shows the representative traces from fluorimetric analysis of cGDPR formation in the absence and presence of 5 mM Zn^{2+}. Similar trends were observed in 6 independent experiments using SRMP from 3 hearts in each group).
C shows a photo showing the increased turbidity of solutions with increasing concentrations of Zn^{2+}.

Note: All experiments were conducted at pH 7.2. NGD assays were conducted at 37 °C. Measurements of NAADP using sea urchin egg homogenates were conducted at 17 °C and samples from incubations (37 °C) were diluted accordingly before addition, in order to achieve optimal measurements. * denotes $p < 0.05$; ** denotes $p < 0.01$ (relative to the control represented by the black bar), determined by one-way ANOVA with post-hoc Dunnett's test. "r.f.u." refers to "relative fluorescence unit".

4.3.5 Effects of catalytic subunit of PKA on NAADP and cGDPR synthesis

It has been reported previously by Terrar's lab and others that β-adrenoceptor activation enhanced the levels of NAADP and cADPR in the heart (Macgregor et al., 2007b; Lewis et al., 2012; Gul et al., 2016). In addition, the effects of isoprenaline in mediating positive inotropy as well as arrhythmogenicity were also shown to be reduced by the pharmacological blockade of the NAADP and cADPR pathways (Macgregor et al., 2007b; Rakovic et al., 1996; Nebel et al., 2013; Capel et al., 2015). These findings are consistent with the hypothesis that the enhanced levels of NAADP and cADPR upon β-adrenoceptor activation contribute to the β-adrenoceptor-mediated positive inotropy and arrhythmogenicity. It was proposed that the enhanced levels of these substances are achieved through an increased activity of enzymes responsible for their synthesis and these enzymes are downstream targets of the β-adrenoceptor pathway. 200 units ml^{-1} of the catalytic

subunit of PKA was able to increase the synthesis of cGDPR significantly by roughly 1.5 times (160 ± 30% of control; n = 4; $p < 0.05$), however a significant increase in the synthesis of NAADP was not detected after PKA treatment (**Figure 16A** and **B**).

Although phosphorylation sites of CD38 have not been reported, it was speculated that PKA might phosphorylate the enzymes that synthesises these molecules and thus enhance the catalytic activity of these enzymes. Although the synthesis of NAADP and cADPR share the same active site, this does not imply that phosphorylation of this enzyme will have similar quantitative and qualitative effects on their rates of synthesis (note: pH has different effects on these catalytic reactions).

In addition, the cGDPR assay allows us to monitor the production of cGDPR continuously throughout the whole experiment, unlike the NAADP-measuring assay where 3 to 4 time points were taken in each experiment. The concentration of cGDPR and the increase in fluorescence can be assumed to have a linear relationship. On the other hand, the log[NAADP concentration] and the measurement of Ca^{2+} release has a classical dose response sigmoidal curve (i.e. even on the linear range of this sigmoidal curve, a relatively drastic difference in concentrations of NAADP is required to have a substantial effect on Ca^{2+} release response). Therefore, the cGDPR assay would have an advantage in terms of resolution and sensitivity compared to the NAADP measurement assay. Last but not least, NAADP can be hydrolysed by the same enzyme which synthesises it while cGDPR is resistant to the hydrolysis (Graeff et al., 1994; Schmid et al., 2011). All these factors could possibly mask the increase in the NAADP synthesis rate (provided that the effect is mild), therefore it is too early to rule out the possibility of a PKA-mediated enhancement of NAADP synthesis. A more sensitive assay for NAADP detection might be useful for future investigation.

As the use of DTT (6 mg ml^{-1}) is normally advised by the manufacturer (Sigma Aldrich, USA) to maintain the activity of PKA, experiments where DTT was included together with PKA treatment showed no significant enhancement of cGDPR synthesis by PKA (82 ± 10 % of control; n = 6, p = 0.18; **Figure 16A**). Consistent with the observations showing DTT as a human CD38 inhibitor (see section 1.2.7.2 on page 12), the data presented here shows that DTT alone can inhibit the cGDPR synthesis in SRMP (26 ± 20% of control; n = 9; p < 0.001; **Figure 16A**). Although a significant enhancement of PKA on cGDPR synthesis was observed when DTT was omitted, the compromised activity of PKA (in the absence of DTT) could have undermined the effect of phosphorylation of cardiac ARC in both the cGDPR and NAADP synthesis.

Figure 16

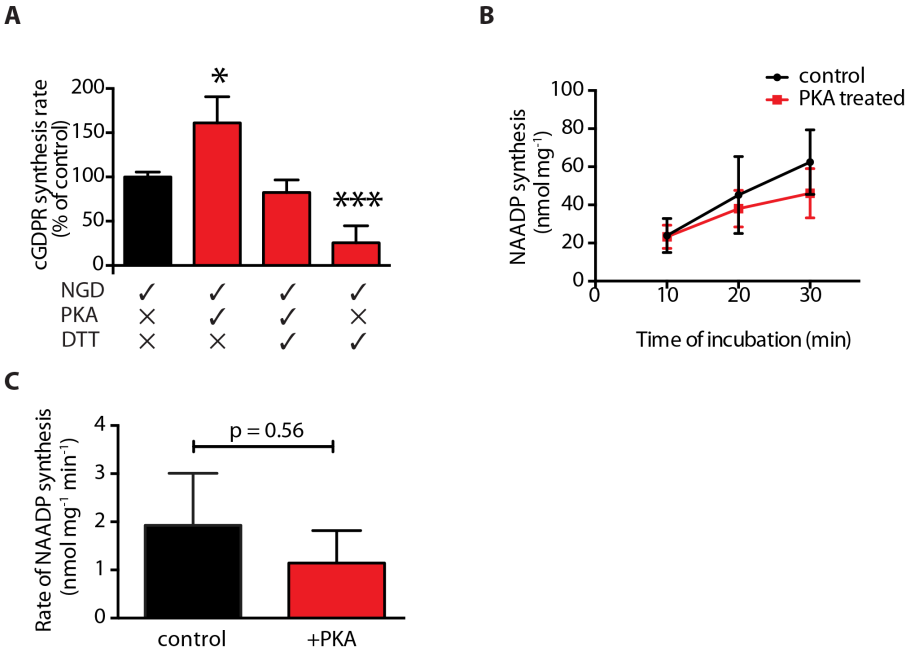


Figure 16: Influence of PKA and DTT on cGDPR and NAADP synthesis

A shows the bar graph of cGPDR synthesis by SRMP with or without PKA (200 units per ml) and/or DTT (6 mg ml^{-1}).
B shows the time course of NAADP synthesis by SRMP with and without the presence of PKA (200 units ml^{-1}).
C shows the average rate of NAADP synthesis with and without the presence of PKA (200 units ml^{-1}).

Note: All experiments were conducted at pH 7.2. All protein-substrates incubations contained a final concentration of 10 mM Mg^{2+} (instead of 0.5 mM), 0.5 mM MgATP, 10 mM phosphocreatine and 10 units ml^{-1} creatine phosphokinase. PKA catalytic subunits were preincubated with protein for 30 min to achieve a stable level of phosphorylation before the addition of substrates. NGD assays were conducted at 37 °C. Measurements of NAADP using sea urchin egg homogenates were conducted at 17 °C and samples from incubations (37 °C) were diluted accordingly before addition, in order to achieve optimal measurements. DTT was omitted in all the experiments unless stated. Numerical data are reported as the mean ± SEM (n = 4 to 13 experiments in each group of **A** and n = 4 experiments in each group of **B** and **C** using SRMP from 4 hearts) * denotes $p < 0.05$; *** denotes $p < 0.001$ relative to the control (represented by black bars), determined by Student's t-test. "mg^{-1}" refers to "per mg protein found in the incubation".

4.4 Discussion

4.4.1 Is there evidence for the existence of a non-CD38 in the SRMP from sheep hearts?

The novel evidence presented here shows that SRMP from sheep hearts is capable of synthesising both cADPR and NAADP. In a substrate competition study, it was demonstrated that the substrates for cyclisation reactions (to produce cGDPR and cADPR) were able to inhibit the base-exchange reaction that produced NAADP; reciprocally, the substrates (NADP and NA) for base-exchange reactions were able to inhibit the cyclisation reaction that produced cADPR (see section 4.3.2 on page 122).

These observations are consistent with the properties of a single active site CD38 enzyme, the only mammalian enzyme known to catalyse both NAADP and cADPR synthesis. Consistent with observations made in purified human CD38 (Aarhus et al., 1995), at an acidic pH, the NAADP production in SRMP occurred at a higher rate. In addition, this characteristic pH bias was supported by the observation that NAADP synthesis was no longer inhibited by the presence of the cADPR substrate, NAD, at pH 4.5, in contrast to those observed at pH 7.2 (see section 4.3.3 on page 125).

By partially purifying the enzymes of interest, some groups have proposed the existence of a non-CD38 cardiac ARC based on their pharmacological and biochemical properties (**Table 4.1 on page 138**). In contrast to the their studies, the cardiac ARC in the SRMP showed a very close resemblance to the CD38 enzyme; this is further supported by the observation that enzymatic activities observed in the SRMP were inhibited by DTT and potentiated by Zn^{2+}. These properties are consistent with the properties of purified human CD38. None of the studies that proposed the existence of a non-CD38 ARC has supported their claim with evidence from a *CD38*$^{-/-}$ model (apart from Ceni et al. (2003a)). On the other hand, in Chapter 5, the pivotal role of CD38 in NAADP and cADPR synthesis in the heart is elucidated. The discrepancies between current studies reported in this thesis and others might be due to species difference (sheep and rats) as well as other factors. For example, unlike other studies, the author of this thesis did not attempt to partially purify or isolate the enzyme of interest from the SRMP. Therefore, the possibility of the existence of non-CD38 ARCs in sheep cardiac tissue could not be ruled out entirely. Without any purification, the sheep SRMP broadly showed CD38-like properties, supporting the hypothesis that the observed ARC activities in SRMP were mostly carried out by CD38. It was speculated that non-CD38 ARCs, if they exist in SRMP, might have been expressed in a much smaller amount and might have had a minor contribution

in these syntheses, compared to the CD38-like enzymes.

Similar approaches have been attempted in other tissues, such as brain tissues, vascular smooth muscles, skeletal muscles, bovine rod outer segments and kidneys (see section 1.2.9 on page 17). The hypothesis that these tissues expressing non-CD38 ARCs was mainly supported by the following: i) A qualitative difference between the effect of divalent ions such as Zn^{2+}, or Cu^{2+} on the enzymatic activities of their proposed ARC and those of CD38. ii) The absence of a detectable protein band in the region of interest (42 – 45 KDa, expected molecular weight of CD38) from immunoblotting experiments. iii) Specific inhibitor-based analyses showing the difference in pharmacological properties. For example, the existence of a distinct ARC was proposed in the kidney since it responded differently to the inhibitor DHAB treatment, compared to CD38 (Nam et al., 2006). Furthermore, the vascular-specific ARC but not CD38 was inhibited by ganglioside GT1b (De Toledo et al., 2000). However, these studies involving non-CD38 ARCs were not without limitations, as listed below:

1) Most of the studies mentioned above have compared the properties of ARC from two different cell types. For example, in Nam's study, the properties of ARC from kidney membrane fractions were compared with those from the membrane fraction from human Jurkat T cells (Nam et al., 2006). Ideally, CD38 should be isolated from kidney tissue and its properties should be compared with the non-CD38 ARC from the same tissue, i.e. from the kidneys, to ensure the differences observed are not due to heterogeneous comparisons.

2) It is unclear at the moment if the proposed ARC is a direct target for divalent ions via a cation-binding site or indirectly via an accessory binding protein. The observed difference in enzymatic properties could arise from the differential expression

of these accessory proteins in different tissues or the omission of these proteins during the purification steps.

3) A lower expression of CD38 in the tissue mentioned above might lead to a weaker staining of CD38 in immunoblotting. Some of these studies have compared CD38 labelling in their tissue of interest to immune cell lines or tissue. As CD38 has other non-enzymatic roles in some immune cells, such as T-cells, their higher expression of CD38 was reasonably expected (Malavasi et al., 2008). Furthermore, CD38 was a typical surface marker for lymphocytes (Vences-Catalán and Santos-Argumedo, 2011). It is not reasonable to dismiss the functional importance or the existence of CD38 in non-immune cells or tissue solely on the basis of the observation that they have a weaker labelling or lower expression, compared to immune cells or tissues. In addition, despite the ubiquitous expression of CD38, it is surprising that some groups reported the lack of CD38 expression in their tissue of interest (see section 1.2.9 on page 17).

4) There was no KO experiment to support the existence of non-CD38 enzymes. In addition, the genomic study comparing the sequence of *Aplysia* cyclase did not reveal sequences other than those which correspond to the CD38 and CD157 (States et al., 1992; Itoh et al., 1994).

5) The non-CD38 ARC was reported to have a lower enzymatic activity (Ceni et al., 2003a). The NADase activity from adult *CD38*$^{-/-}$ brain examined *in vitro* using protein extracts and cells was 3 orders of magnitude lower compared with the CD38-dependent NADase activities found in the same preparation isolated from normal mouse brains (Ceni et al., 2003a). The lower rate of enzymatic activity of these non-CD38 ARCs might put a limit on their physiological contribution, especially in the presence of CD38.

6) There was no substantial converging evidence supporting the existence of these non-CD38 ARCs. Although the effect of cations and DTT were similar on these non-CD38 enzymes, these non-CD38 enzymes seem to have different pharmacological profiles. For example, Nam et al. (2006) reported that DHAB inhibited the kidney-specific ARC but not those in the hearts; on the contrary, Gul et al. (2008) showed that DHAB could inhibit the cardiac ARC. Therefore, the question of whether or not these newly proposed non-CD38 ARCs are identical or unique to their corresponding tissues needs to be addressed.

In the author's opinion, the existence of these non-CD38 enzymes has to be evaluated using *CD38*$^{-/-}$ animals. The ARC enzymatic activities can be assessed in the tissues from *CD38*$^{-/-}$ animals and their biochemical properties (Zn^{2+} or DTT sensitivity) can be investigated. Observations presented in Chapter 5 also show that homogenates and single ventricular myocytes from *CD38*$^{-/-}$ hearts lack the ability to synthesise NAADP and cADPR, providing evidence for CD38 being the main enzyme synthesising these molecules, particularly during the activation of β-adrenoceptors.

4.4.2 Is the assessment of ARC activity in this chapter reliable?

In this chapter, a novel method to measure NAADP is also presented, based on the previous observation regarding the unique homologous inactivation of NAADP-induced Ca^{2+} release (Genazzani et al., 1996). In the past, sea urchin egg homogenates have been used to quantify the amounts of NAADP, mainly in a radioligand binding assay (Lewis et al., 2007) or an NAADP-induced Ca^{2+} release assay (Cancela et al.,

	Human CD38	**Rat cardiac specific cyclase**	**Sheep cardiac SRMP cyclase (this thesis)**	**Reference**
Zn^{2+}	Stimulatory	Inhibitory	Stimulatory/no change*	(Xie et al., 2005; Kannt et al., 2012)
DTT	Inhibitory	No effect	Inhibitory	(Mészáros et al., 1997; Xie et al., 2005)
Cyclase labelling	Positive, 42 KDa (anti-CD38, western blot)	Negative (anti-CD38, western blot), 35 kDa** (in gel fluorescence assay)	Positive*** (anti-CD38, immuno-cytochemistry)	(Kannt et al., 2012; Xie et al., 2005)
Sequence similarity with CD38		No similarity		(Xie et al., 2005)
IC_{50} of SAN4825	$\gg 10^{-6}$M	$\approx 10^{-7}$M	$\approx 10^{-7}$M	(Kannt et al., 2012)

Table 4.1: Summary of properties of the CD38, non-CD38 cardiac specific ARC and ARC from sheep cardiac SRMP
The cardiac specific ARC was reported to have distinct biochemical and pharmacological properties, compared to human CD38. In contrast, the ARC in the sheep cardiac SRMP has similar properties of human CD38. This comparison supports the hypothesis that CD38 is the major ARC in hearts. Similar properties are highlighted in red fonts.
* While Zn^{2+} stimulated NAADP production in the sheep cardiac SRMP, the NGD assay was compromised by the Zn^{2+}-induced turbidity, and hence a stimulatory effect could not be quantified. However, it was clear that no inhibitory effect was observed.
** The type-III CD38 (with cytosolic active site) has recently been reported to be expressed as a non-glycosylated protein around 35 kDa (Zhao et al., 2012, 2015). *** This was done in mouse cardiac cells instead.

1999). Although the former assay has a lower range of detection compared to the assays described in this chapter, it utilises the radioactive analogue of [^{32}P]NAADP which has to be synthesised and treated cautiously. Apart from that, there can

be interference in the performance if the assay by non-NAADP molecules, such as NADP, which bind to a NAADP-binding site and displace NAADP bound to an ARC (Note: The main NAADP-binding sites in sea urchin egg homogenates however are commonly thought to be receptors or binding proteins in the homogenates that are associated with the NAADP-induced Ca^{2+} release). On the other hand, an NAADP-induced Ca^{2+} release assay has a higher detection limit compared to the NAADP-inactivation assay (10^{-8} M versus 10^{-10} M). Given that NAADP is not the only substance known to induce Ca^{2+}release in sea urchin egg homogenates, inhibitors of IP_3 and cADPR might be required in the assay. The NAADP-inactivation assay depends on the homologous inactivation of sea urchin egg homogenates by NAADP. This homologous inactivation was shown to be unique to NAADP and specifically dependent on NAADP concentration. It has an effective range from 10^{-10} to 10^{-8} M (see section 4.3.1 on page 119). Although it is might be not suitable to measure minute amount of NAADP such as the endogenous level of NAADP in the heart, it serves as a reliable and convenient tool for quantifying *in vitro* NAADP production.

4.4.3 Do observations in this thesis support the existence of an ARC in the cardiac SR?

The proposed hypothesis regarding SR-associated ARC is consistent with previous observations by several groups, which demonstrated that SRMP showed enzymatic activities similar to those of ARC (Mészáros et al., 1997; Xie et al., 2005; Kannt et al., 2012). Ideally, a pure SR-only preparation would be the best model for these studies. However, a protocol to achieve this level of purity is not currently available. The sheep SR preparations used for experiments presented in the thesis, in fact, have been widely used for the study of RyR2 and other SR proteins (Mahony, 1988;

Michalak, 1988; Sitsapesan and Williams, 1990; Sitsapesan et al., 1994; Zissimopoulos and Lai, 2005; Laver, 2007; Sikkel et al., 2013; Li et al., 2015). Making preparations from sheep also has the advantage of allowing efficient preparation of amounts of biological material that are orders of magnitude greater than can be prepared from much smaller animals, such as the mouse. The relative purity of similar preparations is supported by electron microscopy and biochemical studies (Mészáros et al., 1997; Saito et al., 1984; Holmberg and Williams, 1990).

The possibility that the contaminating membranes in sheep SRMP are at least partially responsible for the detected and measured ARC activity cannot be excluded. The linear estimation of the NAADP production rate in SRMP is approximately 10^{-9} mol mg^{-1} protein min^{-1} when 500 μM NADP and 7 mM NA were supplemented. This is higher than the CD38 base-exchange activity published using mixed membrane preparation (Chini and Dousa, 1995), which is approximately $10^{-9.5}$ mol mg^{-1} protein min^{-1} when 1 mM NADP and 40 mM NA were supplemented (note: higher substrate concentrations were used in their studies). The sheep SRMP also has a 2- to 3-fold higher rate of NAADP production, compared to mixed membrane preparation from mice (see section 4.3.1 on page 119 and section 5.3.1 on page 148). Although these observations are cross-species comparisons, they are consistent with the idea that substantial amounts of CD38 are expressed in the cardiac SR. If the observed enzymatic activities in SRMP were really a result of contamination of the ARC from organelles other than SR, an SR enriching protocol would in theory reduce the enzymatic activity in the preparation, unless such protocol was enriching other CD38-expressing organelles in addition to SR. The SRMP may be contaminated with a variety of other membranes, but the possibility that an ARC enzyme such as CD38 could be located on SR membranes receives further support from observations from immunocytochemistry experiments

showing CD38 labelling had a striated pattern with a spacing that closely resembled that of RyR labelling (see section 5.3.5 on page 159 and section 5.3.6 on page 164).

4.4.4 Would SR be a suitable place for an ARC enzyme?

The current identified mammalian ARCs are widely regarded as ectoenzymes. While *in vitro* data strongly support their capability to synthesise cADPR and NAADP (only CD38 but not CD157 was shown to synthesise NAADP), their physiological relevance remains questionable due to their paradoxical topologies (see section 1.2.8 on page 15). The location of active sites on the exterior cell surface not only hinders access of substrates such NAD, NADP, and NA to these sites, but also poses questions of how the products of these enzymes might reach their corresponding intracellular targets (such as TPCs and RyRs). A shuttle/transport system, which will facilitate the transport of the substrates and the products across cell membranes, has also been suggested (see section 1.2.8 on page 15). In addition, other scientists have also shown evidence of intraorganellar CD38 being expressed mainly in the endolysosomes (Davis et al., 2008; Cosker et al., 2010).

In the cardiac field, several groups have been looking at the possibility of these enzymes being expressed in SR (see section 1.2.9 on page 17 and 4.1). Their data, as well as the observations reported in this thesis, support the proposal that these ARC enzymes remain intact in the SRMP. One of the reasons why the idea of NAADP synthesis inside lysosomes is favoured is due to the acidic environment that lysosomes provide. It is true that a lower pH enhances the synthesis of NAADP, but current observations reported in this thesis suggest that the synthesis of NAADP is not completely abolished at pH 7.2 (25 % of that observed at pH 4.5). A similar

observation was also published using another model (Aarhus et al., 1995). However, it should also be pointed out that as NAADP is a potent Ca^{2+}-mobilising molecule, and the threshold concentration for NAADP to cause lysosomal Ca^{2+} release is very low (in the tens of nM range (Macgregor et al., 2007a; Nebel et al., 2013)).This implies that even a small amount of synthesised NAADP at pH 7.2 would be sufficient to trigger the NAADP signalling pathway.

Another issue raised regarding these ARCs including CD38, is that they can hydrolyse NAD, cADPR, NADP, and NAADP (Howard et al. 1993; Schmid et al. 2011, see also review by Lee 2006). Therefore, some are convinced that these enzymes, particularly human CD38, are inefficient in making cADPR and NAADP. The compartmentalisation of the products and substrates, for example, having a transport/shuttle system across an organelle such as the lysosome, could potentially facilitate the synthesis of cADPR and NAADP. On the other hand, if the enzymes are indeed expressed on SR, it might also seem to be strategically placed due to the following reasons: 1) The main target of cADPR in hearts, RyRs, are located on the SR (see section 1.2.11 on page 23). 2) It was previously shown that the SR is in close proximity to lysosomes (Aston et al., 2017), where NAADP mobilises Ca^{2+} from. 3) A possible interaction between SR and lysosomes in the NAADP signalling pathway was reported (Capel et al., 2015). It seems that if these enzymes were on the SR, the products made by them would be in close proximity to their targets, be it RyR or a lysosomal protein (such as TPC). Even if the hydrolysis by these enzymes prevents the accumulation of the products, the products being made in a localised area at the pH 7.2 could give rise to a high local concentration, increasing the probability of cADPR and NAADP reaching and binding to their targets. Therefore, the author of this thesis proposes that there might be microdomains, formed by SR proteins, lysosomal proteins, and these enzymes, which are

responsible in facilitating the cADPR and NAADP signalling pathways.

4.5 Conclusion

Taken together, data presented in this chapter are consistent with the hypothesis regarding the existence of CD38-like ARCs in sheep cardiac SRMP, in contrast to those reported in the literature (see section 1.2.9 on page 17). Sheep SRMP is capable of exhibiting both cADPR and NAADP synthesis and their enzymatic properties are similar to those exhibited by human CD38. These observations also supports the hypothesis that CD38 or CD38-like ARC is mainly expressed in the cardiac SR. This hypothesis will be further evaluated in the next chapter.

Chapter 5

Effects of the genetic KO of CD38 on cardiac NAADP and cADPR synthesis, cardiac physiology and cardiac pathophysiology

Majority of the material presented in this chapter was published in Journal of Biological Chemistry (Lin et al., 2017). © the American Society for Biochemistry and Molecular Biology.

5.1 Background

CD38, a mammalian homologue of *Aplysia* cyclase, is the main enzyme being investigated in terms of NAADP and cADPR synthesis in mammalian cells

(Malavasi et al., 2008). The only other identified mammalian homologue of Aplysia cyclase, CD157, has been studied to a lesser extent. However, to date, there is no evidence supporting the hypothesis that CD157 is capable of catalysing *in vitro* NAADP production or endogenous NAADP production.

In mammalian tissues from the liver, spleen and pancreas, CD38 has been shown to be main enzyme for the *in vitro* synthesis of NAADP and cADPR through the base-exchange and cyclisation reactions, respectively (Chini et al., 2002). As mentioned previously (see section 1.2.9 on page 17 and 4.1 on page 115), some studies have proposed a group of non-CD38 ARCs in some tissues including the cardiac tissue. The main limitation these previous studies is the lack of evidence from a KO model. If the cardiac production of cADPR and NAADP is indeed mainly carried out by cardiac specific ARCs that are independent of CD38, the cardiac tissue of *CD38*$^{-/-}$ animals should retain some of ARC activities.

In contrast to these previous studies, the SRMP from sheep hearts exhibited properties which are normally associated with CD38 (see section 4.3 on page 119). To further evaluate whether CD38 is the main enzyme responsible for the *in vitro* synthesis of cADPR and NAADP, a genetic KO model, *CD38*$^{-/-}$, was used. The Ca^{2+} handling of cardiac myocytes and tissue from these *CD38*$^{-/-}$ animals was also investigated, aiming to shed light on the involvement of CD38 in the β-adrenoceptor signalling pathway, which are possibly associated with its ability to synthesise Ca^{2+}-mobilising messengers.

In addition, CD38 is regarded as a type-II ectoenzyme that has extracellular active sites. Not only is their access to the intracellular substrates (NAD and NADP) limited, the delivery of their products (cADPR and NAADP) to intracellular targets (such as RyRs and lysosomal TPCs) cannot be achieved simply

by diffusion. A vesicular hypothesis was proposed to resolve this topological paradox and this hypothesis suggests a process involving the internalisation of CD38 with various substrate transporters that facilitates the bi-directional movements of substrates and products (see review by Bruzzone et al. 2012). On the other hand, Lee's group has proposed that there exists a type-III CD38 with an active site facing the cytosol in human peripheral blood mononuclear cells, promyelocytic leukemic HL60 cells and the monocytic U937 cells (see review by Lee and Zhao 2014). Based on the observations on the sheep cardiac SRMP presented in Chapter 4, the hypotheses regarding expression of CD38 on the cardiac SR and its orientation are also evaluated using the *CD38*$^{-/-}$ model in this chapter.

5.2 Methods

The methods used to carry out experiments in this chapter are described in detail in Chapter 2.

C57BL6 mice (aged 12 – 20 weeks) were killed by cervical dislocation and their hearts were rapidly excised. Each set of membrane preparation was made from 6 hearts as described in section 2.10 on page 67 while ventricular cardiomyocytes were isolated from a type-II collagenase-digested Langendorff-perfused heart (see section 2.2 on page 56).

To initiate the NAADP production, 500 μM NADP and 7 mM NA were preincubated with the membrane preparation and the formation of NAADP was measured using the sea urchin egg homogenate assay (see section 2.11 on page 68).

To initiate the cGPDR production, 500 μM β-NGD was added to the membrane preparation and the formation of cGDPR was measured using fluorimetry (see section 2.12.1 on page 69).

The immunocytochemistry protocol was described in section 2.15 on page 72 and cells were labelled with the rabbit polyclonal anti-CD38 antibody (sc-15362, Santa Cruz Biotech, USA) or mouse monoclonal anti-RyR2 antibody (ab2827, Abcam, UK). Isolations of rabbit ventricular and atrial cardiac myocytes for immunocytochemistry experiments were carried out by Dr Daniel Aston by following the protocol described in section 2.3 on page 57.

For the measurement of Ca^{2+} transients (see section 2.5 on page 60), ventricular cardiomyocytes were incubated with Fluo-5F-AM (5 μM) for 20 – 30 minutes and electrically field stimulated to evoke action potentials at 1 Hz. Global Ca^{2+} transients were recorded with a Nipkow spinning disc confocal microscope (50 frames s^{-1}). Single cell contraction (done in collaboration with Dr. Emma Bolton) and whole heart electrophysiology studies were carried out by following protocols described in section 2.7 on page 62 and in section 2.16 on page 73.

5.3 Results

5.3.1 Lack of cardiac cGDPR and NAADP synthesis in membrane preparation from *CD38*$^{-/-}$ mice at pH 7.2

To investigate the main enzyme responsible for NAADP and cADPR synthesis in cardiac muscle, a model (*CD38*$^{-/-}$) lacking the most common ARC, CD38, was

used. The genetic modification involving the replacement of exons 2 and 3 with the neomycin resistance gene, resulted in the loss of CD38 proteins (Cockayne et al., 1998; Partida-Sánchez et al., 2001). The membrane preparation was isolated from hearts of WT and *CD38*$^{-/-}$ animals. Sea urchin egg homogenates were used to measure the amount of NAADP (see section 2.11 on page 68). The membrane preparation from WT hearts was able to produce NAADP in a time-dependent manner when supplied with 500 μM NADP and 7 mM NA (**Figure 17A**). On the contrary, the membrane preparation from *CD38*$^{-/-}$ hearts failed to produce a detectable amount of NAADP (WT, 0.39 $\pm$ 0.05 nmol mg^{-1} min^{-1}; *CD38*$^{-/-}$, -0.00031 $\pm$ 0.0009 nmol mg^{-1} min^{-1}; n = 3 for both groups; $p < 0.001$; **Figure 17A** and **17B**).

An NGD assay was used to gauge the rate of cADPR synthesis (see section 2.12.1 on page 69). Using this assay, the nicotinamide-sensitive cyclisation of NGD into cGDPR was detected in the membranes from WT hearts but not from *CD38*$^{-/-}$ hearts (WT, 130 $\pm$ 30 r.f.u. mg^{-1} min^{-1} ; *CD38*$^{-/-}$, -9.1 $\pm$ 5 mg^{-1} min^{-1}; n = 6 for both groups; $p < 0.001$; **Figure 17C** and **17D**).

These observations are consistent with the hypothesis that CD38 is the main enzyme responsible for the cardiac synthesis of both NAADP and cADPR.

Figure 17

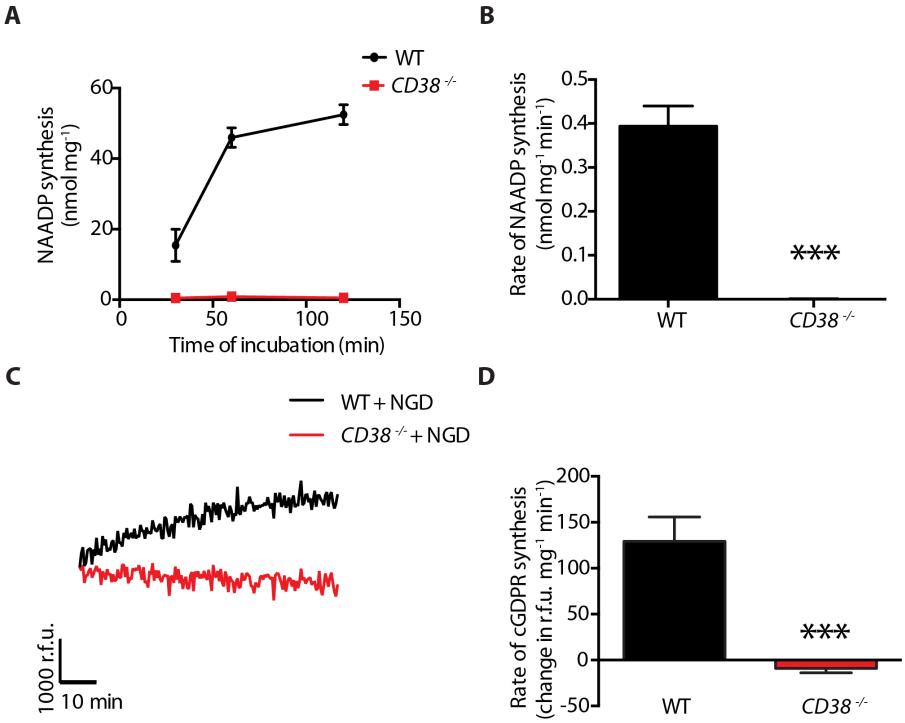


Figure 17: *In vitro* NAADP and cGDPR synthesis was not detectable in cardiac membrane preparation from *CD38*$^{-/-}$ mice at pH 7.2

A and **B** show the time course and average rate of NAADP synthesis by cardiac membrane preparation from WT and *CD38*$^{-/-}$ mice at pH 7.2 (n = 3 in both groups). **C** and **D** show the representative traces of fluorimetric measurement and average rate of cGDPR synthesis by cardiac membrane preparation from WT and *CD38*$^{-/-}$ mice at pH 7.2 (n = 6 in both groups).

Note: All experiments were conducted at pH 7.2. NGD assays were conducted at 37 °C. Measurements of NAADP using sea urchin egg homogenates were conducted at 17 °C and samples from incubations (37 °C) were diluted accordingly before addition, in order to achieve optimal measurements. Numerical data in **A**, **B** and **C** are reported as the mean ± SEM. "n" refers to "the number of independent incubations". Both WT and *CD38*$^{-/-}$ membrane preparation was derived from 3 sets of hearts each, where each set contained 6 individual hearts. *** denotes $p < 0.001$ relative to the WT control, determined by Student's t-test. "mg^{-1}" refers to "per mg protein found in the incubation". "r.f.u." refers to "relative fluorescence unit".

5.3.2 Lack of cardiac NAADP synthesis in the membrane preparation from *CD38*$^{-/-}$ mice at pH 4.5

In Chapter 4, a pH-biased property of ARCs from sheep cardiac SRMP was reported. At an acidic pH of 4.5, these ARCs strongly preferred to carry out the base-exchange reaction to the cyclisation reaction. In other words, at pH 4.5, NAADP synthesis was strongly favoured. This is supported by the observation that NAADP synthesis in the SRMP was not inhibited by high concentration of NAD (2.5 mM), which is the substrate to synthesise cADPR (see section 4.3.3 on page 125). In contrast, at pH 7.2, the NAADP synthesis was inhibited by 2.5 mM NAD (see section 4.3.2 on page 122). The acidic pH also weakened the effect of SAN4825, which is an ARC inhibitor in hindering the NAADP synthesising reaction (see section 6.3.3 on page 200 and 6.3.4 on page 202). One might postulate the existence of an unidentified, non-CD38, NAADP-synthesising enzyme which has one or the combination of the below characteristics: i) It is only functionally efficient in an acidic environment ii) Its rate of NAADP synthesis is greatly enhanced under acidic environment or iii) It has an enzymatic pocket that is structurally different from CD38 and therefore is unaffected by NAD or SAN4825. To address this concern, experiments were carried out to evaluate the NAADP synthesis at pH 4.5 using the membrane preparation from *CD38*$^{-/-}$ hearts. As shown in **figure 18 A** and **B**, the amount of NAADP produced under this condition (*CD38*$^{-/-}$, pH 4.5) remained undetectable and clearly not comparable with the NAADP synthesised in the WT hearts at pH 7.2. It was therefore concluded that the pH bias observed in acidic NAADP synthesis pertained to a CD38 enzyme (see also section 6.3.4 on page 202). In addition, the NAADP synthesis in membrane from *CD38*$^{-/-}$ hearts was not significantly different under different pH (WT at pH 7.2, 0.39 $\pm$ 0.05 nmol mg^{-1} min^{-1}; *CD38*$^{-/-}$ at pH 7.2, -0.00031 $\pm$ 0.0009 nmol mg^{-1} min^{-1}; n = 3 for

both groups *CD38*$^{-/-}$ at pH 4.5, 0.0032 ± 0.001 nmol mg^{-1} min^{-1}; n = 3 for all groups; **figure 18 B**). The loss of functional CD38 seems correlated with the loss of pH dependency of the NAADP synthesis, providing further evidence that CD38 is the major enzyme in cardiac NAADP synthesis.

Figure 18

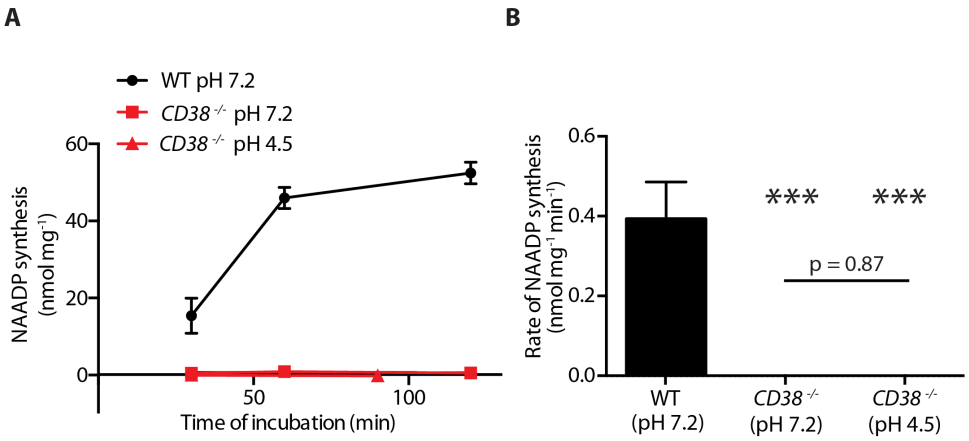


Figure 18: *In vitro* NAADP synthesis remained remained undetectable at pH 4.5 in cardiac membrane preparation from *CD38*$^{-/-}$ mice

A and **B** show the time course and average rate of NAADP synthesis by cardiac membrane preparation from WT and *CD38*$^{-/-}$ mice at pH 4.5 (n = 3)

Note: Measurements of NAADP using sea urchin egg homogenates were conducted at 17 °C and samples from incubations (37 °C) were diluted accordingly before addition, in order to achieve optimal measurements. Numerical data in **A**, **B** and **C** are reported as the mean ± SEM. "n" refers to "the number of independent incubations". Both WT and CD38$^{-/-}$ membrane preparation in these experiments was derived from 3 sets of hearts each, where each set contained 6 individual hearts. *** denotes $p < 0.001$ relative to the WT control, determined by Student's t-test. "mg^{-1}" refers to "per mg protein found in the incubation".

5.3.3 Lack of NAADP synthesis in intact cardiac myocytes from *CD38$^{-/-}$*

The observations regarding the lack of *in vitro* NAADP and cGDPR production in cardiac membrane preparation from *CD38$^{-/-}$* animals are consistent with the previously published observations (Partida-Sánchez et al., 2001; Soares et al., 2007; Cosker et al., 2010). Similarly, they showed that the NAADP and cADPR production in the heart homogenates was not detected when CD38 proteins were not expressed. Their heart homogenates, as well as the membrane preparation used in the experiments described in the thesis, did not discriminate cardiac myocytes from the other cell types found in the heart such as smooth muscle and endothelial cells of the coronary vasculature and the endocardium, fibroblasts and other connective tissue cells, mast cells, and other immune system-related cells. In order to evaluate whether CD38 is the main ARC in cardiac myocytes, the ability of isolated single cardiac myocytes to synthesise NAADP was subsequently assessed.

The enzymatic synthesis of NAADP in intact cardiac ventricular myocytes from WT mice was investigated using the assay procedures used above for the cardiac membrane preparation (see section 2.11 on page 68). Cells were supplemented with 500 μM NAADP and 7 mM NA in the extracellular solution. There was detectable production of NAADP in these intact ventricular cardiomyocytes isolated from WT mice while a similar level of NAADP production was not detected using ventricular myocytes from *CD38$^{-/-}$ mice*. Omission of NA also suppressed NAADP production in myocytes from WT mice, similar to those observed in sheep cardiac SRMP (see section 4.3.1 on page 119) (WT with NA, 0.35 $\pm$ 0.08 nmol mg^{-1} min^{-1}; WT without NA, -0.009 $\pm$ 0.02 nmol mg^{-1} min^{-1}; *CD38$^{-/-}$*, -0.002 $\pm$ 0.001 mg^{-1} min^{-1}; n = 4 or 5 in each group; $p < 0.01$; **Figure 19**).

Figure 19

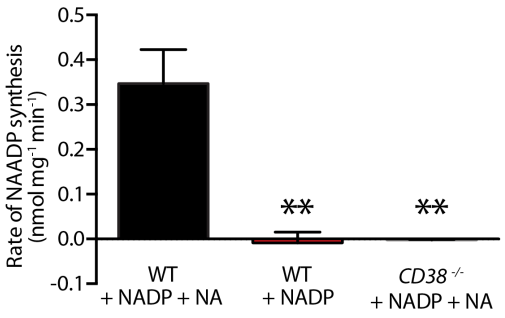


Figure 19: NAADP synthesis was undetectable in single ventricular cardiac myocytes isolated from *CD38$^{-/-}$ mice*

The bar graph shows the rate of NAADP synthesis in WT ventricular cardiac myocytes with and without NA, and in ventricular cardiac myocytes isolated from *CD38$^{-/-}$ mice* (n = 5 for WT with NA and *CD38$^{-/-}$ mice*, n = 4 for WT without NA).

Note: All experiments were conducted at pH 7.2. Measurements of NAADP using sea urchin egg homogenates were conducted at 17 °C and samples from incubations (37 °C) were diluted accordingly before addition, in order to achieve optimal measurements. Numerical data are reported as the mean ± SEM. ** denotes $p < 0.01$ relative to the control (WT + NADP +NA), determined by Student's t-test. "n" refers to "the number of independent experiments using myocytes isolated from two hearts from each group". "mg^{-1}" refers to "per mg protein found in the incubation".

5.3.4 Permeabilisation with Triton X-100 or saponin increased NAADP synthesis rate in single ventricular cardiomyocytes from mice

Since the discovery of CD38, it has been considered as a type-II membrane protein or an ectoenzyme that has an extracellular active site. This topological orientation of CD38 was challenged by Lee's group (Zhao et al., 2011, 2012, 2015). They showed that not only artificial expression of intracellular CD38 resulted in a catalytically

functional and stable CD38, this CD38 was also successfully recognised by a type-III specific CD38 antibody. This highlights the possibility of a functional CD38 with a cytosolic-facing active site.

In section 5.3.3 on page 153, it was demonstrated that the importance of CD38 expression in the NAADP production in the intact single cardiac myocytes. As dead cells were present in the cell culture, it was not possible to determine whether the observed NAADP synthesis is a result of the CD38 expressed extracellularly or the loss of integrity of membranes of dead cells (allowing the access of substrates to intracellular active sites of the CD38) or a combination of both. In section 4.3 on page 119, the possibility of CD38-like ARC expressed in the SR was also demonstrated and this supports the hypothesis regarding the existence of an intracellular CD38 in cardiac tissue.

In this section, as to whether CD38 is exclusively expressed extracellularly in the heart was investigated. If some or all CD38 is indeed expressed intracellularly, permeabilising the cell membrane will allow substrates gaining access to the cell interior and additional production of NAADP will be carried out by enzymes with intracellular active sites. Firstly, it was shown that permeabilisation of the ventricular cardiac myocytes with Triton X-100 (0.1% v/v) caused a substantial increase in the rate of NAADP production compared with intact cells, when both were supplemented with NADP (500 μM) and NA (7 mM) (intact: 0.11 $\pm$ 0.02 nmol mg^{-1} min^{-1} n = 3; Triton X-100-permeabilised: 0.25 $\pm$ 0.03 nmol mg^{-1} min^{-1}; n = 3, $p < 0.05$; **Figure 20A**).

As Triton X-100 does not discriminate the types of membranes (extracellular membrane or organellar membranes), permeabilisation experiments were performed using a milder permeabilising agent, saponin. Saponin was shown to be specific for

cholesterol-dominant membranes such as the cellular membrane, and therefore saponin does not permeabilise the intraorganellar membrane (Lukyanenko and Gyorke, 1999; Böttger and Melzig, 2013). Permeabilisation of the ventricular cardiac myocytes with saponin (0.01% w/v) also caused a substantial increase in the rate of NAADP production compared with intact cells (intact: 0.077 ± 0.01 nmol mg^{-1} min^{-1}; saponin-permeabilised: 0.26 ± 0.1 nmol mg^{-1} min^{-1}; n = 3, $p < 0.05$; **Figure 20B** and **C**). This increase in the rate of NAADP production by saponin was comparable to the increase observed in the Triton X-100 permeabilised cells (**Figure 20C**). These observations are consistent with an intracellularly expressed CD38. Furthermore, the observation that Triton X-100 did not further increase the NAADP synthesis rate of saponin-permeabilised cell (by further exposing luminal proteins) also supports the existence of a type-III intracellular CD38 in cardiac myocytes that has a cytosolic facing active site, instead of a luminal facing active site (Triton X-100 and saponin-permeabilised cell, 0.26 ± 0.01 nmol mg^{-1} min^{-1}; n = 4, $p > 0.05$; **Figure 20B** and **C**).

On the other hand, NAADP production was not revealed or enhanced by permeabilising the ventricular cardiac myocytes from *CD38*$^{-/-}$ mice with Triton X-100 (0.1%) (intact *CD38*$^{-/-}$; -0.001 ± 0.0004 mg^{-1} min^{-1}; Triton X-100-permeabilised *CD38*$^{-/-}$; 0.003 ± 0.0001 mg^{-1} min^{-1}; n = 4 for both groups, $p > 0.05$; **Figure 20C**). This is consistent with the hypothesis that expression of CD38 is not constrained to the cell surface membrane and intracellular CD38 is responsible for the increase in the rate of NAADP production in the permeabilised cells. Control experiments have also been conducted to show the detergents at the concentration used in these experiments did not affect the ability of sea urchin egg homogenates as a bioassay (**Figure 21**).

Figure 20

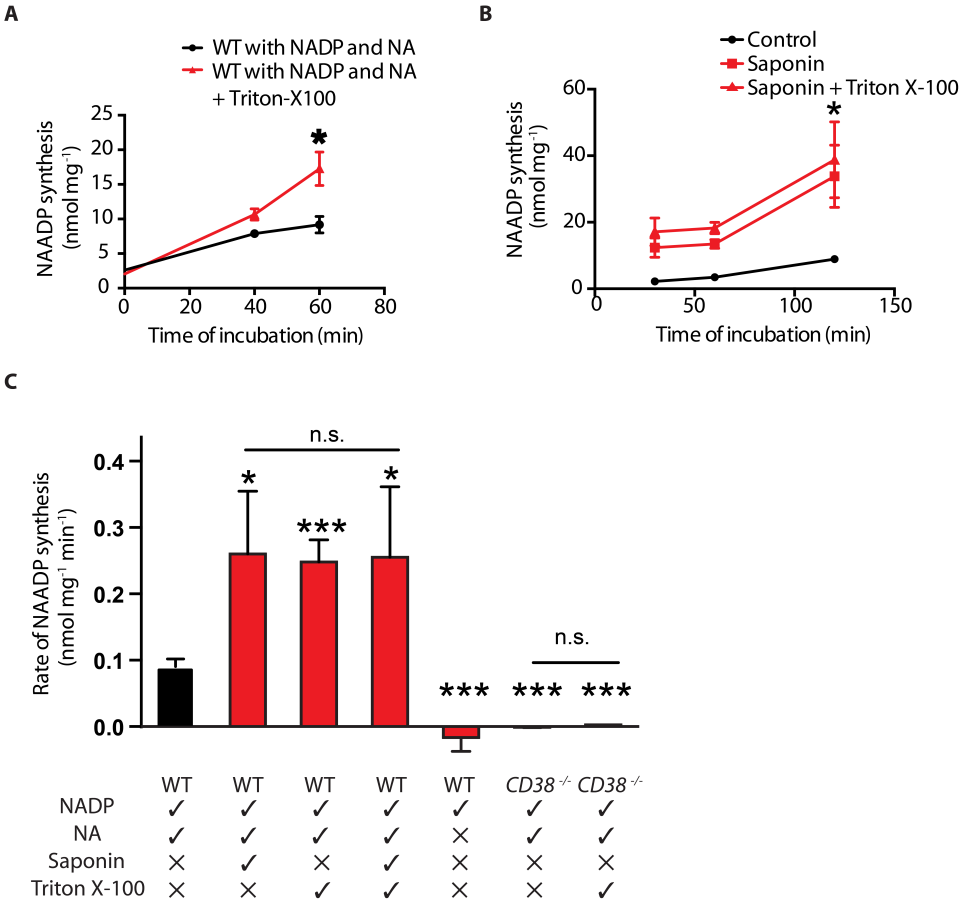

A
WT with NADP and NA
WT with NADP and NA
+ Triton-X100
NAADP synthesis
(nmol mg-1)
Time of incubation (min)
B
Control
Saponin
Saponin + Triton X-100
NAADP synthesis
(nmol mg-1)
Time of incubation (min)
C
Rate of NAADP synthesis
(nmol mg-1 min-1)
n.s.
n.s.
WT WT WT WT WT CD38 -/- CD38 -/-
NADP ✓ ✓ ✓ ✓ ✓ ✓ ✓
NA ✓ ✓ ✓ ✓ × ✓ ✓
Saponin × ✓ × ✓ × × ×
Triton X-100 × × ✓ ✓ × × ✓

Figure 20: Permeabilisation of ventricular cardiomyocytes with saponin (0.01% w/v) and Triton X-100 (0.1% v/v) led to an increased rate of NAADP synthesis

A shows the time course of NAADP synthesis by intact ventricular cardiomyocytes and Triton X-100-permeabilised ventricular cardiomyocytes (n = 3 in each group).
B shows the time course of NAADP synthesis by intact, saponin-permeabilised and Triton X-100 (in addition to saponin)-permeabilised ventricular cardiomyocytes (n = 4 in each group).
C shows a bar graph of the average rate of NAADP production by cardiomyocytes from WT and *CD38*$^{-/-}$ animals under different conditions. The rates of synthesis of intact WT myocytes were pooled from **A** and **B** (n = 7). The rest of the groups has an n number of 4 apart from WT with Triton X-100 (n = 3).

Note: Permeabilisation was achieved by preincubating cardiac myocytes with saponin or Triton X-100 for 15 min before the base exchange reaction was initiated with addition of 500 μM NADP and 7 mM NA. Incubation of substrates and cardiac myocytes were conducted at 37 °C, and the measurements of NAADP using sea urchin egg homogenates were conducted at 17 °C. Samples from incubations were diluted accordingly before addition, in order to achieve optimal measurements. Numerical data are reported as the mean ± SEM. "n" refers to "the number of independent experiments using myocytes isolated from 2 to 3 hearts from WT or *CD38*$^{-/-}$ animals". * denotes $p < 0.05$; *** denotes $p < 0.001$ relative to the intact, non-permeabilised WT myocytes, as determined by Student's t-test. "mg^{-1}" refers to "per mg protein found in the incubation".

Figure 21

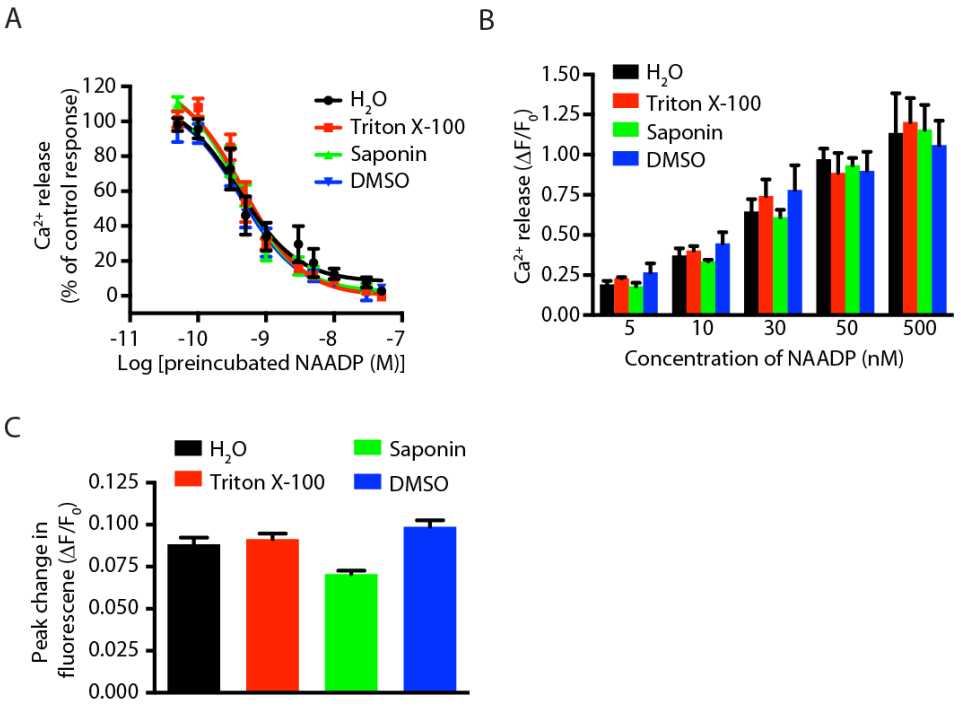


Figure 21: Effects of H_20, Triton X-100, saponin and DMSO on the sea urchin egg homogenate bioassay

The homologous inactivation properties of NAADP (**A**) and the ability of NAADP to mediate Ca^{2+} release (**B**) in sea urchin egg homogenates in the presence of H_20, Triton X-100, saponin or DMSO are shown. **C** shows the change in Ca^{2+}-dependent fluorescence after the addition of H_20, Triton X-100, saponin or DMSO in the sea urchin egg homogenates bioassay. Note: These addition artefacts are relatively small ($< 10\%$) compared to the change in Ca^{2+} dependent fluorescence caused by 500 nM NAADP. These control experiments show that the homologous inactivation properties and the NAADP-mediated Ca^{2+} release are not affected by permeabilising agents or solvents used in current studies reported in this chapter, supporting the reliability of the NAADP measurements using sea urchin egg homogenates under these conditions. Concentrations of Triton X-100 ($5\ x\ 10^{-5}\%$ v/v), saponin ($5\ x\ 10^{-6}\%$ w/v) and DMSO ($5\ x\ 10^{-4}\%$ v/v) used in these experiments correspond to the highest final concentrations present in the sea urchin egg homogenates in studies reported in this thesis. n = 3 wells of sea urchin egg homogenates in each group. No statistical difference in mean was observed between groups in **A** and **B** ($p > 0.05$, determined by StudentâĂŹs t-test).

5.3.5 Permeabilisation with Triton X-100 revealed CD38 labelling in ventricular cardiomyocytes isolated from WT but not *CD38*$^{-/-}$ mice

Following the observation of the effect of membrane permeabilisation on increasing the rate of NAADP synthesis, further investigation was carried out to evaluate whether this permeabilisation had any effect on the immunostaining of CD38.

A rabbit polyclonal antibody (sc-15362, Santa Cruz Biotech, USA) targeting human CD38 was used to validate the presence of this enzyme in mice, since the amino acid sequence (residue 1-170) used to generate the antibody showed extensive ($\approx 70\%$) similarities between the two species (**Figure 22A**). When the surface

membrane was intact in the absence of Triton X-100, there was rather little immunolabelling in WT mouse cardiac myocytes, and this labelling appeared to be concentrated in membrane patches (**Figure 22B**, top panels). When Triton X-100 (0.1% v/v) was used to permeabilise the cell membrane, the labelling by the CD38 antibody was much more extensive and showed striations with a spacing corresponding to the sarcomere length of $\approx$ 2 μm (**Figure 22B**, middle panels). Convincing evidence that the human CD38 antibody was indeed labelling the CD38 proteins was provided by the observation that little or no labelling was detected in permeabilised cardiac ventricular myocytes from *CD38*$^{-/-}$ mice (**Figure 22B**, bottom panels). A striated pattern with a spacing close to 2 μm (shown by representative plots of intensity for a line positioned along the long axis of the cells) was observed in myocytes from WT but not *CD38*$^{-/-}$ mice (**Figure 22C**).

The amino sequence used to raise the rabbit anti-CD38 polyclonal antibody spans through the cytosolic, transmembrane and extracellular portion of the CD38 protein. Further experiments were carried out on mouse spleen tissue (prefixed transcardially with 4% PFA) provided by Daniel Anthony's lab to evaluate the main region of the protein targeted by the antibody. Spleen contains numerous immune cells that possess extracellular CD38 (Malavasi et al., 2008). It was revealed that even without Triton X-100, the antibody was able to label CD38 on the surface of the tissue **Figure 23**. Application of Triton-X100 before the antibody labelling did not alter the staining. Given that the CD38 antibody used is a polyclonal antibody, extra caution needed to be taken to determine its binding site. This preliminary observation provides support for the hypothesis that the polyclonal antibody was mainly targeting the C terminus of the protein where the enzymatic active site was, rather than the N terminus. This also shows that Triton X-100 is not necessary for the binding of antibodies to CD38 proteins; This contrasts with the requirement in cardiac myocytes for permeabilisation

with Triton X-100 to allow antibodies to gain assess to those proteins if they are expressed intracellularly, as seen in the immunolabelling of cardiac myocytes (**Figure 22B**).

Together with the observations in section 5.3.4 on page 154, it seems that the majority of the CD38 proteins (or their C-termini) are expressed intracellularly in the heart (unlike in the spleen tissue) and these cardiac CD38 proteins are likely to have cytosolic-facing active sites.

Figure 22

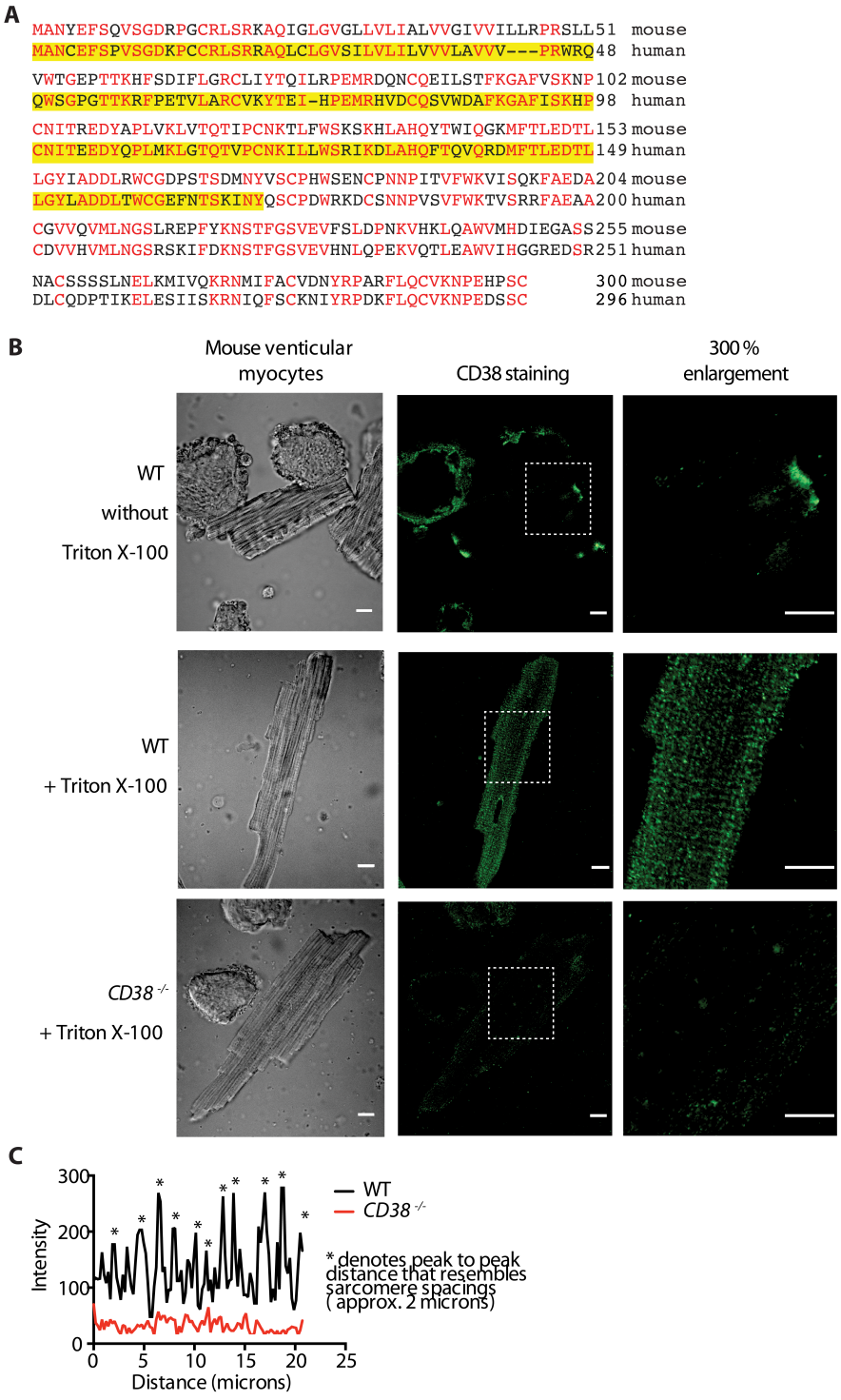

A
MANYEFSQVSGDRPGCRLSRKAQIGLGVGLLVLIALVVGIVVILLRPRSLL51 mouse
MANCEFSPVSGDKPCCRLSRRAQLCLGVSILVLILVVVLAVVV---PRWRQ48 human
VWTGEPTTKHFSDIFLGRCLIYTQILRPEMRDQNCQEILSTFKGAFVSKNP102 mouse
QWSGPGTTKRFPETVLARCVKYTEI-HPEMRHVDCQSVWDAFKGAFISKHP98 human
CNITREDYAPLVKLVTQTIPCNKTLFWSKSKHLAHQYTWIQGKMFTLEDTL153 mouse
CNITEEDYQPLMKLGTQTVPCNKILLWSRIKDLAHQFTQVQRDMFTLEDTL149 human
LGYIADDLRWCGDPSTSDMNYVSCPHWSENCPNNPITVFWKVISQKFAEDA204 mouse
LGYLADDLTWCGEFNTSKINYQSCPDWRKDCSNNPVSVFWKTVSRRFAEAA200 human
CGVVQVMLNGSLREPFYKNSTFGSVEVFSLDPNKVHKLQAWVMHDIEGASS255 mouse
CDVVHVMLNGSRSKIFDKNSTFGSVEVHNLQPEKVQTLEAWVIHGGREDSR251 human
NACSSSSLNELKMIVQKRNMIFACVDNYRPARFLQCVKNPEHPSC 300 mouse
DLCQDPTIKELESIISKRNIQFSCKNIYRPDKFLQCVKNPEDSSC 296 human
B
Mouse venticular myocytes
CD38 staining
300 % enlargement
WT without Triton X-100
WT + Triton X-100
CD38 -/- + Triton X-100
C
Intensity
300
200
100
0
0
5
10
15
20
25
Distance (microns)
WT
CD38 -/-
*denotes peak to peak distance that resembles sarcomere spacings (approx. 2 microns)

Figure 22: Permeabilisation with Triton X-100 revealed immunolabelling of CD38 in ventricular cardiomyocytes isolated from WT but not *CD38*$^{-/-}$ mice

A shows the amino acid sequence of human CD38 and mouse CD38. The region used to raise the antibody is highlighted in yellow. The identical amino acid sequences of mouse and human CD38 are labelled with red fonts.
B shows the immunolabelling of intact WT cardiomyocytes, Triton X-100 permeabilised WT cardiomyocytes and Triton X-100 permeabilised *CD38*$^{-/-}$ cardiomyocytes (by rabbit anti-CD38 polyclonal antibody (sc-15362); scale bar: 10 μm).
C shows the representative plots of fluorescence intensity for a line positioned along the long axes of the WT and *CD38*$^{-/-}$ cardiomyocytes.

Note: Images shown are the representative immunolabelling of the majority ($>$ 75%) observations in each group (number of observed cells $>$ 40, isolated from 4 hearts).

Figure 23

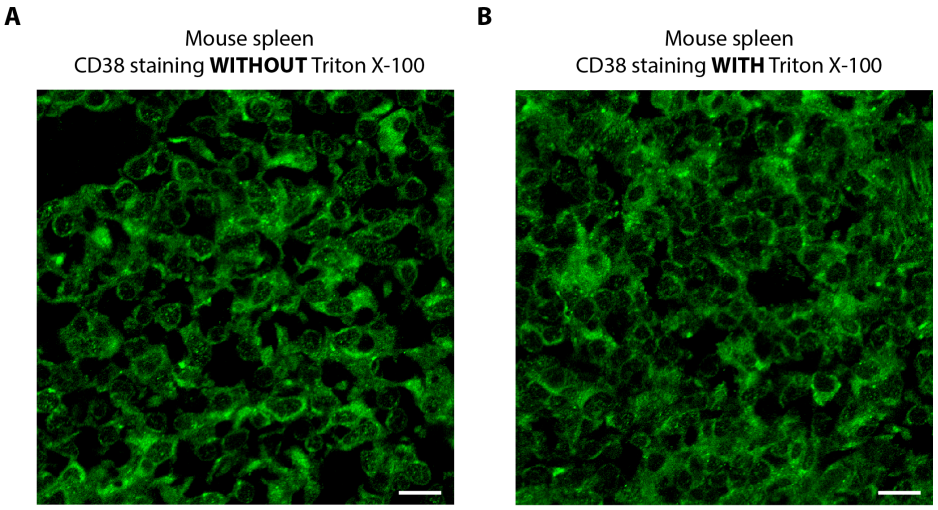


Figure 23: Rabbit anti-human CD38 polyclonal antibodies were able to stain both permeabilised and intact spleen tissue

A shows the immunolabelling of a slice of non-permeabilised mouse spleen tissue (n = 3 slices of tissue; rabbit anti-CD38 polyclonal antibody (sc-15362); scale bar: 10 μm).
B shows the immunolabelling of a slice of Triton X-100-permeabilised mouse spleen tissue (n = 3 slices of tissue; rabbit anti-CD38 polyclonal antibody (sc-15362); scale bar: 10 μm).

5.3.6 Immunolabelling of CD38 and RyR2 on ventricular and atrial cardiomyocytes from rabbits

The presence of t-tubules in ventricular myocytes renders the sarcolemmal L-type Ca^{2+} channels in close proximity to RyRs on SR. This will give rise to an apparent superposition of their corresponding immunolabelling, under a conventional confocal microscope due to the limit of its resolution. Therefore it is unclear whether the ventricular cardiac myocytes express CD38 on the sarcolemma (including t-tubules), SR or both. Since atrial myocytes from small animals such as rabbits do not have t-tubules, the expression of CD38 was investigated in these cell types (note: rabbit myocytes were used instead of mouse myocytes due to the higher yield and higher success rate of rabbit atrial isolation).

The polyclonal antibody (sc-15362) used in section 5.3.5 on page 159 successfully labelled mouse CD38, the labelling of CD38 proteins in both ventricular and atrial myocytes isolated from rabbit hearts was compared, using this antibody. In the presence of Triton X-100, which permeabilises cell membranes, immunolabelling with a striated pattern was again observed (**Figure 24 A**) that appeared to be strikingly similar to that observed in WT mouse myocytes (see section 5.3.5 on page 159) . The separation between striations appeared to be corresponding to the sarcomere length, and labelling of RyR2 with the mouse anti-RyR2 monoclonal antibody showed a similar spacing (**Figure 24 B**). Without Triton X-100, labelling with human CD38 was not only greatly reduced but appeared to show patches similar to those observed in WT mouse myocytes (**Figure 24 C**, see also **Figure 22B**, upper panel). Labelling of CD38 disappeared when the primary antibody was omitted (**Figure 24 D**).

The CD38 staining was performed on rabbit atrial cardiac myocytes and a similar

striation was observed in these atrial myocytes, as shown in **Figure 25, 26**, and **27**. As the majority of atrial myocytes from small animals do not express an extensive t-tubular network (see review by Dibb et al. 2012), these striation patterns probably resulted from the labelling of CD38 on SR. Overall, these observations provide support for the expression of CD38 on cardiac SR and are consistent with the observation of ARC and base-exchange activity in SRMP from sheep hearts (see section 4.3 on page 119).

Figure 24

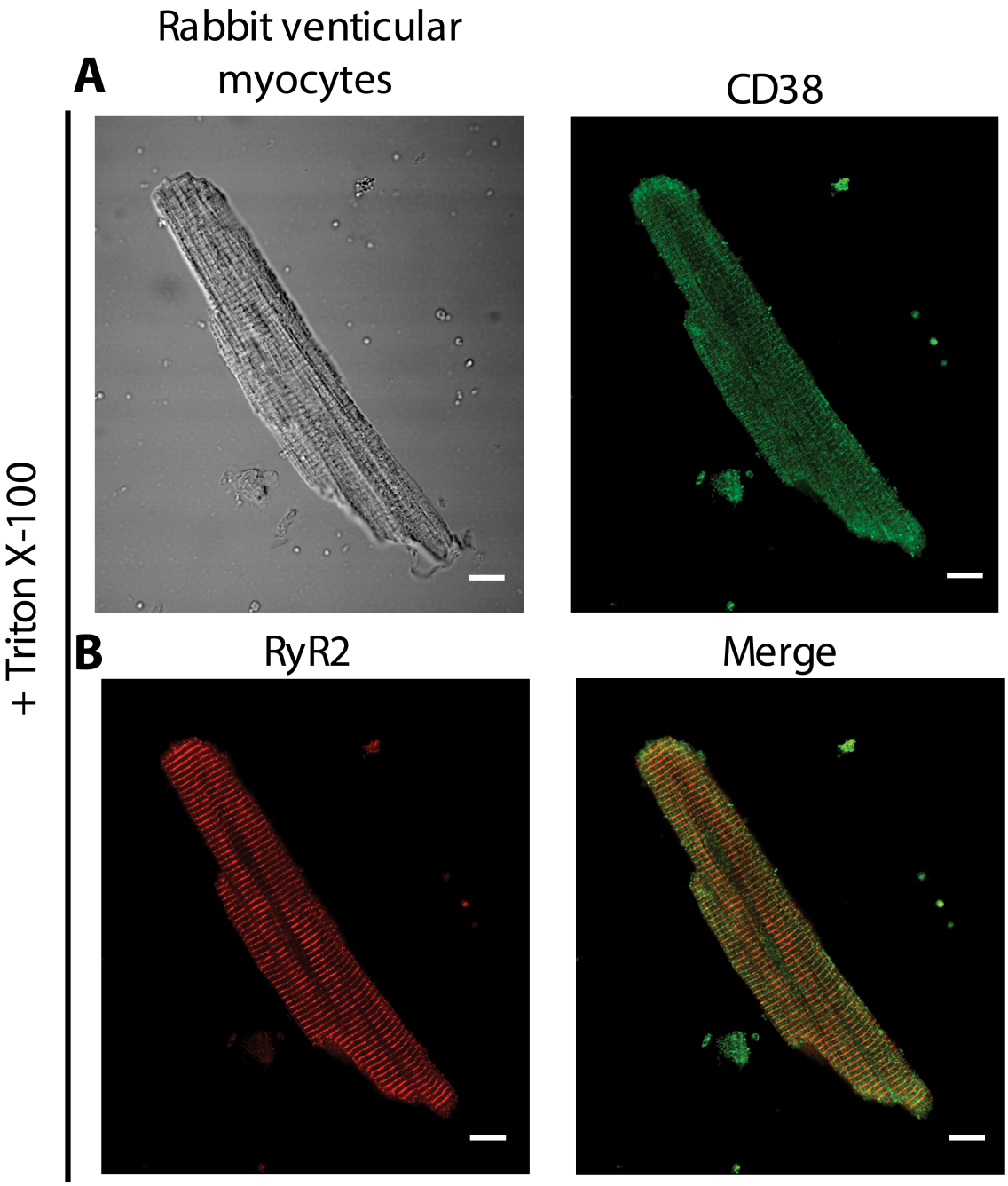


Figure 24

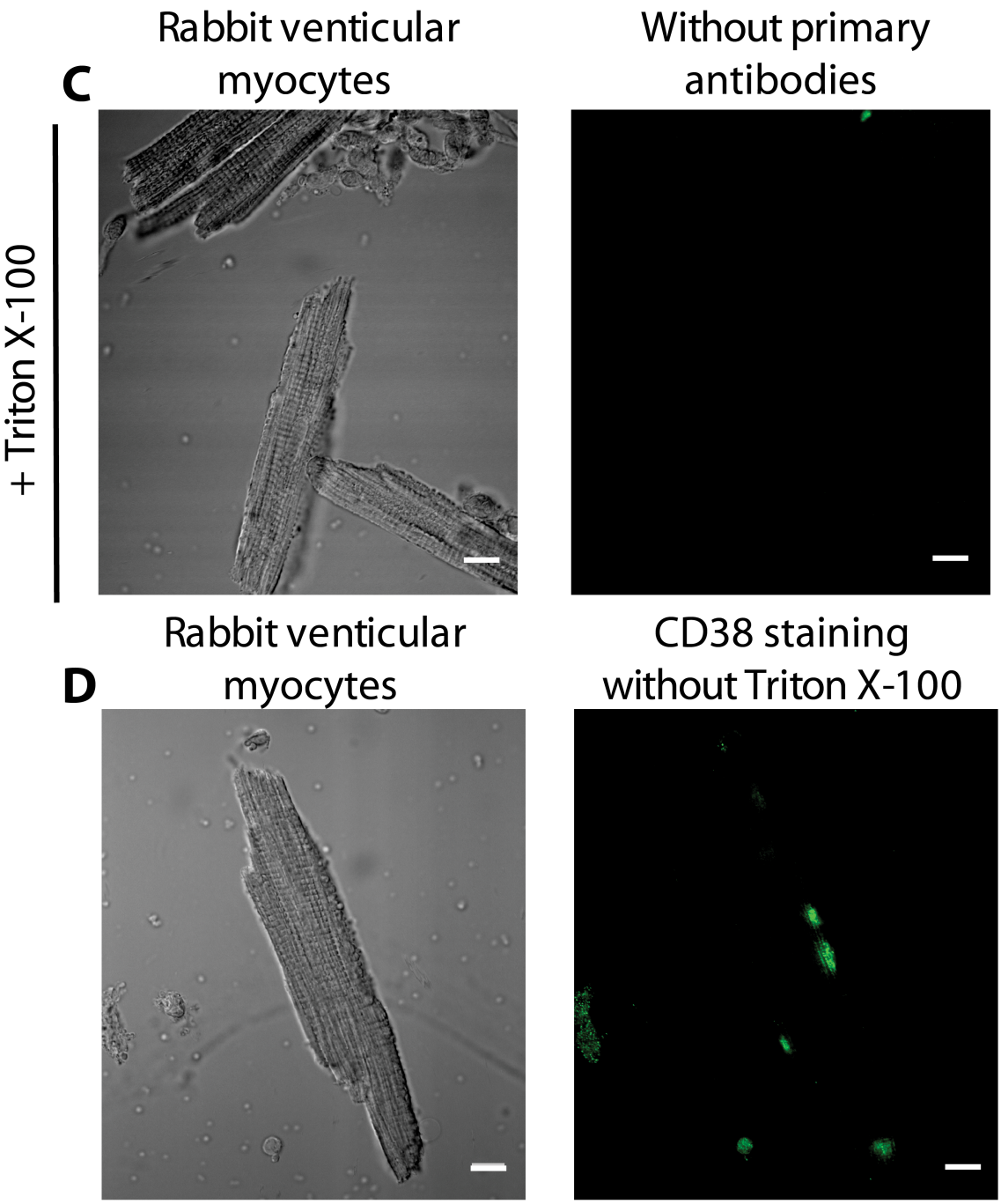

C
Rabbit venticular myocytes
Without primary antibodies
+ Triton X-100
D
Rabbit venticular myocytes
CD38 staining without Triton X-100

Figure 24: Immunolabelling of CD38 on rabbit ventricular myocytes showed a similar pattern to that observed in mouse ventricular myocytes

A shows a bright field image (left) and fluorescence image (right) of a rabbit ventricular myocyte labelled with the rabbit polyclonal anti-CD38 antibody (sc-15362).
B shows a fluorescence image (left) of a rabbit ventricular myocyte labelled with the mouse monoclonal anti-RyR2 antibodies (ab2827) and an image (right) consists of the superposition of images of CD38 and RyR2 immunolabelling.
C shows a bright field image (left) and fluorescence image (right) of a rabbit ventricular myocyte when the rabbit polyclonal anti-CD38 antibody (sc-15362) were omitted.
D shows a bright field image (left) and fluorescence image (right) of a rabbit ventricular myocyte labelled with the rabbit polyclonal anti-CD38 antibody (sc-15362) when Triton X-100 was omitted. Note: Ventricular myocytes in **A**, **B** and **C** were treated with Triton X-100 (0.1% v/v).

Note: Images shown are the representative immunolabelling of the majority ($> 75\%$) observations in each group (number of cells observed > 20, isolated from 3 rabbit hearts; scale bar: 10 μm).

Figure 25

Figure S3

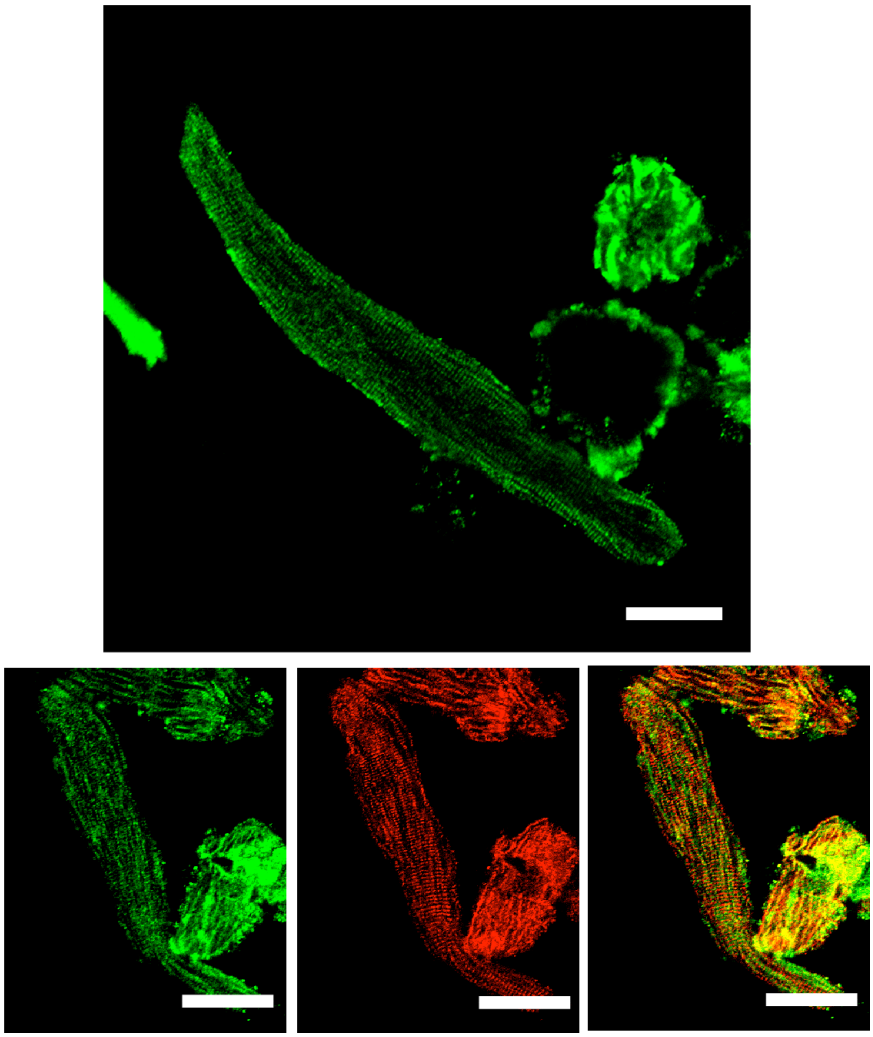


Figure 25: Immunolabelling of CD38 on rabbit atrial myocytes showed a striated pattern instead of a membrane-like staining pattern

Note: The rabbit polyclonal anti-CD38 antibody used was sc-15362. Images shown are the representative immunolabelling of the majority ($> 75\%$) observations in each group (number of cells observed >20, isolated from 2 rabbit hearts; scale bar: 20 μm).

Figure 26

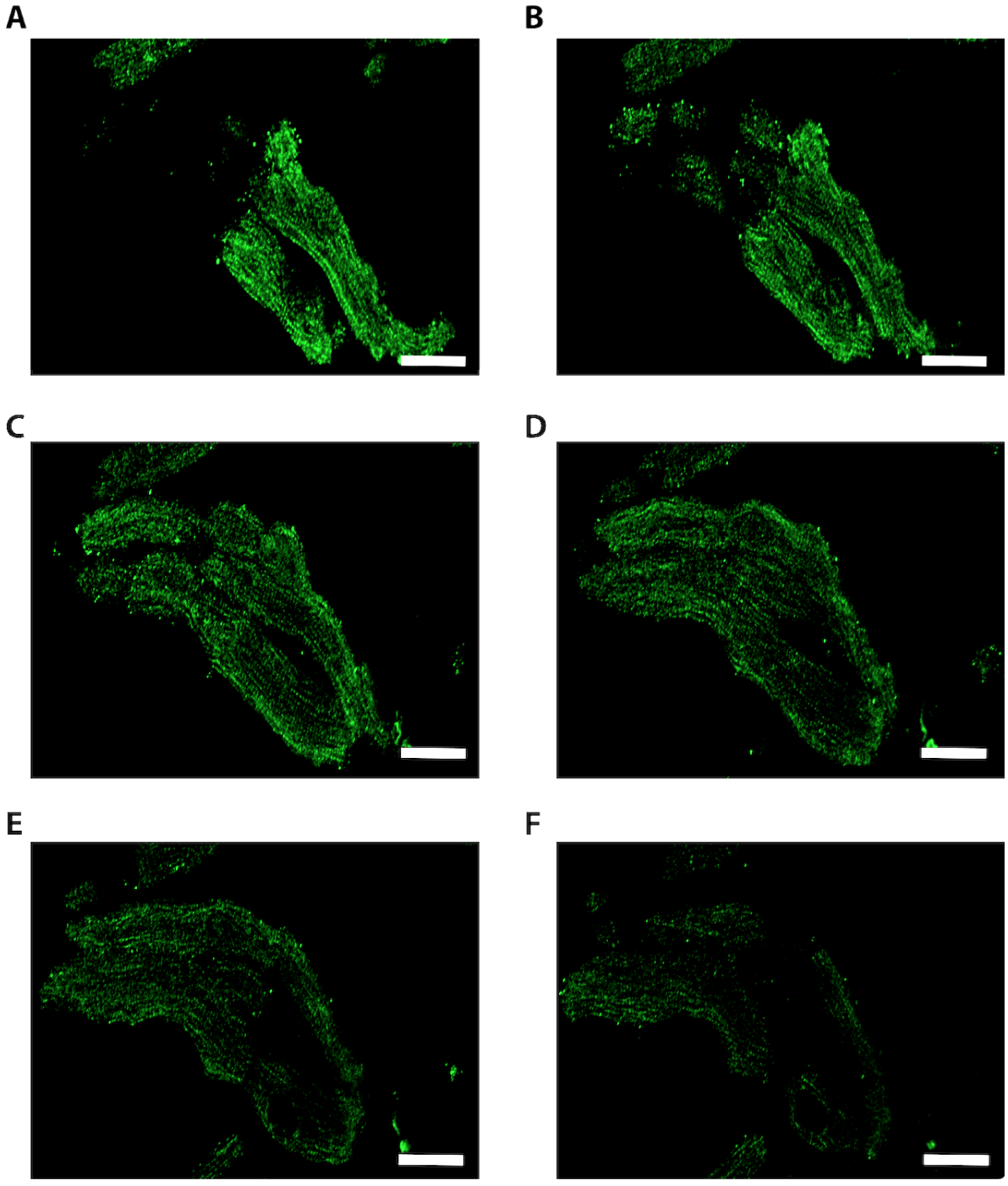


Figure 26: Z series scan of rabbit atrial myocytes labelled by the rabbit polyclonal anti-CD38 antibody

A to **F** show a representative z-series scan of fluorescence images of rabbit atrial myocytes labelled by the rabbit polyclonal anti-CD38 antibody (sc-15362). Each images has a separation of 1.5 μm in z-axis (scale bar: 20 μm).

Note: Images shown are the representative immunolabelling of the majority ($>$ 75%) observations in each group (number of cells observed $>$20, isolated from 2 rabbit hearts).

Figure 27

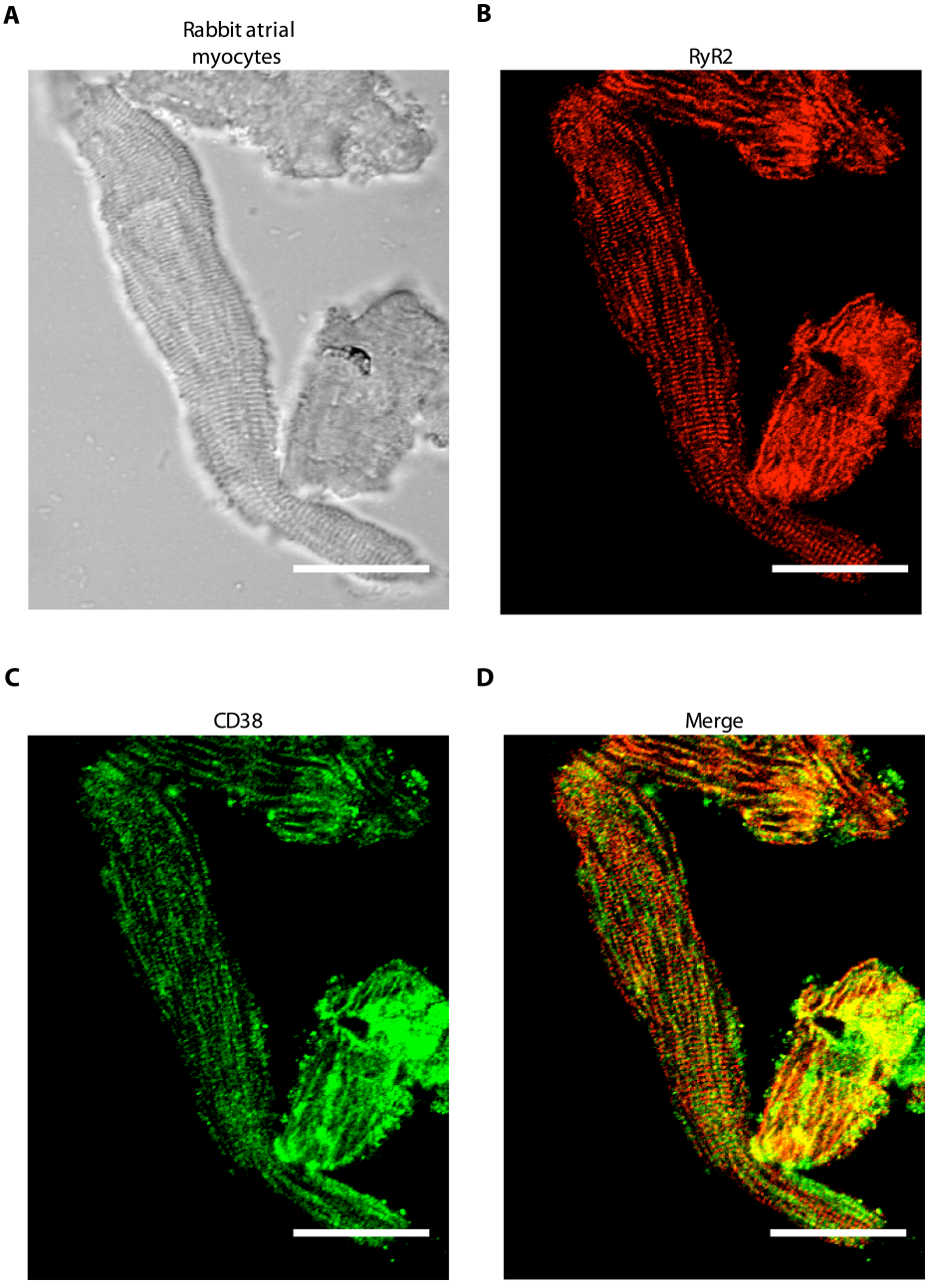


Figure 27: Dual immunolabelling of rabbit atrial myocytes by anti-CD38 and anti-RyR2 antibodies

A shows a bright field image of a rabbit ventricular myocyte labelled with the mouse monoclonal anti-RyR2 antibody (ab2827, **B**) and the rabbit polyclonal anti-CD38 antibody (sc-15362, **C**).
D shows an image consisting of the superposition of images of CD38 and RyR2 immunolabelling (scale bar: 20 μm).

Note: Images shown are the representative staining of the majority (> 75%) observations in each group (number of cells observed >20, isolated from 2 rabbit hearts).

5.3.7 Single ventricular cardiomyocytes from *CD38*$^{-/-}$ mice showed blunted Ca^{2+} transient amplitudes and sarcomere shortening magnitudes during β-adrenoceptor stimulation

In the heart, elevated levels of cADPR and NAADP have been observed following the stimulation of β-adrenoceptors (Macgregor et al., 2007a; Lewis et al., 2012; Gul et al., 2016). In the past, evidence showing cADPR and NAADP having a role in the cardiac EC coupling was reported, both under the basal conditions and during β-adrenoceptor stimulation (Rakovic et al., 1996, 1999; Macgregor et al., 2007a,b; Collins et al., 2011; Capel et al., 2015) (see also section 3.3.3 on page 89). Having shown the effectiveness of the cardiac membrane preparation from mouse hearts in synthesising NAADP and cADPR, the possible roles of CD38 in Ca^{2+} signalling were explored in intact mouse cardiac myocytes. Ventricular myocytes were stimulated with brief current pulses to initiate action potentials and Ca^{2+} transients measured using Fluo-5F-AM. It was observed that both the amplitudes of Ca^{2+} transients and the magnitudes of contractions (expressed as sarcomere

shortening) were less in myocytes from *CD38*$^{-/-}$ hearts compared with WT in the presence of 5 nM isoprenaline (WT: Ca^{2+} transient, 8.1 ± 1.5 (F/F_0), n = 9; *CD38*$^{-/-}$: Ca^{2+} transient, 5.3 ± 0.35 (F/F_0), n = 15, $p < 0.05$, **Figure 28A**; WT: contraction amplitude, 0.17 ± 0.02 μm, n = 17; *CD38*$^{-/-}$: contraction amplitude, 0.14 ± 0.02 μm, n = 11, $p < 0.05$ **Figure 28C**). Representative records are shown in **Figure 28B** and **D**. The difference observed in Ca^{2+} transient amplitudes and contraction magnitudes was interpreted as partly if not completely due to the lack of a contribution from CD38 to the elevation of cADPR and NAADP levels.

Figure 28

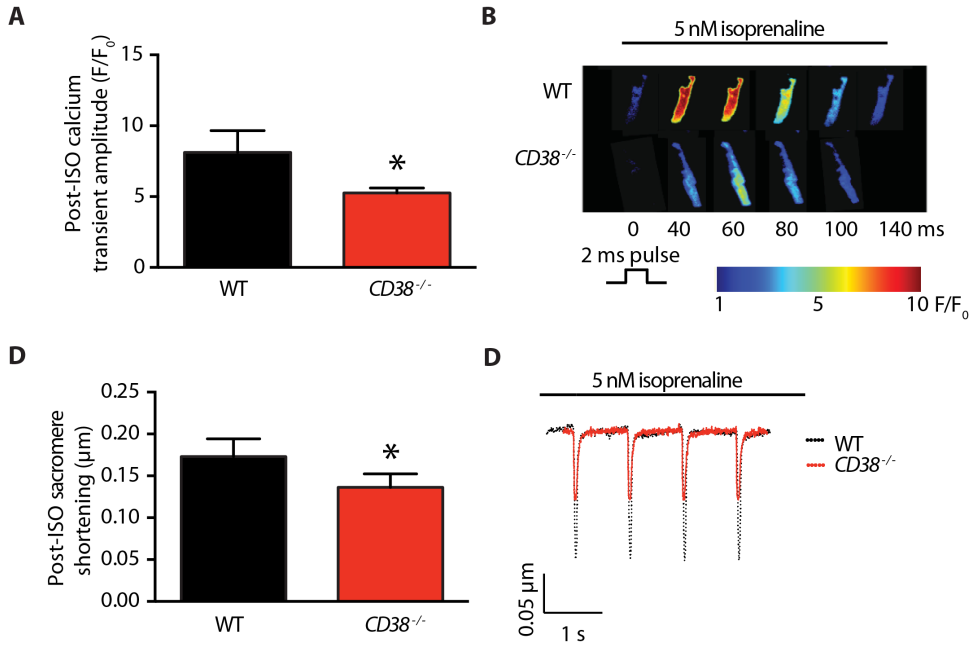


Figure 28: Single ventricular cardiomyocytes from *CD38*$^{-/-}$ mice showed blunted Ca^{2+} transients amplitudes and sarcomere shortenings during β-adrenoceptor stimulation

A shows the average Ca^{2+} transients of WT (n = 9) and *CD38*$^{-/-}$ (n = 15) single ventricular cardiomyocytes in the presence of 5 nM isoprenaline.
B shows the representative images of Ca^{2+} transients of WT and *CD38*$^{-/-}$ single ventricular cardiomyocytes in the presence of 5 nM isoprenaline.
C shows the average sarcomere shortening of WT (n = 17) and *CD38*$^{-/-}$ (n = 11) single ventricular cardiomyocytes in the presence of 5 nM isoprenaline.
D shows the recording traces of sarcomere shortening of WT and *CD38*$^{-/-}$ single ventricular cardiomyocytes in the presence of 5 nM isoprenaline.

Note: Myocytes were electrically paced at 1 Hz and either imaged with a spinning disk confocal microscope (after incubation with Fluo-5F-AM for 20 – 30 min) or imaged with an IonOptix MyoCam system at 36 °C and pH 7.4. Fluorescence data were analysed with Andor software and pClamp, while contraction measurements were analysed with IonWizard 5 software. Contraction measurements were carried out in collaboration with Dr. Emma Bolton. "ISO" refers to "isoprenaline" and "n" refers to "the number of myocytes". Numerical data in **A** and **C** are reported as the mean ± SEM. * denotes $p < 0.05$ relative to the WT control, determined by Student's t-test.

5.3.8 Bafilomycin-A1 blunted Ca^{2+} transient amplitudes in single ventricular cardiomyocytes from WT but not *CD38*$^{-/-}$ mice during β-adrenoceptor stimulation

Following the observation made in section 5.3.7 on page 173, a series of experiments was carried out to find out to what extent of the lack of NAADP production contributed to the blunted magnitude observed in Ca^{2+} transient amplitudes of *CD38*$^{-/-}$ ventricular cardiomyocytes. Bafilomycin-A1 has been reported to inhibit NAADP action in hearts (Macgregor et al., 2007a; Collins et al., 2011). In section 3.3.4 on page 91, it was shown that preincubation with bafilomycin-A1 resulted in weaker Ca^{2+} transient amplitudes of ventricular myocytes

during activation of β-adrenoceptors. Consistent with the hypothesis that CD38 is the main enzyme responsible for NAADP production, preincubation with bafilomycin-A1 (10 μM) was unable to alter the Ca^{2+} transient amplitudes of *CD38*$^{-/-}$ ventricular cardiomyocytes in the presence of isoprenaline (2 nM) to stimulate β-adrenoceptors. (Without bafilomycin-A1: 4.7 ± 0.3 (F/F_0), n = 22, 47 ± 9% increase upon isoprenaline addition, n = 19; with bafilomycin-A1: 4.2 ± 0.3 (F/F_0), n = 16, 49 ± 10% increase upon isoprenaline addition , n = 14; $p > 0.05$; **Figure 29A** and **B**). In contrast, bafilomycin-A1 was able to reduce the Ca^{2+} transient amplitudes in single ventricular cardiomyocytes from WT mice in the presence of isoprenaline (without bafilomycin-A1: 5.7 ± 0.3 (F/F_0), n = 21, 84 ± 10% increase upon isoprenaline addition , n = 10; with bafilomycin-A1: 4.4 ± 0.2 (F/F_0), n = 25, 42 ± 8% increase upon isoprenaline addition, n = 15; $p < 0.05$; **Figure 29A** and **B**). Representative records are shown in **Figure 29C**. It is also worth noting that the Ca^{2+} transient amplitudes both in absolute values and percentage increase were comparable between WT with bafilomycin-A1 pretreatment and *CD38*$^{-/-}$ groups with or without bafilomycin-A1 pretreatment (42 ± 8%, 49 ± 10%, and 47 ± 9% increase, respectively). This suggested that the genetic KO of CD38 and pharmacological inhibition of the NAADP pathway by bafilomycin-A1 have comparable qualitative and quantitative effects on the Ca^{2+} handling of ventricular myocytes, thus providing evidence that CD38 is the main NAADP-synthesising enzyme in cardiac tissue.

These observations support the hypotheses that *CD38*$^{-/-}$ cardiac myocytes are unable to trigger the NAADP signalling pathway upon stimulation of β-adrenoceptors due to the lack of NAADP production by CD38 proteins. This contributes partly if not entirely to the blunted magnitudes observed in both Ca^{2+} transients and contractions, resulting in a weakened β-adrenoceptor-mediated positive inotropic effect.

Figure 29

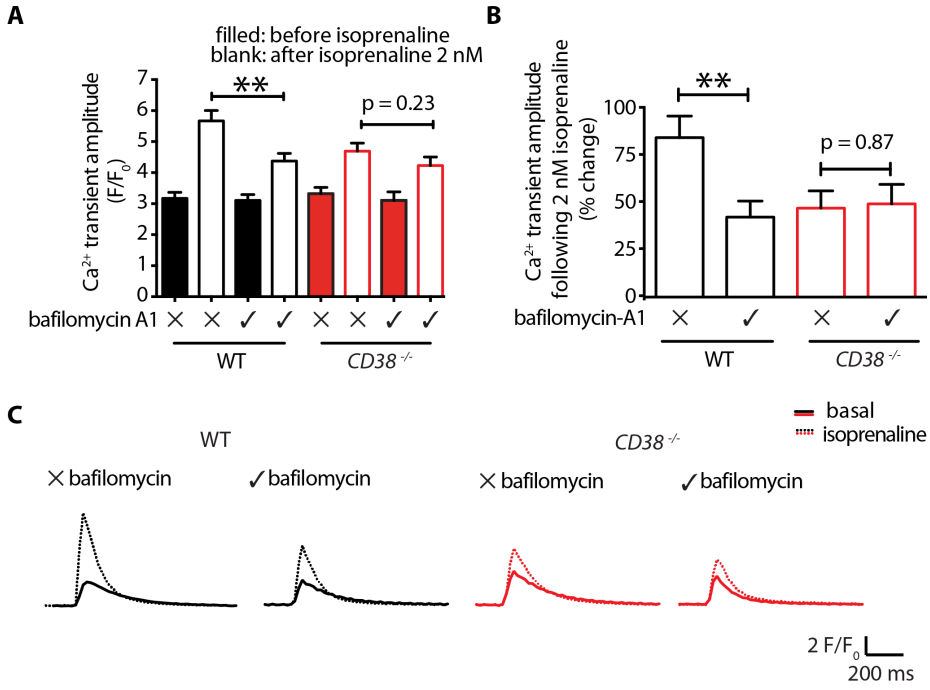


Figure 29: Pretreatment with bafilomycin-A1 did not alter the Ca^{2+} transient amplitudes of single ventricular cardiomyocytes from *CD38*$^{-/-}$ mice during activation of β-adrenoceptors

A shows the average Ca^{2+} transients before and after the addition of 2 nM isoprenaline of WT and *CD38*$^{-/-}$ single ventricular cardiomyocytes pretreated either with bafilomycin-A1 (10 μM) or DMSO (n = 16 – 25).
B shows the percentage increase of Ca^{2+} transients before and after the addition of 2 nM isoprenaline of WT and *CD38*$^{-/-}$ single ventricular cardiomyocytes pretreated either with bafilomycin-A1 (10 μM) or DMSO (n = 10 – 19).
C shows the representative traces of Ca^{2+} transients before and after the addition of 2 nM isoprenaline of WT and *CD38*$^{-/-}$ single ventricular cardiomyocytes pretreated either with bafilomycin-A1 (10 μM) or DMSO.

Note: Myocytes were electrically paced at 1 Hz and either imaged with a spinning disk confocal microscope (after incubation with Fluo-5F-AM for 20 – 30 min) at 36 °C and pH 7.4. Fluorescence data were analysed with Andor software and pClamp. "n" refers to "the number of myocytes". Numerical data in **A** and **B** are reported as the mean ± SEM. * denotes $p < 0.05$, determined by Student's t-test.

5.3.9 Langendorff-perfused hearts from *CD38*$^{-/-}$ mice were more resistant to isoprenaline-induced arrhythmogenocity

It is known that excessive β-adrenoceptor stimulation can lead to cardiac arrhythmias (Shen and Zipes, 2014). These cardiac arrhythmias were often reported to be accompanied by Ca^{2+} mishandling (Cartwright et al., 2011; Kang and Lebeche, 2013). The potential roles of NAADP and cADPR in the pathophysiology of cardiac arrhythmias were also previously published (see section 1.2.11.1 on page 23 and section 1.3.6 on page 50). In brief, an increased in the levels of NAADP and cADPR was observed during strong β-adrenoceptor stimulation (achieved through an application of a high dose of isoprenaline, $\gg 10^{-8}$M) and this could be one of the factors contributing to the development of cardiac arrhythmias. Inhibiting their pathways individually with 8-Br-cADPR (a cADPR inhibitor), BZ194 (an NAADP inhibitor), SAN4825 (an ARC inhibitor) reduced the arrhythmogenocity in single cells and whole animals (Rakovic et al., 1999; Nebel et al., 2013; Warszta et al., 2014). Such resistance to isoprenaline-induced arrhythmogenocity was also observed in the NAADP-insensitive *Tpcn2*$^{-/-}$ mouse hearts, consistent with the hypothesis that an excessive level of NAADP contribute to cardiac arrhythmias (Capel et al., 2015). Since CD38 is the enzyme responsible for the *in vitro* generation of cADPR and NAADP, the resistance of whole hearts from *CD38*$^{-/-}$ mice to isoprenaline-induced arrhythmogenocity was investigated.

The tendency of intact mouse hearts to show arrhythmias was assessed by four different protocols: i) burst pacing with increasing frequency, ii) 50 Hz burst pacing with increasing current, iii) S1S2 pacing, iv) and dynamic pacing (see section 2.16 on page 73 for details and scoring methods). It was demonstrated that WT hearts

showed a significant increase in arrhythmogenicity (determined by arrhythmogenicity score) after the application of 300 nM isoprenaline (WT: score before isoprenaline, 0.75 ± 0.3; score after isoprenaline, 2.3 ± 0.3; n = 8; $p < 0.05$, determined by Mann-Whitney test; **Figure 30A**, left panel). In contrast, no significant increase in the arrhythmogenicity was observed following isoprenaline application in hearts from the *CD38*$^{-/-}$ mice (*CD38*$^{-/-}$: score before isoprenaline, 0.17 ± 0.2; score after isoprenaline, 0.33 ± 0.3; n = 6; $p < 0.05$, determined by Mann-Whitney test; **Figure 30A**, right panel). The post-isoprenaline score of arrhythmogenocity of *CD38*$^{-/-}$ hearts was also significantly lower than WT hearts in the presence of isoprenaline (**Figure 30A**). Further analysis showed that the increase in arrhythmogenocity score was also significantly lower in *CD38*$^{-/-}$ (increase in score of WT: 1.5 ± 0.3; increase in score of *CD38*$^{-/-}$: 0.17 ± 0.2; $p < 0.05$ determined by Mann-Whitney test, figure not shown). The ratio of *CD38*$^{-/-}$ hearts that have one or more arrhythmic events during any of the 4 protocols was also significantly lower than that of WT hearts (WT: 7/8; *CD38*$^{-/-}$: 1/6; $p < 0.05$ determined by Fisher exact test; **Figure 30B**).

The cumulative percentage of hearts which became arrhythmic in the presence of isoprenaline (300 nM) during burst pacing protocol with increasing pacing frequency in **Figure 30C** again show that hearts from *CD38*$^{-/-}$ mice had a reduced tendency to arrhythmias in the presence of isoprenaline. Representative traces obtained from burst pacing experiment are shown in **Figure 30D**.

A further test of isoprenaline-induced arrhythmogenicity is to measure the current threshold for VT (see section 2.16 on page 73 for methods, **Figure 30E** and **F**). Only 1 out of 6 *CD38*$^{-/-}$ mice showed VT in this protocol, and therefore a standard deviation of the threshold cannot be determined. A one sample t-test was computed to determine whether the mean of the current threshold for VT was significantly

different from the 7-fold increase in the pacing current to induce arrhythmias (note: In the *CD38*$^{-/-}$ heart that showed arrhythmias in this protocol, the threshold current to induce VT was equal to 7-fold of the pacing current). This statistical approach assumed an equal standard deviation where the variation of the sample (WT heart in this case) was applied to the value (the threshold current to induce VT in the *CD38*$^{-/-}$ heart, which is 7-fold higher than the pacing current in this case) that it is tested against. The statistical test showed that the mean of current threshold for VT for WT hearts was significantly lower than a 7-fold change in the pacing current (WT: 3.7 $\pm$ 1 folds; *CD38*$^{-/-}$: 7, $p < 0.05$ determined by one-sample t-test; **Figure 30F**). The pacing current required to evoke an action potential in 1:1 ratio in two groups were comparable (data not shown). No significant difference in propensity to arrhythmias was observed between the two groups during dynamic and S1S2 pacing alone (data not shown).

Taken together, these observations show that the tendency for arrhythmias during strong stimulation of β-adrenoceptors was reduced in hearts from *CD38*$^{-/-}$ mice. This is consistent with the hypothesis that the lack of CD38 in *CD38*$^{-/-}$ mice, resulted in a blunted cardiac NAADP/cADPR pathways upon strong β-adrenoceptor stimulation, thus providing these hearts with the resistance to arrhythmias.

Figure 30

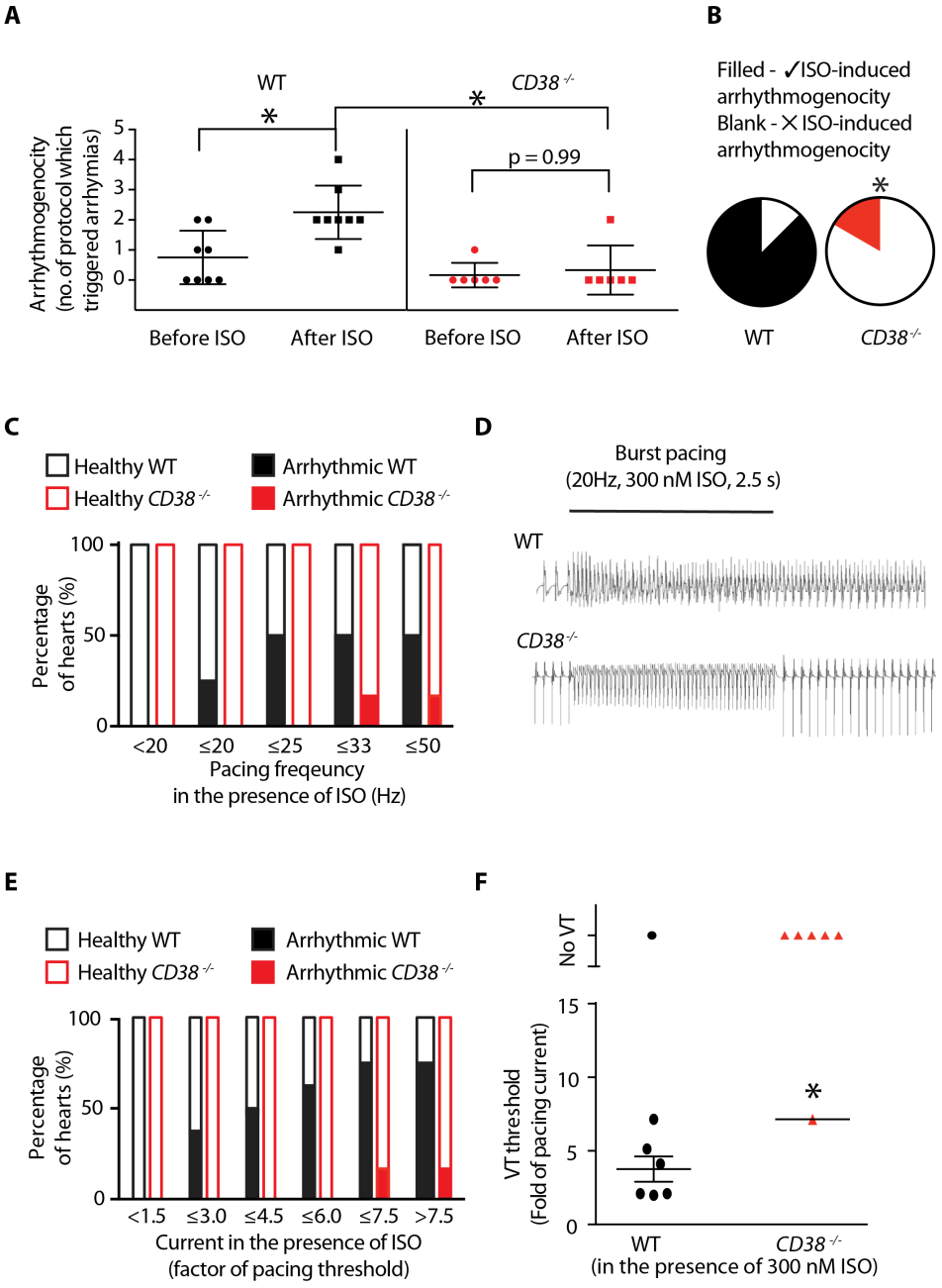

A
WT
CD38 -/-
*
*
p = 0.99
Arrhythmogenocity
(no.of protocol which
triggered arrhymias)
5
4
3
2
1
0
Before ISO
After ISO
Before ISO
After ISO
B
Filled - ✓ISO-induced
arrhythmogenocity
Blank - ✕ISO-induced
arrhythmogenocity
*
WT
CD38 -/-
C
Healthy WT
Arrhythmic WT
Healthy CD38 -/-
Arrhythmic CD38 -/-
Percentage
of hearts (%)
100
50
0
<20
≤20
≤25
≤33
≤50
Pacing freqeuncy
in the presence of ISO (Hz)
D
Burst pacing
(20Hz, 300 nM ISO, 2.5 s)
WT
CD38 -/-
E
Healthy WT
Arrhythmic WT
Healthy CD38 -/-
Arrhythmic CD38 -/-
Percentage
of hearts (%)
100
50
0
<1.5
≤3.0
≤4.5
≤6.0
≤7.5
>7.5
Current in the presence of ISO
(factor of pacing threshold)
F
No VT
VT threshold
(Fold of pacing current)
15
10
5
0
*
WT
CD38 -/-
(in the presence of 300 nM ISO)

Figure 30: Langendorff-perfused from *CD38*$^{-/-}$ mice showed resistance to isoprenaline-induced arrhythmogenocity

A shows the arrhythmogenocity score (determined by the number of programmed electrical stimulation protocols that successfully triggered arrhythmias) of both WT and *CD38*$^{-/-}$ hearts in the absence and presence of isoprenaline (300 nM).
B shows the ratio of hearts from WT and *CD38*$^{-/-}$ animals that exhibited signs of arrhythmias (filled) to those that did not exhibit signs of arrhythmias (blank) during any of the programmed electrical stimulation protocols (in the presence of 300 nM isoprenaline).
C shows the cumulative percentage of hearts that exhibited signs of arrhythmias in response to increasing pacing frequency during burst pacing protocol (in the presence of 300 nM isoprenaline).
D shows the representative traces of monophasic action potentials recorded during burst pacing experiments.
E shows the cumulative percentage of heart that exhibited signs of arrhythmias in response to increasing pacing current during burst pacing (50 Hz) protocol (in the presence of 300 nM isoprenaline).
F shows the current thresholds to trigger VT in both WT and *CD38*$^{-/-}$ hearts (in the presence of 300 nM isoprenaline).

Note: The experiments were conducted with *ex vivo* Langendorff-perfused hearts that were paced with electrodes on their ventricular septa, at 37 °C. The monophasic action potentials from these hearts were recorded with electrodes placed on the left ventricular wall. The terms "arrhythmic" or "arrhythmias" refer to conditions where six or more consecutive regular premature waveforms (VT) or irregular fibrillating waveforms were observed in the Langendorff-perfused heart recordings during the protocols. The term "healthy" refers to conditions where no signs of these events were observed; "n" refers to "the number of hearts". "ISO" refers to "isoprenaline". Numerical data in **A** and **F** are presented as the mean ± SEM. * denotes $p < 0.05$, determined by Mann Whitney test (**A**), Fisher exact test (**B**) and one sample t-test (**F**).

5.3.10 Langendorff-perfused hearts from *CD38*$^{-/-}$ mice showed reduced isoprenaline-induced positive chronotropic effect

The Ca^{2+} handling of SR is known to contribute to the pacemaking mechanisms of the sino atrial node (see review by Capel and Terrar 2015). For example, the reduction and depletion of SR Ca^{2+} stores using CPA and thapsigargin as well as disruption of RyRs using ryanodine have been shown to slow down the beating rate in both single sino atrial nodal cells and atrial tissue preparation (Rigg et al., 2000). Since Ca^{2+} loading and Ca^{2+} release of SR was shown to be dependent on the NAADP and cADPR signalling pathways respectively (see section 1.3.5 on page 46 and section 1.2.11.1 on page 23), there has been an interest in investigating the roles of these two Ca^{2+}-mobilising agents in the pacemaking mechanism. This was examined using the Langendorff heart preparation and the heart rate was derived from the intervals between action potentials (recorded by an electrode) in the ventricle tissue. Interestingly, the loss of CD38 proteins did not alter the basal beating rate of the heart (WT: 270 ± 30 beats per minute (bpm), n = 8; *CD38*$^{-/-}$: 330 ± 20 bpm, n = 6; $p > 0.05$; **Figure 31A**). However, during stimulation of β-adrenoceptors with isoprenaline, hearts from *CD38*$^{-/-}$ mice had a blunted response to β-adrenoceptor-mediated positive chronotropic effect (increase in heart rate (bpm); WT: 240 ± 30 n = 8; *CD38*$^{-/-}$: 150 ± 30 n = 6; $p < 0.05$; **Figure 31B**). This observation shed light on a possible role of these signalling molecules in pacemaking mechanisms, although further investigations have to be carried out to dissect the relevant pathways. Measurements from experiments involving S1S2 protocol and dynamic pacing protocol revealed that there was no significant difference between the post-isoprenaline refractory period of hearts from both

groups as shown in **Figure 31C** and **D** (S1S2 protocol, WT: 0.038 ± 0.007 s, n = 8; *CD38*$^{-/-}$: 0.052 ± 0.003 s, n = 6; p > 0.05; dynamic pacing protocol, WT: 0.051 ± 0.008 s, n = 8; *CD38*$^{-/-}$: 0.054 ± 0.003 s, n = 6; p > 0.05). This shows that the refractory period of the hearts does not depend on the expression of CD38, and the resistance to arrhythmias (shown in section 5.3.9 on page 178) as well as the blunted β-adrenoceptor-mediated positive chronotropic effect observed in *CD38*$^{-/-}$ hearts was probably not a consequence of lengthened refractory periods.

Figure 31

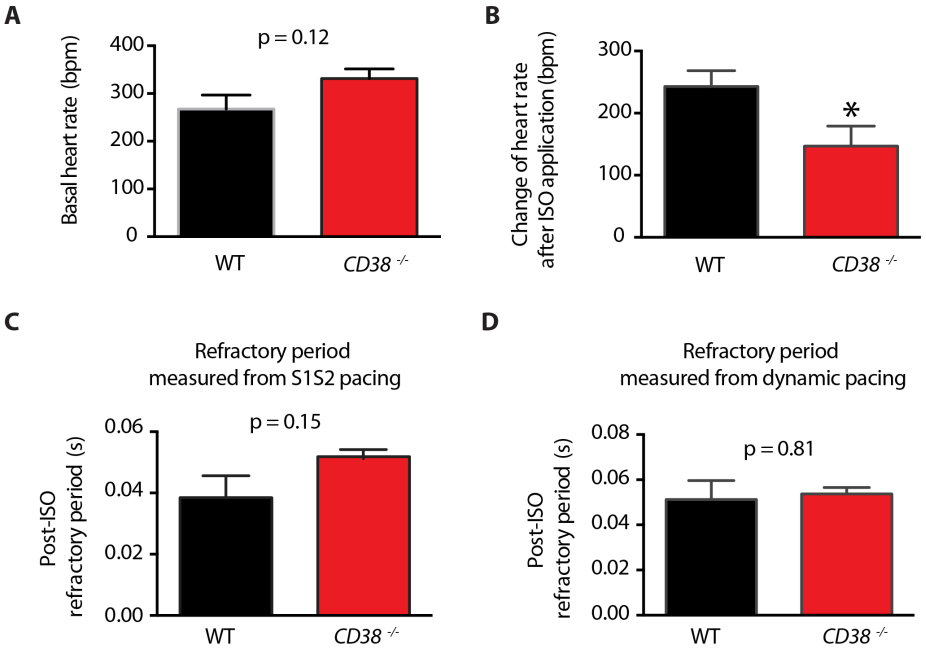


Figure 31: The basal heart rate, heart rate in the presence of isoprenaline and post-isoprenaline refractory periods of Langendorff-perfused hearts from WT and *CD38*$^{-/-}$ mice

A shows the average basal heart rate of Langendorff-perfused heart isolated from WT (n= 8) and *CD38*$^{-/-}$ mice (n = 6).
B shows the average increase of heart rate of Langendorff-perfused hearts isolated from WT (n = 8) and *CD38*$^{-/-}$ (n = 6) mice in the presence of isoprenaline (300 nM).
C and **D** show the average post-isoprenaline (300 nM) refractory period of WT and *CD38*$^{-/-}$Langendorff-perfused hearts, measured from S1S2 and dynamic pacing protocols, respectively.

Note: The experiments were conducted at 37 °C and monophasic action potentials were measured from Langendorff-perfused hearts with an electrode attached to the left ventricular wall. Heart rates were determined from intervals of action potentials, while refractory periods were determined from intervals of action potentials before the hearts become refractory (unable to evoke an action potential in 1:1 manner). "ISO" refers to "isoprenaline". "n" refers to "the number of hearts". Numerical data are reported as the mean ± SEM. * denotes $p < 0.05$ relative to the WT control, determined by Student's t-test.

5.4 Discussion

5.4.1 Is CD38 the main enzyme responsible for NAADP and cADPR synthesis in the heart?

Convincing evidence shows that membrane preparation from *CD38*$^{-/-}$ is not capable of synthesising cGDPR from NGD and is not capable of synthesising NAADP from NADP and NA. The hypothesis that the reduced ability of cardiac muscles from *CD38*$^{-/-}$ to synthesise NAADP and cADPR *in vivo* is mainly extrapolated from the *in vitro* observations, which showed the lack of functional base-exchange reaction and cyclisation reactions to synthesise NAADP and cGDPR respectively. While there is a growing consensus regarding CD38 being the main

enzyme for the *in vitro* synthesis of cADPR and endogenous synthesis of cADPR (Partida-Sánchez et al., 2001; Fukushi et al., 2001; Ceni et al., 2003b; Takahashi et al., 2003; Deshpande et al., 2005), there are still debates about whether CD38 synthesises NAADP (Partida-Sánchez et al., 2001; Soares et al., 2007; Cosker et al., 2010; Gul et al., 2016) (see also section 1.2.10 on page 21). These dichotomous findings perhaps arise from the difficulty to measure minute amounts of endogenous cADPR and NAADP using the available assays (either radioligand binding or enzymatic cycling assay), possibly leading to contradictory observations. On the contrary, the assays for measuring *in vitro* enzymatic activities of CD38 have the advantage of providing a better signal to noise ratio compared to the assays for measuring the endogenous levels of NAADP and cADPR. Also, most of the *in vitro* observations (apart from those observed in brain tissue, (Ceni et al., 2003a)) are consistent with CD38 being the main enzyme to synthesis NAADP and cADPR *in vitro*.

The author of this thesis appreciates the view that the *in vitro* method of synthesising NAADP might not mirror the actual mechanism *in vivo*. As NAADP synthesis was not observed in the membrane preparation and cardiomyocytes isolated from hearts of *CD38*$^{-/-}$ mice was demonstrated, it is very convincing that CD38 is the main enzyme in the heart to synthesise NAADP from NADP and NA, through the base-exchange reaction. As discussed in section 1.2.8 on page 15, some have argued the optimal pH required for the base-exchange reaction is out of the physiological range and the enzymes for base-exchange reaction (ecto-CD38) do not have the desired topology. In Chapter 4, it was demonstrated that NAADP synthesis is feasible at pH 7.2 and evidence in this chapter shows that CD38 proteins are not necessarily expressed as ectoenzymes in the cardiomyocytes.

The hypothesis that there are other physiological mechanisms that may contribute to the increase in the level of NAADP cannot be excluded. Nevertheless, the base-exchange reaction is the only reaction to date that is capable of synthesising NAADP *in vitro*. Some alternative pathways to generate NAADP have been proposed such as the deamidation of NADP or phosphorylation of NAAD by NAD kinase. However, the possibility of a pathway including NAD kinase has already been ruled out (Lerner et al., 2001), whereas deamination of NADP has never been successfully demonstrated.

Unfortunately, the measurements of the endogenous concentration of NAADP in cardiac tissue from WT and *CD38*$^{-/-}$ mice using the sea-urchin radioligand binding assay have not been successful at the times when these studies were carried out (carried out in collaboration with Danni Zhu). Nevertheless, the observation showing single cardiac myocytes from *CD38*$^{-/-}$ animals were insensitive to the effect of bafilomycin-A1 in the presence of isoprenaline (see section 5.3.8 on page 175) is consistent with the hypothesis that these *CD38*$^{-/-}$ cardiac myocytes have impaired NAADP signalling pathways due to the lack of the synthesis of NAADP during activation of β-adrenoceptors. In addition, it was demonstrated that single ventricular cardiomyocytes isolated from the hearts of *CD38*$^{-/-}$ mice have weaker contraction magnitudes and Ca^{2+} transient amplitudes during β-adrenoceptor stimulation. The resistance to β-adrenoceptor-induced arrhythmias was also shown in hearts of *CD38*$^{-/-}$ mice. These observations in single cell functional and *ex vivo* whole heart studies are consistent with the *in vitro* data and they support the hypothesis regarding the involvement of CD38 in producing cADPR and NAADP, which are both known Ca^{2+}-mobilising agents responsible partly for the positive inotropy and arrhythmogenicity mediated by β-adrenoceptors (see section 1.2.11.1 on page 23 and section 1.3.5 on page 46). Future studies to determine to what

extent CD38 KO reduces endogenous levels of cADPR and NAADP in the presence and absence of β-adrenoceptor agonists will give further insight.

5.4.2 Is CD38 expressed as an ectoenzyme in the hearts?

Most authors considered CD38 as a type-II membrane protein, that has a short cytoplasmic N-terminal tail of 21 amino acid residues (see section 1.2.8 on page 15). Gathered from the literature, this hypothesis might be based on, but not limited to, the below observations: i) CD38 was first identified as a surface antigen on lymphocytes. It acts as a co-receptor and binds to other surface antigens. The assumption that CD38 is being expressed extracellularly is extrapolated from lymphocytes to other tissues or cell types (see section 1.2.1 on page 3). ii) CD38 enzymatic activity is sensitive to a reducing condition; a reducing environment such as the cytosol will render it a redundant enzyme (see section 1.2.7 on page 11).

In a paper published by Lee's group (Zhao et al., 2015), the authors have listed examples of proteins that are expressed in two dual topology and opposite orientations, for example prion, multidrug-resistance transporter, diacylglycerol acyltransferase, microsomal epoxide hydrolase, melanocortin-2 receptor accessory protein and lactose permease. Using specific antibodies to target N- and C-termini of CD38, Lee's group has shown that CD38, in fact, exists naturally in two opposite membrane orientations in HL-60 cell lines as well as human primary monocytes and the monocytic U937 cells (Zhao et al., 2012). These cells were shown to expressed both type-II and type-III CD38, with their enzymatic active sites expressed intracellularly and extracellularly respectively. They also showed that CD38 can be expressed preferentially in type-III orientation through the mutation of the three

serine residues to aspartate, which is functional equivalent of phosphorylation of serine residues (Zhao et al., 2015). They postulated the possibility that the endogenous phosphorylation of these residues during protein translation can result in the expression of a mature type-III CD38.

Observations presented in this chapter are consistent with the hypothesis that CD38 is expressed with a type-III membrane orientation in the hearts. Firstly, using a rabbit polyclonal anti-CD38 antibody, little or no specific staining was seen in non-permeabilised cardiomyocytes. However, immunolabelling of CD38 in mouse and rabbit cardiomyocytes that were permeabilised with Triton-X100 revealed a striated-pattern, which has an average spacing of approximately 2 μm. This staining pattern also resembled that from the anti-RyR2 antibody. This observation is consistent with the hypothesis that CD38 is expressed intracellularly, and predominantly on the SR, as discussed in Chapter 4. Secondly, the rate of NAADP production in cardiac myocytes supplemented with NADP and NA increased in the presence of membrane permeabilising agents. The sarcolemmal-specific permeabilisation with saponin alone, non-specific permeabilisation with Triton-X100 alone, or the combination of both resulted in a 3-fold increased rate of NAADP production, compared to those of intact cells. However, the increased activities among these cells permeabilised with different agents were comparable (see section 5.3.4 on page 154). While lysosomal membranes might contain cholesterols which render them prone to saponin permeabilisation, the question of whether saponin can in fact permeabilise lysosomal membranes remains controversial (Böttger and Melzig, 2013; Gilabert-Oriol et al., 2013). On the other hand, saponin, at the concentration used in experiments described in this thesis (0.01% w/v), has been shown to keep the SR intact (Lukyanenko and Gyorke, 1999). This implies there is little or no CD38 expression inside the lumen of organelles (particularly

SR), else a higher increase in the rate of NAADP production would be expected when Triton-X100 was used as a permeabilising agent. Therefore, the favoured hypothesis is that most of the CD38 in the cardiac myocytes are expressed intracellularly in the SR with a type-III membrane orientation.

It was reported that the catalytic domain of CD38 contains six disulphides, which maintain the structure and functionality of enzymatic activities (see section 1.2.7 on page 11). Despite the conventional view that these disulphides might not be stable in cytosol due to the reducing environment it provides, Lee's group have also demonstrated that CD38 with the type-III orientation was capable of producing cADPR and that the expression level of CD38 in HeLa cells was correlated with the intracellular level of cADPR (Zhao et al., 2011). Observations in this chapter support a type-III CD38 expressed on the SR, thus providing alternative solution for the CD38 topological paradox, in contrast to the vesicular hypothesis (see section 1.2.8 on page 15). In addition, there were also recent observations regarding the proximity of SR and lysosomes (Aston et al., 2017). Therefore, instead of having limited access to substrates and hindered delivery of products to targets, type-III CD38 expressed in SR could serve their roles better by producing cADPR and NAADP *in situ*, and delivering them to nearby receptors by simple diffusion without any transporters.

5.5 Conclusion

In the work previously published, the contribution of NAADP and cADPR to the cardiac EC coupling and the development of the cardiac arrhythmias were reported, particularly in the context of the β-adrenoceptor pathway (see

section 1.2.11.1 on page 23, section 1.3.5 on page 46, and section 3.3.3 on page 89). In this chapter, this hypothesis is further supported by evidence showing the effects of CD38 KO in terms of weakening the β-adrenoceptor-mediated positive inotropy and providing resistance to β-adrenoceptor-induced arrhythmias (see section 5.3.7 on page 173 and section 5.3.9 on page 178). Furthermore, the KO of the CD38 gene has an overlapping effect with the bafilomycin-A1 pretreatment. The observation that bafilomycin-A1 blunted the β-adrenoceptor-mediated positive inotropic effect in WT but not *CD38*$^{-/-}$ ventricular myocytes, shows that CD38 is indeed the key protein coupling the activation of β-adrenoceptors and the subsequent activation of the NAADP signalling pathway (see section 5.3.8 on page 175). In other words, without CD38 proteins, the NAADP signalling pathway will not be activated upon the activation of β-adrenoceptors. Therefore, observations in this chapter provide novel evidence of the role of the CD38/NAADP pathway during the fight or flight response of the heart. More importantly, given the high resistance of *CD38*$^{-/-}$ hearts to isoprenaline-induced arrhythmogenocity, CD38 proteins could be a potential therapeutic target for cardiac arrhythmias. In the next chapter, the potential of an inhibitor of ARC, SAN4825, to prevent cardiac arrhythmias will be discussed.

Chapter 6

Effects of SAN4825 on cardiac NAADP and cADPR synthesis, cardiac physiology and cardiac pathophysiology

Majority of the material presented in this chapter was published in Journal of Biological Chemistry (Lin et al., 2017). © the American Society for Biochemistry and Molecular Biology.

6.1 Background

The notion of the existence of a non-CD38 ARC cyclase in cardiac muscle has led to the discovery of a novel drug SAN4825 (Kannt et al., 2012). SAN4825 was

reported as a potent inhibitor of the cardiac non-CD38 ARC with a IC_{50} of 10^{-7} μM.

This work was carried out by Kannt et al. (2012) using high throughput screening. They used a nicotinamide hypoxanthine dinucleotide (NHD)-based assay to gauge the rate of the cyclisation reaction carried out by cardiac ARCs. When the non-fluorescent NHD was converted into the fluorescent cyclic inosine diphosphate-ribose (cIDPR), the increase in fluorescence intensity that corresponded to the rate of cyclisation could be measured. They isolated SR vesicles with differential centrifugation (using a similar method to protocol used in this thesis for isolating SRMP) from pig and rat hearts. They demonstrated that such preparation exhibited the typical ARC activity, shown by the conversion of NHD to cIDPR. Hence, with the NHD assay and their SRMP, the authors have tested more than 17000 molecules, and two drug candidates (SAN4825 and SAN2589) were found to inhibit the cardiac ARC activity.

As mentioned previously (see section 1.2.9 on page 17), the assumption that non-CD38 enzymes were responsible for the observed ARC activity from their SRMP was put forward by demonstrating the differences in biochemical properties between CD38 and cardiac ARCs. The enzymatic activity of purified human CD38 from transfected cell line SF9 was shown to be enhanced by the presence of Zn^{2+}, while the enzymatic activity found in their cardiac SRMP was inhibited by Zn^{2+}. When they performed their NHD assay on their SRMP following the gel electrophoresis, a fluorescent band was found around 35 kDa, as opposed to the molecular weight of a purified human CD38 of 42 kDa. Nonetheless, it is important to point out that the type-III CD38 (with a cytosolic active site) has recently been reported to be expressed as a non-glycosylated protein around 35 kDa (Zhao et al., 2012, 2015).

The comparison of a purified human CD38 and a SRMP may not be straight forward, as the latter is more complex and dynamic. In addition, there are several

questions that need to be addressed. For example, is the observed inhibition of ARC by Zn^{2+} a result from its direct interaction with the responsible enzyme, or with other proteins that indirectly affect ARC? In addition, does the fluorescent band of 35 kDa pertain to proteins that are responsible for producing or degrading the fluorescent cIDPR, or proteins that targeted by the fluorescent molecule (cIDPR)?

As presented in Chapter 5, heart tissue lacking CD38 proteins did not exhibit detectable cADPR and NAADP production. In addition, observations supporting sheep cardiac SRMP exhibits CD38-like ARC activities were presented in Chapter 4. It is therefore hypothesised that the real target of SAN4825 could be CD38 itself, and SAN4825 inhibits enzymatic production of cADPR (or cIDPR) by CD38. In this chapter, evidence from *in vitro* assays, drug docking studies and functional studies, which are consistent with CD38 as the target of SAN4825, is presented. In addition, although Kannt's study showed the inhibition of ARC by SAN4825, some have questioned the extrapolation of observations from experiments performed on an analogue (NHD) rather than the physiological molecule (NAD) itself (Warszta et al., 2014). The observations reported in this chapter also verifies that SAN4825 can inhibit the production of cADPR. Novel evidence showing SAN4825 can inhibit the NAADP production *in vitro* in addition to the cADPR production is also presented. Lastly, observations showing the potential of SAN4825 an anti-arrhythmic drug are also presented and discussed.

6.2 Methods

The methods used to carry out experiments in this chapter are described in detail in Chapter 2.

The cell isolations, Ca^{2+} imaging study, whole heart electrophysiological study were conducted in a manner similar to those mentioned in section 5.2 on page 147. The isolation of SRMP and the measurement of cGDPR and cADPR were again conducted in a manner similar to those described in section 4.2 on page 118 and in section 5.2 on page 147.

A blind docking using the SwissDock webserver was performed to predict the binding sites of SAN4825 in the CD38 proteins (PDB ID: 2HCT, chain B and 2EG9, chain A) (Graeff et al., 2006; Grosdidier et al., 2011). This docking methodology is based on the EADock DSS engine, an approach that has been able to successfully determine small molecule binding modes to proteins. Further docking simulations were also carried out by Dr. Wilian Cortopassi using Glide (see 2.17 for methods).

6.3 Results

6.3.1 SAN4825 inhibited cGDPR and cADPR synthesis in sheep cardiac SRMP at pH 7.2

Using the NGD assay (for methods, see section 2.12.1 on page 69), it was observed that SAN4825 inhibited the synthesis of cGDPR by sheep cardiac SRMP in a dose-dependent way (control: 100 ± 15%; 0.1 μM: 35 ± 20%; 1 μM: 22 ± 20%; 10 μM: 18 ± 10%; 100 μM: 4.8 ± 10%; n = 4 – 7; $p < 0.05$ or 0.01; **Figure 32A**). SAN4825, at a concentration of 10^{-7} M, reduced the rate of cyclisation of NGD to cGDPR by more than 50%; this observation is consistent with the reported IC_{50} of SAN4825 (Kannt et al., 2012).

The NGD assay and other similar fluorescent analogue assays (such as the NHD assay) are widely accepted standards used to measure the ARC activity. Kannt et al. (2012) were the first to predict the ability of SAN4825 to inhibit cADPR synthesis based on an extrapolation from their result showing a similar inhibition (by SAN4825) of cIDPR production. However, such extrapolation may occasionally be challenged by others. For example, as mentioned in a paper (Warszta et al., 2014):

"Kannt and colleagues used nicotinamide hypoxanthine dinucleotide as a surrogate substrate for NAD to measure ADPRC activity...However, since the natural substrate NAD was not used, some uncertainty remains. The differences observed should be tested with the natural substrate NAD and by monitoring both the major reaction to ADPR (NAD-glycohydrolase) and the minor reaction to cADPR (ADP-ribosyl cyclase)."

In addition, not all the enzymes in the ARC family are able to produce significant amounts of cADPR from NAD. For example, although a member of ARC family expressed in *S.Mansoni* was capable of catalysing the cGPDR production efficiently, its capability of catalysing the cADPR production was rather inefficient (yield $<$ 0.02%).

Since the previous study only used analogues of NAD to extrapolate the inhibition by SAN4825 of cADPR synthesis, the inhibition of cADPR synthesis by SAN4825 was further investigated using sea urchin egg homogenates. This approach takes advantage of the ability of sea urchin egg homogenates to release Ca^{2+} in response to addition of cADPR (Clapper et al., 1987). NAD was added to SRMP to give a final concentration of 2.5 mM. This was then incubated for 15 min, and a diluted sample of this mixture was added to the sea urchin egg homogenates to trigger a Ca^{2+} release response that was thought to be mediated by cADPR synthesised from NAD. The Ca^{2+} release

response-mediated by cADPR in sea urchin egg homogenates was then calibrated using known concentrations of cADPR. As expected, SAN4825 (preincubated with the SRMP) reduced the cADPR synthesis, in a concentration-dependent manner (control: 100.0 ± 9%; 1 μM SAN4825: 9.5 ± 3%; 10 μM SAN4825: 7.6 ± 2%; $p < 0.001$; **Figure 32B**). These observations are consistent with the hypothesis that SAN4825 can inhibit both cADPR and cGDPR synthesis.

Figure 32

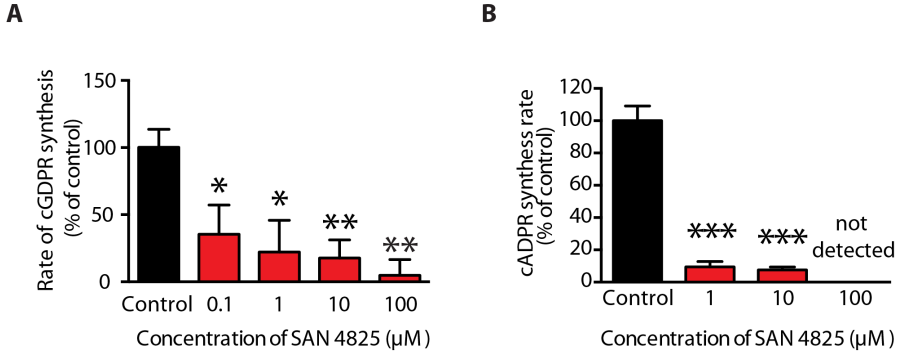


Figure 32: cGDPR and cADPR synthesis carried out by sheep cardiac SRMP were inhibited by SAN4825 at pH 7.2

A shows the inhibitory effect of SAN4825 on the production of cGDPR by sheep cardiac SRMP (n = 4 – 7 in each group). SRMP was either preincubated with DMSO or different concentrations of SAN4825 for 30 min before being supplemented with 500 μM NGD to produce cGDPR.
B shows the inhibitory effect of SAN4825 on the production of cADPR by sheep cardiac SRMP. SRMP was preincubated with either DMSO or different concentrations of SAN4825 for 30 min before being supplemented with 2.5 mM NAD to produce cADPR. (n = 3 in each group).

Note: All experiments were conducted at pH 7.2. NGD assays were conducted at 37 °C. Measurements of cADPR using sea urchin egg homogenates were conducted at 17 °C and samples from incubations (37 °C) were diluted accordingly before addition, in order to achieve optimal measurements. "n" refers to "the number of SRMP incubations". At least three batches of SRMP (isolated from three different hearts) were used in each group. Numerical data are presented as the mean ± SEM. * denotes $p < 0.05$, ** denotes $p < 0.01$, *** denotes $p < 0.001$ relative to the control, determined by one way ANOVA with post-hoc Dunnett's test.

6.3.2 SAN4825 inhibited NAADP synthesis in sheep cardiac SRMP at pH 7.2

Using a sea urchin egg homogenate assay (for methods, see section 2.11 on page 68), it was observed that the ability of sheep cardiac SRMP to synthesise NAADP by the base-exchange reaction was also inhibited in a concentration-dependent manner by SAN4825 at pH 7.2 (**Figure 33A**). Administration of 10^{-7} M SAN4825 reduced the rate of NAADP synthesised by more than 50%. The procedure was carried out by the following method. Either a different final concentration (10^{-8} to 10^{-4} M) of SAN4825 or DMSO (1% v/v) was co-incubated with SRMP for 30 min. NADP and NA were subsequently added to the SRMP (to reach a final concentration of 500 μM and 7 mM, respectively) to initiate the base-exchange reaction. The amount of NAADP synthesised was quantified 15 min after the addition of substrates and the reaction rate was reported as nmol of NAADP synthesised per mg protein per hr. These data are replotted in **Figure 33B**, showing the percentage of inhibition at each concentration of SAN4825 at pH 7.2 (IC_{50} = 1.362 x 10^{-7} M). Together with the observations in section 6.3.1 on page 196, it is convincing that SAN4825 is capable of abolishing NAADP and cADPR synthesis in SRMP from sheep heart. As the lack of NAADP and cADPR production was observed in the membrane preparation from hearts of *CD38*$^{-/-}$ mice (see section 5.3.1 on page 148), the observed inhibitory effect of SAN4825 is hypothesised to be mediated mainly through targeting CD38, resulting in a hindrance of its enzymatic activities.

Figure 33

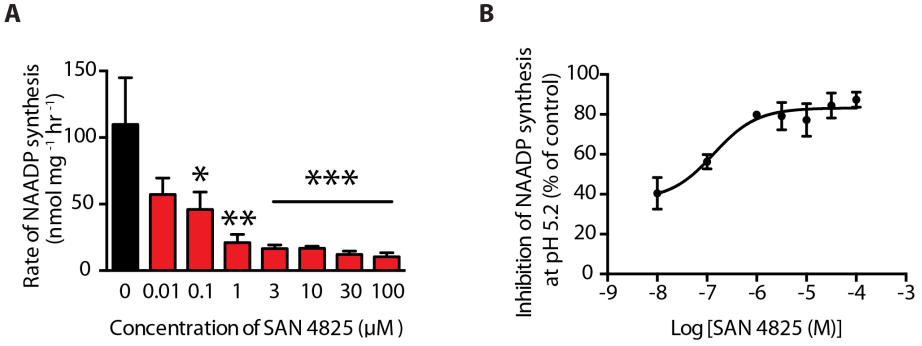


Figure 33: NAADP synthesis carried out by sheep cardiac SRMP was inhibited by SAN4825 at pH 7.2

A and **B** show the inhibitory effect of SAN4825 on the production of NAADP by sheep SRMP, in terms of absolute value and percentage respectively. SRMP was preincubated with SAN4825 (or with DMSO, 1% v/v) before being supplemented with 500 μM NADP and 7 mM NA to produce NAADP (n = 4 in each group).

Note: All experiments were conducted at pH 7.2. All the stated concentrations were the final concentrations in the SRMP-substrate-drug incubation. Measurements of NAADP using sea urchin egg homogenates were conducted at 17 °C and samples from incubations (37 °C) were diluted accordingly before addition, in order to achieve optimal measurements. Numerical data are presented as the mean ± SEM. "n" refers to "the number of SRMP incubations". At least three batches of SRMP (isolated from three different hearts) were used in each group. * denotes $p < 0.05$, ** denotes $p < 0.01$, *** denotes $p < 0.001$ relative to the control (without SAN 4825), determined by one way ANOVA with post-hoc Dunnett's test. "mg^{-1}" refers to "per mg protein found in the incubation".

6.3.3 Lack of SAN4825 inhibition of NAADP synthesis in sheep cardiac SRMP at pH 4.5

Using sea urchin egg homogenates as a bioassay, the effectiveness of SAN4825 was further evaluated at an acidic pH. At pH 4.5, although the inhibition of cADPR synthesis by SAN4825 remained intact (control: 100.0 ± 10%; 10 μM SAN4825: 13 ± 6%; $p < 0.01$; **Figure 34B**), SAN4825 failed to inhibit NAADP synthesis in SRMP

(**Figure 34A**). This observation showed a high resemblance to the observations in the substrate competition study (see section 4.3.2 on page 122). In brief, NAD, the substrate of cADPR is capable of inhibiting NAADP synthesis at pH 7.2 but not pH 4.5. Since inhibitory effect of SAN4825 is similar to those of NAD, the author of this thesis proposes that the inhibition of NAADP and cADPR synthesis by SAN4825 is mediated through occupying the active site in a competitive manner. This idea is supported by observations from silico studies of SAN 4825 (see section 6.3.5 on page 207). Since a known inhibitor of ARC, DHAB, can affect the Ca^{2+} release properties of sea urchin egg homogenates (personal communication, Lianne Davis), observations reported in **Figure 34A** also provide evidence that Ca^{2+} release mediated by NAADP in sea urchin egg homogenates is not affected by 1 μM SAN4825 (final concentration in sea urchin egg homogenates: 1 μM).

Figure 34

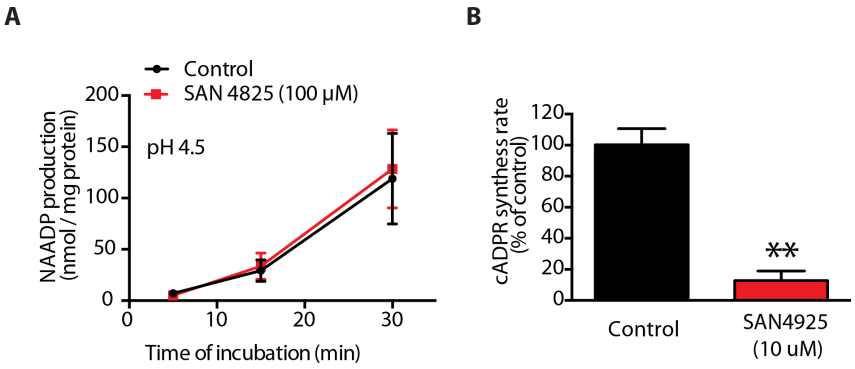


Figure 34: SAN4825 failed to inhibit sheep cardiac NAADP synthesis at pH 4.5 while its inhibition of cADPR synthesis remain intact

A shows the inhibitory effect of SAN4825 on the production of NAADP by sheep SRMP was abolished at pH 4.5. SRMP was supplemented with 500 μM NADP and 7 mM NA to produce NAADP (n = 4 in each group).
B shows the inhibitory effect of SAN4825 on the production of cADPR by sheep SRMP remained intact at pH 4.5. SRMP was supplemented with 2.5 mM NAD to produce cADPR. $^{2+}$ release (n = 4 in each group).

Note: All experiments were conducted at pH 4.5. Measurements of NAADP and cADPR using sea urchin egg homogenates were conducted at 17 °C and samples from incubations (37 °C) were diluted accordingly before addition, in order to achieve optimal measurements. SUEH refers to sea urchin egg homogenates. Numerical data are presented as the mean ± SEM. "n" refers to "the number of SRMP incubations". At least three batches of SRMP (isolated from three different hearts) were used in each group. ** denotes $p < 0.01$ relative to the control (without SAN4825), determined by Student's t-test. "mg^{-1}" refers to "per mg protein found in the incubation".

6.3.4 *In vitro* and *in silico* evidence supports CD38 as the target of SAN4825 in mouse cardiac tissue

As evidence reported in Chapter 5 shows CD38 to be the major enzyme catalysing synthesis of these Ca^{2+}-mobilising messengers in mouse cardiac tissue, the ability of SAN4825 to inhibit the NAADP and cADPR synthesis in mouse membrane preparation was further investigated. SAN4825 was observed to cause a concentration-dependent inhibition of both NAADP synthesis (**Figure 35A**) and cADPR synthesis (**Figure 35B**). At 10^{-7} M, SAN4825 was able to inhibit more than 50% of the NAADP and cADPR synthesis (NAADP synthesis rate in the presence 0.1 μM SAN4825: 47 ± 9%; cADPR synthesis rate in the presence 0.1 μM SAN4825: 37 ± 10%; percentage in relative to control). At pH 4.5, a higher NAADP synthesis rate was observed (160 ± 20% of control) and a weakened inhibition of NAADP synthesis by 10 μM SAN4825 was observed (50 ± 10% of

control); this will be discussed at greater length in Discussion. Similar inhibition of NAADP synthesis by SAN4825 was also observed in saponin-permeabilised myocytes from mouse hearts (3 μM SAN4825: 29 $\pm$ 7% of control; **Figure 35C**).

Using SwissDock (Grosdidier et al., 2011), a docking study involving SAN4825 and the crystal structure of mouse CD38 (PDB ID: 2EG9) was performed. During the simulation, any movement or the change in bond angles of the crystal structure was restricted. A blind docking simulation was carried in a way that the drug molecule was docked into every possible pocket of the protein molecule without specifying the actual active site priorly. The binding energies of each drug-protein conformation were calculated, and 250 conformations with the lowest binding energies were predicted as the possible binding modes between the drug and the protein. These blind docking results using SwissDock showed that all of the 250 conformations were predicted to be inside the catalytic site of CD38 (**Figure 36A**). The active site residues Trp129, Glu150, Asp159, Trp193, and Glu230 in mouse CD38 correspond to Trp125, Glu146, Asp155, Trp189, and Glu226 in human CD38 (**Figure 36C**) . These residues in human CD38 are believed to play an important role for the NAADP and cADPR synthesis following mutagenesis studies (Munshi et al., 2000). The centre of the active site of CD38 was determined to be the centre of these particular amino acid residues (Trp129, Glu150, Asp159, Trp193, and Glu230). The distance between the centre of the drug molecule and the centre of the active site was measured for each prediction. Approximately 90% of the predicted docking sites (250 predictions in total) of SAN4825 in CD38 are within 4.5 Å from the centre of the actual active site (**Figure 36B**).

Crystal structure of WT human CD38 in complex with an analogue of NAADP (PDB ID: 4F46, chain B) shows the π-π stacking between the NA group of the ligand

and Trp189, and the hydrogen bonds between ribose ring of the ligand and Glu226 (Glu230 in mouse, **Figure 36D**, left). Human CD38 in complex with ADPRP also shows hydrogen bonds between one of its ribose rings and Glu226 (Glu230 in mouse, **Figure 36D**, right), and its adenine ring in close proximity to Trp189 (Trp193 in mouse, PDB ID: 4F46, chain A). These binding conformations of ligands from human WT CD38 were superimposed with the most favourable docking conformation of SAN4825 at pH 7.2 in mouse CD38 predicted by Glide (carried out by Dr. Wilian Cortopassi). The superimposed images suggest that SAN4825 occupies the same binding site as the NAADP analogue and ADPRP, in close proximity to Glu226, and its pyridine ring forms π-π stacking with the Trp189 residue of human CD38 (**Figure 36D**).

Observations from *in vitro* experiments show that the inhibitory effect of SAN4825 was qualitatively similar to that of the genetic KO of CD38, while evidence from *in silico* simulations supports the binding of SAN4825 to the active site of mouse CD38. Taken together, evidence presented here support the hypothesis that SAN4825 mediates its inhibition of NAADP and cADPR synthesis, by occupying the active site of CD38.

Figure 35

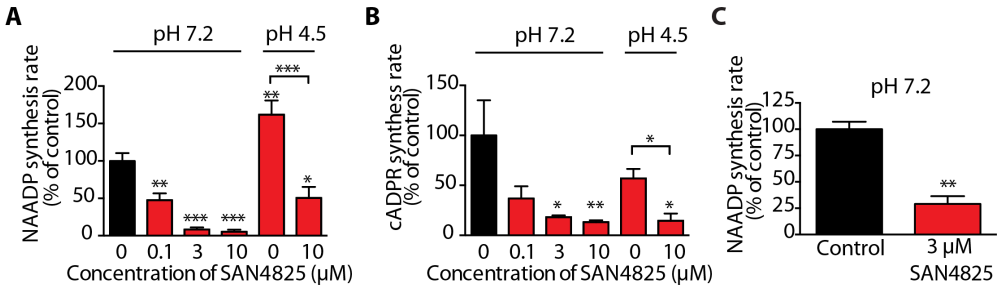


Figure 35: *In vitro* evidence of SAN4825 inhibiting the synthesis of NAADP and cADPR through targeting CD38

A shows the inhibitory effect of SAN4825 on the production of NAADP by mouse membrane preparation. The mouse preparation was supplemented with 500 μM NADP and 7 mM NA to produce NAADP (n = 3 – 4 in each group).
B shows the inhibitory effect of SAN4825 on the production of cADPR by mouse membrane preparation. The mouse preparation was supplemented with 2.5 mM NAD to produce cADPR. (n = 3 in each group).
C shows the inhibitory effect of SAN4825 on the production of NAADP by saponin-permeabilised ventricular cardiomyocytes from mice. The myocytes were supplemented with with 500 μM NADP and 7 mM NA to produce NAADP (n = 3 in each group).

Note: The pH conditions during the incubation were indicated above individual data. Measurements of NAADP and cADPR using sea urchin egg homogenates were conducted at 17 °C and samples from incubations (37 °C) were diluted accordingly before addition, in order to achieve optimal measurements. SUEH refers to sea urchin egg homogenates. "n" refers to "the number of independent incubations". At least three batches of membrane preparation were used in each group, where each batch were made out of 6 hearts. Numerical data are presented as the mean ± SEM. * denotes $p < 0.05$; ** denotes $p < 0.01$; *** denotes $p < 0.001$ relative to the control (black bars) unless indicated by a bar, determined by Student's t-test.

Figure 36

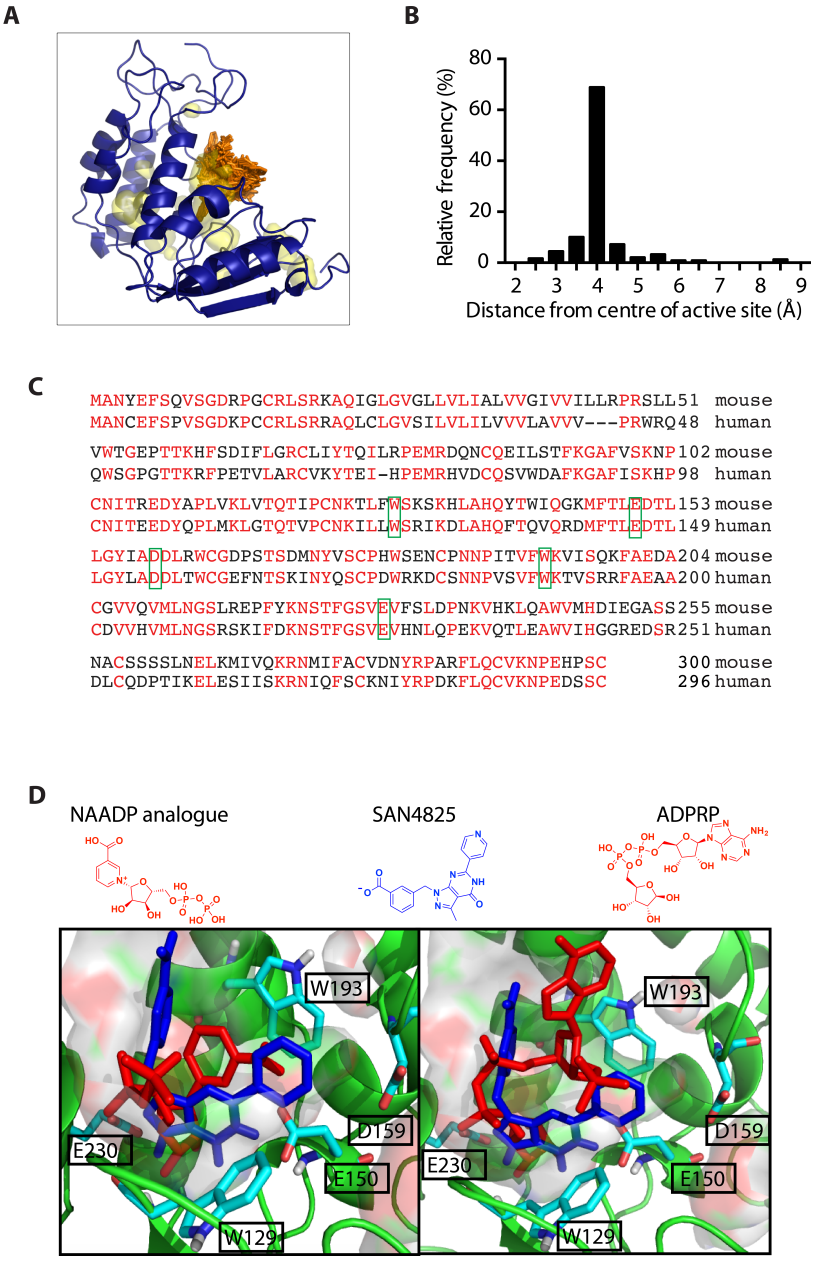

A
B
Relative frequency (%)
Distance from centre of active site (Å)
C
MANYEFSQVSGDRPGCRLSRKAQIGLGVGLLVLIALVVGIVVILLRPRSLL51 mouse
MANCEFSPVSGDKPCCRLSRRAQLCLGVSILVLILVVVLAVVV---PRWRQ48 human
VWTGEPTTKHFSDIFLGRCLIYTQILRPEMRDQNCQEILSTFKGAFVSKNP102 mouse
QWSGPGTTKRFPETVLARCVKYTEI-HPEMRHVDCQSVWDAFKGAFISKHP98 human
CNITREDYAPLVKLVTQTIPCNKTLFWSKSKHLAHQYTWIQGKMFTLEDTL153 mouse
CNITEEDYQPLMKLGTQTVPCNKILLWSRIKDLAHQFTQVQRDMFTLEDTL149 human
LGYIADDLRWCGDPSTSDMNYVSCPHWSENCPNNPITVFWKVISQKFAEDA204 mouse
LGYLADDLTWCGEFNTSKINYQSCPDWRKDCSNNPVSVFWKTVSRRFAEAA200 human
CGVVQVMLNGSLREPFYKNSTFGSVEVFSLDPNKVHKLQAWVMHDIEGASS255 mouse
CDVVHVMLNGSRSKIFDKNSTFGSVEVHNLQPEKVQTLEAWVIHGGREDSR251 human
NACSSSSLNELKMIVQKRNMIFACVDNYRPARFLQCVKNPEHPSC 300 mouse
DLCQDPTIKELESIISKRNIQFSCKNIYRPDKFLQCVKNPEDSSC 296 human
D
NAADP analogue
SAN4825
ADPRP
W193
D159
E230
E150
W129
W193
D159
E230
E150
W129

Figure 36: *In silico* evidence of SAN4825 inhibiting the synthesis of NAADP and cADPR through targeting CD38

A shows the binding site prediction for SAN4825 in mouse CD38. Hydrophobic pockets are shown in yellow. The predicted binding conformations of SAN4825 following blind docking in SwissDock server are shown in orange.
B shows the distances between the predicted docking sites and the center of the active site were plotted in a histogram. The centre of the active site of mouse CD38 was determined to be the centre of residues Trp129, Glu150, Asp159, Trp193, and Glu230, which correspond to the catalytic residue of human CD38 as reported in (Munshi et al., 2000).
C shows the alignment of human and mouse CD38 sequences, with the catalytic residues surrounded by green boxes and identical amino acid residues labelled with red fonts.
D shows the superimposition of NAADP analogue (left, in red) and ADPRP (right, in red) to the most favourable binding conformation of SAN4825 (in blue, both left and right) at the active site of mouse CD38 at pH 7.2 following Glide docking.

Note: This docking study were done in collaboration with Dr. Wilian Cortopassi. The docking simulations of SAN4825 in **A** were carried out using SwissDock with crystal structure of the mouse CD38 (PDB ID: 2EG9, chain A). The binding region was not specified priorly (blind docking) and the flexibility of side chains of the protein were completely restricted.

6.3.5 *In silico* observation predicts human CD38 as the target of SAN4825

Using similar methods described in section 6.3.4 on page 202, a docking study involving SAN4825 and the crystal structure of human CD38 (PDB ID: 2HCT) was performed. Approximately 90% of the predicted docking sites (250 predictions in total) of SAN4825 in CD38 are within 10 Å from the centre of the actual active site (**Figure 37B**). Interestingly, the most energetically favourable conformations of SAN4825 formed π-π interactions with Trp189 and Trp125 of human CD38 (**Figure 37C**). This binding conformation shows high resemblance to the native binding conformation between human CD38 and its substrates such as NAD, NMN, cADPR

and NAADP (Liu et al., 2005, 2006; Zhang et al., 2013). An example of a crystal structure of the mutant CD38(E226Q)-NAD complex was depicted in **Figure 37D** (extracted from Liu et al., 2006). These hydrophobic interactions were hypothesised to contribute to the positioning of substrates inside the enzymatic pocket of CD38. These observations provide support to the prediction that SAN4825 can inhibit the enzymatic reaction of human CD38 by occupying its active site.

Figure 37

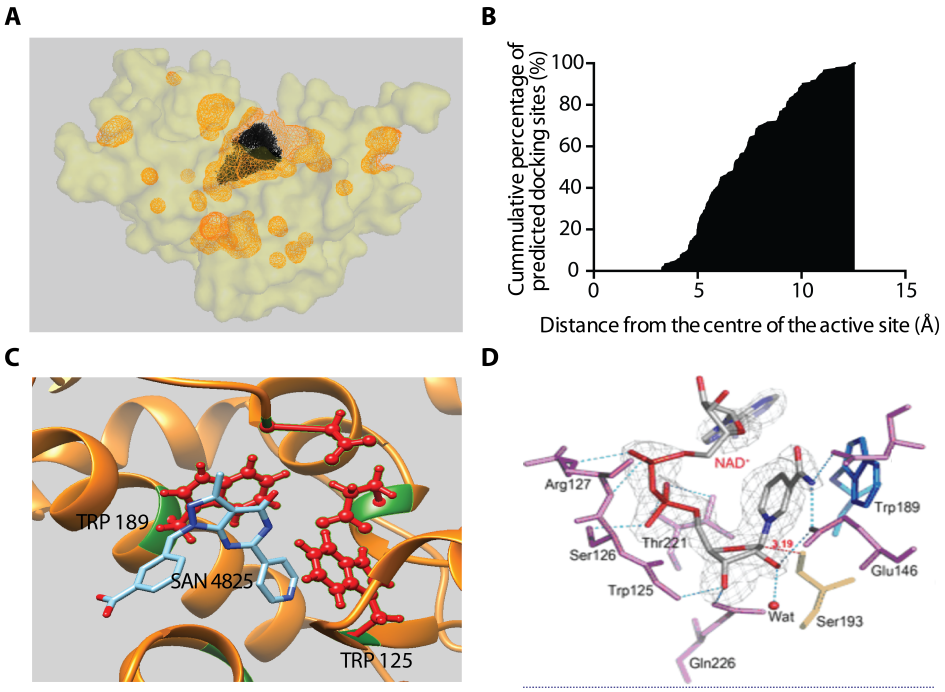


Figure 37: *In silico* observations support the hypothesis that SAN4825 inhibits cADPR and NAADP synthesis by occupying the active site of CD38

A shows the predicted pockets (orange, by PyMol) of CD38 and the 250 predicted docking sites (black, by SwissDock) of SAN4825.
B shows the distances between the centre of the active site of CD38 and the predicted docking sites of SAN4825 in a cumulative percentage graph. The centre of the active site of CD38 was determined to be the centre of catalytic residues Trp125, Glu146, Asp155, Trp189, and Glu226.
C shows the the most energetically favourable conformation of SAN4825 formed π-π interactions with Trp189 and Trp125. These particular π-π interactions were also observed in the crystal structure of the mutant CD38(E226Q)-NAD complex (**D**) (Liu et al., 2006).
D shows a crystal structure of the mutant CD38(E226Q)-NAD complex. Figure **D** was originally published in Journal of Biological Chemistry. (Liu et al., 2006) © the American Society for Biochemistry and Molecular Biology.

Note: The docking simulations of SAN4825 in **A-C** were carried out using SwissDock with crystal structure of the human CD38 (PDB ID: 2HCT, chain B). The binding region was not specified priorly (blind docking) and the flexibility of side chains of the protein were completely restricted. The docking results were illustrated using PyMol (Schrödinger, USA).

6.3.6 Effects of SAN4825 on magnitudes of Ca^{2+} transients and sarcomere shortenings in mouse ventricular myocytes under basal conditions and during the activation of β-adrenoceptors

Both under basal conditions and during β-adrenoceptor stimulation, preincubating mouse ventricular cardiomyocytes with 3 μM SAN4825 resulted in a lower mean of Ca^{2+} transient amplitudes and contraction magnitudes (measured by sarcomere shortenings); however the differences between the SAN4825-treated group and control group did not reach statistical significance (**Figure 38** and **Table 6.1**). It was intriguing that SAN4825 did not cause a significant reduction in the action

potential-triggered Ca^{2+} transients during the activation of β-adrenoceptors, in contrast to those observed in *CD38*$^{-/-}$ mice (see section 5.3.7 on page 173). This discrepancy could be due to factors such as the permeability and the retention of the drug in this experiment. Although 3 μM SAN4825 is sufficient to greatly reduce the synthesis of both cADPR and NAADP *in vitro* (see section 6.3.1 on page 196 and section 6.3.2 on page 199), the actual intracellular concentration of the drug could not be determined. Given that the NAADP signalling pathway, in particular, can be initiated with minute amounts of NAADP (10^{-8} M, Macgregor et al. 2007a; Nebel et al. 2013) due to the high potency of these Ca^{2+}-mobilising agents, a near-complete inhibition of the corresponding enzyme (such as genetic KO) may be required to alter the associated physiological functions to a greater extent. Future experiments can be carried out with higher concentrations of SAN4825; however careful consideration should be taken due to the likelihood of the drug being off-target at high concentration.

On the other hand, it was demonstrated that 3 μM SAN4825 was effective at abolishing the arrhythmias provoked by excessive β-adrenoceptor stimulation, possibly through inhibiting the overproduction of NAADP and cADPR mediated by CD38 (see section 5.3.9 on page 178) . Even though 3 μM SAN4825 could not lower the levels of NAADP and cADPR under the threshold for their positive inotropic effects, it does not necessarily mean similar cases should apply to their arrhythmogenic effect. It is postulated that excessive β-adrenoceptor stimulations produce heightened levels of cADPR and NAADP and therefore trigger arrhythmias. 3 μM SAN4825 might be effective at keeping the levels of cADPR and NAADP below the arrhythmogenic thresholds.

Warszta et al. (2014) have presented similar findings. In their case, up to 30 μM

SAN4825 failed to reduce the amplitude of Ca^{2+} transients, even though 3 μM SAN4825 was successful in reducing the arrhythmic events of cardiac myocytes. Oddly, at 30 μM and in the presence of isoprenaline (200 nM), SAN4825 significantly increased the Ca^{2+} transient amplitude and lengthened the Ca^{2+} decay, and delaying the SR Ca^{2+} uptake instead. In addition, 10 μM SAN4825 by itself (in the absence of isoprenaline) significantly increased the Ca^{2+} efflux from SR. Although Kannt et al. (2012) have reported the lack of SAN4825 binding on other proteins (mainly membrane receptors), the effects observed by Warszta et al. (2014) could still have arisen from additional targets of SAN4825 (perhaps an intracellular protein such as SERCA or RyR), which potentially mask the consequences of CD38 inhibition (such as a negative inotropic effect) by SAN4825 at 3 μM concentration. Nonetheless, genetic KO of CD38 serves as a better model to investigate the physiological function of CD38, and therefore the importance of CD38 in both the β-adrenoceptor-mediated inotropic and arrhythmogenic effect is strongly supported by evidence from experiments using *CD38*$^{-/-}$ mice.

Figure 38

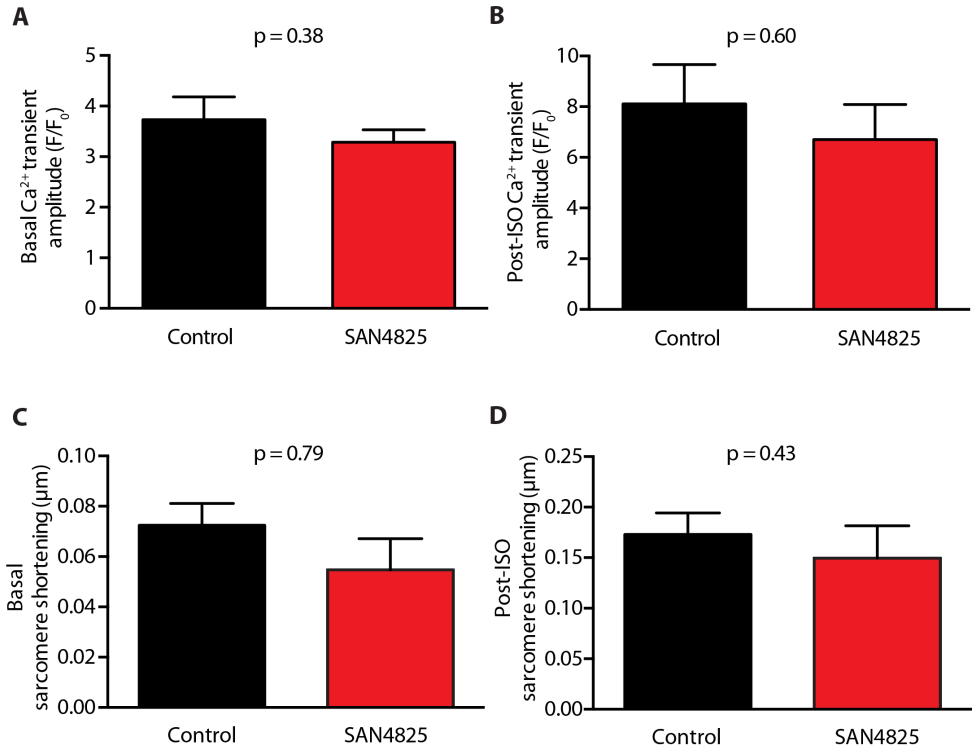


Figure 38: Lack of SAN4825 effect on the amplitudes of Ca^{2+} transients and cell shortenings in mouse ventricular cardiac myocytes under basal conditions and during β-adrenoceptor stimulation

A shows the basal Ca^{2+} transient amplitudes of mouse ventricular cardiac myocytes preincubated either with DMSO or SAN4825 (3 μM).
B shows the post-isoprenaline (5 nM) Ca^{2+} transient amplitudes of mouse ventricular cardiac myocytes preincubated either with DMSO or SAN4825 (3 μM).
C shows the basal sarcomere shortening amplitudes of mouse ventricular cardiac myocytes preincubated with DMSO or SAN4825 (3 μM).
D shows the post-isoprenaline (5 nM) sarcomere shortening amplitudes of mouse ventricular cardiac myocytes preincubated with DMSO or SAN4825 (3 μM).

Note: Myocytes were electrically paced at 1 Hz and either imaged with a spinning disk confocal microscope (after incubation with Fluo-5F-AM for 20 – 30 min) or imaged with an IonOptix MyoCam system at 36 °C and pH 7.4. Fluorescence data were analysed with Andor software and pClamp, while contraction measurements were analysed with IonWizard 5 software. Contraction measurements were carried out in collaboration with Dr. Emma Bolton. Number of independent experiments conducted (n) in each group was stated in **Table 6.1**. Numerical data are presented as the mean ± SEM. Statistical comparisons were carried out using Student's t-test. "ISO" refers to "isoprenaline".

	Control (DMSO)	SAN4825 (μM)
Basal Ca^{2+} transient (F/F_0)	3.7 ± 0.4 (n = 9)	3.3 ± 0.2 (n = 10)
Post-ISO Ca^{2+} transient (F/F_0)	8.1 ± 1.5 (n = 9)	6.7 ± 1.4 (n = 10)
Basal sarcomere shortening (μm)	0.072 ± 0.009 (n = 24)	0.055 ± 0.01 (n = 10)
Post-ISO sarcomere shortening (μm)	0.17 ± 0.02 (n = 17)	0.15 ± 0.03 (n = 9)

Table 6.1: Mean, SEM and n number of Ca^{2+} transient and sarcomere shortening measurements of ventricular myocytes with and without the preincubation of SAN4825 from **Figure 6.3.6**

6.3.7 Effects of SAN4825 on isoprenaline-induced arrhythmogenocity in Langendorff-perfused mouse hearts

Since the possible contribution of CD38 proteins in the isoprenaline-induced arrhythmogenocity was demonstrated in Chapter 5, the anti-arrhythmic effect of SAN4825 was further investigated. Similarly, the tendency intact mouse hearts to show arrhythmias was assessed by four different protocols: i) burst pacing with increasing frequency, ii) 50 Hz burst pacing with increasing current, iii) S1S2 pacing, iv) and dynamic pacing (see section 2.16 on page 73 for details and scoring methods). Control hearts (treated with DMSO) showed a significant increase in arrhythmogenicity after the application of 300 nM isoprenaline (Control: score before isoprenaline, 0.75 ± 0.3; score after isoprenaline, 2.3 ± 0.3; n = 8; $p < 0.05$, determined by Mann-Whitney test; **Figure 39A**, left panel). In contrast, no significant increase in the arrhythmogenicity was observed following isoprenaline application in hearts treated with 3 μM SAN4825 (SAN4825-treated: score before isoprenaline, 0.88 ± 0.4; score after isoprenaline, 1.9 ± 0.4; n = 8; $p > 0.05$,

determined by Mann-Whitney test; **Figure 39A**, right panel).

As shown in the pie chart (**Figure 39B**), after administration of isoprenaline (300 nM), 7 out of 8 control hearts became arrhythmic, but only 4 out of 8 hearts became arrhythmic in the presence of SAN4825. The cumulative percentage of hearts that became arrhythmic in the presence of isoprenaline (300 nM) during the burst pacing protocol with increasing pacing frequency is shown in **Figure 39C**, and again it is clear that hearts preincubated and perfused with SAN4825 had a reduced tendency for arrhythmias during stimulation of β-adrenoceptors.

A further test for isoprenaline-induced arrhythmogenicity is to measure the current threshold for VT. To determine the VT threshold, three trains of 50 Hz burst stimuli were applied with increasing current until either a VT was observed or a current of 32 mA was achieved. The statistical test showed that the threshold current to induce VT in control hearts was significant lower than the SAN4825-treated hearts (Control: 3.7 $\pm$ 0.9 folds; SAN4825-treated: 11 $\pm$ 2.6 folds; n = 8, $p < 0.05$ determined by Student's t-test; **Figure 39D**). Representative traces are shown in **Figure 39E**. The pacing current required to evoke an action potential in 1:1 ratio in two groups were comparable (data not shown). No significant difference in propensity to arrhythmias was observed between the two groups during the dynamic and S1S2 pacing alone (data not shown).

Taken together, these observations show that the tendency to become arrhythmic during stimulation of β-adrenoceptors (with high dose of isoprenaline, 300 nM) was reduced in hearts treated with 3 μM SAN4825. This is consistent with the hypothesis that CD38 is the target of SAN4825 in hearts, and the SAN4825 inhibition of CD38 resulted in blunted NAADP and cADPR pathways during the activation of β-adrenoceptors; hence the hearts are less prone to arrhythmias,

particularly to those mediated by excessive NAADP and cADPR.

Figure 39

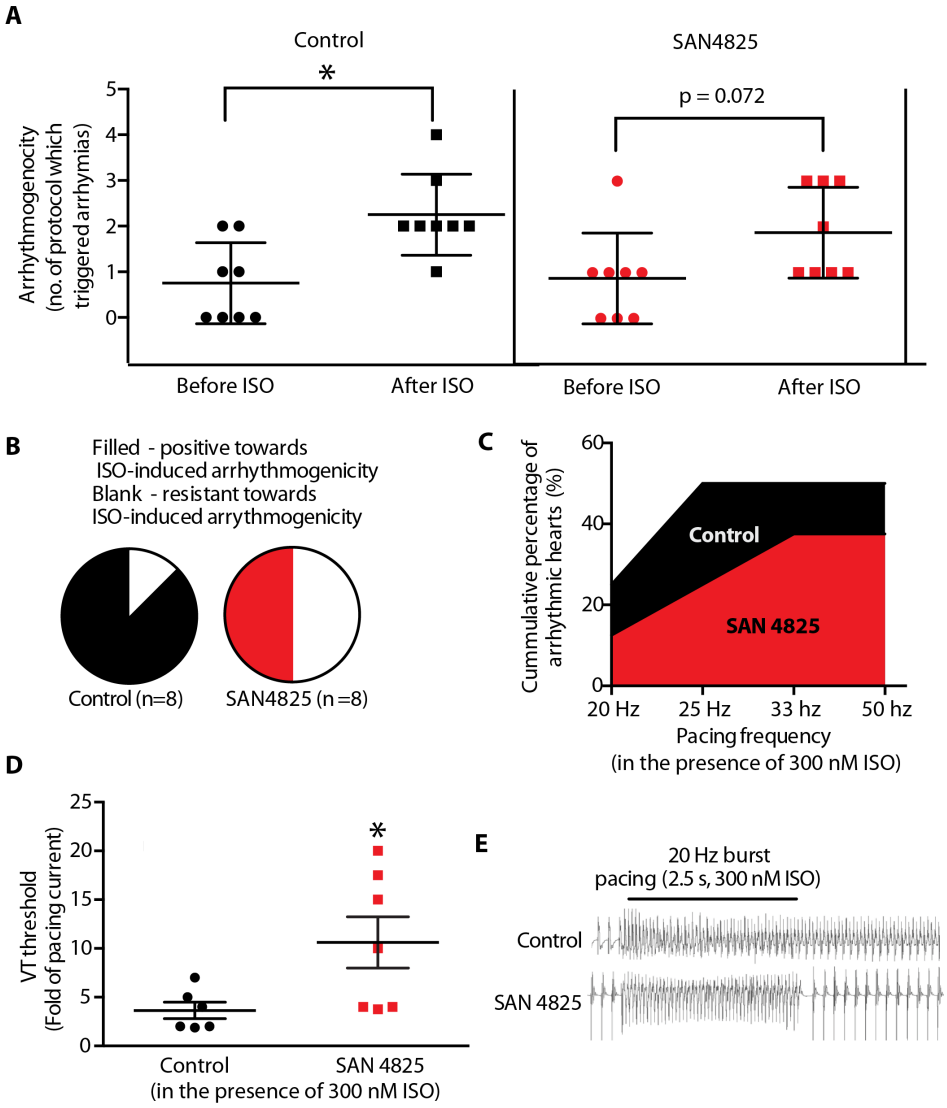


Figure 39: Whole hearts treated with SAN4825 showed resistance to isoprenaline-induced arrhythmogenocity

A shows the arrhythmogenocity score (determined by the number of programmed electrical stimulation protocols that successfully triggered arrhythmias) of Langendorff-perfused hearts in the absence and presence of SAN4825 (3 μM), before and after the application of isoprenaline (300 nM)
B shows the ratio of hearts (with and without SAN4825 treatment) that exhibited signs of arrhythmias (filled) to those that did not exhibit signs of arrhythmias (blank) during any of the programmed electrical stimulation protocols (after the application of 300 nM isoprenaline).
C shows the cumulative percentage of hearts (in the presence of 300 nM isoprenaline) that exhibited signs of arrhythmias in response to increasing pacing frequency during the burst pacing protocol.
D shows the current thresholds to trigger VT (in the presence of 300 nM isoprenaline) in whole hearts in the absence and presence of SAN4825 (3μM). 2 out of 8 hearts from the control group and 1 out of 8 hearts from the SAN4825-treated group did not exhibit VT throughout the current-varying burst pacing experiments.
E shows the representative traces of monophasic action potential recorded during burst pacing experiments (in the presence of 300 nM isoprenaline).

Note: The experiments were conducted with *ex vivo* Langendorff-perfused hearts that were paced with electrodes on their ventricular septa at 37 °C. The monophasic action potentials from these hearts were recorded with electrodes placed on the left ventricular wall. The hearts were either preincubated with DMSO (labelled with Control) or 3 μM SAN4825 (labelled with SAN4825) for 30 min. SAN4825 or DMSO was included in the perfusion solution throughout the experiments. The terms "arrhythmic" and "arrhythmias" refers to conditions where six or more consecutive regular premature waveforms (VT) or irregular fibrillating waveforms were observed in the Langendorff-perfused heart recordings during the protocols, while the term "health" refer to conditions where no signs of these events were observed; n = 8 hearts in each group. ISO refers to isoprenaline. Numerical data in **A** and **D** are presented as the mean ± SEM. * denotes $p < 0.05$, determined by Mann Whitney test (**A**), Student's t-test (**D**). "ISO" refers to "isoprenaline".

6.3.8 Langendorff-perfused mouse hearts treated with SAN4825 showed blunted isoprenaline-induced positive chronotropic effects

During the stimulation of β-adrenoceptors with isoprenaline, whole hearts treated with SAN4825 had a blunted response to β-adrenoceptor-mediated positive chronotropic effect (increase in bpm upon isoprenaline addition; control: 240 $\pm$ 30; SAN4825-treated: 160 $\pm$ 20; n = 8 hearts in each group; $p < 0.5$). This could be a direct effect on the CD38 proteins expressed on sino atrial nodal tissue or the rest of the conduction system, affecting either the intrinsic pacemaking mechanisms or conductivity on the system.

Comparing the refractory periods measured from experiments carried out with the S1S2 protocol (control, 0.038 $\pm$ 0.007 s; SAN4825-treated, 0.061 $\pm$ 0.008 s; n = 8 hearts; p = 0.064) and dynamic pacing protocol (control, 0.051 $\pm$ 0.008 s; SAN4825-treated, 0.075 $\pm$ 0.005 s; n = 8 hearts; $p < 0.05$), hearts treated with SAN4825 had a longer post-isoprenaline refractory period than the control group as shown in **Figure 40E**.

Given that the refractory period of the hearts did not depend on the expression of CD38 (assuming there are no compensatory mechanisms), the effect of SAN4825 in prolonging the refractory period might not be mediated through its inhibition on CD38 (see section 5.3.10 on page 183). The observation regarding the lengthened post-isoprenaline refractory periods in SAN4825-treated hearts were, to an extent, consistent with the observations that SAN4825 was capable of lengthening the Ca^{2+} decay and delaying SR Ca^{2+} uptake in paced ventricular myocytes (Warszta et al., 2014). This lengthened refractory period by SAN4825, in addition to its inhibition

on the excessive production of cADPR and NAADP may partly contribute to the observed protection against arrhythmias (shown in section 6.3.7 on page 213), as well as the resistance to the β-adrenoceptor-induced positive chronotropic effect seen in the SAN4825-treated hearts (this section).

Figure 40

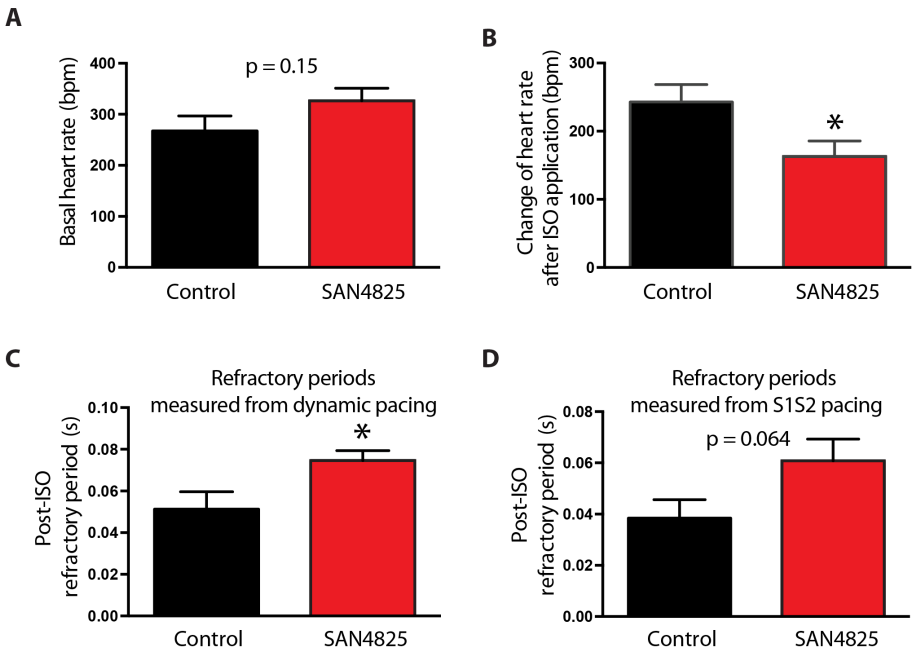


Figure 40: The basal heart rate, heart rate in the presence of isoprenaline, and post-isoprenaline refractory periods of mouse hearts preincubated with either DMSO or SAN4825

A shows the average basal heart rate of Langendorff-perfused heart preincubated with DMSO or SAN4825 (3 μM).
B shows the average increase of heart rate upon the application of isoprenaline (300 nM) in Langendorff-perfused hearts preincubated with DMSO or SAN4825 (3 μM).
C and **D** show the average post-isoprenaline (300 nM) refractory period of Langendorff-perfused hearts preincubated with DMSO or SAN4825 (3 μM), measured from S1S2 and dynamic pacing protocols, respectively.

Note: The experiments were conducted at 37 °C and monophasic action potentials were measured from Langendorff perfused hearts with an electrode attached to the left ventricular wall. Heart rates were determined from intervals of action potentials, while refractory periods were determined from intervals of action potentials before the hearts become refractory (unable to evoke an action potential in 1:1 manner). ISO refers to isoprenaline. n = 8 hearts in each group. Numerical data are reported as the mean ± SEM. * denotes $p < 0.05$ relative to the control (DMSO), determined by Student's t-test. "ISO" refers to "isoprenaline".

6.4 Discussion

6.4.1 Does SAN4825 target CD38?

SAN4825 was one of the drug candidates that was capable of inhibiting the NHD cyclisation reaction of enzymes isolated from SRMP (Kannt et al., 2012). Although the authors claimed that SAN4825 was targeting a cardiac non-CD38 ARC, evidence in this thesis support CD38 as the main target of SAN4825. First of all, in Chapter 5, it was shown that both cardiac membrane preparation and cardiomyocytes from mice lacking CD38 proteins were unable to synthesise NAADP and cADPR. In Chapter 4, it was shown that cardiac SRMP from sheep exhibited CD38-associated properties. The observations from this chapter show that SAN4825 could completely inhibit

the ARC activity of sheep cardiac SRMP and the mouse cardiac mixed membrane preparation and suggests that the administration of SAN4825 mimicked the effect of genetic KO of CD38. Furthermore, the IC_{50} (10^{-7} M) of SAN4825 measured from experiments presented in this chapter is in a similar range to that reported by Kannt et al. (2012). Clearly, the observed inhibition by SAN4825 is not an off-target action, and it seems more likely that SAN4825 indeed targets the main ARC in the heart, CD38, and inhibits its synthesis of NAADP and cADPR.

Interestingly, the inhibition of NAADP but not cADPR synthesis by SAN4825 was observed to be greater at the cytosolic pH of 7.2 than at the acidic pH of 4.5. Further investigation was conducted to evaluate binding conformations of SAN4825 at the active site of mouse CD38 with considerations of different protonation states of SAN4825 and mouse CD38 protein amino acids predicted by Epik and Propka 3.1, respectively (not shown here but included in the supplementary data fromLin et al. (2017)). Despite different conformations at different pH conditions, the most favourable docking conformations of SAN4825 were still in proximity of the main catalytic residues, which are Glu150, Asp159, Glu230, Trp129, and Trp193. When accounting for these observations, the following considerations need to be taken into account i) NAADP synthesis by human CD38 (Aarhus et al., 1995) and mouse CD38 was observed to be enhanced at pH 4.5 (see section 6.3.4 on page 202), ii) inhibition of cADPR synthesis by SAN4825 remains intact at pH 4.5 (see section 6.3.3 on page 200 and section 6.3.4 on page 202), iii) SAN4825 was predicted to bind to the CD38 active site at both pH 7.2 and pH 4.5 (Lin et al., 2017), iv) and no NAADP synthesis was observed in *CD38*$^{-/-}$ at pH 4.5 (see section 18 on page 152). It appears from these considerations that the observed weakened inhibition by SAN4825 at pH 4.5 is therefore not due to a degradation of the drug, a drastic change in the binding conformation of the drug, or a non-CD38 enzyme synthesising NAADP.

To a more extreme extent, the observations in sheep SRMP support the hypothesis that the effect of SAN4825 is weakened by an enhanced NAADP synthesis. In Chapter 4, it was shown that substrates of CD38/ARC were capable of inhibiting each other's reaction. For example, preincubation of high concentration of NAD was shown to inhibit the NAADP synthesis by CD38/ARC. While this observation holds true in the neutral pH, NAADP synthesis was not inhibited by NAD at pH 4.5. Similarly, in the sheep cardiac SRMP, SAN4825 showed similar characteristic with NAD — while SAN4825 was able to inhibit NAADP synthesis at pH 7.2, at pH 4.5, there was a lack of an inhibitory effect of SAN4825 on sheep cardiac SRMP NAADP synthesis (while its inhibition on cADPR at this pH remained intact).

In addition, the *in silico* studies in this chapter shows that SAN4825 was predicted to bind to the active site of CD38. Most of the favourable binding conformations of SAN4825 were predicted to be in close proximity to the CD38 active site. The most favourable Glide docking conformation of SAN4825 at pH 7.2 in mouse CD38 suggests that this compound occupies the same binding site as the NAADP analogue and ADPRP, in close proximity to the residue corresponding to Glu226 of human CD38, and forms π-π stacking with the residue corresponding to Trp189 of human CD38. In addition to the similarity of chemical structures between SAN4825 and NAD, the predicted binding conformations of SAN4825 with both human and mouse CD38 show some resemblance to the native binding conformation between human CD38 and its substrates such as NAD, NMN, cADPR and NAADP (Liu et al., 2005, 2006; Zhang et al., 2013). Bringing this all together, SAN4825 is likely to inhibit CD38 competitively by occupying the catalytic active site of CD38, hindering the access of other substrates.

Due to some complications discussed in section 6.3.6 on page 209, the ability of

SAN4825 to alter the physiological Ca^{2+} handling of cardiac myocytes is yet to be demonstrated. However, consistent with the observation that *CD38*$^{-/-}$ hearts were more resistant to isoprenaline-induced arrhythmias, hearts preincubated and perfused with 3 μM SAN4825 also showed similar resistance to arrhythmias (to a lesser extent with compared with CD38 KO). These observations corroborate those reported by Warszta et al. (2014) who have demonstrated that 3 μM SAN4825 was able to partially block the occurrence of arrhythmic events in single cardiac myocytes, as well as those reported by Kannt et al. (2012) showing that 3 μM SAN4825 reduced the delayed after depolarisations in guinea pig papillary muscle. It was also shown that bolus injection of SAN4825 to anaesthetised guinea pigs could delay ventricular fibrillation and cardiac arrest in ouabain-induced arrhythmias (Kannt et al., 2012). As cADPR and NAADP were both involved in contributing to cardiac arrhythmias (see section 1.2.11.7 on page 33), SAN4825 is proposed to have an anti-arrhythmic effect by preventing the accumulation of these Ca^{2+}-mobilising agents through its inhibition of CD38. Nonetheless, given that 3 μM SAN4825 was capable of altering the refractory period in the whole heart Langendorff experiments, the possible off-targets of SAN4825 at this concentration or higher need to be investigated.

6.5 Conclusion

The observations presented in this chapter support the hypothesis that SAN4825 inhibits the NAADP and cADPR synthesis by CD38, through occupying its active site. Given that whole heart treated with SAN4825 showed resistance to arrhythmias, CD38 is therefore a good therapeutic target for cardiac arrhythmias, therefore SAN4825 serves a promising drug candidate in this context.

Chapter 7

General discussion and future work

7.1 General discussion and conclusion

In Chapter 3, the role of NAADP during the activation of the β-adrenoceptor signalling pathway in mouse ventricular myocytes was investigated. Consistent with the hypothesis that TPC2 proteins are essential in regulating NAADP-induced Ca^{2+} release (Calcraft et al., 2009), cell permeant NAADP-AM was shown to elevate the action potential-triggered Ca^{2+} transients in ventricular cardiomyocytes from WT but not *Tpcn2*$^{-/-}$ mice. These NAADP-insensitive *Tpcn2*$^{-/-}$ cardiomyocytes also showed a blunted response to isoprenaline (3 nM)-induced positive inotropy — the mean Ca^{2+} transient amplitude of these myocytes was lower during activation of the β-adrenoceptor signalling pathway. The effect of genetic KO of *Tpcn2* also mirrors the effect of pharmacological inhibition of the NAADP pathway using bafilomycin-A1, both qualitatively and quantitatively (see section 3.3.4 on page 91). These observations are consistent with previous work done in Terrar's lab showing

that NAADP acts as an inotropic agent in guinea pig ventricular cardiomyocytes (Macgregor et al., 2007a) and guinea pig atrial cardiomyocytes (Collins et al., 2011). Parts of data presented in Chapter 3 were included in a recent published paper (Capel et al., 2015). Observations included in this paper demonstrate that ventricular cardiomyocytes and Langendorff-perfused hearts from *Tpcn2*$^{-/-}$ mice had weaker contractions during the activation of the β-adrenoceptor signalling pathway, compared to the WT control group. Pharmacological blockade of the NAADP signalling pathway using bafilomycin-A1 or Ned-19 (in guinea pig ventricular cardiomyocytes) resulted in blunted Ca^{2+} transients in the presence of isoprenaline (Capel et al., 2015) — an effect similar that observed in *Tpcn2*$^{-/-}$ ventricular myocytes. Taken together, these observations provide evidence that the mobilisation of endolysosomal Ca^{2+} via TPC2 proteins may play a role in β-adrenoceptor-associated positive inotropy. Additional data from the report by Capel et al. (2015) showing the resistance of *Tpcn2*$^{-/-}$ mice to isoprenaline-induced arrhythmias and hypertrophy, also provide additional evidence for the contributions of NAADP and TPC2 in the β-adrenoceptor signalling pathway.

In the second part of Chapter 3, NAADP actions in cardiac tissue were shown to be dependent on functional CaMKII proteins. This NAADP-CaMKII pathway is unlikely to involve phosphorylation of L-type Ca^{2+} channels as there was no significant difference between the amplitude of L-type Ca^{2+} currents between cardiomyocytes from WT and *Tpcn2*$^{-/-}$ mice (see section 3.3.5 on page 93). Similarly, L-type Ca^{2+} currents of guinea pig cardiomyocytes remained comparable with or without the presence of various CaMKII antagonists and Ned-19 (Capel et al., 2015). The intracellular application of NAADP was also shown to increase the SR Ca^{2+} load (Macgregor et al., 2007a; Collins et al., 2011). It is possible that NAADP-induced Ca^{2+} release from lysosomes activates CaMKII proteins, which in

turn phosphorylate SERCA to increase Ca^{2+} uptake and SR Ca^{2+} load, resulting in a positive inotropic effect. Recent evidence showing the lysosomes are found in close proximity to the SR also provides additional support to this hypothesis (Aston et al., 2017). Future experiments demonstrating the effect of NAADP exposure on the phosphorylation states of SERCA and other relevant proteins will provide further evidence on a molecular level.

The interest in NAADP action in cardiac tissue has led to studies investigating how NAADP is synthesised in the heart in this thesis. Despite CD38 being the well-discussed enzyme that catalyses both cADPR and NAADP production, several papers have proposed a non-CD38 enzyme that is responsible for the synthesis of cADPR in the heart (see section 1.2.9 on page 17). This proposed non-CD38 enzyme is expressed intracellularly, with evidence of it being dominant in the SR. It also has different biochemical properties compared to the CD38 enzyme. However, the identity of this enzyme has not been elucidated. In Chapter 4, it was demonstrated that the SRMP from sheep heart was capable of producing NAADP from NADP and NA, and cADPR from NAD. However, the reported biochemical differences in Zn^{2+} and DTT sensitivity by others (Mészáros et al., 1997; Xie et al., 2005; Kannt et al., 2012) were not observed in sheep SRMP. In fact, the enzyme of interest from sheep SRMP shows most, if not all, CD38-associated properties: i) its base-exchange activity shows the typical pH dependency, ii) its base-exchange activity is stimulated by Zn^{2+}, iii) and its cyclisation activity is inhibited by DTT. This enzyme, like the CD38 enzyme, has the ability to catalyse multiple reactions through a single catalytic site. In Chapter 5, it was shown that cardiac membrane preparations and ventricular cardiomyocytes from mice lacking CD38 ($CD38^{-/-}$) were not capable of synthesising NAADP or cGDPR. Further experiments in Chapter 6 also revealed that a drug, SAN4825, that was thought to be an inhibitor of the cardiac non-CD38, cADPR-synthesising enzyme

(Kannt et al., 2012), abolished NAADP and cADPR production in sheep and mouse cardiac tissues. Both *in silico* and *in vitro* evidence shown in Chapter 6 support the hypothesis that SAN4825 inhibits CD38 enzymes through occupying its catalytic site. All together, the data reported in this thesis do not support the existence of a non-CD38 enzyme being the main NAADP and cADPR-synthesising enzyme in the heart; in contrast, the favoured hypothesis is that CD38 is the enzyme responsible for these reactions.

The observations in Chapter 5 further support the role of CD38 during activation of β-adrenoceptors. Ventricular myocytes from *CD38*$^{-/-}$ mice had blunted responses, in terms of Ca^{2+} transients and contractions upon exposure to isoprenaline. In whole heart Langendorff experiments, the genetic KO of CD38 and the pharmacological inhibition of CD38 by SAN4825 were able to provide resistance to isoprenaline-triggered arrhythmias. These observations are consistent with findings of cADPR and NAADP being cardiac inotropic and pro-arrhythmic agents (see section 1.2.11.1 on page 23 and section 1.3.6 on page 50). In addition, several papers have reported the increase in cADPR and NAADP levels in cardiac tissue upon exposure to isoprenaline (see section 1.2.11.3 on page 27). Most importantly, in this chapter, it was demonstrated that while bafilomycin-A1 was capable of blunting the positive inotropic effect of isoprenaline in WT cardiomyocytes and this effect of bafilomycin-A1 was not observed in *CD38*$^{-/-}$ cardiomyocytes. This highlights the role of CD38 in coupling the NAADP and β-adrenoceptors pathways. Therefore, the weaker Ca^{2+} transient amplitudes and greater resistance to arrhythmias seen in *CD38*$^{-/-}$ groups could partly, if not completely be due to the lack of cADPR and NAADP production during activation of β-adrenoceptors. In Chapter 4, it was also reported that one of the main downstream mediators of β-adrenoceptors, PKA, was able to increase the enzymatic production of cGDPR;

however, how an elevated level of NAADP is achieved during activation of β-adrenoceptors remains to be elucidated (see also (Gul et al., 2016)).

There were some major concerns regarding CD38 as the NAADP-synthesising enzyme. For example, as to whether CD38 can catalyse NAADP production at pH 7.2 has been debated. Crystallography studies have suggested that at neutral pH, there might be too much repulsive force between NA and Glu146 (of human CD38), rendering NAADP production not feasible, while in an acidic environment (pH 4.5), NA would be protonated, resulting in less repulsion (see section 1.2.7 on page 11). In Chapter 4, it was shown clearly that NAADP production is feasible at pH 7.2, but is slower, compared to production at pH 4.5 (see section 4.3.3 on page 125). However, given that NAADP is able to trigger Ca^{2+} release in the nanomolar concentration range (Galione, 2014), a lower yield of NAADP can still trigger its physiological signalling pathway. In contrast to the hypothesis that CD38 is a surface antigen expressed extracellularly as seen in lymphocytes, Triton-X100- or saponin-permeabilised cells were able to catalyse NAADP at a higher rate and immunolabelling of CD38 was only observed in permeabilised cells (see section 5.3.4 on page 154 and section 5.3.5 on page 159). Consistent with the data in Chapter 4 and other published papers (cited in section 1.2.9 on page 17), observations from immunolabelling experiments in Chapter 5 revealed a striated labelling pattern of CD38, highlighting the possibility of a relatively higher expression of CD38 in the SR. Coupled with recent observations of lysosomes being in close proximity to the SR (Aston et al., 2017), CD38 expressed on the SR could produce NAADP and cADPR *in situ*, achieving high localised concentrations of these molecules even though the production is at a slower enzymatic rate at pH 7.2.

While researchers in Terrar's lab and other labs were capable of demonstrating

the effect of isoprenaline at 1 – 5 nM (see section 1.3.5 on page 46), Gul et al. (2016) have applied 2 μM isoprenaline to non-pacing cardiac ventricular myocytes from mouse hearts, causing a rise in intracellular [Ca^{2+}] that plateaued at around 400 nM. Assuming that isoprenaline at this concentration has no off-targets, this concentration of isoprenaline would normally result in a strong activation of β-adrenoceptors and would often trigger arrhythmias in whole hearts, let alone single cells. For example, in chapters 5 and 6, it was demonstrated that 300 nM isoprenaline was sufficient to trigger arrhythmias in whole heart experiments (see section 5.3.9 on page 178 and section 6.3.7 on page 213, see also (Capel et al., 2015)). However, the authors did not describe the nature of the observed Ca^{2+} signals, and so it remains unknown as to whether the increased intracellular [Ca^{2+}] is a global sustained Ca^{2+} signal, an episode of recurring Ca^{2+} events, such as Ca^{2+} waves or sparks, or an accumulation of Ca^{2+} in dying cells. In addition to the exceptionally high concentration of isoprenaline used, the lack of Ca^{2+}-induced-Ca^{2+} release at 400 nM in their observations is puzzling; therefore, the physiological relevance of their methods needed to be addressed. They have described the increase in Ca^{2+} upon isoprenaline addition into two phases, which are the initial rise mediated by NAADP and the sustain phase mediated by cADPR. Pharmacological agents which antagonise the NAADP pathway were demonstrated to abolish both phases while those which antagonise cADPR were only capable of inhibiting the latter phase. They also showed that levels of NAADP and cADPR peaked at different time points (one time point apart). From these observations, it was argued that NAADP production precedes cADPR production and the NAADP-regulated Ca^{2+} release from lysosomes initiates cADPR production. However, this argument contradicts a previous observation, which shows that the physiological range of Ca^{2+} has no effect on CD38 enzymatic activity (Liu et al., 2008). As a matter of opinion, the observation that the level of NAADP peaked 15 s

before cADPR does not necessarily support the argument put forward by Gul et al. (2016), especially as these molecules have different potencies and ranges of endogenous levels. It should also be noted that the time resolution of their studies is exactly 15 s. Furthermore, the determination of peaks and comparisons of peaked time lacked appropriate statistical analyses and considerations of uncertainties and errors. Despite disagreeing on the fact that the preceding NAADP production is indispensable for cADPR production, the author of this thesis speculates that NAADP and/or cADPR can influence the enzymatic activity of CD38, through their Ca^{2+}-mobilising effect, indirectly rather than directly. It is possible that this feed forward mechanism is mediated by Ca^{2+} sensitive proteins (see section 7.2.3 on page 235 and section 7.2.4 on page 236).

It is important to point out that Gul et al. (2016) also demonstrated that without functional CD38, cardiac NAADP and cADPR production were not observed *in vitro*. However, in addition to showing that the KO of CD38 only abolished the sustenance of intracellular Ca^{2+} (proposed to be mediated by cADPR) but not the initial spike (proposed to be mediated by NAADP), they further demonstrated that the KO of CD38 prevented the isoprenaline-induced increase in the endogenous levels of cADPR but not NAADP. They concluded that CD38 is the main enzyme for cADPR production but NAADP production is catalysed by another NAADP-synthesising enzyme. Interestingly, Gul et al. (2016) showed that bafilomycin-A1 was able to inhibit the rise of intracellular Ca^{2+} completely and inhibit the increase in levels of NAADP and cADPR in cardiomyocytes exposed to isoprenaline. Observations from previous experiments conducted in Terrar's lab and from experiments shown in this thesis showed that the effects of isoprenaline were only partially blunted in *Tpcn2*$^{-/-}$ and *CD38*$^{-/-}$ myocytes as well as myocytes preincubated with bafilomycin-A1 (see Chapter 3, 5 and 6). This is completely

justifiable as a major part of this flight and fight response was mediated by PKA phosphorylation of RyRs, SERCA and L-type Ca^{2+} channels (Bers, 2002). However, surprisingly, Gul et al. (2016) showed that by merely antagonising the NAADP signalling pathway with bafilomycin-A1, the effect of isoprenaline in their Ca^{2+} measuring assay was completely abolished. Furthermore, it is in a way contradictory for them to propose that bafilomycin-A1 inhibited a non-CD38 NAADP-synthesising enzyme through alkalinising the lysosomes, as the acid dependency of NAADP production is the quintessential property of the CD38 enzyme and of the base-exchange reaction. In their reports, the basal levels of NAADP and cADPR (in the absence of β-adrenoceptor stimulation) remained intact in CD38 KO animals as well as in the presence of different pharmacological agents, including those which were shown to inhibit the production of cADPR during the activation of β-adrenoceptors. This raised the question of whether the endogenous levels of these molecules were beyond the detection limits of their assays.

Although the author of this thesis agrees that measurements of endogenous levels of NAADP provide additional insights, however, it should be pointed out that the minute amounts of NAADP in the hearts might challenge the reliability of these measurements. For this reason, one should be cautious when interpreting such observation and the role of CD38 in synthesising NAADP should not be evaluated solely based on the measurement of endogenous NAADP levels in CD38 KO models. The evidence that CD38 and the base-exchange reaction are, by far, the main enzyme and the main reaction for the synthesis of NAADP *in vitro* should be weighted and considered carefully. Functional assays such as the one showing the lack of a bafilomycin-A1-mediated effect in $CD38^{-/-}$ myocytes (see section 5.3.8 on page 175) should be employed to provide further evidence.

In conclusion, observations in this thesis have provided evidence for the role of an intracellular CD38 expressed on the SR that involves the NAADP signalling pathway. These signalling pathways have overlapping contributions in modulating the EC coupling of the heart especially during the activation of β-adrenoceptors. During extreme activation of β-adrenoceptors, these pathways play a significant role in the development of cardiac arrhythmias and therefore they are potential therapeutic targets.

7.2 Future work

7.2.1 Type-III CD38 in the heart

Following observations reported in this thesis that support the expression of CD38 on the SR (see section 5.3.5 on page 159 and section 5.3.6 on page 164), the topological orientation of cardiac CD38 is yet to be determined. While the expression of Type-III CD38 was shown in several cells lines and mammalian cells (Zhao et al., 2011, 2012, 2015), its expression in a vital organ demands further investigation. As discussed above, type-III CD38 is catalytically functional and does not possess the topological paradox of a type-II CD38 (see section 1.2.8 on page 15). Lee's group have designed several antibodies that specifically label human type-III CD38 (Zhao et al., 2012). These tools, or similar specific labelling agents, for targeting experimental animals will be useful in the study of type-III CD38 in the heart. Human induced pluripotent stem cell (iPSC)-derived cardiomyocytes or human atrial myocytes isolated from atrial appendages can also be used as models to study the expression of CD38. The regulation of the expression of type-II or

type-III CD38 is also worth studying as this will provide further insight into whether their expression levels in cardiac tissue is altered in the disease state or upon hormonal stimulation. The relative contribution of type-III CD38 versus the type-II CD38 in terms of generating Ca^{2+}-mobilising molecules can also be investigated using pharmacological agents that inhibit the substrate/product transport mechanisms, which are pivotal for the type-II CD38 to act as an efficient enzyme.

7.2.2 Contribution of CD38 in atrial tissue

Most, if not all, of the CD38 work has focussed on the ventricles of the heart (see section 1.2.11 on page 23). In this thesis, immunolabelling of CD38 in rabbit atrial myocytes also showed labelling with a striated pattern (see section 5.3.6 on page 164). As most of the atrial tissue lacks of t-tubules, observations from the immunolabelling experiments suggested a SR-predominant expression of CD38 in atrial tissue. As to whether CD38 is the main enzyme in catalysing NAADP and cADPR production in atrial tissue remains to be addressed. In the past, Terrar's group has demonstrated the role of NAADP in EC coupling of atrial myocytes (Collins et al., 2011). As CD38 was shown to mediate EC coupling of ventricular myocytes particularly during the activation of β-adrenoceptors, CD38 could similarly mediate the EC coupling of atrial tissue. In whole heart experiments, it was demonstrated that inhibition of the CD38 pathway provided protection to the heart against β-adrenoceptor-mediated arrhythmias (see section 5.3.9 on page 178 and section 6.3.7 on page 213). CD38 and its Ca^{2+}-mobilising products could also alter the Ca^{2+} handling properties of atrial tissue. This extrapolation can be verified using myocytes isolated from atrial tissue or isolated atrial myocytes. In addition, it was demonstrated (in this thesis) that inhibition of CD38 also blunted the positive chronotropic effect of isoprenaline (see

section 5.3.10 on page 183 and section 6.3.8 on page 217). Since the Ca^{2+} signalling pathway has been shown to be pivotal for the regulation of pacemaking mechanisms (see review by Capel and Terrar 2015), CD38 could have a role in the pacemaking mechanism of the sino-atrial node. The positive chronotropic effect of isoprenaline in isolated sino-atrial nodal tissue from WT and *CD38*$^{-/-}$ would be a suitable model for such an investigation. More importantly, future experiments demonstrating the downstream mechanisms of the CD38/NAADP/cADPR pathway in regulating the heart beat can be carried out.

7.2.3 Relationship of CaMKII and NAADP/CD38

In Chapter 3, it was shown that CaMKII could be a significant downstream mediator of the NAADP signalling pathway (see section 3.3.6 on page 94). The current hypothesis is that CaMKII proteins are activated by the high concentration, localised NAADP-regulated Ca^{2+} release from lysosomes. Colocalisation studies involving TPC proteins, CaMKII proteins and/or lysosomes will provide further support for this hypothesis. Future experiments can be carried out to further evaluate the involvement of CaMKII as a downstream mediator of the NAADP signalling pathway; for example, i) quantitative analysis of the phosphorylation states of proteins phosphorylated by CaMKII (such as RyR and phospholamban), using western blot or phosphoproteomics, ii) investigation of the effect of intracellular application of NAADP in mutant mice that express mutant proteins that cannot be phosphorylated by CaMKII (such as mice with a point mutation on Thr-17 site of phospholamban), iii) and/or detection of CaMKII activation after intracellular application of NAADP through Förster resonance energy transfer (FRET) responses in transgenic mice. Furthermore, there could be a dynamic

interaction between CD38 and CaMKII. For example, CD38 could be an upstream mediator of CaMKII by producing NAADP while CaMKII might regulate the CD38 enzymatic activity through phosphorylation. Such potential feed forward mechanism is consistent by several observations: i) application of NAADP further triggered an intracellular accumulation of cADPR and NAADP (Djerada and Millart, 2013; Djerada et al., 2013), ii) and application of bafilomycin-A1 inhibit the production of both NAADP and cADPR (Gul et al., 2016). Experiments can be carried out to evaluate the the enzymatic production of NAADP and cADPR upon β-adrenoceptor stimulation in the presence and absence of CaMKII inhibitors such as KN93 or AIP.

7.2.4 Possible complementary actions of NAADP and cADPR

Following the discussion above regarding a role of CaMKII/NAADP in modulating CD38 enzymatic activity, it is also of interest to study in the possible complementary actions of NAADP and cADPR. In Chapter 5, it was shown that the bafilomycin-A1 preincubation and the genetic KO of CD38 reduced the isoprenaline effect to a similar level (see section 5.3.8 on page 175), while in the past it was demonstrated that 8-Br-cADPR (cADPR inhibitor) has a negative inotropic effect (Rakovic et al., 1996). If the *CD38*$^{-/-}$ animals cannot produce both cADPR and NAADP and that cADPR and NAADP signalling pathways has little or no overlapping, genetic KO of CD38 should have a greater effect than that of inhibiting NAADP pathway alone. Given that cADPR mainly has an effect on SR Ca^{2+} release while NAADP actions are mediated partly through increasing SR Ca^{2+} load (see section 1.2.11.1 on page 23 and section 1.3.5 on page 46), the current speculation is that these two molecules might work in a complementary manner in increasing

systolic intracellular Ca^{2+} concentration. Their synchronisation is very likely to be controlled by CD38 that can produce both cADPR and NAADP. One interesting experiment to support this is to evaluate whether intracellular application of NAADP has a lesser effect in *CD38*$^{-/-}$ myocytes compared to its WT. Similarly, if the hypothesis is that NAADP initiates the activation of CaMKII which subsequently enhances CD38 enzymatic activity, CaMKII might also be a key mediator of this synchronisation of NAADP and cADPR by CD38. One obvious caveat in this hypothesis is that if the stimulation of CaMKII by NAADP-regulated Ca^{2+} release precedes the enhancement of CD38 activity, which process/protein is responsible to initiate or augment the NAADP-regulated Ca^{2+} release if not CD38 itself? Interestingly, some published work has demonstrated the endogenous level of NAADP upon the stimulation of receptors has three phases: an initial spike followed by a rapid drop and slowly ramping up to a sustained increase (Lewis et al., 2012; Djerada and Millart, 2013). These observations are consistent with the hypothesis proposed below: CD38 is first transiently stimulated by other modulators (such as PKA) and subsequently produces NAADP and cADPR that indirectly activates a second modulator (such as the Ca^{2+}-activated CaMKII), which then steps in and further stimulates CD38, giving rise to a sustained and enhanced enzymatic activity of CD38.

References

Aarhus, R., Dickey, D. M., Graeff, R. M., Gee, K. R., Walseth, T. F., and Lee, H. C. (1996). Activation and inactivation of Ca^{2+} release by $NAADP^{+}$. *Journal of Biological Chemistry* **271**, 8513–8516.

Aarhus, R., Graeff, R. M., Dickey, D. M., Walseth, T. F., and Lee, H. C. (1995). ADP-ribosyl cyclase and CD38 catalyze the synthesis of a calcium-mobilizing metabolite from NADP. *Journal of Biological Chemistry* **270**, 30327–30333.

Adebanjo, O. A., Anandatheerthavarada, H. K., Koval, A. P., Moonga, B. S., Biswas, G., Sun, L., Sodam, B. R., Bevis, P. J., Huang, C. L., Epstein, S., Lai, F. A., Avadhani, N. G., and Zaidi, M. (1999). A new function for CD38/ADP-ribosyl cyclase in nuclear Ca^{2+} homeostasis. *Nature Cell Biology* **1**, 409–414.

Alessio, M., Roggero, S., Funaro, A., De Monte, L. B., Peruzzi, L., Geuna, M., and Malavasi, F. (1990). CD38 molecule: structural and biochemical analysis on human T lymphocytes, thymocytes, and plasma cells. *Journal of Immunology* **145**, 878–884.

Aley, P. K., Singh, N., Brailoiu, G. C., Brailoiu, E., and Churchill, G. C. (2013). Nicotinic acid adenine dinucleotide phosphate (NAADP) is a second messenger in muscarinic receptor-induced contraction of guinea pig trachea. *Journal of Biological Chemistry* **288**, 10986–10993.

Arredouani, A., Ruas, M., Collins, S. C., Parkesh, R., Clough, F., Pillinger, T., Coltart, G., Rietdorf, K., Royle, A., Johnson, P., Braun, M., Zhang, Q., Sones, W., Shimomura, K., Morgan, A. J., Lewis, A. M., Chuang, K. T., Tunn, R., Gadea, J., Teboul, L., Heister, P. M., Tynan, P. W., Bellomo, E. A., Rutter, G. A., Rorsman, P., Churchill, G. C., Parrington, J., and Galione, A. (2015). Nicotinic acid adenine dinucleotide phosphate (NAADP) and endolysosomal two-pore channels modulate membrane excitability and stimulus-secretion coupling in mouse pancreatic β cells. *Journal of Biological Chemistry* **290**, 21376–21392.

Aston, D. (2017). The influence of nicotinic acid adenine dinucleotide phosphate (NAADP) signalling and the significance of the organization of lysosomes in cardiac myocytes. *DPhil Thesis, University of Oxford* .

Aston, D., Capel, R. A., Ford, K. L., Christian, H. C., Mirams, G. R., Rog-Zielinska, E. A., Kohl, P., Galione, A., Burton, R. A. B., and Terrar, D. A. (2017). High resolution structural evidence suggests the sarcoplasmic reticulum forms microdomains with acidic stores (lysosomes) in the heart. *Scientific Reports* **7**, 10.1038/srep40620.

Bacher, I., Zidar, A., Kratzel, M., and Hohenegger, M. (2004). Channelling of substrate promiscuity of the skeletal-muscle ADP-ribosyl cyclase isoform. *The Biochemical Journal* **381**, 147–154.

Bainton, D. F. (1981). The discovery of lysosomes. *Journal of Cell Biology* **91**, 66s–76s.

Bak, J., Billington, R. A., Timar, G., Dutton, A. C., and Genazzani, A. A. (2001). NAADP receptors are present and functional in the heart. *Current Biology* **11**, 987–990.

Benito, J. M., López, M., Lozano, S., Martinez, P., González-Lahoz, J., and Soriano, V. (2004). CD38 expression on CD8 T lymphocytes as a marker of residual virus replication in chronically HIV-infected patients receiving antiretroviral therapy. *AIDS Research and Human Retroviruses* **20**, 227–233.

Bers, D. M. (2002). Cardiac excitation-contraction coupling. *Nature* **415**, 198–205.

Berthelier, V., Laboureau, J., Boulla, G., Schuber, F., and Deterre, P. (2000). Probing ligand-induced conformational changes of human CD38. *European Journal of Biochemistry* **267**, 3056–3064.

Billington, R. A. and Genazzani, A. A. (2007). PPADS is a reversible competitive antagonist of the NAADP receptor. *Cell Calcium* **41**, 505–511.

Böttger, S. and Melzig, M. F. (2013). The influence of saponins on cell membrane cholesterol. *Bioorganic and Medicinal Chemistry* **21**, 7118–7124.

Brailoiu, E., Churamani, D., Cai, X., Schrlau, M. G., Brailoiu, G. C., Gao, X., Hooper, R., Boulware, M. J., Dun, N. J., Marchant, J. S., and Patel, S. (2009). Essential requirement for two-pore channel 1 in NAADP-mediated calcium signaling. *Journal of Cell Biology* **186**, 201–209.

Brooks, B. R., Brooks, C. L., Mackerell, A. D., Nilsson, L., Petrella, R. J., Roux, B., Won, Y., Archontis, G., Bartels, C., Boresch, S., Caflisch, A., Caves, L., Cui, Q., Dinner, A. R., Feig, M., Fischer, S., Gao, J., Hodoscek, M., Im, W., Kuczera, K., Lazaridis, T., Ma, J., Ovchinnikov, V., Paci, E., Pastor, R. W., Post, C. B., Pu, J. Z., Schaefer, M., Tidor, B., Venable, R. M., Woodcock, H. L., Wu, X., Yang, W., York, D. M., and Karplus, M. (2009). CHARMM: The biomolecular simulation program. *Journal of Computational Chemistry* **30**, 1545–1614.

Bruzzone, S., Guida, L., Franco, L., Zocchi, E., Corte, G., and De Flora, A. (1998). Dimeric and tetrameric forms of catalytically active transmembrane CD38 in transfected HeLa cells. *FEBS letters* **433**, 275–278.

Bruzzone, S., Guida, L., Sturla, L., Usai, C., Zocchi, E., and De Flora, A. (2012). Subcellular and intercellular traffic of NAD^+, NAD^+ precursors and NAD^+-derived signal metabolites and second messengers: old and new topological paradoxes. *Messenger* **1**, 34–52.

Bruzzone, S., Guida, L., Zocchi, E., Franco, L., and De Flora A (2001). Connexin 43 hemi channels mediate Ca^{2+}-regulated transmembrane NAD^+ fluxes in intact cells. *The FASEB Journal* **15**, 10–12.

Calcraft, P. J., Ruas, M., Pan, Z., Cheng, X., Arredouani, A., Hao, X., Tang, J., Rietdorf, K., Teboul, L., Chuang, K.-T., Lin, P., Xiao, R., Wang, C., Zhu, Y., Lin, Y., Wyatt, C. N., Parrington, J., Ma, J., Evans, A. M., Galione, A., and Zhu, M. X. (2009). NAADP mobilizes calcium from acidic organelles through two-pore channels. *Nature* **459**, 596–600.

Cancela, J. M., Churchill, G. C., and Galione, A. (1999). Coordination of agonist-induced Ca*ext*2+-signalling patterns by NAADP in pancreatic acinar cells. *Nature* **398**, 74–76.

Cang, C., Aranda, K., and Ren, D. (2014). A non-inactivating high-voltage-activated two-pore Na^+ channel that supports ultra-long action potentials and membrane bistability. *Nature Communications* **5**, 10.1038/ncomms6015.

Cang, C., Zhou, Y., Navarro, B., Seo, Y. J., Aranda, K., Shi, L., Battaglia-Hsu, S., Nissim, I., Clapham, D. E., and Ren, D. (2013). MTOR regulates lysosomal ATP-sensitive two-pore Na^+ channels to adapt to metabolic state. *Cell* **152**, 778–790.

Cantó, C., Menzies, K. J., and Auwerx, J. (2015). NAD^+ metabolism and the control of energy homeostasis: A balancing act between mitochondria and the nucleus. *Cell Metabolism* **22**, 31–53.

Capel, R. A., Bolton, E. L., Lin, W. K., Aston, D., Wang, Y., Liu, W., Wang, X., Burton, R.-A. B. A. B., Bloor-Young, D., Shade, K.-T. T., Ruas, M., Parrington, J., Churchill, G. C., Lei, M., Galione, A., and Terrar, D. A. (2015). Two pore channels (TPC2s) and nicotinic acid adenine dinucleotide phosphate (NAADP) at lysosomal-sarcoplasmic reticular junctions contribute to acute and chronic β-adrenoceptor signaling in the heart. *Journal of Biological Chemistry* **290**, 30087–30098.

Capel, R. A. and Terrar, D. A. (2015). The importance of Ca^{2+}-dependent mechanisms for the initiation of the heartbeat. *Frontiers in Physiology* **6**, 10.3389/fphys.2015.00080.

Cartwright, E. J., Mohamed, T., Oceandy, D., and Neyses, L. (2011). Calcium signaling dysfunction in heart disease. *BioFactors* **37**, 175–181.

Ceni, C., Muller-Steffner, H., Lund, F., Pochon, N., Schweitzer, A., De Waard, M., Schuber, F., Villaz, M., and Moutin, M.-J. (2003a). Evidence for an Intracellular ADP-ribosyl Cyclase/NAD^+-glycohydrolase in Brain from CD38-deficient Mice. *Journal of Biological Chemistry* **278**, 40670–40678.

Ceni, C., Pochon, N., Brun, V., Muller-Steffner, H., Andrieux, A., Grunwald, D., Schuber, F., De Waard, M., Lund, F., Villaz, M., and Moutin, M.-J. (2003b). CD38-dependent ADP-ribosyl cyclase activity in developing and adult mouse brain. *The Biochemical Journal* **370**, 175–183.

Ceni, C., Pochon, N., Villaz, M., Muller-Steffner, H., Schuber, F., Baratier, J., De Waard, M., Ronjat, M., and Moutin, M.-J. (2006). The CD38-independent ADP-ribosyl cyclase from mouse brain synaptosomes: a comparative study of neonate and adult brain. *The Biochemical journal* **395**, 417–426.

Chidambaram, N. and Chang, C. F. (1998). Functional role of glycosylation on the recombinant CD38/ADP-ribosyl cyclase in CHO cells. *International Journal of Biochemistry and Cell Biology* **30**, 1011–1018.

Chidambaram, N., Wong, E. T., and Chang, C. F. (1998). Differential oligomerization of membrane-bound CD38/ADP-ribosyl cyclase in porcine heart microsomes. *Biochemistry and Molecular Biology International* **44**, 1225–1233.

Chini, E. N., Chini, C. C. S., Kato, I., Takasawa, S., and Okamoto, H. (2002). CD38 is the major enzyme responsible for synthesis of nicotinic acid-adenine dinucleotide phosphate in mammalian tissues. *The Biochemical Journal* **362**, 125–130.

Chini, E. N. and Dousa, T. P. (1995). Enzymatic-synthesis and degradation of nicotinate adenine dinucleotide phosphate (NAADP), a Ca^{2+}-releasing agonist, in rat tissues. *Biochemical and Biophysical Research Communications* **209**, 167–174.

Christensen, K. A., Myers, J. T., and Swanson, J. A. (2002). pH-dependent regulation of lysosomal calcium in macrophages. *Journal of Cell Science* **115**, 599–607.

Churchill, G. C. and Galione, A. (2001). NAADP induces Ca^{2+} oscillations via a two-pool mechanism by priming IP_3- and cADPR-sensitive Ca^{2+} stores. *EMBO Journal* **20**, 2666–2671.

Churchill, G. C., Okada, Y., Thomas, J. M., Genazzani, A. A., Patel, S., and Galione, A. (2002). NAADP mobilizes Ca^{2+} from reserve granules, lysosome-related organelles, in sea urchin eggs. *Cell* **111**, 703–708.

Clapper, D. L., Walseth, T. F., Dargie, P. J., and Lee, H. C. (1987). Pyridine nucleotide metabolites stimulate calcium release from sea urchin egg microsomes desensitized to inositol trisphosphate. *Journal of Biological Chemistry* **262**, 9561–9568.

Cockayne, D. A., Muchamuel, T., Grimaldi, J. C., Muller-Steffner, H., Randall, T. D., Lund, F. E., Murray, R., Schuber, F., and Howard, M. C. (1998). Mice deficient for the ecto-nicotinamide adenine dinucleotide glycohydrolase CD38 exhibit altered humoral immune responses. *Blood* **92**, 1324–1333.

Collins, T. P., Bayliss, R., Churchill, G. C., Galione, A., and Terrar, D. A. (2011). NAADP influences excitation-contraction coupling by releasing calcium from lysosomes in atrial myocytes. *Cell Calcium* **50**, 449–458.

Copello, J. A., Qi, Y., Jeyakumar, L. H., Ogunbunmi, E., and Fleischer, S. (2001). Lack of effect of cADP-ribose and NAADP on the activity of skeletal muscle and heart ryanodine receptors. *Cell Calcium* **30**, 269–284.

Cosker, F., Cheviron, N., Yamasaki, M., Menteyne, A., Lund, F. E., Moutin, M. J., Galione, A., and Cancela, J. M. (2010). The ecto-enzyme CD38 is a nicotinic acid adenine dinucleotide phosphate (NAADP) synthase that couples receptor activation to Ca^{2+} mobilization from lysosomes in pancreatic acinar cells. *Journal of Biological Chemistry* **285**, 38251–38259.

Crider, B. P., Xie, X. S., and Stone, D. K. (1994). Bafilomycin inhibits proton flow through the H^+ channel of vacuolar proton pumps. *Journal of Biological Chemistry* **269**, 17379–17381.

Cui, Y., Galione, A., and Terrar, D. A. (1999). Effects of photoreleased cADP-ribose on calcium transients and calcium sparks in myocytes isolated from guinea-pig and rat ventricle. *The Biochemical journal* **342**, 269–273.

Curran, J., Tang, L., Roof, S. R., Velmurugan, S., Millard, A., Shonts, S., Wang, H., Santiago, D., Ahmad, U., Perryman, M., Bers, D. M., Mohler, P. J., Ziolo, M. T., and Shannon, T. R. (2014). Nitric oxide-dependent activation of CaMKII increases diastolic sarcoplasmic reticulum calcium release in cardiac myocytes in response to adrenergic stimulation. *PLoS ONE* **9**, 10.1371/journal.pone.0087495.

Dammermann, W., Zhang, B., Nebel, M., Cordiglieri, C., Odoardi, F., Kirchberger, T., Kawakami, N., Dowden, J., Schmid, F., Dornmair, K., Hohenegger, M., Flügel, A., Guse, A. H., and Potter, B. V. L. (2009). NAADP-mediated Ca^{2+} signaling via type 1 ryanodine receptor in T cells revealed by a synthetic NAADP antagonist. *Proceedings of the National Academy of Sciences of the United States of America* **106**, 10678–10683.

Davidson, S. M., Foote, K., Kunuthur, S., Gosain, R., Tan, N., Tyser, R., Zhao, Y. J., Graeff, R., Ganesan, A., Duchen, M. R., Patel, S., and Yellon, D. M. (2015). Inhibition of NAADP signalling on reperfusion protects the heart by preventing lethal calcium oscillations via two-pore channel 1 and opening of

the mitochondrial permeability transition pore. *Cardiovascular Research* **108**, 357–366.

Davis, L. C., Morgan, A. J., Chen, J. L., Snead, C. M., Bloor-Young, D., Shenderov, E., Stanton-Humphreys, M. N., Conway, S. J., Churchill, G. C., Parrington, J., Cerundolo, V., and Galione, A. (2012). NAADP Activates two-pore channels on T cell cytolytic granules to stimulate exocytosis and killing. *Current Biology* **22**, 2331–2337.

Davis, L. C., Morgan, A. J., Ruas, M., Wong, J. L., Graeff, R. M., Poustka, A. J., Lee, H. C., Wessel, G. M., Parrington, J., and Galione, A. (2008). Ca^{2+} signaling occurs via second messenger release from intraorganelle synthesis sites. *Current Biology* **18**, 1612–1618.

De Flora, A., Zocchi, E., Guida, L., Franco, L., and Bruzzone, S. (2004). Autocrine and paracrine calcium signaling by the CD38/NAD^+/cyclic ADP-ribose system. *Annals of the New York Academy of Sciences* **1028**, 176–191.

De Toledo, F. G., Cheng, J., Liang, M., Chini, E. N., and Dousa, T. P. (2000). ADP-ribosyl cyclase in rat vascular smooth muscle cells: properties and regulation. *Circulation Research* **86**, 1153–1159.

Deshpande, D. A., White, T. A., Guedes, A. G. P., Milla, C., Walseth, T. F., Lund, F. E., and Kannan, M. S. (2005). Altered airway responsiveness in CD38-deficient mice. *American Journal of Respiratory Cell and Molecular Biology* **32**, 149–156.

Dibb, K. M., Clarke, J. D., Eisner, D. A., Richards, M. A., and Trafford, A. W. (2012). A functional role for transverse (t-) tubules in the atria. *Journal of Molecular and Cellular Cardiology* **58**, 84–91.

Djerada, Z. and Millart, H. (2013). Intracellular NAADP increase induced by extracellular NAADP via the P2Y11-like receptor. *Biochemical and Biophysical Research Communications* **436**, 199–203.

Djerada, Z., Peyret, H., Dukic, S., and Millart, H. (2013). Extracellular NAADP affords cardioprotection against ischemia and reperfusion injury and involves the P2Y11-like receptor. *Biochemical and Biophysical Research Communications* **434**, 428–433.

Egea, P. F., Muller-Steffner, H., Kuhn, I., Cakir-Kiefer, C., Oppenheimer, N. J., Stroud, R. M., Kellenberger, E., and Schuber, F. (2012). Insights into the mechanism of bovine CD38/NAD^+glycohydrolase from the X-ray structures of its michaelis complex and covalently-trapped intermediates. *PLoS ONE* **7**, 10.1371/journal.pone.0034918.

Elson, L. (2011). Regulation of cardiac Ca^{2+} signalling mechanisms and contractile function by nicotinic acid adenine dinucleotide phosphate. *DPhil Thesis, University of Oxford* .

Elson, L., Churchill, G., Terrar, D. A., and Rakovic, S. (2016). Actions of the NAADP antagonist trans-Ned19 in cardiac ventricular myocytes. *Biophysical Journal* **100**, 81a–82a.

Elson, L. C., Owen, W. D., Gafson, A. R., Parrington, J., Galione, A., Terrar, D. A., and Rakovic, S. (2010). Role of the putative NAADP receptor, two-pore channel 2, in ventricular myocyte responses to isoproterenol. *Biophysical Journal* **98**, 100a.

Fabiano, A., Panfoli, I., Calzia, D., Bruschi, M., Ravera, S., Bachi, A., Cattaneo, A., Morelli, A., and Candiano, G. (2011). Catalytic properties of the retinal rod outer segment disk ADP-ribosyl cyclase. *Visual Neuroscience* **28**, 121–128.

Favia, A., Desideri, M., Gambara, G., D'Alessio, A., Ruas, M., Esposito, B., Del Bufalo, D., Parrington, J., Ziparo, E., Palombi, F., Galione, A., and Filippini, A. (2014). VEGF-induced neoangiogenesis is mediated by NAADP and two-pore channel-2-dependent Ca^{2+} signaling. *Proceedings of the National Academy of Sciences of the United States of America* **111**, E4706–E5715.

Favia, A., Pafumi, I., Desideri, M., Padula, F., Montesano, C., Passeri, D., Nicoletti, C., Orlandi, A., Del Bufalo, D., Sergi, M., Ziparo, E., Palombi, F., and Filippini, A. (2016). NAADP-dependent Ca^{2+} signaling controls melanoma progression, metastatic dissemination and neoangiogenesis. *Scientific Reports* **6**, 10.1038/srep18925.

Fernandez, J. E., Deaglio, S., Donati, D., Svoboda Beusan, I., Corno, F., Aranega, A., Forni, M., Falini, B., and Malavasi, F. (1998). Analysis of the distribution of human CD38 and of its ligand CD31 in normal tissues. *Journal of Biological Regulators and Homeostatic Agents* **12**, 81–91.

Friesner, R. A., Banks, J. L., Murphy, R. B., Halgren, T. A., Klicic, J. J., Mainz, D. T., Repasky, M. P., Knoll, E. H., Shelley, M., Perry, J. K., Shaw, D. E., Francis, P., and Shenkin, P. S. (2004). Glide: a new approach for rapid, accurate docking and scoring. 1. Method and assessment of docking accuracy. *Journal of Medicinal Chemistry* **47**, 1739–1749.

Fruen, B. R., Mickelson, J. R., Shomer, N. H., Velez, P., and Louis, C. F. (1994). Cyclic ADP-ribose does not affect cardiac or skeletal muscle ryanodine receptors. *FEBS letters* **352**, 123–126.

Fukushi, Y., Kato, I., Takasawa, S., Sasaki, T., Ong, B. H., Sato, M., Ohsaga, A., Sato, K., Shirato, K., Okamoto, H., and Maruyama, Y. (2001). Identification of cyclic ADP-ribose-dependent mechanisms in pancreatic muscarinic Ca^{2+} signaling using CD38 knockout mice. *Journal of Biological Chemistry* **276**, 649–655.

Galione, A. (2014). A primer of NAADP-mediated Ca^{2+} signalling: from sea urchin eggs to mammalian cells. *Cell Calcium* **58**, 27–47.

Galione, a., Lee, H. C., and Busa, W. B. (1991). Ca^{2+}-induced Ca^{2+} release in sea urchin egg homogenates: modulation by cyclic ADP-ribose. *Science* **253**, 1143–1146.

Gan, L., Jiang, W., Xiao, Y. F., Deng, L., Gu, L. D., Guo, Z. Y., Zhou, Z. C., Wu, D., and Xin, H. B. (2011). Disruption of CD38 gene enhances cardiac functions by elevating serum testosterone in the male null mice. *Life Sciences* **89**, 491–497.

Gao, L., Blair, L. A. C., and Marshall, J. (2006). CaMKII-independent effects of KN93 and its inactive analog KN92: reversible inhibition of L-type calcium channels. *Biochemical and Biophysical Research Communications* **345**, 1606–1610.

Gao, Y. and Mehta, K. (2007). N-linked glycosylation of CD38 is required for its structure stabilization but not for membrane localization. *Molecular and Cellular Biochemistry* **295**, 1–7.

Garrity, A. G., Wang, W., Collier, C. M., Levey, S. A., Gao, Q., and Xu, H. (2016). The endoplasmic reticulum, not the pH gradient, drives calcium refilling of lysosomes. *eLife* **5**, 10.7554/eLife.15887.

Genazzani, A. A., Empson, R. M., and Galione, A. (1996). Unique inactivation properties of NAADP-sensitive Ca^{2+} release. *Journal of Biological Chemistry* **271**, 11599–11602.

Genazzani, A. A., Mezna, M., Dickey, D. M., Michelangeli, F., Walseth, T. F., and Galione, A. (1997). Pharmacological properties of the Ca^{2+}-release mechanism sensitive to NAADP in the sea urchin egg. *British Journal of Pharmacology* **121**, 1489–1495.

Gilabert-Oriol, R., Mergel, K., Thakur, M., Von Mallinckrodt, B., Melzig, M. F., Fuchs, H., and Weng, A. (2013). Real-time analysis of membrane permeabilizing effects of oleanane saponins. *Bioorganic and Medicinal Chemistry* **21**, 2387–2395.

Goodrich, S. P., Muller-Steffner, H., Osman, A., Moutin, M. J., Kusser, K., Roberts, A., Woodland, D. L., Randall, T. D., Kellenberger, E., LoVerde, P. T., Schuber, F., and Lund, F. E. (2005). Production of calcium-mobilizing metabolites by a novel member of the ADP-ribosyl cyclase family expressed in schistosoma mansoni. *Biochemistry* **44**, 11082–11097.

Graeff, R. and Lee, H. C. (2002). Novel cycling assays for cADPR and NAADP. In *Cyclic ADP-ribose and NAADP*. Springer US.

Graeff, R., Liu, Q., Kriksunov, I. A., Hao, Q., and Hon, C. L. (2006). Acidic residues at the active sites of CD38 and ADP-ribosyl cyclase determine nicotinic acid adenine dinucleotide phosphate (NAADP) synthesis and hydrolysis activities. *Journal of Biological Chemistry* **281**, 28951–28957.

Graeff, R., Munshi, C., Aarhus, R., Johns, M., and Lee, H. C. (2001). A single residue at the active site of CD38 determines its NAD cyclizing and hydrolyzing activities. *Journal of Biological Chemistry* **276**, 12169–12173.

Graeff, R. M., Franco, L., De Flora, A., and Lee, H. C. (1998). Cyclic GMP-dependent and -independent effects on the synthesis of the calcium messengers cyclic ADP-ribose and nicotinic acid adenine dinucleotide phosphate. *Journal of Biological Chemistry* **273**, 118–125.

Graeff, R. M., Walseth, T. F., Fryxell, K., Branton, W. D., and Lee, H. C. (1994). Enzymatic synthesis and characterizations of cyclic GDP-ribose. A procedure for distinguishing enzymes with ADP-ribosyl cyclase activity. *Journal of Biological Chemistry* **269**, 30260–30267.

Grosdidier, A., Zoete, V., and Michielin, O. (2011). SwissDock, a protein-small molecule docking web service based on EADock DSS. *Nucleic Acids Research* **39**, W270–W277.

Guedes, A. G., Deshpande, D., Dileepan, M., Walseth, T., Panettieri, R. J., Subramanian, S., and Kannan, M. (2015). CD38 and airway hyper-responsiveness: studies on human airway smooth muscle cells and mouse models. *Canadian Journal of Physiology and Pharmacology* **93**, 145–153.

Guida, L., Bruzzone, S., Sturla, L., Franco, L., Zocchi, E., and De Flora, A. (2002). Equilibrative and concentrative nucleoside transporters mediate influx of extracellular cyclic ADP-ribose into 3T3 murine fibroblasts. *Journal of Biological Chemistry* **277**, 47097–47105.

Guida, L., Franco, L., Zocchi, E., and De Flora, A. (1995). Structural role of disulfide bridges in the cyclic ADP-ribose related bifunctional ectoenzyme CD38. *FEBS Letters* **368**, 481–484.

Gul, R., Kim, S.-Y., Park, K.-H., Kim, B.-J., Kim, S.-J., Im, M.-J., and Kim, U.-H. (2008). A novel signaling pathway of ADP-ribosyl cyclase activation by angiotensin II in adult rat cardiomyocytes. *American Journal of Physiology Heart and Circulatory Physiology* **295**, H77–H88.

Gul, R., Park, D.-R., Shawl, A. I., Im, S.-Y., Nam, T.-S., Lee, S.-H., Ko, J.-K., Jang, K. Y., Kim, D., and Kim, U.-H. (2016). Nicotinic acid adenine dinucleotide phosphate (NAADP) and cyclic ADP-ribose (cADPR) Mediate Ca^{2+} signaling in cardiac hypertrophy induced by β-adrenergic stimulation. *PLoS One* **11**, 10.1371/journal.pone.0149125.

Gul, R., Shawl, A. I., Kim, S.-H., and Kim, U.-H. (2012). Cooperative interaction between reactive oxygen species and Ca^{2+} signals contributes to angiotensin II-induced hypertrophy in adult rat cardiomyocytes. *American Journal of Physiology Heart and Circulatory Physiology* **302**, H901–H909.

Guse, A. H., da Silva, C. P., Berg, I., Skapenko, A. L., Weber, K., Heyer, P., Hohenegger, M., Ashamu, G. A., Schulze-Koops, H., Potter, B. V., and Mayr, G. W. (1999). Regulation of calcium signalling in T lymphocytes by the second messenger cyclic ADP-ribose. *Nature* **398**, 70–73.

Haberthur, U. and Caflisch, A. (2008). FACTS: fast analytical continuum treatment of solvation. *Journal of Computational Chemistry* **29**, 701–715.

Halgren, T. A. (2009). Identifying and characterizing binding sites and assessing druggability. *Journal of Chemical Information and Modeling* **49**, 377–389.

Halgren, T. A., Murphy, R. B., Friesner, R. A., Beard, H. S., Frye, L. L., Pollard, W. T., and Banks, J. L. (2004). Glide: a new approach for rapid, accurate docking and scoring. 2. enrichment factors in database screening. *Journal of Medicinal Chemistry* **47**, 1750–1759.

Hara-Yokoyama, M., Kukimoto, I., Nishina, H., Kontani, K., Hirabayashi, Y., Irie, F., Sugiya, H., Furuyama, S., and Katada, T. (1996). Inhibition of NAD^+ glycohydrolase and ADP-ribosyl cyclase activities of leukocyte cell surface antigen CD38 by gangliosides. *Journal of Biological Chemistry* **271**, 12951–12955.

Hara-Yokoyama, M., Kukimoto-Niino, M., Terasawa, K., Harumiya, S., Podyma-Inoue, K. A., Hino, N., Sakamoto, K., Itoh, S., Hashii, N., Hiruta, Y., Kawasaki, N., Mishima-Tsumagari, C., Kaitsu, Y., Matsumoto, T., Wakiyama, M., Shirouzu, M., Kasama, T., Takayanagi, H., Utsunomiya-Tate, N., Takatsu, K., Katada, T., Hirabayashi, Y., Yokoyama, S., and Yanagishita, M. (2012). Tetrameric interaction of the ectoenzyme CD38 on the cell surface enables its catalytic and raft-association activities. *Structure* **20**, 1585–1595.

Hara-Yokoyama, M., Sugiya, H., Furuyama, S., Hirabayashi, Y., Nagatsuka, Y., Katsumata, O., Irie, F., Kontani, K., Hoshino, S. I., Katada, T., Ono, Y., and Fujita-Yoshigaki, J. (2001). Complex gangliosides as cell surface inhibitors for the ecto-NAD^+ glycohydrolase of CD38. *Biochemistry* **40**, 888–895.

Heidemann, A. C., Schipke, C. G., and Kettenmann, H. (2005). Extracellular application of nicotinic acid adenine dinucleotide phosphate induces Ca^{2+} signaling in astrocytes in situ. *Journal of Biological Chemistry* **280**, 35630–35640.

Hellmich, M. R. and Strumwasser, F. (1991). Purification and characterization of a molluscan egg-specific NADase, a second-messenger enzyme. *Cell Regulation* **2**, 193–202.

Higashida, H., Egorova, A., Higashida, C., Zhong, Z.-G. G., Yokoyama, S., Noda, M., and Zhang, J.-S. S. (1999). Sympathetic potentiation of cyclic ADP-ribose formation in rat cardiac myocytes. *Journal of Biological Chemistry* **274**, 33348–33354.

Higashida, H., Liang, M., Yoshihara, T., Akther, S., Fakhrul, A., Stanislav, C., Nam, T.-S., Kim, U.-H., Kasai, S., Nishimura, T., Al Mahmuda, N., Yokoyama, S., Ishihara, K., Gerasimenko, M., Salmina, A., Zhong, J., Tsuji, T., Tsuji, C., and Lopatina, O. (2017). An immunohistochemical, enzymatic, and behavioral study of CD157/BST-1 as a neuroregulator. *BMC Neuroscience* **18**, 35.

Higashida, H., Zhang, J., Hashii, M., Shintaku, M., Higashida, C., and Takeda, Y. (2000). Angiotensin II stimulates cyclic ADP-ribose formation in neonatal rat cardiac myocytes. *The Biochemical journal* **352**, 197–202.

Hirata, Y., Kimura, N., Sato, K., Ohsugi, Y., Takasawa, S., Okamoto, H., Ishikawa, J., Kaisho, T., Ishihara, K., and Hirano, T. (1994). ADP ribosyl cyclase activity of a novel bone marrow stromal cell surface molecule, BST-1. *FEBS letters* **356**, 244–248.

Hohendanner, F., McCulloch, A. D., Blatter, L. A., and Michailova, A. P. (2014). Calcium and IP_3 dynamics in cardiac myocytes: experimental and computational perspectives and approaches. *Frontiers in Pharmacology* **5**, 10.3389/fphar.2014.00035.

Holmberg, S. R. M. and Williams, A. J. (1990). The cardiac sarcoplasmic reticulum calcium-release channel: modulation of ryanodine binding and single-channel activity. *Biochimica et Biophysica Acta* **1022**, 187–193.

Howard, M., Grimaldi, J. C., Bazan, J. F., Lund, F. E., Santos-Argumedo, L., Parkhouse, R. M., Walseth, T. F., and Lee, H. C. (1993). Formation and hydrolysis of cyclic ADP-ribose catalyzed by lymphocyte antigen CD38. *Science* **262**, 1056–1059.

Huang, Y., Liu, T., Wang, D., Wang, X., Li, R., Chen, Y., Tang, Y., Wang, T., and Huang, C. (2015). Calmodulin kinase II inhibitor regulates calcium homeostasis changes caused by acute β-adrenergic receptor agonist stimulation in mouse ventricular myocytes. *In Vitro Cellular and Developmental Biology - Animal* **52**, 156–162.

Iino, S., Cui, Y., Galione, A., and Terrar, D. A. (1997). Actions of cADP-ribose and its antagonists on contraction in guinea pig isolated ventricular myocytes. Influence of temperature. *Circulation Research* **81**, 879–884.

Inui, M., Wang, S., Saito, A., and Fleischer, S. (1988). Characterization of junctional and longitudinal sarcoplasmic reticulum from heart muscle. *Journal of Biological Chemistry* **263**, 10843–10850.

Ishibashi, K., Suzuki, M., and Imai, M. (2000). Molecular cloning of a novel form (two-repeat) protein related to voltage-gated sodium and calcium channels. *Biochemical and Biophysical Research Communications* **270**, 370–376.

Itoh, M., Ishihara, K., Tomizawa, H., Tanaka, H., Kobune, Y., Ishikawa, J., Kaisho, T., and Hirano, T. (1994). Molecular cloning of murine BST-1 having homology with CD38 and Aplysia ADP-ribosyl cyclase. *Biochemical and Biophysical Research Communications* **203**, 1309–1317.

Jackson, D. G. and Bell, J. I. (1990). Isolation of a cDNA encoding the human CD38 (T10) molecule, a cell surface glycoprotein with an unusual discontinuous pattern of expression during lymphocyte differentiation. *Journal of Immunology* **144**, 2811–2815.

Jacobson, M. P., Friesner, R. A., Xiang, Z., and Honig, B. (2002). On the role

of the crystal environment in determining protein side-chain conformations. *Journal of Molecular Biology* **320**, 597–608.

Jacobson, M. P., Pincus, D. L., Rapp, C. S., Day, T. J. F., Honig, B., Shaw, D. E., and Friesner, R. A. (2004). A hierarchical approach to all-atom protein loop prediction. *Proteins* **55**, 351–367.

Jha, A., Ahuja, M., Patel, S., Brailoiu, E., and Muallem, S. (2014). Convergent regulation of the lysosomal two-pore channel-2 by Mg $^{2+}$, NAADP, PI(3,5)P2 and multiple protein kinases. *EMBO Journal* **33**, 501–511.

Jin, D., Liu, H.-X., Hirai, H., Torashima, T., Nagai, T., Lopatina, O., Shnayder, N. A., Yamada, K., Noda, M., Seike, T., Fujita, K., Takasawa, S., Yokoyama, S., Koizumi, K., Shiraishi, Y., Tanaka, S., Hashii, M., Yoshihara, T., Higashida, K., Islam, M. S., Yamada, N., Hayashi, K., Noguchi, N., Kato, I., Okamoto, H., Matsushima, A., Salmina, A., Munesue, T., Shimizu, N., Mochida, S., Asano, M., and Higashida, H. (2007). CD38 is critical for social behaviour by regulating oxytocin secretion. *Nature* **446**, 41–45.

Jorgensen, W. L., Maxwell, D. S., and Tirado-Rives, J. (1996). Development and testing of the OPLS all-atom force field on conformational energetics and properties of organic liquids. *Journal of the American Chemical Society* **118**, 11225–11236.

Kalogeris, T., Bao, Y., and Korthuis, R. J. (2014). Mitochondrial reactive oxygen species: a double edged sword in ischemia/reperfusion vs preconditioning. *Redox Biology* **2**, 702–714.

Kang, S. and Lebeche, D. (2013). Myocardial calcium signaling in physiology and disease. *Journal of Receptor, Ligand and Channel Research* **6**, 1–13.

Kannt, A., Sicka, K., Kroll, K., Kadereit, D., and Gögelein, H. (2012). Selective inhibitors of cardiac ADPR cyclase as novel anti-arrhythmic compounds. *Naunyn–Schmiedeberg's Archives of Pharmacology* **385**, 717–727.

Kato, I., Yamamoto, Y., Fujimura, M., Noguchi, N., Takasawa, S., and Okamoto, H. (1999). CD38 disruption impairs glucose-induced increases in cyclic ADP-ribose, $[Ca^{2+}]_i$, and insulin secretion. *Journal of Biological Chemistry* **274**, 1869–1872.

Katz, F., Povey, S., Parkar, M., Schneider, C., Sutherland, R., Stanley, K., Solomon, E., and Greaves, M. (1983). Chromosome assignment of monoclonal antibody-defined determinants on human leukemic cells. *European Journal of Immunology* **13**, 1008–1013.

Keng, M. K., Han, M. K., Park, J. B., Soo Wan Chae, Kim, U. H., Hon Cheung Lee, Boon Huat Bay, and Chan Fong Chang (2000). Localization of the cyclic ADP-ribose-dependent calcium signaling pathway in hepatocyte nucleus. *Journal of Biological Chemistry* **275**, 24807–24817.

Kim, H., Jacobson, E. L., and Jacobson, M. K. (1993). Synthesis and degradation of cyclic ADP-ribose by NAD glycohydrolases. *Science* **261**, 1330–1333.

Kim, S. Y., Cho, B. H., and Kim, U. H. (2010). CD38-mediated Ca^{2+} signaling contributes to angiotensin II-induced activation of hepatic stellate cells: Attenuation of hepatic fibrosis by CD38 ablation. *Journal of Biological Chemistry* **285**, 576–582.

Kontani, K., Nishina, H., Ohoka, Y., Takahashi, K., and Katada, T. (1993). NAD glycohydrolase specifically induced by retinoic acid in human leukemic HL-60 cells: Identification of the NAD

glycohydrolase as leukocyte cell surface antigen CD38. *Journal of Biological Chemistry* **268**, 16895–16898.

Kukimoto, I., Hoshino, S., Kontani, K., Inageda, K., Nishina, H., Takahashi, K., and Katada, T. (1996). Stimulation of ADP-ribosyl cyclase activity of the cell surface antigen CD38 by zinc ions resulting from inhibition of its NAD^+ glycohydrolase activity. *European Journal of Biochemistry* **239**, 177–182.

Kumasaka, S., Shoji, H., and Okabe, E. (1999). Novel mechanisms involved in superoxide anion radical-triggered Ca^{2+} release from cardiac sarcoplasmic reticulum linked to cyclic ADP-ribose stimulation. *Antioxidants & Redox Signaling* **1**, 55–69.

Lahouratate, P., Guibert, J., and Faivre, J. F. (1997). cADP-ribose releases Ca^{2+} from cardiac sarcoplasmic reticulum independently of ryanodine receptor. *American Journal of Physiology* **273**, H1082–H1089.

Laver, D. R. (2007). Ca^{2+} stores regulate ryanodine receptor Ca^{2+} release channels via luminal and cytosolic Ca^{2+} sites. *Clinical and Experimental Pharmacology and Physiology* **34**, 889–896.

Lee, H. C. (2001). Physiological functions of cyclic ADP-ribose and NAADP as calcium messengers. *Annual Review of Pharmacology and Toxicology* **41**, 317–345.

Lee, H. C. (2006). Structure and enzymatic functions of human CD38. *Molecular Medicine* **12**, 317–323.

Lee, H. C. (2012). *Cyclic ADP-ribose and NAADP: structures, metabolism and functions*. Springer Science & Business Media.

Lee, H. C. and Aarhus, R. (1991). ADP-ribosyl cyclase: an enzyme that cyclizes NAD^+ into a calcium-mobilizing metabolite. *Cell Regulation* **2**, 203–209.

Lee, H. C. and Aarhus, R. (1995). A derivative of NADP mobilizes calcium stores insensitive to inositol trisphosphate and cyclic ADP-ribose. *Journal of Biological Chemistry* **270**, 2152–2157.

Lee, H. C. and Aarhus, R. (1997). Structural determinants of nicotinic acid adenine dinucleotide phosphate important for its calcium-mobilizing activity. *Journal of Biological Chemistry* **272**, 20378–20383.

Lee, H. C. and Aarhus, R. (2000). Functional visualization of the separate but interacting calcium stores sensitive to NAADP and cyclic ADP-ribose. *Journal of Cell Science* **113**, 4413–4420.

Lee, H. C. and Zhao, Y. J. (2014). The type III calcium signaling mechanism of CD38. *Messenger* **3**, 59–64.

Lerner, F., Niere, M., Ludwig, A., and Ziegler, M. (2001). Structural and functional characterization of human NAD kinase. *Biochemical and Biophysical Research Communications* **288**, 69–74.

Lewis, A. M., Aley, P. K., Roomi, A., Thomas, J. M., Masgrau, R., Garnham, C., Shipman, K., Paramore, C., Bloor-Young, D., Sanders, L. E. L., Terrar, D. A., Galione, A., and Churchill, G. C. (2012). β-Adrenergic receptor signaling increases NAADP and cADPR levels in the heart. *Biochemical and Biophysical Research Communications* **427**, 326–329.

Lewis, A. M., Masgrau, R., Vasudevan, S. R., Yamasaki, M., O'Neill, J. S., Garnham, C., James, K., Macdonald, A., Ziegler, M., Galione, A., and Churchill, G. C. (2007). Refinement of a radioreceptor binding assay for nicotinic acid adenine dinucleotide phosphate. *Analytical Biochemistry* **371**, 26–36.

Li, L., Mirza, S., Richardson, S. J., Gallant, E. M., Thekkedam, C., Pace, S. M., Zorzato, F., Liu, D., Beard, N. A., and Dulhunty, A. F. (2015). A new cytoplasmic interaction between junctin and ryanodine receptor Ca^{2+} release channels. *Journal of Cell Science* **128**, 951–963.

Lin, S. J. and Guarente, L. (2003). Nicotinamide adenine dinucleotide, a metabolic regulator of transcription, longevity and disease. *Current Opinion in Cell Biology* **15**, 241–246.

Lin, W. K., Bolton, E. L., Cortopassi, W. A., Wang, Y., O'Brien, F., Maciejewska, M., Jacobson, M. P., Garnham, C., Ruas, M., Parrington, J., Lei, M., Sitsapesan, R., Galione, A., and Terrar, D. A. (2017). Synthesis of the Ca^{2+}-mobilizing messengers, NAADP and cADPR, by intracellular CD38 enzyme in mouse heart: role in β-adrenoceptor signaling. *Journal of Biological Chemistry* **292**, 13243–13257.

Lin-Moshier, Y., Walseth, T. F., Churamani, D., Davidson, S. M., Slama, J. T., Hooper, R., Brailoiu, E., Patel, S., and Marchant, J. S. (2012). Photoaffinity labeling of nicotinic acid adenine dinucleotide phosphate (NAADP) targets in mammalian cells. *Journal of Biological Chemistry* **287**, 2296–2307.

Liu, J., Zhao, Y., Li, W., Hou, Y., Li, T., Zhao, Z., Fang, C., Li, S., and Lee, H. (2017). Cytosolic interaction of type III human CD38 with CIB1 modulates cellular cyclic ADP-ribose levels. *Proceedings of the National Academy of Sciences of the United States of America* **114**, 8283–8288.

Liu, Q., Graeff, R., Kriksunov, I. A., Lam, C. M. C., Lee, H. C., and Hao, Q. (2008). Conformational closure of the catalytic site of human CD38 induced by calcium. *Biochemistry* **47**, 13966–13973.

Liu, Q., Kriksunov, I. A., Graeff, R., Munshi, C., Hon, C. L., and Hao, Q. (2005). Crystal structure of human CD38 extracellular domain. *Structure* **13**, 1331–1339.

Liu, Q., Kriksunov, I. A., Graeff, R., Munshi, C., Hon, C. L., and Hao, Q. (2006). Structural basis for the mechanistic understanding of human CD38-controlled multiple catalysis. *Journal of Biological Chemistry* **281**, 32861–32869.

Lloyd-Evans, E., Morgan, A. J., He, X., Smith, D. A., Elliot-Smith, E., Sillence, D. J., Churchill, G. C., Schuchman, E. H., Galione, A., and Platt, F. M. (2008). Niemann-Pick disease type C1 is a sphingosine storage disease that causes deregulation of lysosomal calcium. *Nature Medicine* **14**, 1247–1255.

Lukyanenko, V., Györke, I., Wiesner, T. F., and Györke, S. (2001). Potentiation of Ca^{2+} release by cADP-ribose in the heart is mediated by enhanced SR Ca^{2+} uptake into the sarcoplasmic reticulum. *Circulation Research* **89**, 614–622.

Lukyanenko, V. and Gyorke, S. (1999). Ca^{2+} sparks and Ca^{2+} waves in saponin-permeabilized rat ventricular myocytes. *Journal of Physiology* **521**, 575–585.

Luzio, J. P., Pryor, P. R., and Bright, N. A. (2007). Lysosomes: fusion and function. *Nature Reviews Molecular Cell Biology* **8**, 622–632.

Macgregor, A. (2014). Possible effects of cyclic ADP-ribose and related endogenous substances on calcium release and contraction in isolated ventricular myocytes. *DPhil Thesis, University of Oxford* .

Macgregor, A., Yamasaki, M., Rakovic, S., Sanders, L., Parkesh, R., Churchill, G. C., Galione, A., and Terrar, D. A. (2007a). NAADP controls cross-talk

between distinct Ca^{2+} stores in the heart. *Journal of Biological Chemistry* **282**, 15302–15311.

Macgregor, A. T., Rakovic, S., Galione, A., and Terrar, D. A. (2007b). Dual effects of cyclic ADP-ribose on sarcoplasmic reticulum Ca^{2+} release and storage in cardiac myocytes isolated from guinea-pig and rat ventricle. *Cell Calcium* **41**, 537–546.

Mahony, L. (1988). Maturation of calcium transport in cardiac sarcoplasmic reticulum. *Pediatric Research* **24**, 639–643.

Maier, L. S. and Bers, D. M. (2007). Role of Ca^{2+}/calmodulin-dependent protein kinase (CaMK) in excitation-contraction coupling in the heart. *Cardiovascular Research* **73**, 631–640.

Malavasi, F., Deaglio, S., Funaro, A., Ferrero, E., Horenstein, A. L., Ortolan, E., Vaisitti, T., and Aydin, S. (2008). Evolution and function of the ADP ribosyl cyclase/CD38 gene family in physiology and pathology. *Physiological Reviews* **88**, 841–886.

Malavasi, F., Funaro, A., Alessio, M., DeMonte, L. B., Ausiello, C. M., Dianzani, U., Lanza, F., Magrini, E., Momo, M., and Roggero, S. (1992). CD38: a multi-lineage cell activation molecule with a split personality. *International Journal of Clinical & Laboratory Research* **22**, 73–80.

Malavasi, F., Funaro, A., Roggero, S., Horenstein, A., Calosso, L., and Mehta, K. (1994). Human CD38: a glycoprotein in search of a function. *Immunology Today* **15**, 95–97.

Massion, P. B., Feron, O., Dessy, C., and Balligand, J. L. (2003). Nitric oxide and cardiac function: ten years after, and continuing. *Circulation Research* **93**, 388–398.

Mellman, I., Fuchs, R., and Helenius, A. (1986). Acidification of the Endocytic and Exocytic Pathways. *Annual Review of Biochemistry* **55**, 663–700.

Meszaros, L. G., Bak, J., and Chu, A. (1993). Cyclic ADP-ribose as an endogenous regulator of the non-skeletal type ryanodine receptor Ca^{2+} channel. *Nature* **364**, 76–79.

Mészáros, L. G., Wrenn, R. W., and Váradi, G. (1997). Sarcoplasmic reticulum-associated and protein kinase C-regulated ADP-ribosyl cyclase in cardiac muscle. *Biochemical and Biophysical Research Communications* **234**, 252–256.

Michalak, M. (1988). Identification of the Ca^{2+}-release activity and ryanodine receptor in sarcoplasmic-reticulum membranes during cardiac myogenesis. *Biochemical Journal* **253**, 631–636.

Mitsui-Saito, M., Kato, I., Takasawa, S., Okamoto, H., and Yanagisawa, T. (2003). CD38 gene disruption inhibits the contraction induced by alpha-adrenoceptor stimulation in mouse aorta. *Journal of Veterinary Medical Science* **65**, 1325–1330.

Mojzisová, A., Krizanová, O., Záciková, Ä., Komínková, V., and Ondrias, K. (2001). Effect of nicotinic acid adenine dinucleotide phosphate on ryanodine calcium release channel in heart. *Pflugers Archiv: European Journal of Physiology* **441**, 674–677.

Moreno-García, M. E., Partida-Sánchez, S., Primack, J., Sumoza-Toledo, A., Muller-Steffner, H., Schuber, F., Oppenheimer, N., Lund, F. E., and Santos-Argumedo, L. (2004). CD38 is expressed as noncovalently associated homodimers on the surface of murine B lymphocytes. *European Journal of Biochemistry* **271**, 1025–1034.

Moreschi, I., Bruzzone, S., Bodrato, N., Usai, C., Guida, L., Nicholas, R. A., Kassack, M. U., Zocchi, E., and De Flora, A. (2008). $NAADP^+$ is an agonist of the human P2Y11 purinergic receptor. *Cell Calcium* **43**, 344–355.

Moreschi, I., Bruzzone, S., Nicholas, R. A., Fruscione, F., Sturla, L., Benvenuto, F., Usai, C., Meis, S., Kassack, M. U., Zocchi, E., and De Flora, A. (2006). Extracellular NAD^+ is an agonist of the human P2Y11 purinergic receptor in human granulocytes. *Journal of Biological Chemistry* **281**, 31419–31429.

Morgan, A. J. and Galione, A. (2007). NAADP induces pH changes in the lumen of acidic Ca^{2+} stores. *The Biochemical Journal* **402**, 301–310.

Morgan, A. J. and Galione, A. (2014). Two-pore channels (TPCs): current controversies. *BioEssays* **36**, 173–183.

Muller-Steffner, H., Kuhn, I., Argentini, M., and Schuber, F. (2010). Identification of the N-glycosylation sites on recombinant bovine CD38 expressed in Pichia pastoris: their impact on enzyme stability and catalytic activity. *Protein Expression and Purification* **70**, 151–157.

Munshi, C., Aarhus, R., Graeff, R., Walseth, T. F., Levitt, D., and Lee, H. C. (2000). Identification of the enzymatic active site of CD38 by site-directed mutagenesis. *Journal of Biological Chemistry* **275**, 21566–21571.

Mutafova-Yambolieva, V. N., Hwang, S. J., Hao, X., Chen, H., Zhu, M. X., Wood, J. D., Ward, S. M., and Sanders, K. M. (2007). Beta-nicotinamide adenine dinucleotide is an inhibitory neurotransmitter in visceral smooth muscle. *Proceedings of the National Academy of Sciences of the United States of America* **104**, 16359–16364.

Nam, T.-S., Choi, S. H., Rah, S.-Y., Kim, S.-Y., Jang, W., Im, M.-J., Kwon, H. J., and Kim, U.-H. (2006). Discovery of a small-molecule inhibitor for kidney ADP-ribosyl cyclase: implication for intracellular calcium signal mediated by cyclic ADP-ribose. *Experimental & Molecular Medicine* **38**, 718–726.

Naylor, E., Arredouani, A., Vasudevan, S. R., Lewis, A. M., Parkesh, R., Mizote, A., Rosen, D., Thomas, J. M., Izumi, M., Ganesan, A., Galione, A., and Churchill, G. C. (2009). Identification of a chemical probe for NAADP by virtual screening. *Nature Chemical Biology* **5**, 220–226.

Nebel, M., Schwoerer, A. P., Warszta, D., Siebrands, C. C., Limbrock, A. C., Swarbrick, J. M., Fliegert, R., Weber, K., Bruhn, S., Hohenegger, M., Geisler, A., Herich, L., Schlegel, S., Carrier, L., Eschenhagen, T., Potter, B. V. L., Ehmke, H., and Guse, A. H. (2013). Nicotinic acid adenine dinucleotide phosphate (NAADP)-mediated calcium signaling and arrhythmias in the heart evoked by β-adrenergic stimulation. *Journal of Biological Chemistry* **288**, 16017–16030.

Noguchi, N., Takasawa, S., Nata, K., Tohgo, A., Kato, I., Ikehata, F., Yonekura, H., and Okatnoto, H. (1997). Cyclic ADP-ribose binds to FK506-binding protein 12.6 to Release Ca^{2+} from islet microsomes. *Journal of Biological Chemistry* **272**, 3133–3136.

Parkesh, R., Lewis, A. M., Aley, P. K., Arredouani, A., Rossi, S., Tavares, R., Vasudevan, S. R., Rosen, D., Galione, A., Dowden, J., and Churchill, G. C. (2008). Cell-permeant NAADP: A novel chemical tool enabling the study of Ca^{2+} signalling in intact cells. *Cell Calcium* **43**, 531–538.

Partida-Sánchez, S., Cockayne, D. A., Monard, S., Jacobson, E. L., Oppenheimer, N., Garvy, B., Kusser,

K., Goodrich, S., Howard, M., Harmsen, A., Randall, T. D., and Lund, F. E. (2001). Cyclic ADP-ribose production by CD38 regulates intracellular calcium release, extracellular calcium influx and chemotaxis in neutrophils and is required for bacterial clearance in vivo. *Nature Medicine* **7**, 1209–1216.

Pitt, S. J., Funnell, T. M., Sitsapesan, M., Venturi, E., Rietdorf, K., Ruas, M., Ganesan, A., Gosain, R., Churchill, G. C., Zhu, M. X., Parrington, J., Galione, A., and Sitsapesan, R. (2010). TPC2 is a novel NAADP-sensitive Ca^{2+} release channel, operating as a dual sensor of luminal pH and Ca^{2+}. *Journal of Biological Chemistry* **285**, 35039–35046.

Pitt, S. J., Lam, A. K. M., Rietdorf, K., Galione, A., and Sitsapesan, R. (2014). Reconstituted human TPC1 is a proton-permeable ion channel and is activated by NAADP or Ca^{2+}. *Science Signaling* **7**, 10.1126/scisignal.2004854.

Pollak, N., Dölle, C., and Ziegler, M. (2007). The power to reduce: pyridine nucleotides - small molecules with a multitude of functions. *Biochemical Journal* **402**, 205–218.

Powell, T., Terrar, D. a., and Twist, V. W. (1980). Electrical properties of individual cells isolated from adult rat ventricular myocardium. *Journal of Physiology* **302**, 131–153.

Prakash, Y. S., Kannan, M. S., Walseth, T. F., and Sieck, G. C. (2000). cADP ribose and $[Ca^{2+}]_i$ regulation in rat cardiac myocytes. *American Journal of Physiology Heart and Circulatory Physiology* **279**, H1482–H1489.

Prasad, G. S., McRee, D. E., Stura, E. A., Levitt, D. G., Lee, H. C., and Stout, C. D. (1996). Crystal structure of Aplysia ADP ribosyl cyclase, a homologue of the bifunctional ectozyme CD38. *Nature Structural Biology* **3**, 957–964.

Rah, S. Y., Mushtaq, M., Nam, T. S., Kim, S. H., and Kim, U. H. (2010). Generation of cyclic ADP-ribose and nicotinic acid adenine dinucleotide phosphate by CD38 for Ca^{2+} signaling in interleukin-8-treated lymphokine-activated killer cells. *Journal of Biological Chemistry* **285**, 21877–21887.

Rakovic, S., Cui, Y., Iino, S., Galione, A., Ashamu, G. A., Potter, B. V. L., and Terrar, D. A. (1999). An antagonist of cADP-ribose inhibits arrhythmogenic oscillations of intracellular Ca^{2+} in heart cells. *Journal of Biological Chemistry* **274**, 17820–17827.

Rakovic, S., Galione, A., Ashamu, G. A., Potter, B. V., and Terrar, D. A. (1996). A specific cyclic ADP-ribose antagonist inhibits cardiac excitation-contraction coupling. *Current Biology* **6**, 989–996.

Rakovic, S. and Terrar, D. A. (2002). Calcium Signaling by cADPR in Cardiac Myocytes. In *Cyclic ADP-Ribose and NAADP*. Springer US, Boston, MA.

Reinherz, E. L., Kung, P. C., Goldstein, G., Levey, R. H., and Schlossman, S. F. (1980). Discrete stages of human intrathymic differentiation: analysis of normal thymocytes and leukemic lymphoblasts of T-cell lineage. *Proceedings of the National Academy of Sciences of the United States of America* **77**, 1588–1592.

Reyes, L. A., Boslett, J., Varadharaj, S., De Pascali, F., Hemann, C., Druhan, L. J., Ambrosio, G., El-Mahdy, M., and Zweier, J. L. (2015). Depletion of NADP(H) due to CD38 activation triggers endothelial dysfunction in the postischemic heart. *Proceedings of the National Academy of Sciences of the United States of America* **112**, 11648–11653.

Rigg, L., Heath, B. M., Cui, Y., and Terrar, D. A. (2000). Localisation and functional significance of ryanodine receptors during beta-adrenoceptor stimulation in the guinea-pig sino-atrial node. *Cardiovascular Research* **48**, 254–264.

Rosen, D., Lewis, A. M., Mizote, A., Thomas, J. M., Aley, P. K., Vasudevan, S. R., Parkesh, R., Galione, A., Izumi, M., Ganesan, A., and Churchill, G. C. (2009). Analogues of the nicotinic acid adenine dinucleotide phosphate (NAADP) antagonist Ned-19 indicate two binding sites on the NAADP receptor. *Journal of Biological Chemistry* **284**, 34930–34934.

Ruas, M., Davis, L. C., Chen, C.-C., Morgan, A. J., Chuang, K.-T., Walseth, T. F., Grimm, C., Garnham, C., Powell, T., Platt, N., Platt, F. M., Biel, M., Wahl-Schott, C., Parrington, J., and Galione, A. (2015). Expression of Ca^{2+}-permeable two-pore channels rescues NAADP signalling in TPC-deficient cells. *The EMBO Journal* **34**, 1743–1758.

Ruas, M., Rietdorf, K., Arredouani, A., Davis, L. C., Lloyd-Evans, E., Koegel, H., Funnell, T. M., Morgan, A. J., Ward, J. A., Watanabe, K., Cheng, X., Churchill, G. C., Zhu, M. X., Platt, F. M., Wessel, G. M., Parrington, J., and Galione, A. (2010). Purified TPC isoforms form NAADP receptors with distinct roles for Ca^{2+} signaling and endolysosomal trafficking. *Current Biology* **20**, 703–709.

Rybalchenko, V., Ahuja, M., Coblentz, J., Churamani, D., Patel, S., Kiselyov, K., and Muallem, S. (2012). Membrane potential regulates nicotinic acid adenine dinucleotide phosphate (NAADP) dependence of the pH- and Ca^{2+}-sensitive organellar two-pore channel TPC1. *Journal of Biological Chemistry* **287**, 20407–20416.

Saito, A., Seiler, S., Chu, A., and Fleischer, S. (1984). Preparation and morphology of sarcoplasmic reticulum terminal cisternae from rabbit skeletal muscle. *Journal of Cell Biology* **99**, 875–885.

Sakurai, Y., Kolokoltsov, A. A., Chen, C.-C., Tidwell, M. W., Bauta, W. E., Klugbauer, N., Grimm, C., Wahl-Schott, C., Biel, M., and Davey, R. A. (2015). Two-pore channels control Ebola virus host cell entry and are drug targets for disease treatment. *Science* **347**, 995–998.

Sanchez, L., Wang, Y., Siegel, D. S., and Wang, M. L. (2016). Daratumumab: a first-in-class CD38 monoclonal antibody for the treatment of multiple myeloma. *Journal of Hematology & Oncology* **9**, 10.1186/s13045–016–0283–0.

Schieder, M., Rötzer, K., Brüggemann, A., Biel, M., and Wahl-Schott, C. A. (2010). Characterization of two-pore channel 2 (TPCN2)-mediated Ca^{2+} currents in isolated lysosomes. *Journal of Biological Chemistry* **285**, 21219–21222.

Schmid, F., Bruhn, S., Weber, K., Mittrücker, H. W., and Guse, A. H. (2011). CD38: a NAADP degrading enzyme. *FEBS Letters* **585**, 3544–3548.

Schmid, F., Fliegert, R., Westphal, T., Bauche, A., and Guse, A. H. (2012). Nicotinic acid adenine dinucleotide phosphate (NAADP) degradation by alkaline phosphatase. *Journal of Biological Chemistry* **287**, 32525–32534.

Shen, M. J. and Zipes, D. P. (2014). Role of the autonomic nervous system in modulating cardiac arrhythmias. *Circulation Research* **114**, 1004–1021.

Sikkel, M. B., Collins, T. P., Rowlands, C., Shah, M., O'Gara, P., Williams, A. J., Harding, S. E., Lyon, A. R., and MacLeod, K. T. (2013). Flecainide reduces Ca^{2+} spark and wave frequency

via inhibition of the sarcolemmal sodium current. *Circulation Research* **98**, 286–296.

Singaravelu, K. and Deitmer, J. W. (2006). Calcium mobilization by nicotinic acid adenine dinucleotide phosphate (NAADP) in rat astrocytes. *Cell Calcium* **39**, 143–153.

Sitsapesan, R., McGarry, S. J., and Williams, A. J. (1994). Cyclic ADP-ribose competes with ATP for the adenine nucleotide binding site on the cardiac ryanodine receptor Ca^{2+}-release channel. *Circulation Research* **75**, 596–600.

Sitsapesan, R. and Williams, A. J. (1990). Mechanisms of caffeine activation of single calcium-release channels of sheep cardiac sarcoplasmic reticulum. *Journal of Physiology* **423**, 425–439.

Smyth, J. T., Abbott, A. L., Lee, B., Sienaert, I., Kasri, N. N., De Smedt, H., Ducibella, T., Missiaen, L., Parys, J. B., and Fissore, R. A. (2002). Inhibition of the inositol trisphosphate receptor of mouse eggs and A7r5 cells by KN-93 via a mechanism unrelated to Ca^{2+}/calmodulin-dependent protein kinase II antagonism. *Journal of Biological Chemistry* **277**, 35061–35070.

Soares, S., Thompson, M., White, T., Isbell, A., Yamasaki, M., Prakash, Y., Lund, F. E., Galione, A., and Chini, E. N. (2007). NAADP as a second messenger: neither CD38 nor base-exchange reaction are necessary for in vivo generation of NAADP in myometrial cells. *American Journal of Physiology Cell Physiology* **292**, C227–C239.

States, D. J., Walseth, T. F., and Lee, H. C. (1992). Similarities in amino acid sequences of Aplysia ADP-ribosyl cyclase and human lymphocyte antigen CD38. *Trends in Biochemical Sciences* **17**, 495.

Sun, L., Adebanjo, O. A., Koval, A., Anandatheerthavarada, H. K., Iqbal, J., Wu, X. Y., Moonga, B. S., Wu, X. B., Biswas, G., Bevis, P. J. R., Kumegawa, M., Epstein, S., Huang, C. L.-H., Avadhani, N. G., Abe, E., and Zaidi, M. (2002). A novel mechanism for coupling cellular intermediary metabolism to cytosolic Ca^{2+} signaling via CD38/ADP-ribosyl cyclase, a putative intracellular NAD^+ sensor. *FASEB Journal* **16**, 302–314.

Takahashi, J., Kagaya, Y., Kato, I., Ohta, J., Isoyama, S., Miura, M., Sugai, Y., Hirose, M., Wakayama, Y., Ninomiya, M., Watanabe, J., Takasawa, S., Okamoto, H., and Shirato, K. (2003). Deficit of CD38/cyclic ADP-ribose is differentially compensated in hearts by gender. *Biochemical and Biophysical Research Communications* **312**, 434–440.

Takasawa, S., Tohgo, A., Noguchi, N., Koguma, T., Nata, K., Sugimoto, T., Yonekura, H., and Okamoto, H. (1993). Synthesis and hydrolysis of cyclic ADP-ribose by human leukocyte antigen CD38 and inhibition of the hydrolysis by ATP. *Journal of Biological Chemistry* **268**, 26052–26054.

Talukder, M. A. H., Zweier, J. L., and Periasamy, M. (2009). Targeting calcium transport in ischaemic heart disease. *Cardiovascular Research* **84**, 345–352.

Terrar, D. (2015). The roles of NAADP , two pore channels and lysosomes in Ca^{2+} signaling in cardiac muscle. *Messenger* **4**, 23–33.

Tohgo, A., Takasawa, S., Noguchi, N., Koguma, T., Nata, K., Sugimoto, T., Furuya, Y., Yonekura, H., and Okamoto, H. (1994). Essential cysteine residues for cyclic ADP-ribose synthesis and hydrolysis by CD38. *Journal of Biological Chemistry* **269**, 28555–28557.

Torti, M., Bertoni, A., Canobbio, I., Sinigaglia, F., and Balduini, C. (1999). Hydrolysis of $NADP^+$ by platelet CD38 in the absence of synthesis and degradation of cyclic ADP-ribose 2'-phosphate. *FEBS Letters* **455**, 359–363.

Vasudevan, S. R., Galione, A., and Churchill, G. C. (2008). Sperm express a Ca^{2+}-regulated NAADP synthase. *The Biochemical journal* **411**, 63–70.

Veech, R. L., Eggleston, L. V., and Krebs, H. A. (1969). The redox state of free nicotinamide-adenine dinucleotide phosphate in the cytoplasm of rat liver. *Biochemical Journal* **115**, 609–619.

Vences-Catalán, F. and Santos-Argumedo, L. (2011). CD38 through the life of a murine B lymphocyte. *IUBMB Life* **63**, 840–846.

Venturi, E., Pitt, S., Galfré, E., and Sitsapesan, R. (2012). From eggs to hearts: what is the link between cyclic ADP-ribose and ryanodine receptors? *Cardiovascular Therapeutics* **30**, 109–116.

von Heijne, G. (1989). Control of topology and mode of assembly of a polytopic membrane protein by positively charged residues. *Nature* **341**, 456–458.

von Heijne, G. (2006). Membrane-protein topology. *Nature Reviews Molecular Cell Biology* **7**, 909–918.

Walseth, T. F., Lin-Moshier, Y., Jain, P., Ruas, M., Parrington, J., Galione, A., Marchant, J. S., and Slama, J. T. (2012). Photoaffinity labeling of high affinity nicotinic acid adenine dinucleotide phosphate (NAADP)-binding proteins in sea urchin egg. *Journal of Biological Chemistry* **287**, 2308–2315.

Wang, X., Zhang, X., Dong, X. P., Samie, M., Li, X., Cheng, X., Goschka, A., Shen, D., Zhou, Y., Harlow, J., Zhu, M. X., Clapham, D. E., Ren, D., and Xu, H. (2012). TPC proteins are phosphoinositide-activated sodium-selective ion channels in endosomes and lysosomes. *Cell* **151**, 372–383.

Warszta, D., Nebel, M., Fliegert, R., and Guse, A. H. (2014). NAD derived second messengers: role in spontaneous diastolic Ca^{2+} transients in murine cardiac myocytes. *DNA Repair* **23**, 69–78.

Wei, W.-J., Sun, H.-Y., Ting, K. Y., Zhang, L.-H., Lee, H.-C., Li, G.-R., and Yue, J. (2012). Inhibition of cardiomyocytes differentiation of mouse embryonic stem cells by CD38/cADPR/Ca^{2+} signaling pathway. *Journal of Biological Chemistry* **287**, 35599–35611.

Wilson, H. L. (1998). Regulation of calcium mobilisation by pyridine nucleotide metabolites. *DPhil Thesis, University of Oxford* .

Xie, G.-H., Rah, S.-Y., Kim, S.-J., Nam, T.-S., Ha, K.-C., Chae, S.-W., Im, M.-J., and Kim, U.-H. (2005). ADP-ribosyl cyclase couples to cyclic AMP signaling in the cardiomyocytes. *Biochemical and Biophysical Research Communications* **330**, 1290–1298.

Xie, G.-H. H., Rah, S.-Y. Y., Yi, K. S., Han, M.-K. K., Chae, S.-W. W., Im, M.-J. J., and Kim, U.-H. H. (2003). Increase of intracellular Ca^{2+} during ischemia/reperfusion injury of heart is mediated by cyclic ADP-ribose. *Biochemical and Biophysical Research Communications* **307**, 713–718.

Xu, M., Li, X. X., Ritter, J. K., Abais, J. M., Zhang, Y., and Li, P. L. (2013). Contribution of NADPH oxidase to membrane CD38 internalization and activation in coronary arterial myocytes. *PLoS ONE* **8**, 10.1371/journal.pone.0071212.

Yalcintepe, L., Albeniz, I., Adin-Cinar, S., Tiryaki, D., Bermek, E., Graeff, R. M., and Lee, H. C. (2005). Nuclear CD38 in retinoic acid-induced HL-60 cells. *Experimental Cell Research* **303**, 14–21.

Yamada, M., Mizuguchi, M., Otsuka, N., Ikeda, K., and Takahashi, H. (1997). Ultrastructural localization of CD38 immunoreactivity in rat brain. *Brain Research* **756**, 52–60.

Yamaguchi, S., Jha, A., Li, Q., Soyombo, A. A., Dickinson, G. D., Churamani, D., Brailoiu, E., Patel, S., and Muallem, S. (2011). Transient receptor potential mucolipin 1 (TRPML1) and two-pore channels are functionally independent organellar ion channels. *Journal of Biological Chemistry* **286**, 22934–22942.

Yamasaki, M., Masgrau, R., Morgan, A. J., Churchill, G. C., Patel, S., Ashcroft, S. J. H., and Galione, A. (2004). Organelle selection determines agonist-specific Ca^{2+} signals in pancreatic acinar and beta cells. *Journal of Biological Chemistry* **279**, 7234–7240.

Yang, L. Z., KockskĬĹmper, J., Khan, S., Suarez, J., Walther, S., Doleschal, B., Unterer, G., Khafaga, M., MÌĹcHler, H., Heinzel, F. R., Dillmann, W. H., Pieske, B., and Spiess, J. (2011). CAMP- and Ca^{2+}/calmodulin-dependent protein kinases mediate inotropic, lusitropic and arrhythmogenic effects of urocortin 2 in mouse ventricular myocytes. *British Journal of Pharmacology* **162**, 544–556.

Yu, Q. and Heikal, A. A. (2009). Two-photon autofluorescence dynamics imaging reveals sensitivity of intracellular NADH concentration and conformation to cell physiology at the single-cell level. *Journal of Photochemistry and Photobiology B: Biology* **95**, 46–57.

Zhang, F., Jin, S., Yi, F., and Li, P. L. (2009a). TRP-ML1 functions as a lysosomal NAADP-sensitive Ca^{2+} release channel in coronary arterial myocytes. *Journal of Cellular and Molecular Medicine* **13**, 3174–3185.

Zhang, F. and Li, P. L. (2007). Reconstitution and characterization of a nicotinic acid adenine dinucleotide phosphate (NAADP)-sensitive Ca^{2+} release channel from liver lysosomes of rats. *Journal of Biological Chemistry* **282**, 25259–25269.

Zhang, H., Graeff, R., Lee, H. C., and Hao, Q. (2013). Crystal structures of human CD38 in complex with NAADP and ADPRP. *Messenger* **2**, 44–53.

Zhang, X., Tallini, Y. N., Chen, Z., Gan, L., Wei, B., Doran, R., Miao, L., Xin, H. B., Kotlikoff, M. I., and Ji, G. (2009b). Dissociation of FKBP12.6 from ryanodine receptor type 2 is regulated by cyclic ADP-ribose but not β-adrenergic stimulation in mouse cardiomyocytes. *Cardiovascular Research* **84**, 253–262.

Zhao, Y. J., Lam, C. M. C., Lee, H. C., and Watson, P. (2012). The membrane-bound enzyme CD38 exists in two opposing orientations. *Science Signaling* **5**, 10.1126/scisignal.2002700.

Zhao, Y. J., Zhang, H. M., Lam, C. M. C., Hao, Q., and Lee, H. C. (2011). Cytosolic CD38 protein forms intact disulfides and is active in elevating intracellular cyclic ADP-ribose. *Journal of Biological Chemistry* **286**, 22170–22177.

Zhao, Y. J., Zhu, W. J., Wang, X. W., Zhang, L.-H. H., and Lee, H. C. (2015). Determinants of the membrane orientation of a calcium signaling enzyme CD38. *Biochimica et Biophysica Acta* **1853**, 2095–2103.

Zhu, M. X., Ma, J., Parrington, J., Calcraft, P. J., Galione, A., and Evans, A. M. (2010). Calcium signaling via two-pore

channels: local or global, that is the question. *American Journal of Physiology Cell Physiology* **298**, C430–C441.

Zielinska, W., Barata, H., and Chini, E. N. (2004). Metabolism of cyclic ADP-ribose: Zinc is an endogenous modulator of the cyclase/NAD glycohydrolase ratio of a CD38-like enzyme from human seminal fluid. *Life Sciences* **74**, 1781–1790.

Zissimopoulos, S. and Lai, F. A. (2005). Interaction of FKBP12.6 with the cardiac ryanodine receptor C-terminal domain. *Journal of Biological Chemistry* **280**, 5475–5485.

Zocchi, E., Franco, L., Guida, L., Calder, L., and De Flora, A. (1995). Self-aggregation of purified and membrane-bound erythrocyte CD38 induces extensive decrease of its ADP-ribosyl cyclase activity. *FEBS Letters* **359**, 35–40.

Zong, X., Schieder, M., Cuny, H., Fenske, S., Gruner, C., Rötzer, K., Griesbeck, O., Harz, H., Biel, M., and Wahl-Schott, C. (2009). The two-pore channel TPCN2 mediates NAADP-dependent Ca^{2+}-release from lysosomal stores. *Pflugers Archiv European Journal of Physiology* **458**, 891–899.